PROCEEDINGS

1st International

PhD. SYMPOSIUM

28-30. May 1996. BUDAPEST

Technical University of Budapest
Faculty of Civil Engineering

Edited by G. L. Balázs

PROCEEDINGS

1st International

Ph.D. Symposium

28-30. May 1996, Budapest

Technical University of Budapest

Faculty of Civil Engineering

edited by G.L. Balázs

PREFACE

The Proceedings here is the result of an initiative concerning Ph.D. studies.

Every university has its own programme for Ph.D. studies. These programmes may be very different but always try to help the Ph.D. students to reach their Ph.D. title within a limited number of years.

I think that the Ph.D. students need a special forum above the Ph.D. programmes to present the results of their ongoing research and to discuss them collecting advices how to continue the research. This forum should be very similar to that we generally have for technical or scientific presentations and as wide as possible to collect opinion on a large scale. It was then called as *Ph.D. Symposium*.

The system of the symposium is to have short oral presentations by the Ph.D. students themselves. The presentations are discussed immediately afterwards. Main results of the studies are summarized in the symposium proceedings.

Nevertheless, the objectives of the **Ph.D. Symposium 1996 Budapest** are:

1. to provide a forum for Ph.D. students in civil engineering to present the progress of their work,
2. to discuss the results of the ongoing Ph.D. studies in order to support the future work,
3. to give the possibility for Ph.D. students to establish contact for international communication,
4. to compare Ph.D. studies in various countries.

We received contributions from all over the world (*BOKU-Wien, EPFL Lausanne, ETH Hönggerberg, National Technical University of Athens, Romanian Academy Timisoara Branch, Stanford University, Technical University of Budapest, Tohoku Gakuin University, University of Karlsruhe, University of Stuttgart*) which helped very much to reach above objectives.

I appreciate the huge effort of *Ph.D. students* preparing their oral and written contributions, respectively, and especially those six Ph.D. students (*Á. Barsi, T. Hajnal, A. Köpecsiri, Z. Orbán, B. Vásárhelyi*) who served on the Organizing Committee.

Many thanks for the advices and support by the dean *Prof. J. Megyeri* and vice-dean *Prof. J. Farkas*, session chairmen *Profs. Á. Detrekői, Zs. Gáspár, M. Iványi, Ottó Haszpra* and other professors and assoc. professors of our faculty.

Support and understanding by *Profs. K. Bergmeister, D. Dubina, J. Eibl, R. Eligehausen, R. Favre, P. Marti, K. Otsuka, G.S. Springer, T.P. Tassios* of this initiative sending Ph.D. students to the symposium in a foreign country were especially appreciated.

Last but not least the financial support of the Faculty of Civil Engineering at the Technical University of Budapest and the support of the initiation by the CEB (Comité Euro-International du Béton) are gratefully acknowledged.

G.L. Balázs

Participating universities:

BOKU Wien

EPFL Lausanne

ETH Hönggerberg

National Technical University of Athens

Romanian Academy, Timisoara Branch

Stanford University

Technical University of Budapest

Tohoku Gakuin University

University of Karlsruhe

University of Stuttgart

Sponsored by:

Faculty of Civil Engineering

Technical University of Budapest

Organizing Committee:

György L. BALÁZS,	Assoc. Prof.
Árpád BARSI,	Ph.D. Student
Tünde HAJNAL,	Ph.D. Student
András KÖPECSIRI,	Ph.D. Student
Zoltán ORBÁN,	Ph.D. Student
Balázs VÁSÁRHELYI,	Ph.D. Student

GENERAL PROGRAM

28. (Tuesday) May 1996	OPENING
	SESSION 1 Concrete structures, masonry and composites (*in English*)
29. (Wednesday) May 1996	SESSION 2 Road construction (in English) SESSION 3 Steel structures (*in English*)
	SESSION 4 Hydraulic engineering (in English) SESSION 5 Mechanics (*in English*)
	Evening: Discussion about the life of Ph.D. students in various countries (*in English*)
30. (Thursday) May 1996	SESSION 6 Geodesy (*in Hungarian*) SESSION 7 Mechanics, materials (*in Hungarian*)
	SESSION 8 Hydraulic engineering (*in Hungarian*)
	CLOSING
	Small symposium banquet

Meeting room: Műegyetem rkp 3, H-1111 Budapest
Building K, 1st Floor, Room 40

B

C

CONTENT

SESSION 2
Road constiction

SESSION 3
Steel structures

SESSION 4
Hydraulic engineering

SESSION 5
Mechanics

SESSION 1

Concrete structures, masonry and composites

IRREVERSIBLE DEFORMATIONS OF POST-TENSIONED STRUCTURES UNDER CYCLIC LOADS

Favre R., Charif H. & Rotilio J.-D.
Swiss Federal Institute of Technology, Reinforced and Post-tensioned Concrete
CH- 1015 Lausanne

1. INTRODUCTION

Several post-tensioned concrete bridges continue to deform in time even though the period relative to concrete's time dependent effects (creep, shrinkage, relaxation) is over.
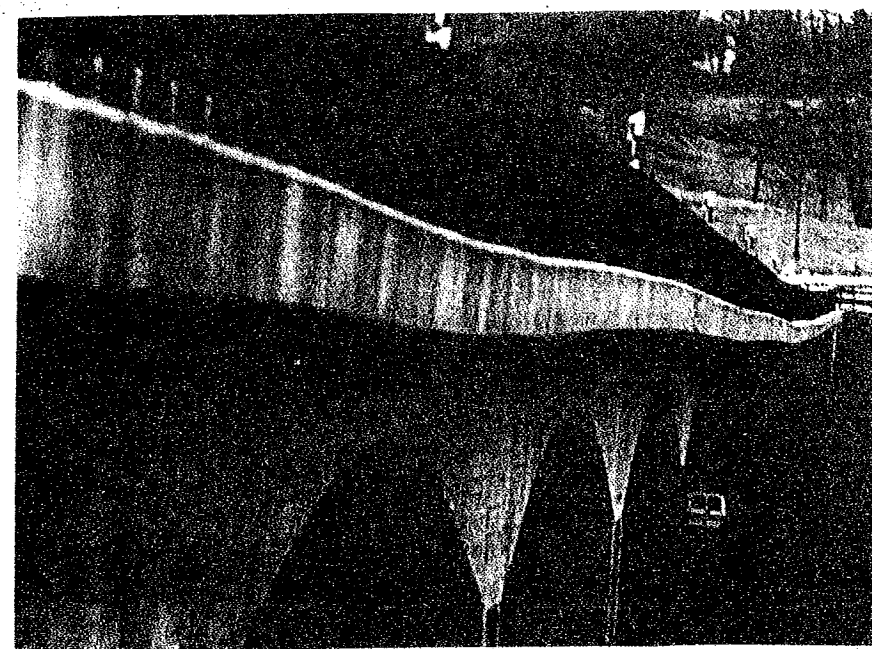
Fig.1 Excessive deformations / Fégire's Bridge, Switzerland

One of the reasons of such an unstabilized behaviour could be the appearance of irreversible deformations increasing in time caused by cyclic loads, especially for partially post-tensioned structures which allow cracking under permanent loads.

The Institute of Reinforced and Post-tensioned Concrete (IBAP) at the Swiss Federal Institute of Technology (EPFL) aims at a satisfactory long term behaviour of concrete structures. This effort recently materialised into a major publication, that summarises two Ph.D. thesis and other researches [1]. Basically it ended up into recommendations

meant to guide the design engineer in his choice of the post-tensioning level[1] in order to guarantee a structure's satisfactory behaviour in time.

However the possible influence of cyclic loads was not considered. The research presented here has to be seen as a natural evolution of the work accomplished so far at the IBAP, since one of its main purposes is to *observe the post-tensioning level's influence on concrete structures' irreversible deformations due to a repeated loading*. Another expected result is the development of a theoretical model, based on an « improved » Moment - Curvature law which will take into account the long term non-reversible behaviour. Such a law could then be implemented into a finite elements program's algorithm.

2. TWO NOTIONS

2.1 Irreversible deformations

What we mean by irreversible deformations is simply the difference between a reference state's deformation (D0) characterised by a certain load level and a further state's deformation (D2) under the same load level, after the structure has been loaded at a higher load and reached deformation D1 (figure2). Even if this difference is very small, the repetition of a loading-unloading cycle will lead to an accumulation of these small differences, which will result in irreversible deformations.
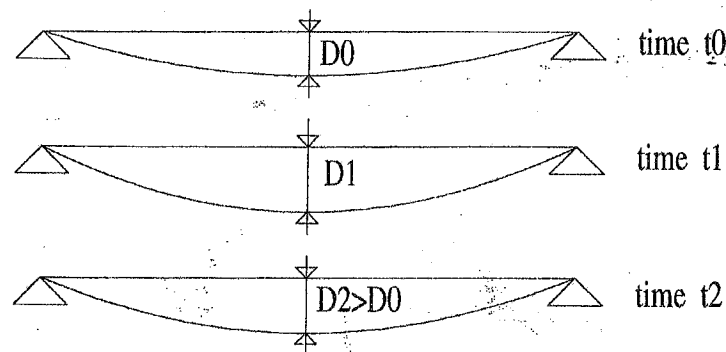
Fig.2   *Irreversible deformations*

This irreversible behaviour is closely related to cracking, because the load repetition causes a damaging between concrete and steel. Therefore the post-tensioning level plays a major role since it determines whether the structure will be cracked or not.

From a design code stand point, it has to be recognised that even though some works were carried out in this area, very little guidance (if none) is given in design codes [2] on how repeated loading should be considered. Moreover the influence of a possible post-tensioning force is not addressed.

---

[1] The post-tensioning level is based on a general concept which could be related to the amount of post-tension. In fact it is a factor called β, going from 0 for a reinforced concrete beam to 1 for a fully post-tensioned beam. But actually it is a deflection's compensation factor. That is to say it gives the proportion of the total deflection, compensated by post-tensioning. Thus $\beta = 1$ means a total compensation.

2.2 Cyclic loads

The loads considered can be seen as assuming a double function. Firstly they can crack the structure when applied. Secondly they can increase the deformations by appearing repeatedly, leading so to irreversible deformations.

Changes in temperatures can produce stresses of the same order of magnitude as the dead or live loads provided that the thermal expansion or contraction is restrained [3]. As far as bridges are concerned, *traffic* (especially the heaviest portion of it) has an impact also. Beside the two types of loads mentioned above, there are also the loads that appear during the construction phase. Theses loads could crack the structure even before it is finished.

The influence of cyclic loads on modern structures is actual. In fact thanks to the technological progresses made on materials, construction methods and design by using computer programs, the modern bridges tend to become slenderer and more elegant. But the slenderer the structure gets, the greater the influence of varying loads becomes.

3. TESTS

The first part of this research consisted in setting up a series of experimental tests to be performed on post-tensioned concrete beams, which post-tensioning level varies from one beam to another. The reference static model is a simple supported beam with a parabolic cable. However the tested beams are characterised by a rectilinear post-tension and the vertical balancing load is directly taken into account at the jack by applying a smaller load. This way of proceeding was chosen to solve several practical matters (transportation, application of the post-tensioning force before any load is applied, creep induced deflections).

The post-tensioning force runs from P = 0 [kN] (reinforced concrete) to P = 259 [kN] (fully post-tensioned beam : deflections due to permanent loads and post-tensioning are equal to zero).
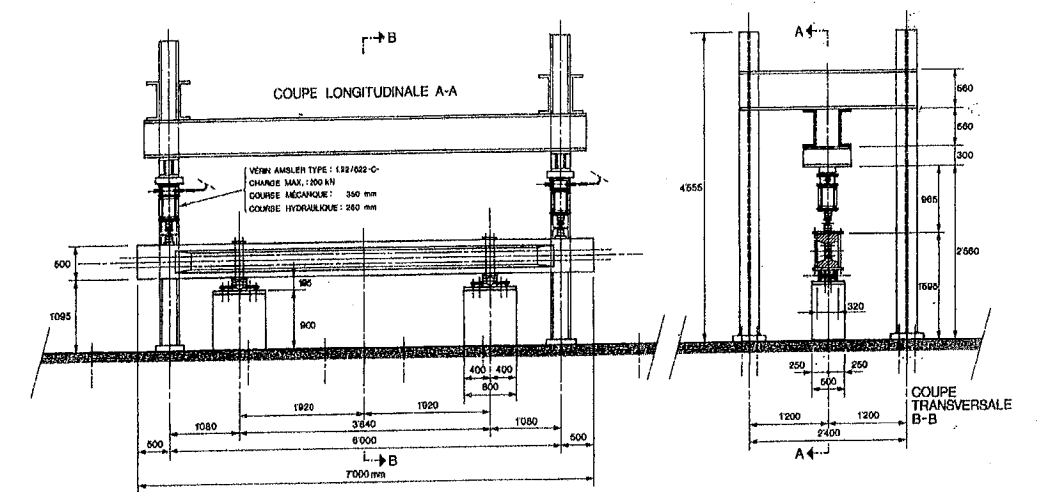
Fig.4   *Tested beam*

The first approach consists in considering the tested beam as a bridge to be built with its loads defined. At that stage the design engineer has to choose the post-tensioning force. The purpose of these tests is to illustrate the consequences of that choice with respect to a long term deterioration due to cyclic loads. By keeping the ultimate load constant for all the beams, which are differently post-tensioned, it automatically implies that the beams will be tested at different load levels. The four beams tested under this approach, are presented below.

A second approach has been investigated, which consists in keeping the load level constant, close to cracking. This approach will not be presented here.

3.1 Cycles

The sinus shaped cycles were applied at a rate of 3 cycles per minute. The minimum and maximum load correspond respectively to the long term permanent loads and to the total of dead and live loads. A total of more than 7000 cycles has been applied. If we consider that one load cycle correspond to an actual daily temperature cycle, then it would mean that 20 years have been simulated. This value is only indicative.

3.2 Measuring devices

- Five inductive captors

- Two parallel rows of 15 strain gauges (Omega gauges) on the top and bottom fiber at mid span over a length of 1.5 m.
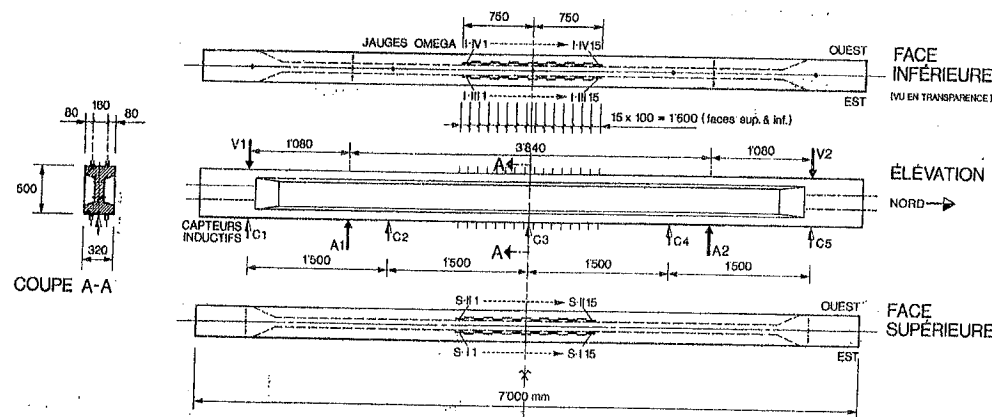
Fig.5   Measuring devices

4. FIRST RESULTS

Since data analysis is not over yet, only a small part of the results are presented. A complete report will be published later this year [4].

The four beams tested according to the first approach, were post-tensioned as follows:

Beam	Post-tensioning force P [kN]	Post-tensioning level β
G00	0	0.0
G03	80	0.3
G06	150	0.6
G10	260	1.0

The first graph presented here below shows the maximum deflections' envelops versus the number of cycles. Obviously the load repetition leads to an increase in deflections which varies from one beam to another. This increase diminishes with the number of cycles, but after 7000 cycles the deflections are still increasing.
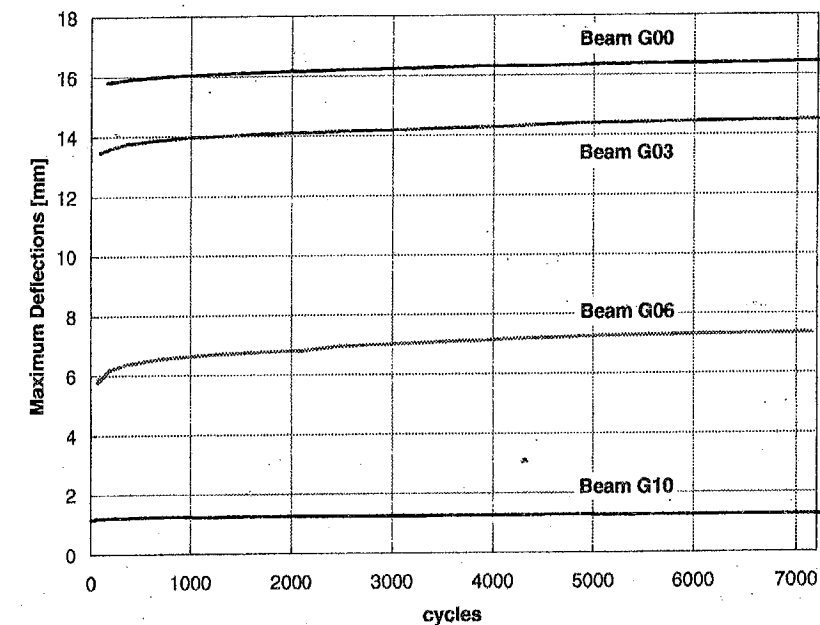
Fig.6   Maximum deflections versus cycles

The increase in deflection can better be seen in the second graph (figure 7). It is interesting to notice that the increase in deflections is smaller for G00 and G10 than for the two other beams. This can be explained by seeing that for G10 the maximum applied load is below cracking - therefore G10 is loaded elastically - and that for G00 the beam is completely cracked at first loading. However for G03 and G06 the cracking process is still evolving in time.

Another interesting observation to point out is that about 80% of the measured deflection's increase after 7000 cycles, has taken place after 1000 cycles.
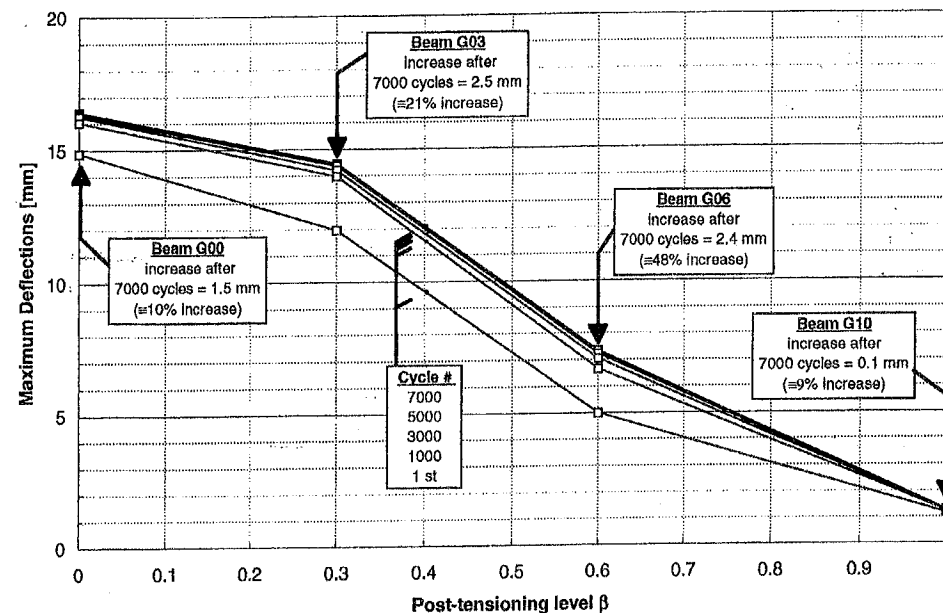
Fig.7   Maximum deflections versus β

5. CONCLUSIONS

Even though few results are known, some interesting observations were made. Concerning the choice of the post-tensioning level, we can say that in order to avoid large deformations and an "unacceptable" (obviously to be defined!) irreversible behaviour, high post-tensioning level should be used. As a comparison the recommended β based on long term observations of more than 200 bridges and on non linear simulations is equal to 0.8 for a standard quality requirement [1]. Even if this research on irreversible deformations is far from being finished, it could be expected, that it will end up in recommending high levels of post-tensioning to guarantee a satisfactory behaviour in time.

REFERENCES

[1]   Favre R. & al., "Learnings from load testing and long term observations for the evaluations of concrete bridges. Recommendations for the choice of post-tensioning", *OFR Report*, July 95.

[2]   Ghali A. & Favre R., "Concrete Structures; Stresses and deformations", *E & FN Spon*, Second edition, 1994.

[3]   "CEB-FIP Model code 1990", *Design code*, Thomas Telford, 1993.

[4]   Rotilio J.-D. & Charif H., " Irreversible deformations of post-tensioned beams under cyclic loads : Tests report", *to be published*.

SAFETY OF REINFORCED CONCRETE BEAMS SUBJECTED TO COMBINED STRESS

Kálmán Koris
Technical University of Budapest, Department of Reinforced Concrete Structures
H-1521 Budapest, Hungary

1. INTRODUCTION

At our engineering structures, the applied loads, the structural dimensions and material properties are random functions. Due to such random fluctuations, the value of the structural resistance is a random function, itself. This uncertain behaviour of our structures can be taken into account using a stochastic analysis. Probabilistic methods in mechanics, for problems involving time-independent uncertainties, can be comprehensively classified into two major categories: methods using a statistical approach and methods using non-statistical approach [1]. Simulation, e. g. Monte Carlo simulation is the most prevalent statistical approach. Non-statistical approaches include second-moment analysis and stochastic finite element methods (SFEM).

Stochastic finite element methods have recently become an active area of research. Researchers in this field attempt to combine the finite element analysis and the stochastic analysis. The modern engineering structures are quite complex to analyse. The finite element method (FEM) has proven by far the most effective tool available to engineers solving a large class of such complex engineering problems. The formulation of the stochastic finite element method is a natural extension of the basic ideas of the deterministic finite element method to accommodate random functions.

The usual reliability analysis of reinforced concrete structures compares cross-sectional resistance with locally acting forces. However, this process involves inconsistencies, so it would be favourable to compare acting loads with resisting loads at system level rather than at cross-sectional level [3]. The purpose of this paper is to present a stochastic finite element technique that gives us the ability to compare globally acting forces with structural resistance at system level.

2. EXPLANATION OF STRUCTURAL SAFETY

Safety of a structure means the probability of the load effect (S) not exceeding the value of the structural resistance (R). The safety of a structure is satisfactory if

$$\text{Prob}[R - S \geq 0] \geq (1 - p)$$

where p is the probability of failure [8]. The structural safety is generally described by the safety index (β). The distance between the mean values of the structural resistance (R_m) and the load effect (S_m) can be expressed using the safety index as

$$R_m - S_m = \beta \cdot s_{RS}$$

where s_{RS} is the standard deviation of the resultant distribution (Fig. 1).
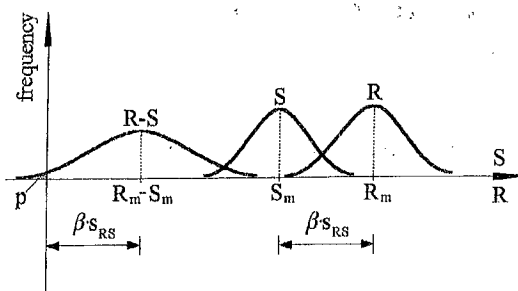
Fig. 1 Explanation of safety index (β)

To be able to determine the safety index, the knowledge of the distributions of external loads and structural resistance is needed. The distribution of different types of loads can be experimentally quite well examined, however the distribution of the structural resistance is much more complicated to determine. Expecting normal distribution, the mean value and standard deviation of structural resistance are needed to describe its distribution.

3. MEAN VALUE OF STRUCTURAL RESISTANCE

To analyse a reinforced concrete structure, the finite element method is applied. Since we use the mean values of structural dimensions and material properties for the calculations, the result we get is the mean value of the structural resistance.

3.1. Considering the material characteristic of reinforced concrete

For the finite element calculations, the stress-deformation relation of a reinforced concrete element is required. To describe the post-cracking behaviour of structural concrete in combined stress-state, a method based on discretized space truss model is used (Fig. 2).
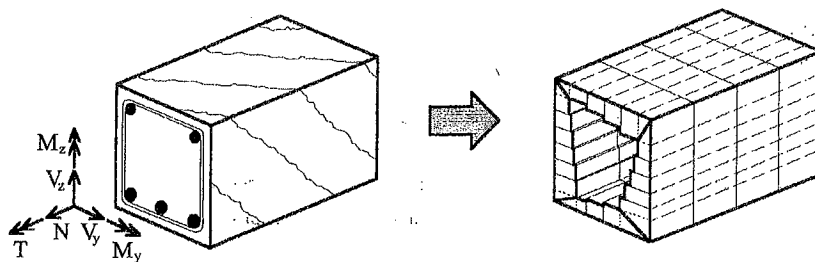
Fig 2. Multiaxially loaded reinforced concrete bar and its discretization

According to this method, the deformations can be determined to a given load combination considering the equilibrium conditions, the geometry of deformation, elastic-plastic stress-strain characteristics of the steel and non-linear stress-strain relation of the concrete [6], [7].

3.2. Analysing the structure using finite element method

For the finite element analysis, a 1D bar element with deformations of order three is used (Fig. 3). The deformation functions are approximated with $C^{(0)}$ continuous functions.
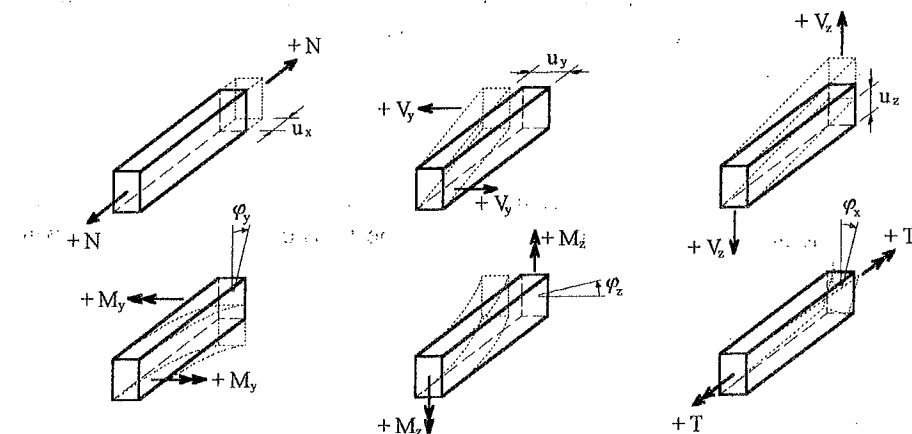
Fig. 3 Linear and angular flexibilities of a bar element

The examined reinforced concrete beam is loaded with single-parameter load. The value of the load-intensity is increased in steps until the structure fails. According to the method described in Chapter 3.1., the stiffnesses of the finite elements are calculated by successive approximation to each value of the load-intensity. Using the evaluated stiffnesses, a chord stiffness matrix of the structure can be compiled and the computations can be proceeded. The value of maximum load that can be carried without the failure of the structure can be accepted as the structural resistance.

4. DISTRIBUTION OF THE STRUCTURAL RESISTANCE

4.1. The variational approach

The expression for the deterministic finite element system of equations in a displacement format can be written as

$$K \cdot u = q \tag{4.1.1}$$

where K is the stiffness matrix, u includes the unknown nodal displacements and q is the vector of external loads. In case of single-parameter load, q can be expressed as a product of the load-intensity (F) and a load-distribution vector (Φ):

$$q = F \cdot \Phi$$

The displacement is influenced by the variation in the stiffness properties and the load-intensity and can be split up into its mean and fluctuating components as

$$(\overline{K} + \delta K) \cdot (\overline{u} + \delta u) = (\overline{q} + \delta q) \tag{4.1.2}$$

From equation (4.1.2) we get:

$$\overline{K} \cdot \overline{u} + \overline{K} \cdot \delta u + \delta K \cdot \overline{u} + \delta K \cdot \delta u = \overline{q} + \delta q \qquad (4.1.3)$$

The product of $\delta K \cdot \delta u$ can be neglected from (4.1.3), since its influence on the results is expected to be insignificant. Considering (4.1.1), the fluctuating components can be separated into an independent system of equations:

$$\delta K \cdot \overline{u} = \delta q - \overline{K} \cdot \delta u \qquad (4.1.4)$$

In ultimate limit state, assuming the variation of displacement (δu_i) to be zero at node i (where the structure fails), the equation (4.1.4) can be transformed into the following expression [3]:

$$\delta K \cdot \overline{u} = -\tilde{K} \cdot \delta \tilde{q} = - \begin{bmatrix} k_{1,1} & \cdots & k_{1,i-1} & -\Phi_1 & k_{1,i+1} & \cdots & k_{1,n} \\ \vdots & & \vdots & \vdots & \vdots & & \vdots \\ k_{i-1,1} & \cdots & k_{i-1,i-1} & -\Phi_{i-1} & k_{i-1,i+1} & \cdots & k_{i-1,n} \\ k_{i,1} & \cdots & k_{i,i-1} & -\Phi_i & k_{i,i+1} & \cdots & k_{i,n} \\ k_{i+1,1} & \cdots & k_{i+1,i-1} & -\Phi_{i+1} & k_{i+1,i+1} & \cdots & k_{i+1,n} \\ \vdots & & \vdots & \vdots & \vdots & & \vdots \\ k_{n,1} & \cdots & k_{n,i-1} & -\Phi_n & k_{n,i+1} & \cdots & k_{n,n} \end{bmatrix} \cdot \begin{bmatrix} \delta u_1 \\ \vdots \\ \delta u_{i-1} \\ \delta F \\ \delta u_{i+1} \\ \vdots \\ \delta u_n \end{bmatrix} \qquad (4.1.5)$$

Considering (4.1.5), the variation of load-intensity (δF) can be evaluated from:

$$\delta \tilde{q} = -\tilde{K}^{-1} \cdot \delta K \cdot \overline{u} \qquad (4.1.6)$$

4.2. Evaluation of covariance using stochastic finite element method

In (4.1.6) the variation of the load-intensity has been expressed, however, the variation of the stiffness matrix (δK) is still not known. The stochastic finite element method gives the possibility to expand K about its mean value via Taylor series [1], [4], [5]. Assuming that K is function of an α random variable, δK can be approximately expressed with the first order partial derivative of K as

$$\delta K = \frac{\partial K}{\partial \alpha} \delta \alpha \qquad (4.2.1)$$

where $\delta \alpha$ is the variation of α. It should be noted, that higher order partial derivatives have been neglected from (4.2.1). This approximation is reasonable if the variation of the stiffness matrix is less than about 15 per cent [5], [8]. Substituting (4.2.1) into (4.1.6) and forming the covariance matrix, we get:

$$C_{\tilde{q}} = \delta \tilde{q} \cdot \delta \tilde{q}^T = \tilde{K}^{-1} \cdot \frac{\partial K}{\partial \alpha} \cdot \overline{u} \cdot \delta \alpha \cdot C_p \cdot \delta \alpha^T \cdot \overline{u}^T \cdot \frac{\partial K^T}{\partial \alpha} \cdot \tilde{K}^{-T}$$

where $\delta \alpha$ includes the standard deviations of random variables and C_ρ is the correlation matrix. The correlation between different elements can be described by an exponentially decaying function of the distance between two elements and the length of correlation [3].

Using the method described previously, we are able to evaluate the mean value (F) and the standard deviation (δF) of the load-intensity. Since F was calculated in ultimate limit state, it can be interpreted as the value of the structural resistance at system level. If the distribution of resistance (R) is assumed to be normal, F and δF can be used to describe the distribution function:

$$P(\xi < x) = \frac{1}{\sqrt{2\pi} \cdot \delta F} \cdot \int_{-\infty}^{x} e^{-\frac{(t-F)^2}{2 \cdot \delta F^2}} dt \qquad (4.2.2)$$

According to expression (4.2.2) and Chapter 2., the safety index and the structural safety can be evaluated.

5. CONCLUSIONS

This paper presents a stochastic finite element technique that is capable of predicting the distribution of the structural resistance, and the safety of structure at system level. In this approach, the distributions of structural dimensions, material properties and the structural resistance were assumed to be normal. However, in reality these distributions are rather asymmetrical, such as Pearson III., Gumbel or Weibull distribution. Using these distributions for statistical evaluations, third-moment (skewness) analysis is also necessary. The finite element calculations mentioned in this paper can be also improved using more accurate 2D or 3D model to describe the behaviour of reinforced concrete.

6. REFERENCES

[1] Belytschko, T.; Liu, W.K.; Mani, A., "Random Field Finite Elements", *International Journal for Numerical Methods in Engineering*, Vol. 23, 1986, pp. 1831-1845.

[2] Bojtár I.; Gáspár Zs., "Tartók statikája IV. - A végeselem-módszer", *Egyetemi jegyzet*, Bp. 1993.

[3] Eibl, J.; Schmidt-Hurtienne, B., "Grundlagen für ein neues Sicherheitskonzept", *Bautechnik*, 72 (1995), Heft 8, pp. 501-506.

[4] Ghanem, R.G.; Spanos, P.D., "Stochastic Finite Elements: A Spectral Approach", *Springer-Verlag*, New York 1991.

[5] Handa, K.; Andersson, K., "Application of Finite Element Methods in the Statistical Analysis of Structures", *ICOSSAR '75 - 3rd International Conference on Structural Safety and Reliability*, 1975, pp. 409-417.

[6] Lucero-Cimas, H.N., "Zur Berechnung prismatischer Stahlbetonbalken mit verschiedenen Querschnittsformen für allgemeine Beanspruchungen", *Forschungs- und Seminarberichte aus dem Bereich der Mechanik der Universität Hannover*, Bericht-Nr. F90/1, April 1990.

[7] Mitchell, D; Collins, M. P., "Diagonal Compression Field Theory - A Rational Model for Structural Concrete in Pure Torsion", *ACI Journal*, Title No. 71-28., August 1974, pp. 396-408.

[8] Szalai K., "Vasbeton szerkezetek - Vasbeton szilárdságtan", *Tankönyvkiadó*, Budapest 1990.

PROPERTIES OF MICROCRACKS FORMED ON SURFACE OF CONCRETE AT STEAM CURING PERIOD

Minoru ABA
Graduate student of Civil Engineering
Tohoku Gakuin University
1-13-1, Chuo, Tagajo, 985, JAPAN

Koji OTSUKA
Professor of Civil Engineering
Tohoku Gakuin University
1-13-1, Chuo, Tagajo, 985, JAPAN

1. INTRODUCTION

Accelerated curing of concrete by atmospheric pressure steam is used extensively in the production of precast concrete structural members. However, sometimes micro cracks are formed on the surface of these concrete products. Such microcracks are difficult to detect by the naked eye and some defective concrete products may pass through the quality check. After the steam curing period, if concrete products suffer early drying, microcracks may grow much bigger. This will make for a lower durability of the precast concrete structure. However, there is no proper technique for detection of such microcracks, and relationships between these microcracks and the durability of concrete have not been investigated clearly.

The purpose of this investigation was to study the properties of microcracks formed on the surface of concrete at the steam curing period and at the early drying period. A new X-ray technique using a contrast medium was developed for this study to detect microcracks. Relationships between surface microcracks and durability of concrete were also studied by freeze-thaw resistance tests.

2. MATERIALS USED IN TESTS AND TESTING METHOD

2.1 Materials and specimens

The cement used was high-early-strength portland cement. The fine aggregate was a river product and the coarse aggregate was crushed stone. The mix proportions of the concrete were given in a water-cement ratio of 0.5, air content of 5 percent $\pm$ 1 as shown in Tab.1. The dimensions of specimen used were 100 $\times$ 100 $\times$ 400 mm as shown in Fig.1.

Tab.1 Mix proportions of concrete

Gmax	Slump	Air	W/C	s/a	Unite weight (kg/m³)				
(mm)	(cm)	(%)	(%)	(%)	Water	Cement	Fine aggregate	Coarse aggregate	AE
20	8±1	5	50	46	192	384	744	923	0.096

2.2 Steam curing conditions

Tab.2 shows the steam curing conditions that were used in the tests. Four types of different presteaming period were used.

Tab.2 Steam curing conditions

Series	Pre-steaming period* (hr)	Rate of temperature rise (C/hr)	Maximum temperature · period (C) · (hr)	Rate of cooling (C/hr)
1	6			3.1
2	4	12	55	4.0
3	2			4.9
4	0			5.8
5	Ordinary moist curing(O.M.C.)			-3

*Presteaming temperature : 20 C

The other conditions; the presteaming temperature, the rate of temperature rise, the maximum temperature and the rate of cooling, were each constant at 20 C, 12 C per hr, 55 C and -3 C per hr, in order to lessen, as much as possible, these influences. Besides, the ordinary moist curing (O.M.C.) condition was used for a comparison.

2.3 Detection of surface microcracks

After the curing period, the bottom 20 mm of the specimen were removed using a diamond saw, and the surface microcracks formed in the curing period were detected. And a X-ray technique using a contrast medium was used to detect the surface microcracks. The contrast medium was permeated into the microcracks formed on the surface of the concrete. The X-ray inspection was made, and microcracks were detected by a sharkasten (film viewing device) from X-ray shadowgraph film. The total length of the cracks were measured by the curvimeter on traced cracks, and the density of crack length was calculated as the total length of cracks divided by the traced area.
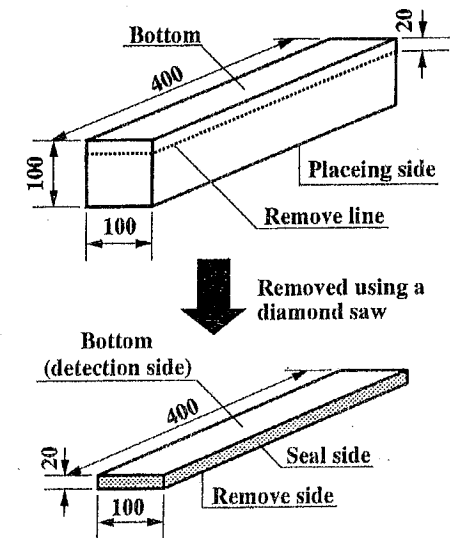
Fig.1 Shape and dimensions of specimen (mm)

Then, as shown in Fig.1, all the surfaces of the specimen, except the bottom (detection side of the microcracks) were sealed with epoxy resins. The specimens were placed in a climate room for 91 days at 50 percent relative humidity and 20 C to replicate the early drying period. During the early drying period, X-ray inspection was made at 3, 7, 14, 21, 28, 56 and 91 days.

2.4 Test for resistance to freezing and thawing

The test was conducted in accordance with ASTM-C666 A (a method of rapid freezing and thawing in water). However, all the surfaces of the specimen, except the bottom were sealed with epoxy resins in order to allow deterioration only from the bottom side. Change in the dynamic modulus of elasticity during freezing and thawing regime was measured every 30 cycles up to the 300th cycle. The dried specimen was submerged in water for 1 week after the early drying period. It was then sealed and the test was started.

3. EXPERIMENTAL RESULTS

3.1 Properties of surface microcracks

3.1.1 Types of surface microcracks

Fig.2 shows an example of the cracks traced from an X-ray film, obtained by an X-ray technique using a contrast medium, at the end of the steam curing period. It can be seen from this figure that at the end of the steam curing period there were many microcracks on the surface of the concrete. On closer investigation, surface microcracks could be

classified into three types, separation cracks between aggregate and paste, mortar cracks and vapor cracks. In the following, enlarged shadowgraphs of these cracks shown on the X-ray film are presented.
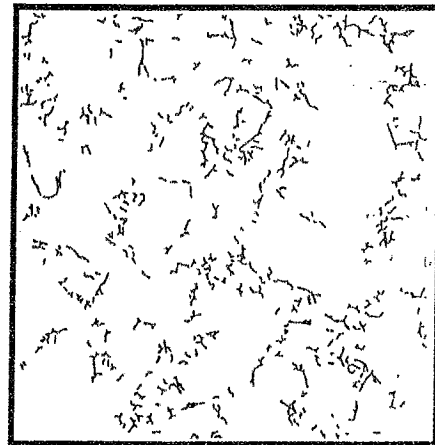
Fig.2 Microcracks traced from X-ray film

Photo.1 Separation cracks between aggregate and paste

Photo.2 Mortar cracks
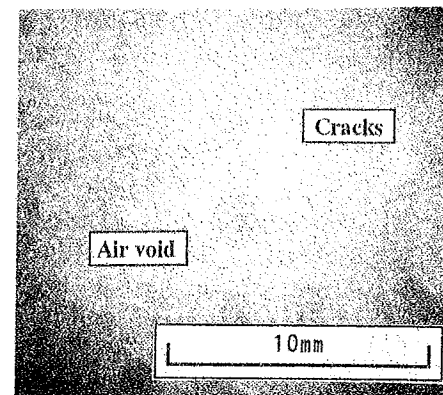
Photo.3 Vapor cracks

Photo.1 shows an enlarged shadowgraph of separation cracks between aggregate and paste. In the photograph, the arcshaped white line around the aggregate is the separation crack where the contrast medium permeated into chinks between the aggregate and the paste.

Photo.2 shows an enlarged shadowgraph of mortar cracks. The gray part in the center is an aggregate, the white curve around the aggregate is the separation crack, and the cloudy parts around the separated aggregate are considered groups of many microcracks formed in the mortar.

Photo.3 shows an enlarged shadowgraph of vapor cracks. The spherical part in the center is an air void, and the radial white lines starting from the air void are the vapor cracks.

3.1.2 Influence of steam curing conditions

Fig.3 shows the density of surface microcrack length formed in the curing period for different curing conditions. It can be seen that the shorter presteaming period tended to form more microcracks. In the case of the presteaming period of 0 hr, relatively many mortar cracks in addition to separation cracks were detected, and a few vapor cracks were also detected. In the case of the presteaming period of 6 hr, almost all of the cracks detected were separation cracks. These microcracks were observed by SEM and the widths were between 0.01 and 0.03 mm.

3.1.3 Influence of early drying period after steam curing period

Fig.4 shows changes in the density of surface microcrack length during the early drying period. It can be seen from this figure that the densities of surface microcrack length rapidly increased during the first month of the early drying period. After 1 month, the rates of increase slowed. Further, in the case of the steam curing, the rate of increase of microcracks was much greater than that in the case of the ordinary moist curing. In the case of the microcracks formed during the early drying period, both separation cracks and mortar cracks were detected. These microcracks were observed by SEM and the widths were between 0.05 and 0.1 mm, which were bigger than that at the end of the steam curing period.

3.2 Relationship between surface microcracks and freeze-thaw resistance

3.2.1 Influence of steam curing conditions

Fig.5 shows the results of the freeze-thaw resistance tests at the end of the steam curing
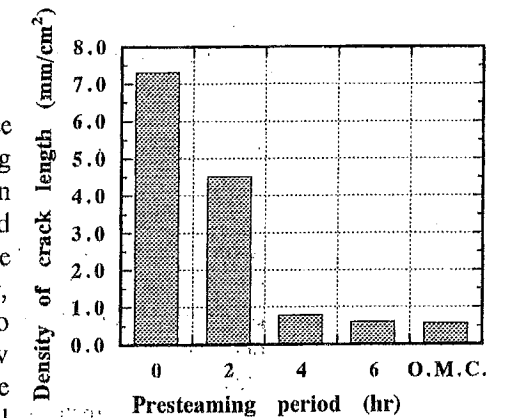
Fig.3 Density of crack length for different curing conditions
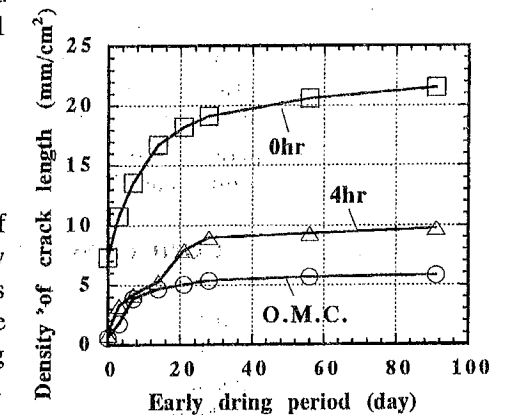
Fig.4 Relationship between early drying period and density of crack length
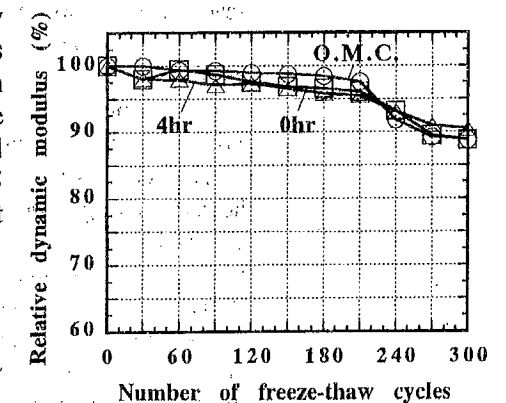
Fig.5 Results of freeze-thaw resistance tests at end of steam curing period

period. In the all cases, the differences in changes in the relative dynamic modulus of elasticity are small. From this result, the surface microcracks formed during the steam curing period had a small influence on the freeze-thaw resistance of the concrete. It is considered that the reason for small influence is that the widths of the surface microcracks formed at the curing period were exceedingly small.

3.2.2 Influence of early drying period after steam curing period

Fig. 6 shows the results of the freeze-thaw resistance tests at the end of the early drying period of 1 month. In the case of the presteaming period of 0 hr, the rate of decrease of the relative dynamic modulus of elasticity was much greater than that in the case of the presteaming period of 4 hr. From this result, the surface microcracks increased during the early drying period had a big influence on the freeze-thaw resistance of the concrete. It is considered that the reason for big influence is that the surface microcracks formed in the steam curing period, suffered early drying and the widths grown much bigger.
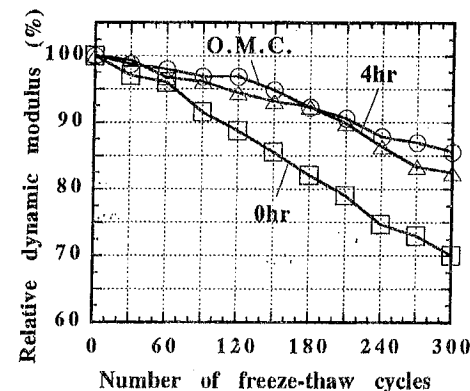
Fig.6 Results of freeze-thaw resistance tests at end of early drying period of 1 month

4. CONCLUSIONS

Experiments were carried out by X-ray technique using a contrast medium to detect the surface microcracks formed at the steam curing period and at the early drying period. Relationships between surface microcracks and durability of concrete were also studied by the freeze-thaw resistance tests. The following conclusions can be drawn.

(1) Using a X-ray technique with contrast medium, the surface microcracks formed at the steam curing period could be detected. The surface microcracks could be classified into three types, separation cracks between aggregate and paste, mortar cracks and vapor cracks.
(2) The Shorter presteaming period tended to form more microcracks. In case of the shorter presteaming period relatively many mortar cracks were detected.
(3) The densities of surface microcrack length rapidly increased during the first month of the early drying period. After the 1 month, the rates of increase slowed. Further, in the case of the steam curing, the rate of increase of microcracks was much greater than that in the case of the ordinary moist curing.
(4) The surface microcracks formed during the steam curing period had a small influence on the freeze-thaw resistance of concrete. However, such surface microcracks suffered early drying and the widths grown much bigger. This made for a lower freeze-thaw resistance of the concrete.

REFERENCES
[1]Otsuka K., Shoya M., Koseki K. and Aba M., "Properties of microcracks formed on surface of concrete at steam curing period", *Proceedings of JSCE*, No.520/V-28, pp.143-155, 1995.8

LARGE-SCALE TESTS ON STRUCTURAL CONCRETE GIRDERS UNDER SHEAR AND NORMAL FORCES

Walter Kaufmann
Institute of Structural Engineering, ETH Zürich
CH-8093 Zürich, Switzerland

1 INTRODUCTION

1.1 General considerations

Truss models with variable inclination of the concrete diagonals and related stress field approaches are common tools in the shear design of structural concrete girders with transverse reinforcement [CEB-FIP (1990)]. These approaches are based on a sound physical basis through the theory of plasticity. In order to achieve the ultimate loads predicted by these models, sufficient ductility of the stirrups has to be provided and an appropriate value of the effective compressive concrete strength must be used.

Test results related to the effective compressive concrete strength as well as the ductility of stirrups are however scarce, especially for flat inclinations of the concrete compressive struts at failure. Codes therefore usually provide limitations of the inclinations of the struts and a seemingly low value for the effective compressive concrete strength in order to prevent web crushing failures.

Investigations on the behaviour of wall elements [Collins (1979)] show that the effective concrete compressive strength depends on various parameters and that it may be reduced to values well below usual code assumptions if large strains perpendicular to the principal compressive direction occur, which has to be expected for flat inclinations of the concrete compressive struts at failure. In these cases, even failures due to rupture of the stirrups cannot be excluded since bond stresses for small, vertical bars are in fact much higher than predicted by common design formulas.

In the structural assessment of existing structures which have been designed according to empirical design formulas of older codes, the above mentioned limitations of the inclination of the concrete compressive struts often constitute a severe restriction which inhibits a successful verification of the load bearing capacity in shear. Many of these structures are heavily posttensioned with only slightly curved tendons which therefore contribute only a small part to the shear resistance. By using a flatter inclination of the concrete compressive struts the load bearing capacity could often be demonstrated considering the fact that the strong posttensioning usually provides substantial reserves in the longitudinal reinforcement.

1.2 Objective of the experiments

The goal of the tests described in this contribution was to investigate the behaviour (ultimate loads, deformations) of webs of structural concrete girders with low shear reinforcement ratios and correspondingly flat inclinations of the concrete compressive struts at failure.
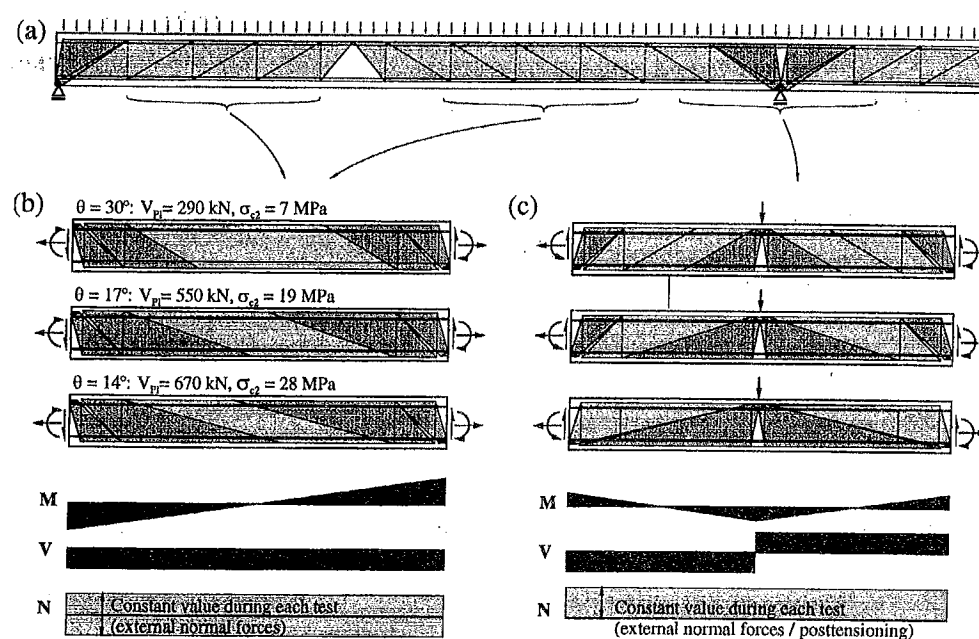
Fig. 1: (a) Continuous girder and assumed stress-fields; (b) and (c) development of stress-fields for increasing load, corresponding to test series VN and MVN, respectively.

In the shear design of girders by means of stress-fields [Sigrist, Alvarez and Kaufmann (1995)], two generally different cases can be distinguished [Fig. 1]. On one hand, outside the support regions there are continuous stress-fields in the web [Fig. 1(b)], i.e. parallel bands of inclined concrete compressive bands and vertical tension-bands (stirrups); for usual situations no plastic deformations of the chords will occur until failure. On the other hand, at the supports there are fans [Fig. 1(c)], i.e. discontinuous stress-fields consisting of radiating concrete compressive struts transferring the shear forces to the nodal zone at the support; large plastic deformations of the tension chord will occur especially at intermediate supports of continuous girders designed by limit analysis.

These two cases have been studied in test series VN and MVN, respectively. Of the various parameters influencing the behaviour of webs of structural concrete girders, the following have been investigated in detail:

- Normal forces (required re-orientation of the inclination of the compressive struts from cracking until failure);

- Pre-existing, vertical cracks in the web caused by preceding loading in tension (restraints);

- Plastic deformations of the tension chord in the support region;

- Posttensioning and differences between posttensioning and externally applied normal forces.

In all tests the behaviour of the girders under monotonically increasing load until failure was investigated. Forces acting on the specimen, deformations, average strains and crack widths were measured and continuously recorded.

2 EXPERIMENTS

2.1 Beam Element Tester

The experiments have been carried out using a novel testing facility called "Beam Element Tester" (BET). Since the BET has been designed by the author and was used for the first time in these tests, some details of the facility are given below.

The basic idea of the BET is to investigate elements of beams rather than entire girders. In this way realistic cross-sections can be treated while the total element size remains within reasonable limits for fabrication and transportation.

The facility [Fig. 2] consists of two reaction frames, two connectors transferring the applied loads to the element and a varying number of jacks and reaction struts depending on the test type. Element sizes of up to 6 m length and 0.8 x 0.8 m in cross-section can be tested. Two horizontal 2.5 MN jacks acting on the connector in a distance of 1.20 m allow to subject the element ends to up to 5 MN in tension/compression, 3 MN in bending or any combination in between. These capacities allow to overcome the resistances of even heavily reinforced elements already at their ends; failures should however always occur in the central portion of the elements in order to get reliable results. Shear forces are introduced through the vertical jack and are limited to 1 MN in the configuration of Fig. 2. Together with additional jacks acting in the span of the element, almost any desired combination of in-plane loads can be generated.

Tensile forces are introduced at the element ends through longitudinal reinforcement welded to T-shaped blocks which in turn are fixed to the connectors with high-strength bolts. In this way, up to 5 MN of tension may be introduced in a flange of 0.8 x 0.15 m.
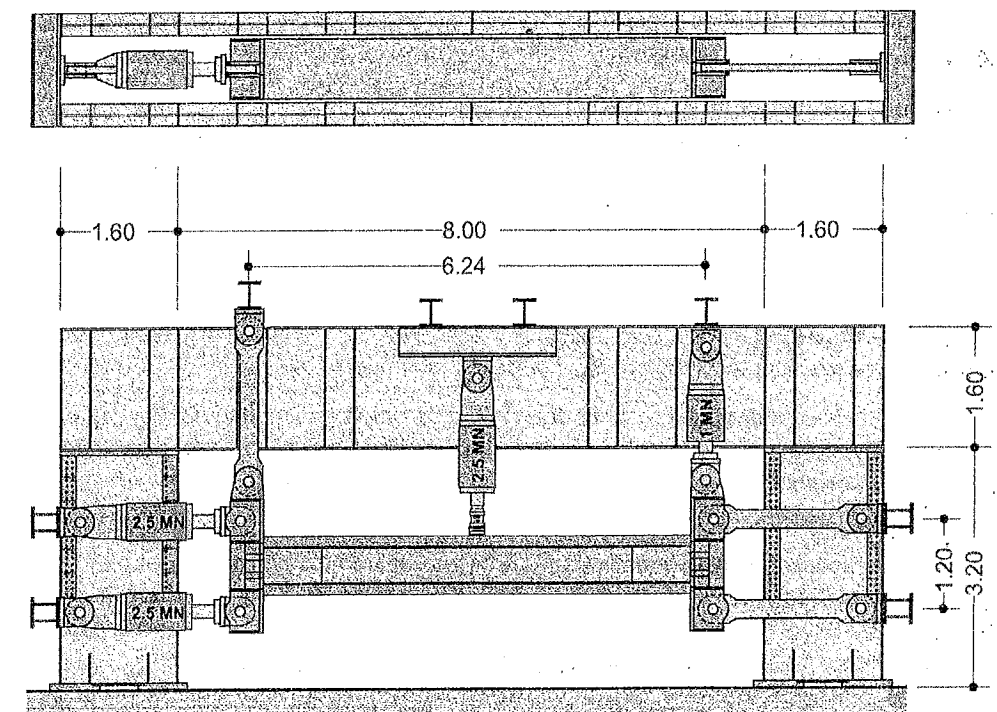
Fig. 2: Beam Element Tester (BET), plan and elevation (jack at midspan used for test series MVN only; dimensions [m]).

2.2 Specimen geometry and material properties

The geometry of the specimens was identical for both test series. The elements measured 5.84 m in length, 0.78 m in height and were of I-shaped cross-section. Top and bottom flanges were 0.80 m wide and 0.14 m high; web thickness was 0.15 m in the central portion of the elements. In order to prevent failures at the element ends, the web was thickened to 0.45 m in the end-regions and additional vertical reinforcement was provided.

The shear reinforcement in the central portion of all specimens consisted of vertical, closed stirrups $\emptyset 8$ @ 200 mm corresponding to a geometrical shear reinforcement ratio of $\rho_w = 0.34$ %. The stirrups as well as the longitudinal reinforcement were made from standard deformed bars with an average yield strength of about 520 MPa, Young's Modulus of 208 GPa and an ultimate strain of 5-8 % for the stirrups and 12-15 % for the longitudinal bars. The average concrete compressive strength for both test series was $f_c' = 57$ MPa and $f_{cc} = 68$ MPa for the cylinders and the cubes tested, respectively.

2.3 Test Series VN

The four specimens of series VN were monotonically loaded in shear until failure, with zero moment at midspan as shown in Fig. 1(b). The longitudinal reinforcement was identical for all specimens and designed to remain elastic during the test.

Before the actual test, specimen VN1 was subjected to all combinations of maximum normal forces and moments (with V=0) produceable by the *BET*, which resulted in vertical cracks over the entire specimen height at a distance of 200 mm (stirrup spacing). Specimens VN3 and VN4 were subjected to axial tension and compression of 1.00 MN, respectively, before being loaded in shear; the axial force was then held constant during the test.

2.4 Test Series MVN

The four specimens of series MVN were also monotonically loaded in shear until failure, but in contrast to series VN an additional vertical jack was provided at midspan. The loading procedure [Fig. 1(c)] simulated the behaviour of an (inverted) intermediate support of a continuous girder designed by limit analysis. In the first phase of the test, horizontal forces were controlled such that moments at the element ends were zero. In the second phase, after reaching the yield moment at midspan, rotations of both element ends were prevented and moments arising from the increasing force at midspan were thereafter primarily taken at the element ends. Vertical forces were continuously adjusted such that moments at both ends of the element were equal throughout the test.

MVN1 to 3 were designed to reach the yield moment at midspan under the same net web shear (i.e. total shear - contribution of the inclined posttensioning cable, see below); MVN4 was designed not to yield at midspan during the entire test.

Specimens MVN2 and MVN4 were subjected to axial compression of 1.30 MN before being loaded in shear and the axial force was again held constant during the test. Specimens MVN3 and MVN4 were posttensioned with a bonded VSL 6-7 cable ($P_u = 1.85$ MN) tensioned to an initial force of 1.30 MN and anchored on the backside of the connectors of the *BET*. The cables were directed straight downward from the element ends until midspan where they were deviated with the minimum allowable radius of curvature.
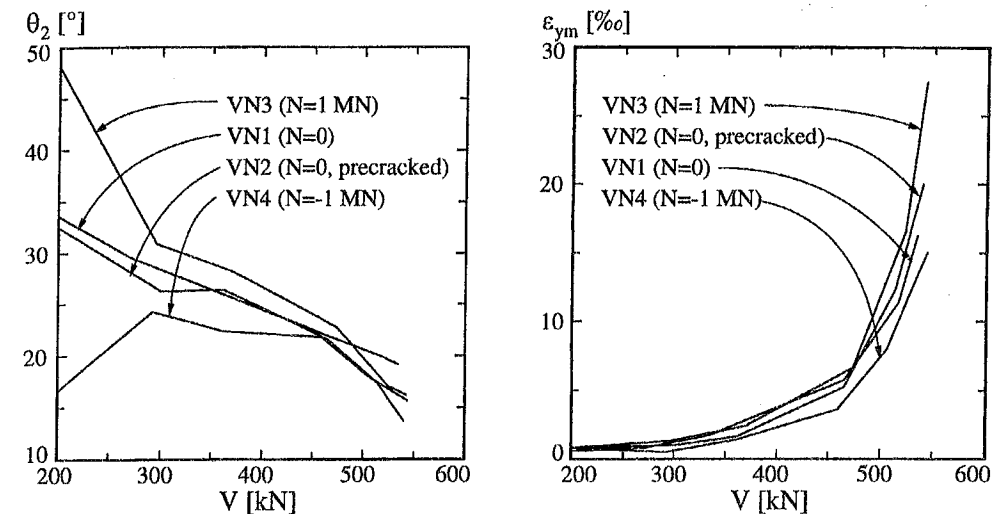
Fig. 3: Principal compressive strain directions and average vertical strains measured in the central portion of the specimens, test series VN.

3 PRELIMINARY RESULTS

The tests have shown that the *BET* enables tests on elements instead of entire girders, even when relatively high forces have to be applied to the element ends. No specimen failed within the end regions, even in series VN where the maximum loads occurred at the element ends.

Test results of both series indicate that, as predicted by stress-field solutions, longitudinal forces, pre-existing cracks and yielding of the tension-chord reinforcement only slightly influence the shear resistance of girders with appropriately designed chords. For example [Fig. 3], all specimens of series VN reached about the same ultimate loads and measured principal strain directions were very similar after cracking. The major influence of normal forces observed was that principal tensile strains at the same shear load significantly increase with applied axial tension and decrease with axial compression arising from external forces or prestressing. In cases without axial compression the resulting large vertical tensile strains may therefore lead to premature failures due to breaking of the stirrups rather than crushing of the web concrete as predicted by the theory of plasticity. Such failures are much less critical if axial compression is provided by either external normal forces or prestressing. A detailed presentation of the test results will be published in a test report [Kaufmann and Marti (1996)].

REFERENCES

CEB-FIP (1990). CEB-FIP Model-Code for Concrete Structures. Comité Euro-International du Béton, Bulletin d'Information No. 213/214, Lausanne, May 1993, 437 pp.

Collins, M.P. (1979). "Stress-Strain Characteristics of Diagonally Cracked Concrete", *Final Report*, IABSE Colloquium Copenhagen 1979, pp. 27-34.

Kaufmann, W. and Marti, P. (1996). Test report, to be published in 1996.

Sigrist, V., Alvarez, M. and Kaufmann, W. (1995). "Shear and Flexure in Reinforced Concrete Beams", *Bulletin d'Information No. 223*, Comité Euro-International du Béton, Lausanne, June 1995, pp. 7-49.

LARGE-SCALE TENSION TESTS ON WALL ELEMENTS

Manuel Alvarez
ETH Zurich, Institute of Structural Engineering
8093 Zurich, Switzerland

1. INTRODUCTION

The bearing capacity of reinforced concrete structures is usually determined using limit analysis methods based on the theory of plasticity. The application of this theory requires that the plastically deformed regions of the structure possess a sufficient deformation capacity. In fact the ultimate state can only be attained if a premature failure due to any critical deformations is excluded by providing an adequate ductility of all structural components. When using design methods based on the theory of plasticity, a verification of the compatibility of deformations is often neglected. The deformation capacity required for the redistribution of internal forces has then to be ensured by considering general design rules. In some cases however a strict verification of the deformation capacity of the structure is unavoidable to justify the chosen state of equilibrium.

The deformation capacity of reinforced concrete structures is governed by the material ductility of concrete and steel, the structural ductility of the composite elements and by characteristic geometrical dimensions of the statical system such as slenderness and shape of cross-sections. In structures subjected to bending failure occurs at locations where so-called plastic hinges develop during the loading process. The rotation capacity of these regions depends on the elongation capacity of the tension chord and on the admissible strains in the compression zone and in the web. The amount of plastic rotation in the hinge region is mainly due to the elongation of the tension chord. The deformation behaviour of the tension chord can be described by a constitutive law which strongly depends on the mechanical properties of the reinforcing steel and the bond behaviour between concrete and steel bars.

In structural elements subjected to tension the ductility of reinforcing bars is restricted by the so-called tension stiffening effect. The tension stiffening is due to bond between concrete and steel bars which causes a variation of the steel stresses and strains between maximum values at the cracks and minimum values between two cracks. The average value of the steel strains between two cracks is therefore only a portion of the maximum steel strain at the crack. The ratio of these two values quantifies the restraint action caused by the tension stiffening effect. This restraint action increases in the post-yield range of the reinforcing steel, since the decrease of steel strains starting from a crack is much more pronounced than in the elastic range. This is due to the fact that the low strain-hardening modulus of the reinforcing steel demands for a higher gradient of steel strains in order to satisfy the equilibrium and compatibility conditions of the bonded steel bar. As a consequence, the plastic strains of steel are concentrated in relatively narrow areas around the cracks and the average value of steel strains is only a small portion of the maximum plastic steel strain. However, this increase of the tension stiffening effect in the post-yield range of steel is mitigated by the gradual deterioration of bond conditions [4].

2. RESEARCH SIGNIFICANCE

Load tests in pure tension allow for a direct experimental determination of the relation between average steel strains and maximum steel stresses in cracked structural elements. This constitutive law in tension is an important basis for any calculation of deformations of reinforced concrete structures. The large-scale tension tests presented in this contribution aimed at investigating some main influences on the elongation behaviour and capacity of tensile structural elements:

- mechanical properties of the reinforcing steel and in particular the shape of the strain-hardening branch of its constitutive law,
- reinforcement ratio,
- prestressing,
- transverse reinforcement,
- strength of concrete.

In addition to the large-scale tension tests a series of pull-out tests were performed to determine the bond characteristics of the reinforcing bars. The resulting bond laws may be used to predict the tension stiffening effect by means of analytical or numerical models.

3. EXPERIMENTS

The test series consisted of nine large-scale tension tests on reinforced as well as prestressed wall elements and of 21 pull-out tests on concrete cubes. The reinforcement consisted of steel bars Ø 14 mm of three different ductility classes (H, N, L) and post-tensioning cables VSL 6-7 (1850 kN at ultimate) in plastic ducts. The ductility properties of reinforcing steel are usually quantified by the ratio of ultimate and yield stress (f_{su}/f_{sy}) as well as the ultimate strain ε_{su}. Figs. 1 (a) and (b) show the conception of the tests and Tabs. 1 and 2 contain the parameters chosen in the tests. The ratios of longitudinal reinforcement in the wall elements varied from 1 % in the specimens Z1 through Z6 to 0.7 % in specimens Z7 and Z8 and 2 % in specimen Z9. In the pull-out tests, centric and eccentric pull-out with different concrete covers of the bars were investigated as well as the influence of plastic deformations of the bar on the bond law.

4. EXPERIMENTAL RESULTS

Fig. 2 (a) shows the stress-strain diagrams of the reinforcement and Fig. 2 (b) the constitutive law of the structural wall elements Z1, Z3, Z4 and Z8 up to failure. Note that the specimen reinforced with steel of ductility class H reached an elongation at ultimate of about 6 % while specimen Z4, reinforced with steel N, failed at an elongation of approximately 0.6 %. Therefore, ratios $(\varepsilon_{sm}/\varepsilon_{smax})$ at ultimate of about 0.5 and 0.2 are to be expected for reinforcing steel of ductility class H and N, respectively. A detailed presentation of the test results will be published in a test report [1].
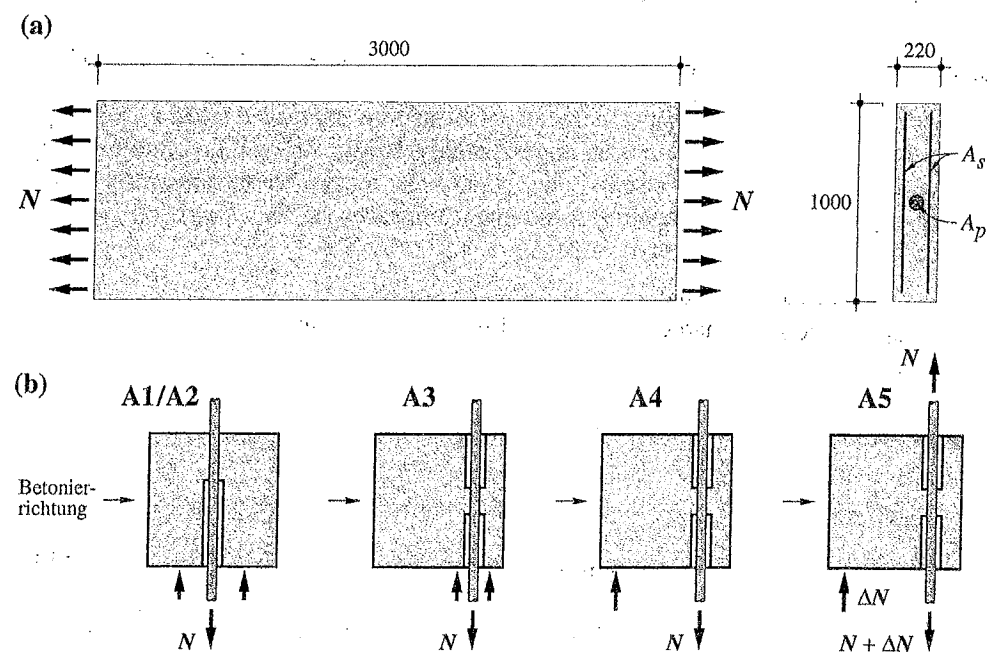
Fig. 1 – Conception of (a) tension tests and (b) pull-out tests, [mm].

Specimen	Z1	Z2	Z3	Z4	Z5	Z6	Z7	Z8	Z9
Longitudinal reinforcement $A_s = n \cdot A_{s(\varnothing 14)}$ [mm²]			2156			1232	616	1540	4312
Prestressed reinforcement A_p [mm²]			0				1050		0
Ductility class of reinforcing steel		H		N	L		H		
Transverse reinforcement	Ø 8 @ 200	0				Ø 8 @ 200			
Concrete cube strength f_{cw} [MPa]	50	90				50			

Tab. 1 – Test program for the tension tests.

Series	A1	A2	A3	A4	A5
Type of test	centric pull-out			eccentric pull-out	
Concrete cover [mm]	93			38	
Plastic steel strain at begin of pull-out [‰]	0				20
Concrete cube strength f_{cw} [MPa]	50	90		50	
Ductility class of reinforcing steel	H/N/L		H		

Tab. 2 – Test program for the pull-out tests.
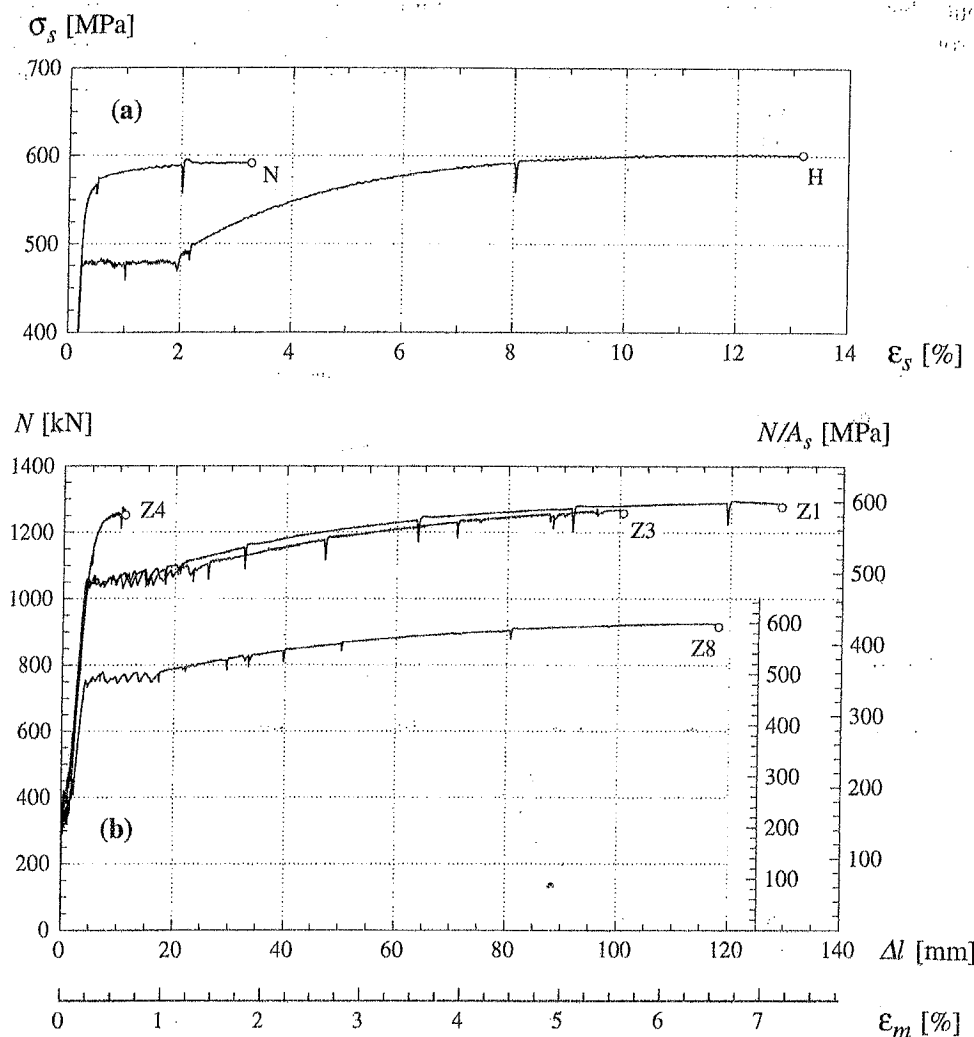
Fig. 2 – (a) Stress-strain diagrams of reinforcing steel; (b) Force-elongation diagrams for specimens Z1, Z3, Z4, Z8.

5. CONCLUSIONS

The large-scale tests on wall elements presented in this paper allowed for an experimental determination of the constitutive law of structural concrete in tension up to failure. These constitutive law demonstrates the restraint of the elongation capacity of the naked steel bars due to bond action. The influence of tension stiffening on the elongation capacity of structural elements was shown to be particularly pronounced when using steel reinforcement with poor ductility properties. This fact can be explained by considering both that a lower strain-hardening modulus (equivalent to a smaller ratio (f_{su}/f_{sy})) causes a more pronounced localization of plastic steel strains near the cracks and that a large ultimate steel strain ε_{su} along with the deterioration of bond conditions would be needed to gradually reduce this localization. As a main result it must be pointed

out that the elongation capacity of a structural element diminishes more than proportionally with a decrease of the ultimate steel strain ε_{su} assuming that the ratio (f_{su}/f_{sy}) and the bond conditions remain the same. In cases where a substantial deformation capacity is required to allow for the redistribution of forces needed to reach the assumed design ultimate state, minimum requirements for the steel ductility are necessary to supply the required deformation capacity.

Notation

A_s	cross-section of reinforcing steel	δ	bond slip
A_p	cross-section of prestressed steel	ε_m	average strain
f_{su}	ultimate steel stress	ε_m	steel strain
f_{sy}	yield steel stress	ε_{su}	ultimate strain of reinforcing steel
f_{cw}	concrete cube strength	σ_s	steel stress
N	normal force	τ_b	bond stress
Δl	elongation	ρ	geometrical reinforcement ratio

References

[1] Alvarez, M., and Marti, P., test report, to be published in summer 1996.

[2] Eligehausen, R., Popov, E.P., and Bertero, V.V., "Local Bond Stress-Slip Relationships of Deformed Bars under Generalized Excitations", *Report No. UCB/EERC-83/23*, Earthquake Engineering Research Center, University of California, Berkeley 1983, 162 pp.

[3] Rehm, G., *Über die Grundlagen des Verbundes zwischen Stahl und Beton*, Deutscher Ausschuss für Stahlbeton, Heft 138, Verlag von Wilhelm Ernst & Sohn, Berlin 1961, 59 pp.

[4] Shima, H., Chou, L., and Okamura, H., Micro and Macro Models for Bond in Reinforced Concrete, Journal of the Faculty of Engineering, University of Tokyo, Vol. 39, No.2, pp. 133-194, 1987.

EARTHQUAKE RESISTANT DESIGN OF TALL BUILDINGS BY THE CONTINUUM METHOD

András Köpecsiri
Technical University of Budapest
Dept. of Reinforced Concrete Structures
H-1521 Budapest, Hungary

Abstract

High-rise buildings are investigated for earthquake using the continuum method. A replacement Timoshenko-beam is analysed using the Response Modal Analysis with Mode Superposition. A model is presented which enables the designer to determine easily and quickly the base shear, the overturning moment, the top displacement and the maximum inter-story drift ratio of tall buildings subjected to earthquake.

1. INTRODUCTION

The analysis of high-rise building structures for earthquake requires extensive numerical calculations, even at the beginning of the design procedure. These "exact" calculations do not show directly the effect of the different geometrical and material properties on the behaviour of the structure under seismic loads.

Structure   Replacement beam

Ground motion   Ground motion
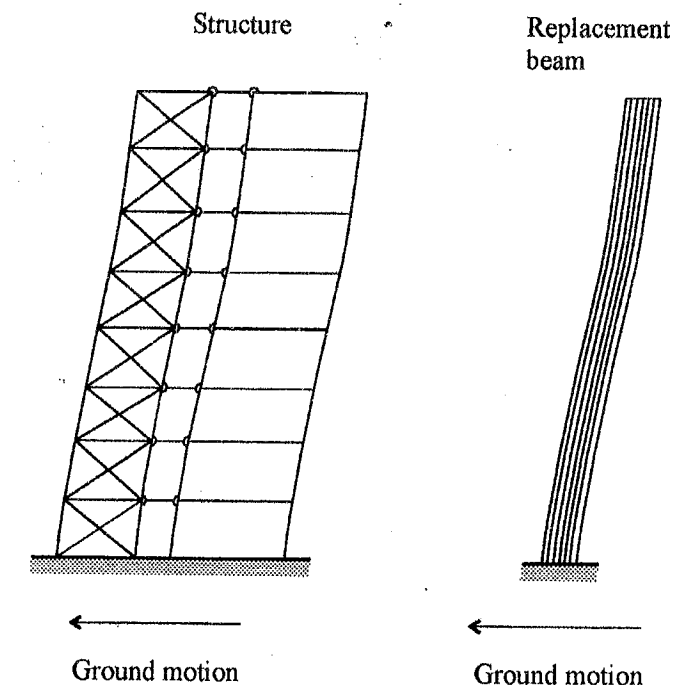
Fig. 1 Response of the original structure and the replacement column to ground motion

To overcome these shortcomings, approximate calculations were proposed in the past [1, 2, 3]. One of the best candidates for a quick approximate calculation is the continuum method. The basic idea is that the real structure, containing different discrete elements e.g. beams, columns, walls, etc. is replaced by a continuous column. The overall behaviour of the original structure has to be the same as that of the replacement column. This is illustrated in Fig. 1, where both the original discrete structure and the replacement column are subjected to the same ground motion. The horizontal displacement of the two structures must be the same, however the local behaviour (e. g. the slope of the columns) can be different.

The replacement continuum was determined by several authors for uniformly distributed horizontal load [4, 5, 6, 7, 8], seismic load [3, 9, 10] or for the stability analysis under vertical loads [11, 12, 13]. To achieve a good accuracy the replacement column has to be more general than the classical beam having flexural deformations only. (In the following the replacement bar will be referred as "beam", and not as column). Many authors [9, 14, 15] proposed a *"sandwich bar with thick faces"* as a replacement continuum.

A sandwich beam (see Fig. 2) contains three different layers: two face sheets and a core in between. The faces are more rigid than the core. The sandwich is characterised by three stiffnesses, the global bending stiffness $\left(B_g\right)$, which is due to the compressibility of the faces, the local bending stiffness $\left(B_l\right)$, which is due to the bending of the faces and the shear stiffness (S). The basic idea is that the individual beams or braces between the columns are "smeared" through the height of the building.

$$B_g = \frac{btd^2}{2}E$$

$$B_l = \frac{bt^3}{6}E$$

$$S = bdG$$
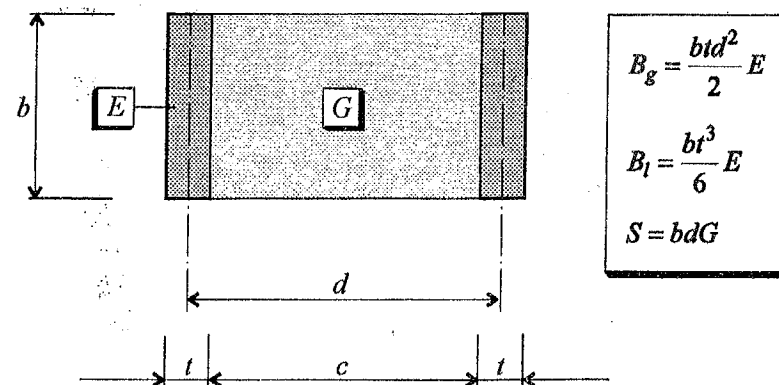
Fig. 2 Cross section of a sandwich beam.
The Young modulus of the face sheets is denoted by E,
the shear modulus of the core is denoted by G.

The calculation of the replacement stiffnesses from the properties of the structure is given in [3, 13]. Because of the relative difficulties in the analysis of the above mentioned sandwich beam with thick faces simplified models were also suggested [8, 10].

For wide rigid frames the global stiffness can be assumed to be infinite, $B_g = \infty$. In this case we obtain the columns supported by a "shear type" foundation.

For narrow building structures the global bending stiffness could be negligible, $B_l = 0$, while B_g plays an important role. In this case we obtain a Timoshenko-beam i.e. a beam having flexural and shear deformation with the stiffnesses B_g and S.

Stafford Smith [16] worked out an approximate, simple solution for the sandwich bar with thick faces. In his paper design charts are also presented to determine the first two periods of vibration and the seismic base shear forces. However, his solution is not applicable for the analysis of rigid frame and braced frame structures.

Several authors investigated the Csonka-beam. Basu [17] and Kollár [10] also presented design charts to get quick answers.

Neither Stafford Smith's solution nor the analysis based on the Csonka-beam are applicable for the analysis of narrow buildings which are common structures in practice. The Timoshenko-beam is a good candidate for the analysis of these structures. However, no analysis seems to be available on the basis of a replacement Timoshenko-beam.

2. PROBLEM STATEMENT

We consider high-rise buildings having a symmetrical stiffening system. The members of the shear walls, rigid frames and braced frames are assumed to be the same at each level, hence the individual levels have the same stiffness characteristics. The mass of the floors are also assumed to be identical through the height of the building.

Our aim is to give a quick approximate analysis for the design of the elements of the building for earthquake loads.

3. METHOD OF SOLUTION

In the analysis we assume that the elements of the building behave in a linearly elastic manner, no plastic deformations or energy dissipation occur. Because of the symmetry of the building only in-plane motions are considered, the torsional motions are negligible.

The high-rise building is replaced by a continuum, by a Timoshenko-beam, having flexural $\left(B_g\right)$ and shear (S) stiffness. The calculation of these stiffnesses are given by Stafford Smith [3] and Hegedűs and Kollár [13].

Building code prescriptions (e.g. UBC, DIN, EUROCODE, HUNGARIAN STANDARD, etc.) are determining the loads on a building using the Response Modal Analysis with Mode Superposition [18, 19]. Due to this method the horizontal forces acting on the building depend on the period of free vibration and on the mode shape functions.

Knowing the distribution of the horizontal seismic forces $\left(F(x)\right)$, the displacements and internal forces can be calculated performing a simple static analysis of the building.

The free vibration of the Timoshenko-beam was investigated by Köpecsiri and Kollár [20] and a computer code and design charts were also developed to analyse high-rise buildings subjected to earthquake.

4. NUMERICAL EXAMPLE

Rigid frame. Stafford Smith [22] investigated a 20-story rigid frame structure for uniformly distributed load. The same structure will be investigated for earthquake in the following. The geometrical and material characteristics of the frame are given in Table 1 and Fig. 3. Both "exact" and the approximate method based on the Timoshenko-beam were considered in analysing the structure. The exact calculation was carried out using the ETABS code [21].

Table 1 Geometrical and material characteristics of the rigid frame

Number of stories = 20
Total height, $H = 61$m
Story height, $h = 3.05$m
Clear span of openings: $L_1 = 5.49$m,
$L_2 = 4.88$m, $L_3 = 4.27$m.
Weight/unit height: $mg=588.6$kN/m.
Modulus of elasticity:
$E=2.780 \times 10^7$ kN/m^2.
Area of columns:
$A_{c1} = A_{c2} = 0.182$m^2,
$A_{c3} = A_{c4} = 0.208$ m^2.
Area of beams:
$A_{b1} = A_{b2} = 0.178$m^2, $A_{b3} = 0.2$m^2.
Moment of inertia of columns:
$I_{c1} = I_{c2} = 0.277$m^4,
$I_{c3} = I_{c4} = 0.413$ m^4.
Moment of inertia of beams:
$I_{b1} = I_{b2} = 0.354$m^4, $I_{b3} = 0.505$m^4.
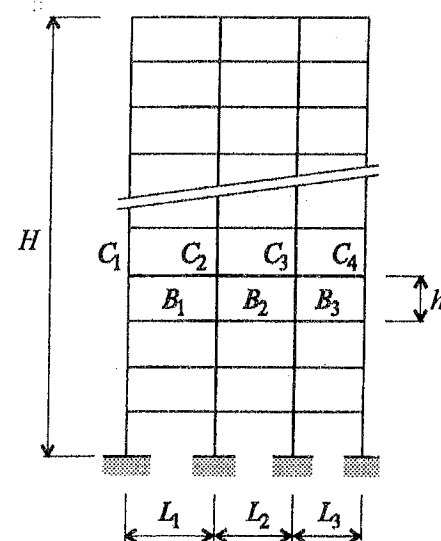
Fig. 3 Rigid frame example. Stafford Smith [22]

The results and the relative differences are summarised in Table 2. The differences are always under 5%.

The effect of the total height of the building was investigated in Fig. 4a and b. Three sets of data are shown : results produced by ETABS, by the present method (Timoshenko-beam) and by Kollár [10] (Csonka-beam). In this case Stafford Smith's solution [16] is applicable only under 7 stories. The comparison of results shows that the Timoshenko-beam gives quite accurate results above 10 stories while the Csonka-beam is inaccurate in the same region.
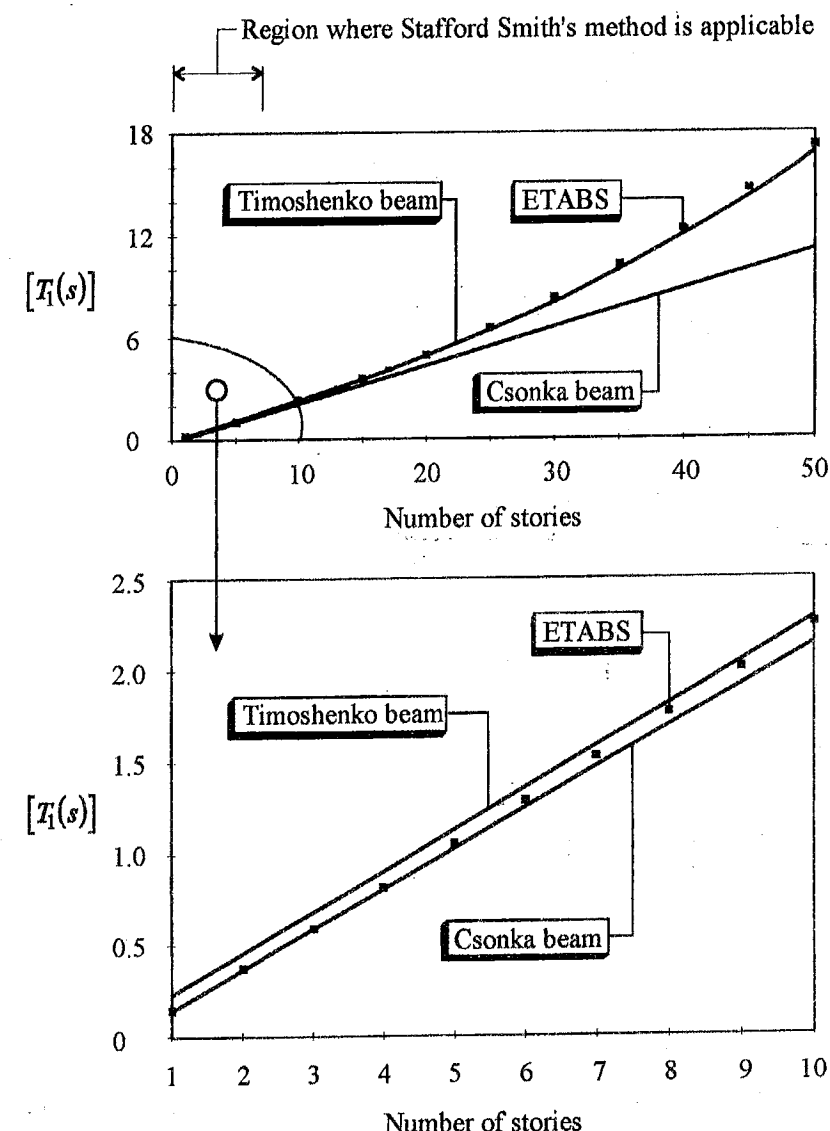
Fig. 4 First period of vibration of the rigid frame in function of the number of stories

Table 2 Comparison of results and assessment of accuracy

Mode of Vibr. (i)	Present method	ETABS	Percentage discrepancies with FEM analysis $\varepsilon(\%)$
Periods of vibration T(sec)			
1	4.88	4.98	2.0
2	1.60	1.61	0.6
3	0.91	0.90	1.1
Base shear V(kN)			
1	193.8	188.9	2.6
2	29.79	30.02	0.8
3	15.55	16.18	3.9
Maximum probable base shear V_{max}(kN)			
	196.7	192.0	2.4
Base moment M(kN)			
1	7698	8080	4.7
Top deflection Δ_1(m)			
1	0.055	0.057	3.5
Maximum inter-story drift-ratio δ_1			
1	0.00116	0.00122	4.9

5. CONCLUSIONS

The approximate method based on the Timoshenko-beam model is applicable for narrow buildings where the known approximate methods [10, 16] brake down.

Comparisons with FE (ETABS) [21] analysis show that this simple method can be an effective and reliable tool for the design of buildings for earthquake.

6. ACKNOWLEDGEMENTS

7. REFERENCES

[1] Tso, W. and Rutenberg, A., "Seismic spectral response analysis of coupled shear walls", *J. Struct. Engrg., ASCE,* 103 (1), 1977, pp. 181-196.

[2] Basu, A. K., "Seismic design charts for coupled shear walls", *J. Struct. Engrg., ASCE,* 109 (2), 1983, pp. 335-352.

[3] Stafford Smith, B. and Crowe, E., "Estimating periods of vibration of tall buildings" *J. Struct. Engrg., ASCE,* 112 (5), 1986, pp. 1005-1019.

[4] Beck, H., "Contribution to the analysis of coupled shear walls", *Journal of the American Concrete Institute,* 59, 1962, pp. 1055-1069.

[5] Csonka, P., "Beitrag zur Berechnung waagerecht belasteter Stockwerkrahmen", *Die Bautechnik,* Vol. 39, 1962, pp. 237-240.

[6] Rosman, R., "Static und Dynamic der Sch eibensysteme des Hochbaues", *Springer-V.* 1968.

[7] Szerémi L., "Stiffening system of multistorey buildings by the continuum modell", *Periodica Politechnica Civ. Engrg.,* Vol. 22, 1978, pp. 205-218.

[8] Szerémi, L., "Épületmerevítések számítása" (Calculation of stiffening systems of buildings). Budapest, Mérnöki Kézikönyv II. Ed. Palotás László, *Műszaki Könyvkiadó.* 1984, pp. 868-896. (In Hungarian)

[9] Skattum, S. K., "Dynamic analysis of coupled shear walls and sandwich beams", *California Institute of Technology.* Thesis.

[10] Kollár, L. P., "Calculation of plane frames braced by shear walls for seismic load", *Acta Technica Acad. Sci. Hung.,* 104 (1-3), 1991 pp. 187-209.

[11] Goshy, B., "Lemezvázas épületek statikája és dinamikája (Statics and dynamics of coupled shear wall structures", *Műszaki Könyvkiadó,* 1981. (In Hungarian)

[12] Rosman, R., "Dynamics and Stability of shear wall building structures", *Proc. Instn. Civ. Engs,* 55, 1973, pp. 411-423.

[13] Hegedűs, I. and Kollár, L. P., "Szendvicsrúdmodell alkalmazása mérnöki szerkezetek stabilitásvizsgálatában" (Stability analysis of engineering structures using the szendvics bar model). Chapter of the book "A mérnöki stabilitáselmélet különleges problémái" (Special problems of the theory of structural stability) edited by Kollár L. *Akadémiai Kiadó,* 1991. (In Hungarian)

[14] Murashev, V., et al., "Design of reinforced concrete structures", *Mir Publishers,* 1971.

[15] Hegedűs, I. and Kollár, L. P., "Generalized bar models and their physical interpretation", *Acta Technica Hung. Civil Engrg.* 101, 1991, pp. 67-93.

[16] Stafford Smith, B., and Yoon Y-S., "Estimating seismic base shears of tall wall-frame buildings", *J. Struct. Engrg., ASCE,* vol. 117, No. 10, 1991, pp. 3026-3041.

[17] Basu, A. K., Nagpal, K. and Surinder, K., "Charts for seismic design of frame-wall systems", *J. of Struct. Engrg.,* 110(1), 1984, pp. 31-45.

[18] Paz, M., "International Handbook of Earthquake Engineering. Codes, Programs and Examples", *Chapman&Hall.* 1994.

[19] Csák, B., Hunyadi, F. and Vértes, Gy., "Földrengések hatása az építményekre" (Earthquake effect on the buildings). *Műszaki Könyvkiadó.* 1981. (In Hungarian)

[20] Köpecsiri, A. and Kollár, L. P., "Approximate analysis of tall building structures for earthquake using the Timoshenko-beam", submitted for publication to *Periodica Politechnica,* 1996.

[21] Habibullah, A., "ETABS. Three Dimensional Analysis of Building Systems", *Computers & Structures Inc.* 1995.

[22] Stafford Smith, B., Kuster, M. and Hoenderkamp J. C. D., "A generalised approach to the deflection analysis of braced frame, rigid frame, and coupled wall structures. *Can. J. Civ. Engrg.,* 1981. No. 8, pp. 230-240.

SEISMIC BEHAVIOUR OF REINFORCED MASONRY WALLS

Nikoletta PSILLA
National Technical University of Athens
Laboratory of Reinforced Concrete
5, Iroon Polytechniou St, 157 73, Zografou, Greece

INTRODUCTION

Unreinforced masonry, constitutes a non ductile, brittle material with almost no energy absorbtion, thus exhibiting unsatisfactory performance under seismic loading. In order to enhance strength and ductility against service conditions and mainly against seismic actions, masonry structures are usually vertically and horizontally reinforced with steel reinforcement. In fact, it has been reported [1] that reinforced masonry structures could be designed to adequately perform under major earthquakes, provided that careful design and detailing requirements are followed. Hence, concerning low and medium-rise buildings, reinforced masonry could constitute an easier and more economical construction system compared to that of reinforced concrete, nowadays commonly used. It should be noted, however that, despite its several merits, the technique of reinforced masonry finds a rather limited application. As illustrated in most recent international regulatory codes, for several aspects related to reinforced masonry design and construction, research has not yet succeeded to provide the necessary quantitative information which would allow for a rational and economical design and construction of reinforced masonry buildings. Thus, the design of reinforced masonry is still more or less based on empirical equations and minimal measures. It is therefore obvious that for the full development of this technology, a design level, similar to that of concrete, should be succeeded.

STATEMENT OF THE PROBLEM

Masonry walls constitute the basic structural elements of reinforced masonry buildings, designed to provide the major seismic resistance of the building, carrying the in-plane lateral forces.

Depending on their position in the structural system, their effective aspect ratio, quantity and arrangement of vertical and horizontal reinforcement and on the mechanical properties of the materials, two distinct inelastic deformation mechanisms can be exhibited by shear walls subjected to in-plane seismic loads:
- the flexural mechanism characterised by tensile yielding of vertical reinforcement at the tensioned side and crushing of masonry units at the compressed toe,
- the shear mechanism, characterised by diagonal tensile cracking.

Results of previous research [3], [4], [10] have indicated that shear mechanism is less desirable than the flexural one. In fact, wall components dominated by the shear mechanism are more brittle than those dominated by flexure, thus leading to a severe reduction of the overall ductility of a structural system and thereby severely jeopardising the overall seismic resistance of the structure. It is therefore necessary to know the strength and deformability capability of masonry walls under different behaviour modes to avoid undesirable brittle shear failure in reinforced masonry design.

Previous research has provided detailed description of the flexural failure mode (which is similar to that of R.C.) and quite accurate theoretical models for the estimation of the flexural capacity of a reinforced masonry wall [1], [5], [8]. On the contrary, referring to the resistance of a wall failing to a shear mode, the available data are not sufficient to lead to definite conclusions. In general, the shear resistance of a wall depends on several different mechanisms, e.g. the dowel action of vertical reinforcement, the tension capacity of horizontal reinforcement (see Fig. 1), the truss and beam action of vertical and horizontal steel and masonry as well as the interlocking forces between the parts of the wall, separated by diagonal cracking. Moreover, significant role to the effectiveness of horizontal reinforcement plays the bond between mortar and reinforcement in mortar joints, the anchoring conditions at the wall's vertical edges as well as the mechanical properties of the masonry units.
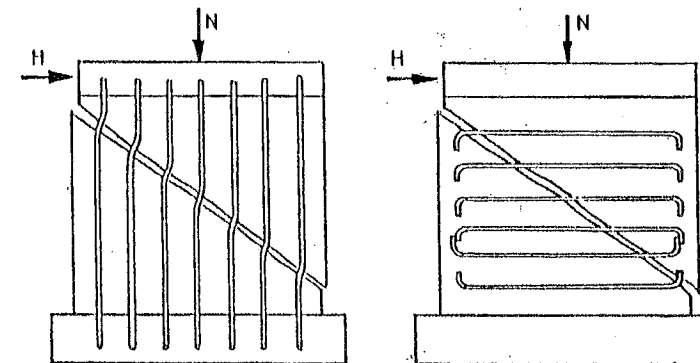
Fig. 1 Mechanism of reinforcement action at shear failure of a reinforced masonry wall [2]

Due to the complexity of the mechanisms involved, there is a lack of validated theoretical models for the evaluation of shear strength and ductility of wall panels. On the other hand, although the rather large amount of the available experimental data, in many cases contradictory results have been obtained, owing to the large number of design parameters involved and the different testing techniques followed. This is the reason why, codes provisions are usually based on experience from the behaviour of masonry walls in reinforced masonry structures, thus being in many cases oversimplistic and overconservative.

Therefore, the need becomes obvious for a rational model to predict the mode of failure to be expected for the masonry element under consideration and its corresponding strength and ductility. Thus, this work is focused to the investigation of the behaviour of reinforced masonry walls against seismic loading, to obtain qualiquative and quantitative information on their strength and ductility. The aim is to enhance the data base and improve somehow the current design methodology concerning the analytical calculation of the resistance characteristics of a masonry wall, as well as the appropriate minimal measures.

PLAN OF THE WORK

Although reinforced masonry includes a wide range of material types and various construction forms our investigation is concentrated in the specific materials and

construction technology developed in Greece, within the frame of a Brite-Euram european programme entitled " Industrial Development of Reinforced Masonry Buildings". In our case the reinforced masonry system is obtained with the horizontal reinforcing bars embedded in the horizontal mortar joints and a diffused vertical reinforcement inserted in special holes made out in special vertically perforated clay units (see Fig. 2); only the holes where the reinforcement is placed are filled with grout.
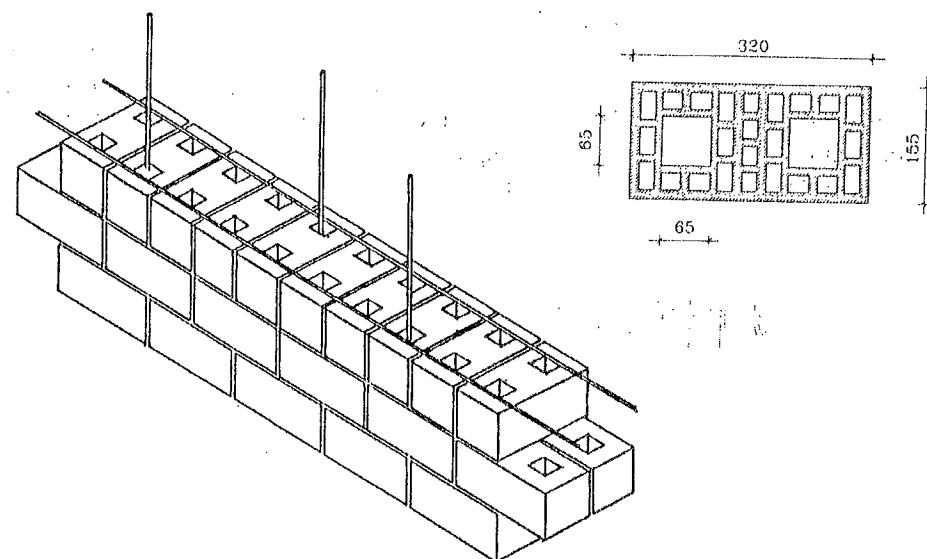
Fig. 2 Clay unit and form of reinforced masonry construction developed in Greece

In the first stage of our work, the mechanical characteristics of the constituent materials namely clay unit, mortar and grout and unreinforced masonry (against compression, tension and diagonal compression) are experimentally investigated, to obtain their full stress-strain curves. This constitutes a necessary information to be used in models to be developed in the following stages.

Further, the different force transfer mechanisms developing along an uncontinuity (crack or joint) of a reinforced masonry wall and conditioning its strength and deformability characteristics are isolated and experimentally investigated. Thus, a series of reduced scale tests on various mechanisms are carried out, namely on friction between brick and brick or between brick and mortar, on dowel and on pull-out, push-in action of vertical and horizontal reinforcement. On the basis of the experimental results obtained analytical models on the different mechanisms are calibrated and corrected. Our intention is, these models to be used as input for the development of a model describing the strength and deformability characteristics of masonry shear walls, taking into account the participation proportion of each mechanism.

This model is calibrated and corrected on the basis of test results on full scale reinforced wall panels under seismim loading. To this purpose the shear behaviour of five full-scale cantilever walls are experimentally examined. Although the inelastic behaviour of reinforced masonry walls is influenced by many factors, in this work the parameters investigated are the effective aspect ratio, the quantity of vertical and horizontal reinforcement and the magnitude of axial compressive stress (see Tab. 1). All

N^o	h x l (mm^2)	t (mm)	aspect ratio	σ_o (MPa)	ρ_v (‰)	vertical steel	ρ_h (‰)	horizontal steel
1	2650 x 1850	320	1.43	0.2	0.48	1Φ10/51	0.59	2Φ8/53
5	1855 x 1850	320	1.00	0.2	0.48	1Φ10/51	0.59	2Φ8/53
6	1855 x 1850	320	1.00	0.4	0.48	1Φ10/51	0.59	2Φ8/53
7	1855 x 1850	320	1.00	0.4	0.94	1Φ14/51	0.93	2Φ10/53
8	1590 x 2700	320	0.59	0.2	0.48	1Φ10/51	0.59	2Φ8/53

Tab. 1 Reinforced masonry wall specimens
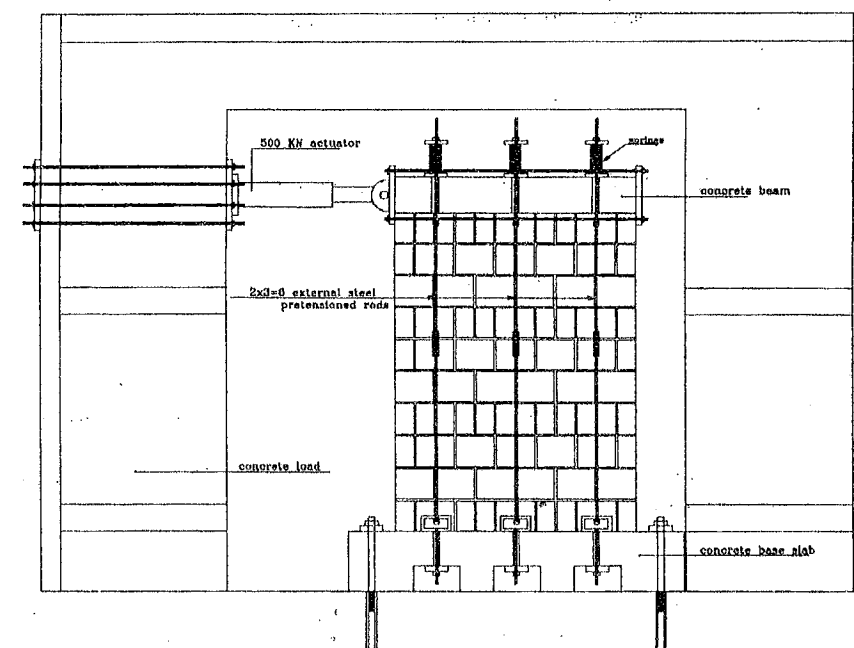
Fig. 3 Test set-up for testing the seismic resistance of reinforced masonry walls
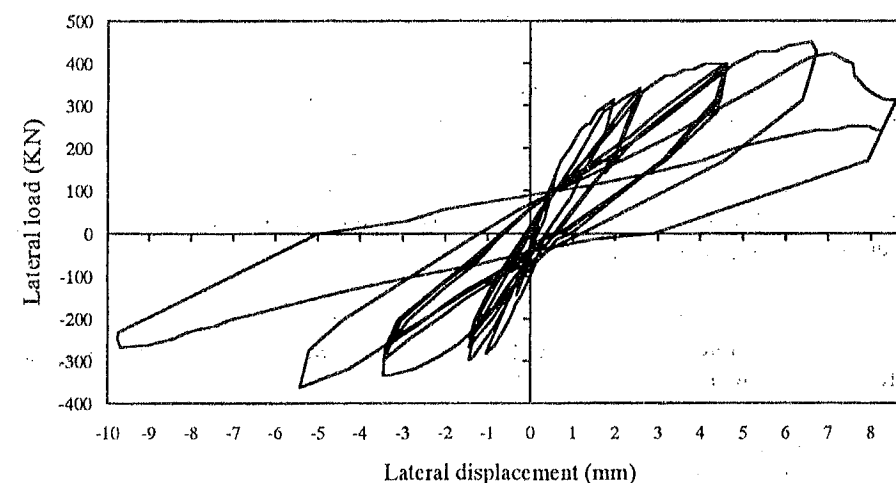
Fig. 4 Hysteresis curves of specimen 8

specimens are subjected to a standard displacement history, while the axial compressive stress is maintained constant during each test (see Fig. 3 and 4).

Finally, by means of this model an attempt is made to make clear the role of the minimum ratio of reinforcement.

CONCLUSIONS

From the results up to now it seems that the development of a model describing the strength and deformability characteristics of masonry shear walls, taking into account the participation proportion of each mechanism could be possible. Nevertheless, analytical work is still to be carried out for the full evaluation of the experimental work completed so far.

REFERENCES

1. Paulay T., Priestley M.J.N., *Seismic Design of Reinforced Concrete and Masonry Buildings*, John Wiley & Sons, Inc., New York, 1992.

2. Priestley, M.J.N., " Masonry", *Design of Earthquake Resistant Structures*, ed. Emilio Rosenblueth, John Wiley & Sons, New York - Toronto, 1980.

3. Priestley, M.J.N. and Elder D., "Cyclic Loading Tests of Slender Concrete Masonry Shear Walls", *Bul. of the New Zealand National Society for Earthquake Engineering*, Vol. 15, No 1, 1982.

4. Shing, P.B., Noland, J.L., Klamerus, E., Spaeh H., "Inelastic Behaviour of Concrete Masonry Shear Walls", *Journal of Structural Engineering*, Vol. 115, No 9, September, 1989.

5. Shing, P.B., Schuller, M., Hoskere, V.S., "In-plane resistance of Reinforced Masonry Shear Walls", *Journal of Structural Engineering*, Vol. 116, No 3, March, 1990.

6. Tassios, T.P. , *Mechanics of masonry*, Symmetria, Athens, 1987.

7. Tassios, T.P. , "Masonry, infill and R.C. walls under cyclic loading", *CIB Symposium on Wall Structures*, Warsaw, 1984.

8. Tomazevic, M., "Fundamentals of Earthquake Resistant Design of Masonry Buildings", *XV Regional Seminar on Earthquake Engineering*, European Association for Earthquake Engineering, Ravello, Italy, 1989.

9. Tomazevic, M., Lutman, M., Petkovic, L., "In-plane Behaviour of Reinforced Masonry Walls Subjected to Cyclic Lateral Loads", *Report No ZRMK/PI-92/06*, Institute for Testing and Research in Materials and Structures, Ljubljana, 1993.

10. Wakabayashi, M., and Nakamura, T., "Reinforced Principle and Seismic Resistance of Brick Masonry Walls", *Proc. 8th World Conference on Earthquake Engineering*, Vol. V, San Fransisco, 1984.

COMPOSITE RETROFITTING OF MASONRY WALLS

John Jai   and
Stanford University
Dept. of Aeronautics and Astronautics
Stanford, CA USA

Rita Kiss
Technical University of Budapest
Dept. of Reinforced Concrete Structures
Budapest, Hungary

1. INTRODUCTION

Unreinforced masonry construction (UMC) is a popular building method found world-wide because of its low cost and simplicity. However, the tensile and shear strengths of unreinforced masonry are insufficient to sustain seismic forces. Many of the fatalities resulting from earthquakes are caused by the collapse of UMC. Although most modern construction is either steel frame or reinforced concrete, some unreinforced masonry structures still remain in use.

Many retrofit techniques have been developed, most involving the addition of steel reinforcement bars to masonry walls. These procedures suffer from a number of dis-advantages. The reinforcing steel is expensive, cumbersome, and subject to corrosion. These retrofit techniques are also time-consuming and labor-intensive.

In recent years, numerous applications for composite materials have arisen in the field of civil engineering [1-6]. In particular, composites have been examined as a possible alternative to steel as the reinforcement material in reinforced concrete [7-9]. Additionally, composites have been proposed as a repair material for bridges [10-12] and columns and to build offshore constructions [1]. The reason for the rise of composite materials stems from its advantages over traditional building materials. It is superior to steel in strength, weight, and corrosion resistance.

In this work, the use of composite materials to retrofit unreinforced masonry is explored. The benefits of composites offer a retrofit technique to overcome the usual problems associated with unreinforced masonry. It is proposed that fiber-reinforced plastics can be used to resist the tensile load incurred by a structure and combine with the masonry to form a single load-bearing unit capable of sustaining compressive, shear and tensile loads. To achieve this, fiberglass sheets can be applied to the surface of masonry structures at strategic locations in a "wallpaper" fashion, as illustrated in Figure 1.

The purpose of this work is to evaluate the feasibility of such a retrofit technique, to determine appropriate materials and methods, and to examine the basic behavior of composite reinforced masonry.

Two types of test arrangements are considered:

- Single Brick
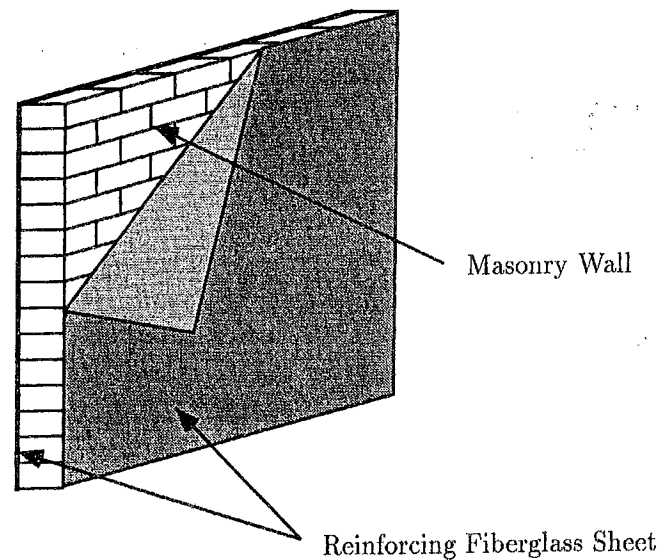
Figure 1 Fiberglass "wallpaper" retrofit method

Figure 2 Single brick delamination test specimens: (a) Flush, (b) Initial delamination, (c) Staggered

- Beams

2. SINGLE BRICK TESTS

During loading, the reinforcement may separate (delaminate) from the masonry. To utilize composite reinforcement effectively, the delamination phenomenon must be understood. To gain some understanding of this delamination process, reinforced single bricks were tested in under three different conditions.

- Two half-bricks (Figure 2a).

- Two "staggered" half-bricks with a $\frac{1}{8}$ inch step between the halves (Figure 2b).

- Two half-bricks with a $\frac{1}{2}$ inch initial (before loading) delamination between the reinforcement and the brick along the center of the brick (Figure 2c).

Each brick was subjected to three-point bending. During the test, the applied load and the crosshead deflection were measured and recorded. Delamination was also observed visually.

2.1 Test results

The data obtained with the reinforced single bricks subjected to three-point bending are shown in Figure 3.

Figure 3 Load vs. deflection of single bricks reinforced with composites (Ref. Figure 2)

The following observations may be made:

1) When the two half-bricks are aligned, that is, with no stagger (Figures 2a and b), the load varies linearly with deflection until failure. The load-deflection curve for the case with no delamination (Figure 2a) is practically identical to that for the case with delamination (Figure 2b). Up to failure, no significant delamination of the reinforcement was observed in these two cases.

2) When the two half-bricks are staggered (Figure 2c), the load vs. deflection is linear until the reinforcement begins to delaminate. Once the delamination begins and the delamination area grows, the load varies with deflection in a nonlinear manner. It is noteworthy that the load carrying capability of the staggered bricks is considerably lower than the non-staggered bricks. This is due to the fact that delamination weakens the structure.

The aforementioned results indicate that delamination between the brick and the reinforcement is caused mostly by misalignment of the bricks. Once such misalignment exists (which is likely to be the case in practice), the delamination grows and the load carrying capacity decreases.

3. BEAM TESTS

To study the effect of composite reinforcement on the bending behavior of masonry beams, beam bending tests were conducted.

Masonry beams constructed of fourteen bricks (Figure 4) were fully covered with reinforcement on one of the faces.

Beams of the following construction were tested:

1 - Unreinforced

2 - Reinforced with epoxy resin and woven fiberglass cloth

3 - Reinforced with epoxy resin and chopped-fiber fiberglass mat

4 - Reinforced with polyester resin and woven fiberglass cloth

5 - Reinforced with polyester resin and chopped-fiber fiberglass mat

Each beam was tested in four-point bending. Load was applied via two $\frac{1}{2}$ inch steel rollers, 14 inches apart. Between these two rollers, the beam is in pure bending, such that shear is negligible and the bending moment is constant. The load was applied by a mechanical tester under displacement control at a constant rate of 0.002 inches per second. During the test, the applied force and crosshead deflection were monitored and recorded and delamination was visually observed.

3.1 Test results

The moment in the portion of the beam between the load points was used to provide a normalized basis for comparing the bending strengths of beams of different lengths. A typical moment vs. midpoint deflection curve obtained from the tests is shown in Figure 4. A comparison of the average failure moments in shown in Figure 5.

From the experimental results, the following observations may be made:

1) The reinforced beams were able to support more load than the unreinforced beams. Figure 5 shows that the beams reinforced with epoxy resin and chopped-fiber mat were over 16 times stronger than the unreinforced beams and that the weakest reinforced beams were still nearly 7 times stronger than the unreinforced beams. The reinforced beams were able to sustain tensile loads in the reinforcing sheets after the mortar joints had cracked, leading to increased load capacity.

2) The reinforced beams were also able to sustain loads beyond the first failure. This damage tolerance can be seen in the ductile behavior shown in Figure 4. While the unreinforced beams failed suddenly and brittly, the reinforced beams all demonstrated some ductility. During loading, delamination was observed in the bending region. These delaminations serve as an energy dissipation mechanism and cause the observed ductility.
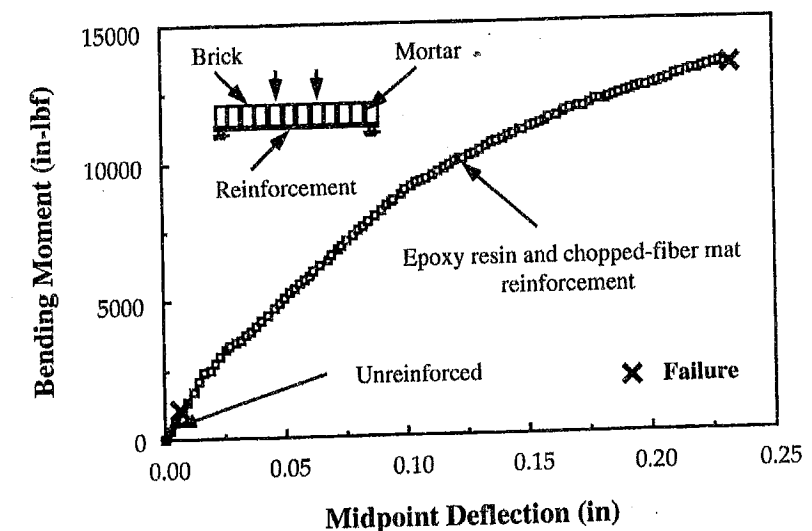
Figure 4 *Load vs. deflection of a masonry beam reinforced with epoxy resin and chopped-fiber fiberglass mat, subjected to four-point bending*
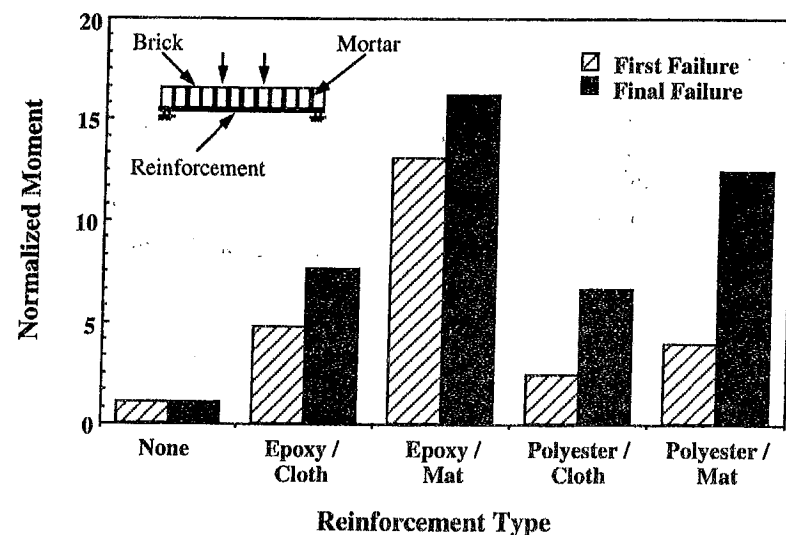
Figure 5   Average bending strength of reinforced masonry beams subjected to four-point bending, normalized to unreinforced strength

CONCLUSIONS

This study was conducted to determine the feasibility of using composites to retrofit unreinforced masonry structures. From the data obtained from the experiments, it is evident that composite retrofitting increases both the damage capacity and the damage tolerance of masonry structures. The beam specimens were able to sustain loads beyond first failure, demonstrating ductile behavior.

Four different reinforcement materials were tested to evaluate the differences between different fiber configurations and resins. The polyester resin was rejected for further tests because of practical considerations and the cloth did not provide sufficient strength. Further experiments will be conducted with the epoxy-mat combination because of its superior engineering qualities and for economic considerations.

There appear to be many possibilities of applying composite materials to the reinforcement of masonry. Further studies must be performed to determine other factors such as the environmental effects on fiberglass. These tests are currently being conducted at Stanford University as part of this ongoing research. Analytical methods are also being developed to aid in the investigation of this promising technology.

REFERENCES

[1]   Barrio D.S., "The Use of Structural Composites in 21st Century Infrastructure Technology", *Plastics Composites for 21st Century Construction*, AICHE, 1993,

pp. 1-14.

[2]   Bank L.C., "Composite Materials in Civil Engineering Applications: The Age of New Materials", *Society of the Plastics Industry (SPI) Annual Management Meeting*, Orlando, Florida, 1992.

[3]   Barbero E. and H.V.S. GangaRao, "Structural Applications of Composites in Infrastructure", *SAMPE Journal*, Vol. 27, No. 6, November-December 1991, pp. 9-16.

[4]   Ballinger C.A., "Development of Composites for Civil Engineering", *Proceedings of the First Advanced Composite Materials in Civil Engineering Structures Conference*, ASCE, January 1991.

[5]   Meier U. and H. Kaiser, "Strengthening of Structures with CFRP Lamination", *Proceedings of the First Advanced Composite Materials in Civil Engineering Structures Conference*, ASCE, January 1991, pp. 224-232.

[6]   Leonard L., "Rebuilding the Infrastructure with Advanced Composites", *Advanced Composites*, May-June 1990, pp. 43-47.

[7]   Faza S.S. and H.V.S. GangaRao, "Composite materials as Concrete Reinforcement", *Plastics Composites for 21st Century Construction*, AICHE, 1993, pp. 12-22.

[8]   Bank L.C. and Z. Xi, "Pultruded FRP Grating as a Reinforcement for Concrete", *48th SPI Conference*, 1993, 13-B.

[9]   Roll R.D., "Use of GFRP Rebar in Concrete Structures", *Proceedings of the First Advanced Composite Materials in Civil Engineering Structures*, ASCE, January 1991, pp. 93-98.

[10]   Iyer S. I., A. Khubchandani, and J. Feng, "Fiberglass and Graphite Cables for Bridge Decks", *International Congress on Polymers in Concrete*, September 1991.

[11]   Cooper J.D., "Advanced Composites - Backbone for a New Era in Bridge Engineering Research", *Proceedings of the First Advanced Composite Materials in Civil Engineering Structures*, ASCE, January 1991, pp. 111-122.

[12]   Noritake K., S. Kumagi, et. al., "Aramid FRP Pretensioned Road Bridge", *Materials: Performance and Prevention of Deficiencies and Failure*, November 1990, pp. 65-70.

ACKNOWLEDGEMENTS

and the Department of Reinforced Concrete Structures at the Technical University of Budapest.

The tests reported here were conducted with András Köpecsiri of the Technical University of Budapest, and under the guidance of Professors G. Springer (Department of Aeronautics and Astronautics, Stanford University), H. Krawinkler (Department of Civil Engineering, Stanford University), and L. Kollár (Department of Reinforced Concrete Structures, Technical University of Budapest).

SPLITTING FORCES OF HEADED STUDS AND UNDERCUT ANCHORS

Jörg Asmus
Institut für Werkstoffe im Bauwesen
University of Stuttgart
D-70550 Stuttgart, Pfaffenwaldring 4

1. INTRODUCTION

The failure of a fastener can be caused by rupture of steel, anchor pullout or giving a sufficiently high steel capacity by a concrete cone failure. These failure modes have been investigated intensively and the associated failure loads can be calculated with known equations [1, 2].

For the failure mode splitting there is no satisfactory, general equation to calculate the failure load. Splitting of the concrete member can be expected if the member dimensions are small. The splitting failure load depends on the dimensions of the concrete member, the material properties, the installation parameters and above all on the splitting forces of the fastener. For this reason the transformation of the tension force into splitting force has to be considered for the determination of the splitting failure load.

Therefore, the influencing factors on the splitting forces of fastenings with mechanical interlock (e.g. headed studs and undercut anchors) are experimentally studied. The results are evaluated and discussed.

2. LITERATURE

The main influencing factor on the ratio of splitting and tension forces ($R_{SP/T}$) of headed studs and undercut anchors is the load bearing area, which is calculated with the width of shoulder and the bolt diameter. The ratio $R_{SP/T}$ should be described with the pressure, which is the effective concrete stress on the shoulder. The pressure is calculated as the tension force divided by the load bearing area. Furthermore, the ratio $R_{SP/T}$ is influenced by the angle of cone α (Fig. 1a).

In the literature only a few investigations into the ratio $R_{SP/T}$ have been found. According to theoretical investigations in [3] a ratio $R_{SP/T} = 0,25$ can be assumed. Based on only 4 tests with undercut anchors a ratio $R_{SP/T} = 0,35$ [4] was found. In [5] the lateral blow out failure of headed studs near to a free edge was investigated. According to this investigation a ratio $R_{SP/T} = 0,2$ for low pressure ($p \sim 4$ N/mm^2) and $R_{SP/T} = 0,4$ for high pressure ($p \sim 15$ N/mm^2) was recommended.

3. TESTS

3.1 Test program

More than 150 tests with headed studs and different sizes of 3 types of undercut anchors have been carried out (Fig. 1).

The bolt diameter was varied from 8 to 16 mm and the width of the shoulder (a_s) from 0.5 to 8 mm, which means a variation of the load bearing area from 12 to 564 mm². Furthermore, the angle of cone was varied ($\alpha = 15°$, 45° and 90°). With each version at least 5 tests were made.
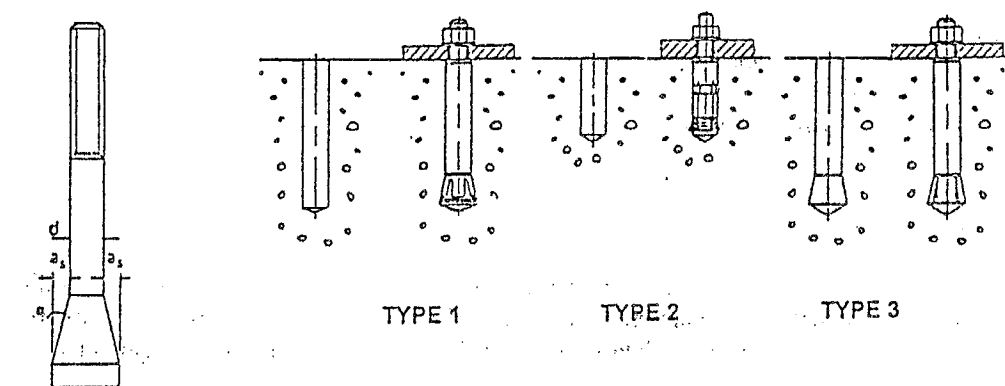
a) Headed stud   b) Undercut anchors

Fig. 1 Applied fasteners

3.2 Test setup

For the realization of the tests a special test setup was used (Fig. 2). After installing the fastener, the application of the prestressing load started and the resulting splitting force was measured by a servo-hydraulic machine. During the test the crack width was kept constant.

4. TEST RESULTS

In Fig. 3 typical test results for headed studs (d = 16 mm, $\alpha = 90°$, a_s = 3 or 8 mm) are shown. Fig. 3a) indicates the splitting force as a function of the prestressing force. With increasing prestressing force the splitting force increases. In Fig. 3b) is shown that for a prestressing force ≥ 10 kN the ratio $R_{SP/T}$ is roughly constant. From these curves, the ratio $R_{SP/T}$ are evaluated for a prestressing force equal to 30 % of the yield force. A smaller load bearing area produces larger displacements (Fig. 3c). For undercut anchors similar tendencies were observed.

To investigate the influence of the cone angle, test series with constant values of the bolt diameter (12 mm) and width of shoulder (8 mm) were carried out. For an angle of cone 45°and 90° the results are similar. For an angle of cone of 15° approximately 20% higher splitting forces were measured (Fig. 4). This confirms with results from [5, 6]. For an angle of cone $\alpha < 20°$ the splitting forces increase with decreasing angle.

The investigations have shown that the splitting forces depend mainly on the splitting area (Fig. 5). With higher pressure the splitting forces increase. Up to a pressure of 300 N/mm² the influence is not so strong. For a pressure higher than 300 N/mm², which corresponds to a ratio pressure/concrete compressive strength of roughly 10, the concrete is pulverized and a quasi-hydrostatic state of stress distribution arises. Therefore for p ≥ 300 N/mm² the ratio $R_{SP/T}$ increases significantly (Fig. 6).
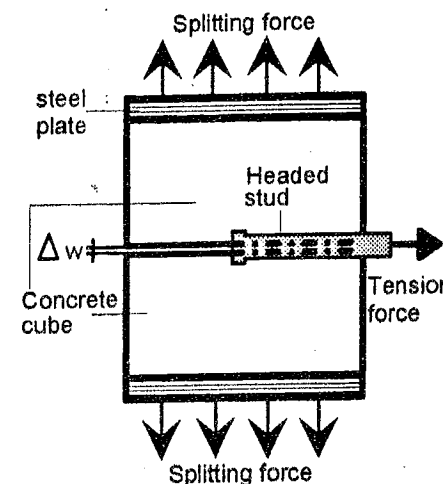
Fig. 2 Schematic test setup
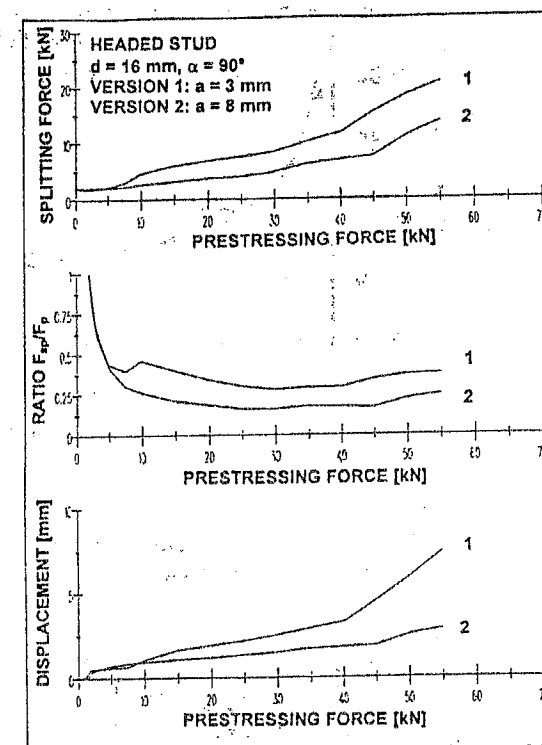
Fig. 3 Typical test results: Splitting force, Ratio $R_{SP/T}$ and displacement as a function of prestressing force
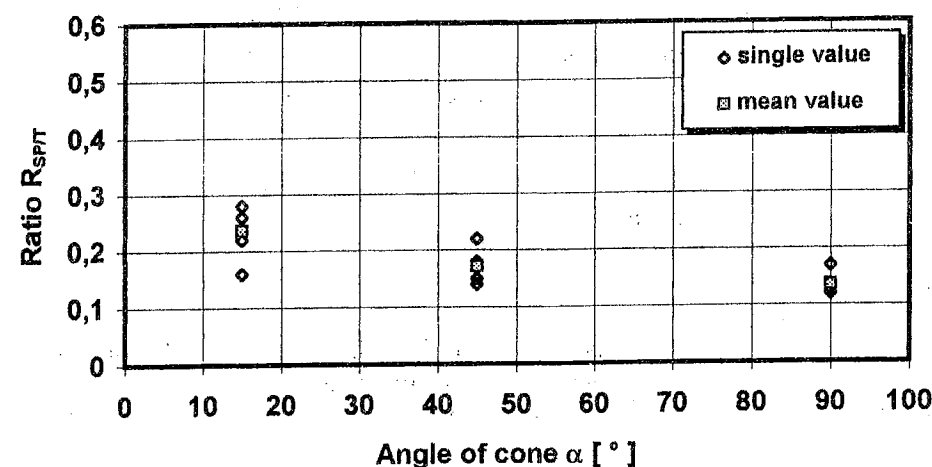
Fig. 4 Ratio $R_{SP/T}$ as a function of angle of cone α, Headed studs (d = 12 mm, a_s = 8 mm)
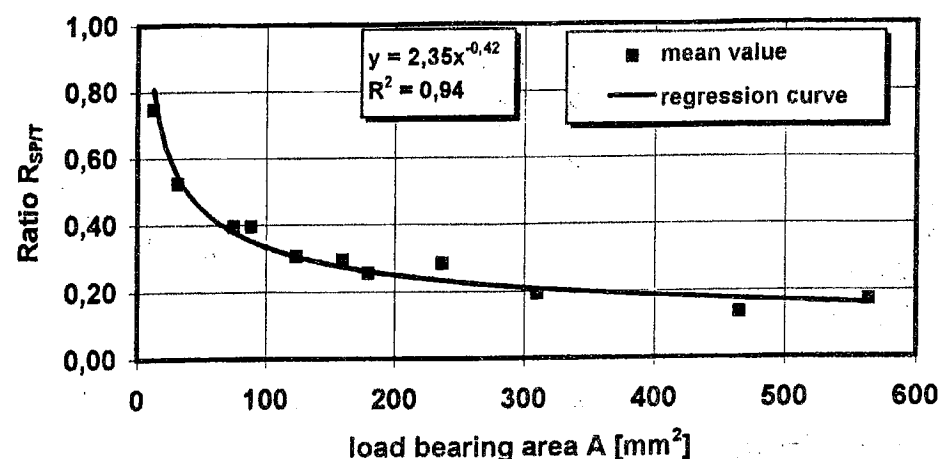
Fig. 5 Ratio $R_{SP/T}$ as a function of the load bearing area, Headed studs (d = 8 -16 mm, $\alpha = 90°, f_c = 35,6 \, N/mm^2$)
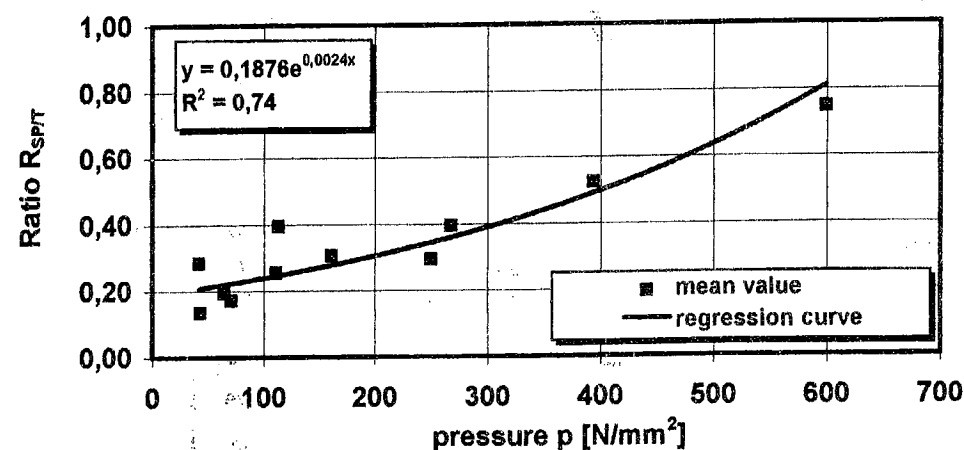
Fig. 6 Ratio $R_{SP/T}$ as a function of the pressure, Headed studs (d = 8 -16 mm, $\alpha = 90°, f_c = 35,6 \, N/mm^2$)

5. CONCLUSIONS

In order to find a general equation to describe the splitting failure load of headed studs and undercut anchors the transformation of tension force into splitting forces have to be considered. In several tests with headed studs and undercut anchors the influencing factors on the ratio of splitting to tension force $R_{SP/T}$ were investigated.

The ratio $R_{SP/T}$ mainly depends on the size of load bearing area or the pressure under the head respectively. For angles of cone $\alpha < 20°$ the splitting forces increase with decreasing angle.

6. REFERENCES

[1] Deutsches Institut für Bautechnik, "Bemessungsverfahren für Dübel zur Verankerung in Beton", 1993.

[2] CEB-Guide on the design of fastenings, Draft 2/1994.

[3] Leonhardt F., „Vorlesung über Massivbau", Teil 2. Springer Verlag, Berlin, 1986, pp. 53-60.

[4] Faoro M., „Untersuchungen zur Frage der Spalt- und Spreizkräfte von Befestigungssystemen (Teil I), Bericht Nr. 3/4 - 85/2, Institut für Werkstoffe im Bauwesen, Universität Stuttgart, 1985.

[5] Furche J., Eligehausen R., „Lateral Blow-Out Failure of Headed Studs Near a Free Edge", ACI - special publication, Anchors in Concrete, Detroit, 1990.

[6] Bohner R., „Spalten des Ankergrundes Beton infolge zentrisch belasteter formschlüssiger Befestigungsmittel", Diplomarbeit, Institut für Werkstoffe im Bauwesen, Universität Stuttgart, 1988

[7] Asmus J., „Einflußgrößen auf die Umsetzung der Zugkräfte in Spaltkräfte bei formschlüssigen Befestigungsmitteln", Bericht Nr. 16/13 - 95/16, Institut für Werkstoffe im Bauwesen, Universität Stuttgart, 1995.

[8] Scheer S., „Untersuchungen zur Frage der Spaltkräfte von formschlüssigen Befestigungsmitteln", Diplomarbeit, Institut für Werkstoffe im Bauwesen, Universität Stuttgart, 1994

DESIGN MODEL FOR BONDED ANCHORS

Dipl. Ing. Bernhard Lehr,
University of Stuttgart - Institut für Werkstoffe im Bauwesen
Pfaffenwaldring 4, D - 70 550 Stuttgart

1. INTRODUKTION

The importance of bonded anchors is increasing because of the low costs of these anchors and the possibility of various applications.

A design model for torque controled expansion and undercut anchors is available, but not for bonded anchors. Our aim is to find a desing model for bonded anchors.

The behavior of single anchors away from edges is studied by Cook [1]. The load bearing behavior of group fastenings is investigated by the IWB. Single anchors at the edge and the corner of the element are tested by the Imperial College in London. The present article deals with the tests of the IWB and the Imperial College.

2. BONDED ANCHORS

A bonded anchor system consists of a threaded rod, washer, hexagon nut and a resin mortar. There are two types of bonded anchors: capsule type anchors and injection type anchors.

The typical capsule-type anchor consists of a cylindrical glass ampule containing an uncured polymeric compound and an accelerator or catalyst in isolated form. After inserting the cartridge in the drilling hole the threaded rod is driven into the required depth with the aid of a hammer drill applying percussive/rotary movements.

For resin based injection anchors plastic cartridges containing premeasured amounts of resin and hardener allow for controlling the mixing of polymer compounds. These compounds are normally mixed through a special mixing nozzle. The mixed mortar has to be injected before pushing the threaded rod into the drilling hole.

After drilling the holes must be cleaned carefully, because in uncleaned drilling holes the dust remains in the area between the mortar and the concrete. This causes an unfavorable load bearing behavior of bonded anchors due to less bond.

The anchors can be loaded after the curing time (appr.~ 30 min. at 20°C).

3. LOADBEARING AND FAILURE OF BONDED ANCHORS

Under tensil loading a bonded anchor exhibts approximately elastic behavior close to the maximum load. Normally they fail by pullout (Fig. 1a). The fracture area is between the mortar and the concrete or beetween the mortar and the anchor rod. In the case of a short embedment depth ($h_{ef} \leq 4\ d_{nom}$) there occures concrete cone failure (Fig. 1b). With increasing of the embedment depth the bonded anchors fail by a combined concrete cone and pullout failure (Fig. 1c). When the embedment depth is great enough ($h_{ef} \leq 10\ d_{nom}$), there will be steel failure (Fig. 1d).

4. TESTS WITH BONDED ANCHORS

Tables 1 and 2 give an overview of the tests are made at the IWB. The test programm of the Imperial College in London is shown in the Tables 3 and 4.

Till April 1996 there were done 138 centric tension tests with quadruple fastenings and 15 tests with double fastenings at the IWB. To compare the test results, 40 single

anchors were tested too. 79 tests with bonded amchors near the edge and 23 tests near the corner were carried out in the Imperial College.

a) *Bond failure* b) *Concrete cone failure*

c) *Concrete cone failure combined with bond failure* d) *Steel failure*
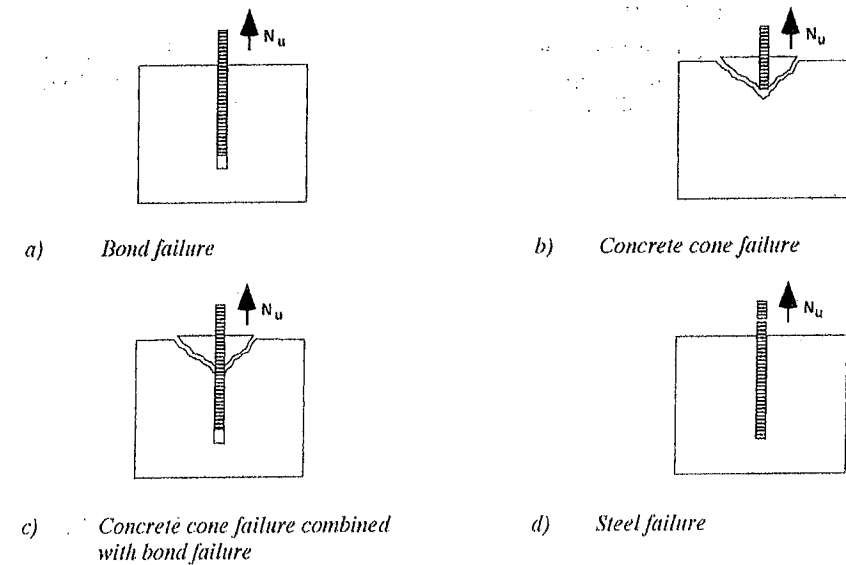
Fig. 1 *Failure modes of single bonded anchors far away from the edge*

Ø d_{nom}	h_{ef}/d_{nom}	h_{ef} [mm]	number of tests: c/h_{ef}					
			0,5	1,0	1,5	2,0	2,5	3,0
M 8	6	48		4				
	8	64		9	4	4	3	
	10	80		4				
	12	96		3				
	16	128		3				
	20	160		3				
M 12	4	48		8	9	8	12	11
	6	72		3				
	8	96	4	5	4	4	6	
	10	120		5				
	12	144	6	5	3			
	16	192		4				
M 16	8	128		4				

Tab. 1 *Centric tension tests with bonded anchors: Influence of spacing for quadruple fastenings, test programm in IWB [2]*

Ø d_{nom}	h_{ef}/d_{nom}	h_{ef} [mm]	number of tests: postion	
			perpendicular to edge	corner
M 12	8	96	4	3
	12	144	4	4

Tab. 2 *Centric tension tests with fastenings with two bonded anchors: Influence of edge distance and spacing ($s = 1\ h_{ef}/c = 0,5\ h_{ef}$) test programm in IWB [2]*

Ø d_{nom}	h_{ef}/d_{nom}	h_{ef} [mm]	number of tests: s/h_{ef}				
			0,25	0,5	0,75	1,0	1,25
M 8	8	64		5			
	12	96		5			
	16	128		5			
	20	160		2			
M 12	4	48			5	4	3
	8	96		4	4	4	
	12	144	5	5	5	3	
	16	192	5	5	5	5	
M 20	12	240		3			

Tab. 3 *Centric tension tests with bonded anchors: Influence of edge distance for single anchors, test programm in Imperial College [3]*

Ø d_{nom}	h_{ef}/d_{nom}	h_{ef} [mm]	number of tests: c/h_{ef}		
			0,5	0,75	1,0
M 12	8	96	4	3	4
	12	144	4		
	16	192	4		
	20	240	4		

Tab. 4 *Centric tension tests with bonded anchors: Influence of edge distance for fastenings at the corner, test programm in Imperial College [3]*

The tests, which were done at the Imperial College [3] to check the influence of the edge and the corner effects are shown in Fig. 2. The failure load was calculated according CC-method (Eq. (1)) [4].

In Fig. 3 the results of the tests at the IWB [2] are shown over the relationship between the spacing and the embedment depth. Furthermore, the calculated failure load according to Eq. (1) [4] and the pullout failure load according Eq. (2) can be seen.

$$N_U = A_{c,N} / A_{c,N}^0 \cdot N_0^u \cdot \psi_{s,N} \qquad (1)$$

$$N_{U,p} = n / N_{u,p}^0 \qquad (2)$$

with:
$N_u^0 = 13.5 \cdot f_{cc}^{0.5} \cdot h_{ef}^{1.5}$
$A_{c,N} = (s + 3 h_{ef})^2$
$A_{c,N}^0 = 9 \cdot h_{ef}^2$
$\psi_{s,N} = 0.3 + 0.7 \cdot c / (1.5 \cdot h_{ef})$

with:
$N_{u,p}^0 = \tau_u \cdot \pi \cdot d_0 \cdot h_{ef}$
n = number of anchors
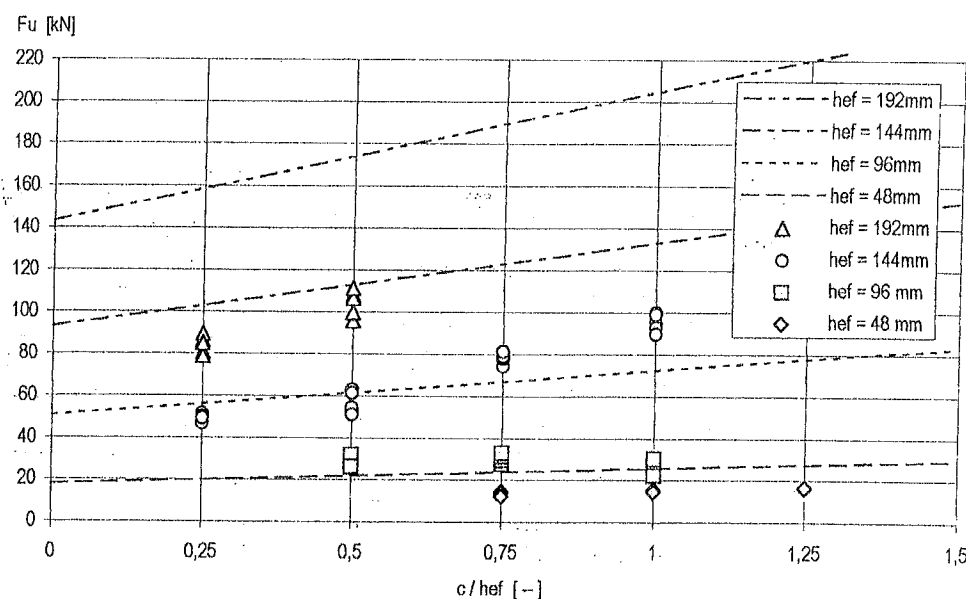
Fig.2 Centric tension tests with bonded anchors M12: Influence of edge distance
hef = 48 / 96 / 144 / 192 mm

5. MODIFIED CC-METHOD

Assuming that in genreral the concrete cone model of metal anchors is correct and also the equitation to calculate the influence of spacings is correct [4], it is possible to use this model for bonded anchors too. The most anchors failed with a combined concrete cone failur with bond failure like Fig. 1c. Only the embedment depth h_{ef} is to modify with a faktor α like it happens in Eq. (3).

Faktor α is unknown. It can be find for each test with the condition, that the relation beetween the failure load of the test and the calculated failure load is about 1,00. If this is done with all tests together of the Imperial Collage and of IWB [2,3], there can be found the factor $\alpha = 0,73$ with a standard devition of $s = 0,24$ and a coefficient of vari-
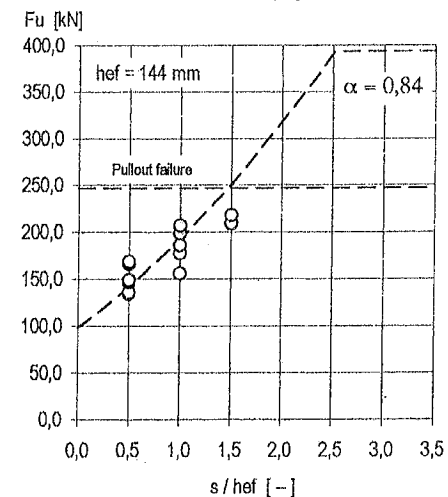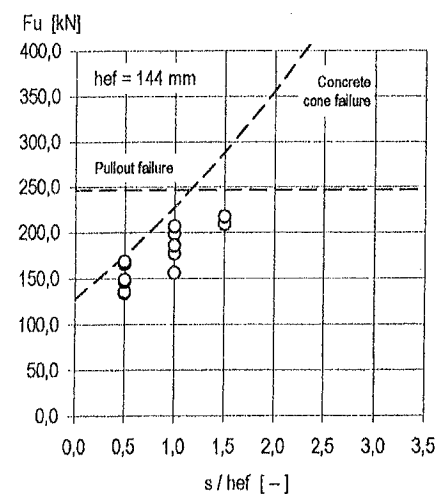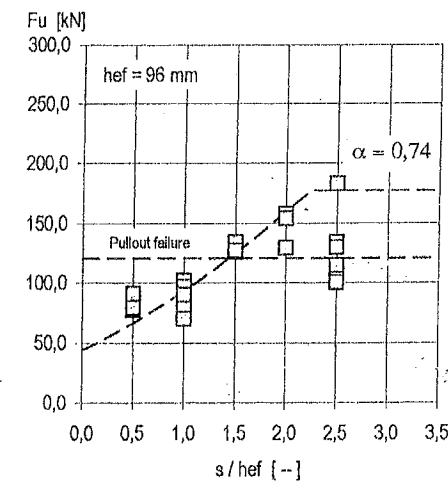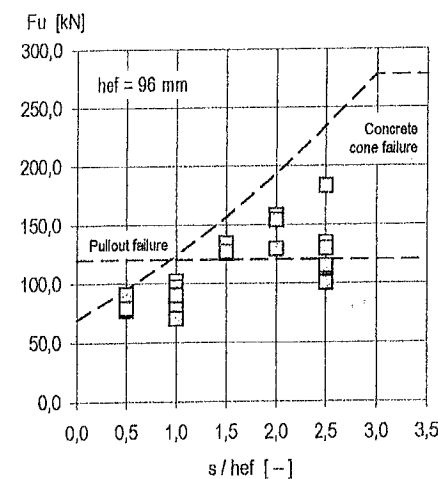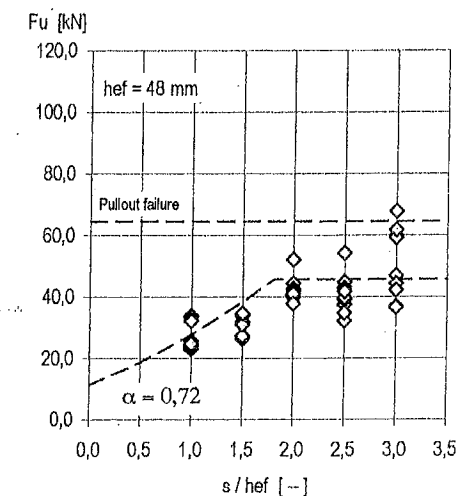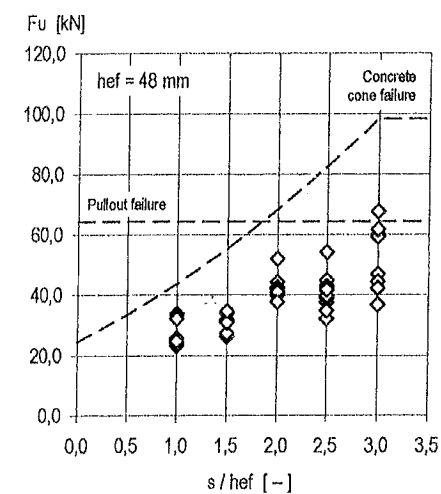
Fig. 3 Centric tension tests at the IWB with bonded anchors M12: Influence of spacing for quadruple fastenings, h_{ef} = 48 / 96 / 144 mm, comparision with CC- method

Fig. 4 Centric tension tests at the IWB with bonded anchors M12: Influence of spacing for quadruple fastenings, h_{ef} = 48 / 96 / 144 m, comparision with modified CC- method

ation v = 24,3 % (Fig. 5). In the case of tests with quadruple fastenings used an other mortar than at the Imperial Collage and at the IWB [5], there can be found the factor α = 0,87 with a standard devition of s = 0,13 and a coefficient of variation v = 11,5 % (Fig. 6).

$$N_U = A_{c,N} / A_{c,N}^0 \cdot N_u^0 \cdot \psi_{s,N} \tag{3}$$

with:
$N_u^0 = 13,5 \cdot f_{cc}^{0,5} \cdot (\alpha \cdot h_{ef})^{1,5}$ (Quadruple anchorgroup far away from the edge)
$A_{c,N} = (s + 3 \cdot \alpha \cdot h_{ef})^2$ (Single anchor at the edge)
$A_{c,N} = 3 \cdot \alpha \cdot h_{ef} \cdot (c + 1,5 \cdot \alpha \cdot h_{ef})$
$A_{c,N}^0 = 9 \cdot (\alpha \cdot h_{ef})^2$ α from tests
$\psi_{s,N} = 0,3 + 0,7 \cdot c / (1,5 \cdot \alpha \cdot h_{ef})$
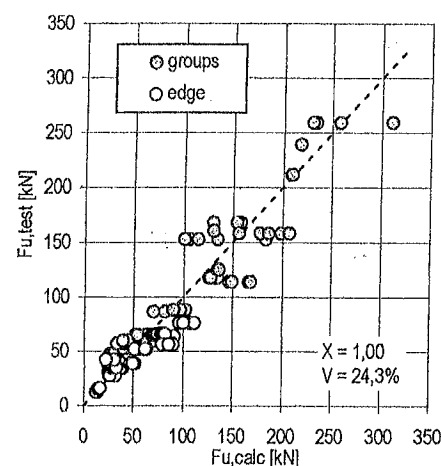
Fig. 5   Comparision of measured and calculated failure loads: test results from IWB and mperial College (α = 0,73)
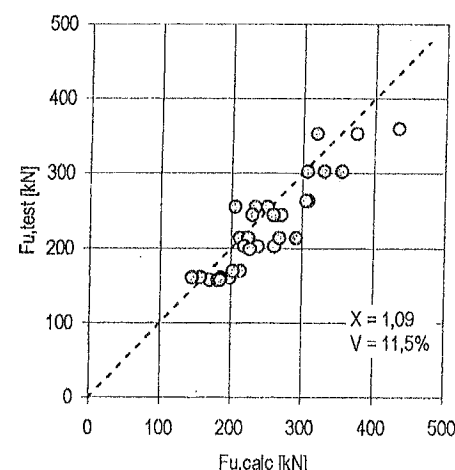
Fig. 6   Comparision of measured and calculated failure loads: test results from University of Florida (α = 0,87)

Our next study will simulate the behavior of unconfined single bonded anchors and quadruple fastenings with bonded anchors using the finite element method.

6. CONLUSIONS

A lot of tests were carried out with bonded anchors at the IWB and the Imperial College [2,3,5]. The load bearing behavior of these anchors, which are fail with a concrete cone failure or a combined concrete cone failure with bond failure, seems to be similar to that predicted by the modified CC-method.

Factor α, wich is needed to consider h_{ef}, seems to depend on the type of mortar and the embedmenth depth. Further tests are needed to study the influence of the concrete strength, the type of mortar and the embedment depth on the behavior of anchor groups.

Numerical simulations should be carried out to clarify the failure mechnanism of simple anchors and anchor groups.

7. REFERENCES

[1] Cook R.A. et al., "Adhesive-Bonded Anchors: Bond Properties and Effects of In-service and Installation Conditions", *Structures and Materials Research Report No. 94-2A*, Draft Final Projekt Report, Dezember 1994

[2] Eligehausen R., Lehr B., "Design of Fastenings with Bonded Anchors", *IWB-Report No. 20/4-96/8*, Stuttgart 1996

[3] Popo-Ola S.O., Newman J.B., "Centric Tensile Tests of Bonded Anchors in Non-cracked Concrete", *IWB-Report No. 20/3-95/17*, London 1995

[4] Rehm G., Eligehausen R., Mallee R.: "Befestigungstechnik", in *Betonkalender*, Ernst & Sohn, Verlag für Architektur und technische Wissenschaften, Berlin 1992.

[5] Spieth, H.: Bemessung von Befestigungen mit Verbunddübeln in ungerissenem Beton, *Diplomarbeit* am Institut für Werkstoffe im Bauwesen, Stuttgart 1995.

SAFETY OF REINFORCED CONCRETE STRUCTURES AS A FUNCTION OF CONCRETE STRENGTH

Zoltán Orbán
Technical University of Budapest, Department of Reinforced Concrete Structures
H-1521 Budapest

1. INTRODUCTION

Construction industry nowadays places more and more demand on the material properties of concrete and by that the importance of tensile strength has also increased. As an example tensile strength of concrete became an important material parameter in airport and roadway paving applications as well as in industrial concrete floors, building floors or roof decks where flexural failure is more probable than failure in compression. Tensile strength was long considered inferior and negligible compared to compressive strength.

Current researches prove, however, that the significance of tensile strength in structure resistance is equal or even higher than that of compressive strength.
In most cases the variability or relative uncertainty in tensile strength influences structural safety more unfavourably than that in compressive strength.

Tensile strength is usually derived from the compressive strength of concrete but this relation shows a great uncertainty.

This study first deals with the reasons of uncertainty and then there is a brief summary on what we mean by safety and how we can calculate it. In the second part an example shows the effects of the above mentioned strength properties on the safety level of a reinforced concrete beam.

2. UNCERTAINTY IN TENSILE STRENGTH

Origin and determination of tensile strength is a major argument point. Standards derive the tensile strength exclusively from the compressive strength based on different empirical relations that are mainly regression curves fitted to experimental results. These usually are in the form of $f_t = a \cdot f_c^k$, where f_t is the tensile strength, f_c is the compressive strength of concrete, a and k are constants. They also show big variance in the determination of tensile strength especially for the high strength concrete (Fig.1). This is not merely the result of varying cautiousness of standard makers but it also comes from the fact that at the different experiments the conditions influencing the strength properties of concrete are usually not the same.

As we all know the strength of concrete depends on several parameters and many of these have different effect on tensile and compressive strength. Therefore it is not possible to find a general relation between the tensile and compressive strength.

To find a more accurate formula for the relation between the strengths we should involve other material parameters beside the compressive strength.
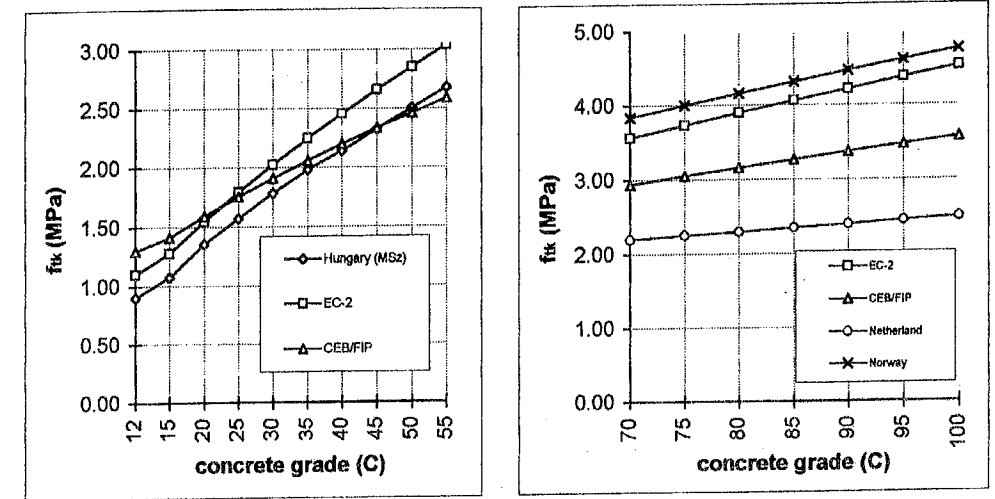
a) for normal strength concrete *b) for high strength concrete*

Fig.1   The characteristic values of concrete tensile strength (f_{tk}) versus concrete grade according to different standards

3. SAFETY OF STRUCTURES

3.1 Definition of safety

The relative uncertainty of parameters involved in structural analysis and design is an important factor influencing structural safety. The reliability of a structure is defined as the complement of the probability of failure and represents the probability that the structure will not fail.

Reliability = $1-p_f$, where p_f is the probability of failure.
In other words reliability refers to the probability that the structural loads do not exceed the structure's ability to resist them.
The safety is satisfactory if $prob[R - S = Z \geq 0] \geq 1 - p_{RS}$, where p_{RS} is the acceptable probability of failure, Z is the safety margin or failure function, R is the resistance and S is the load effect. Both S and R are treated as random variables. Failure occurs if Z is less than or equal to zero.

Structural safety can be conveniently measured with the so called *safety index* (β) as

$$\beta = \frac{\overline{Z}}{\sigma_Z}$$,in which $\overline{Z}$ and σ_Z refer to the mean value and the relative standard deviation of Z, respectively. This measure is directly related to the probability of failure (Fig.2).
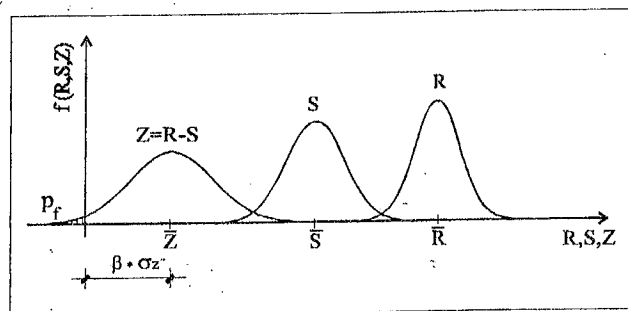
Fig. 2 Geometrical representation of safety index (β)

3.2 Calculation of safety

The theory of reliability has developed rapidly in the last decades. Several probabilistic methods have been worked out in order to calculate the safety level of structures. These include methods like exact methods, first-order reliability methods (FORM), second - order reliability methods (SORM) and point estimation methods. Due to the difficulties in using the above mentioned methods the distribution of random variables are usually assumed to be normal or close to normal in order to simplify the calculation.

However, if the number of factors is extremely large or they show significant difference to the normal distribution or the analytical method is impossible to use for some other reason it is the Monte-Carlo simulation that can be used effectively. In this method a random number generator is used to generate individual simulations. Disadvantage of the method that numerical complications arise when the probability of failure is relatively small.

4. RESULTS OF THE ANALYSIS

In the analysis the structural safety dependence on the strength properties of concrete is shown using a reinforced concrete beam as an example. Two types of failure have been examined. In the first case the resistance(R) is the resistance moment of the beam's cross section and is determined by the compressive strength of the concrete(f_c). In the second case R is the cracking moment of the cross section and is determined by the tensile strength(f_t).

Both the material and geometrical parameters as well as the load effect were treated as random variables. For the relative standard deviations of the parameters the current CEB assumptions were used. The probability distribution functions for all parameters were assumed to be normal. The mean value and the relative standard deviation were fixed in each parameter except in the strength parameters of concrete.

For the sake of simplicity it is assumed that the probability of failure in the structure is equal to the probability of failure in the cross section. Monte-Carlo simulation was used for calculation.
Figure 3 and Figure 4 show the effect of changes in the mean value and the relative standard deviation of concrete compressive- and tensile strengths on the safety level of the beam.

As we can see, the safety index (β) and the probability of failure (p_f) are significantly dependent on the relative standard deviation of the tensile strength in the case of analysing the safety for cracking (Fig.3/b). It is important to observe that the safety cannot be improved significantly by increasing the mean value of tensile strength if there is a great relative uncertainty in it. There is a definitely less dependence in the case of analysing ultimate flexural capacity in which the resistance is determined by the compressive strength of concrete (Fig.3/a).

a) R = Resistance Moment   *b) R = Cracking Moment*
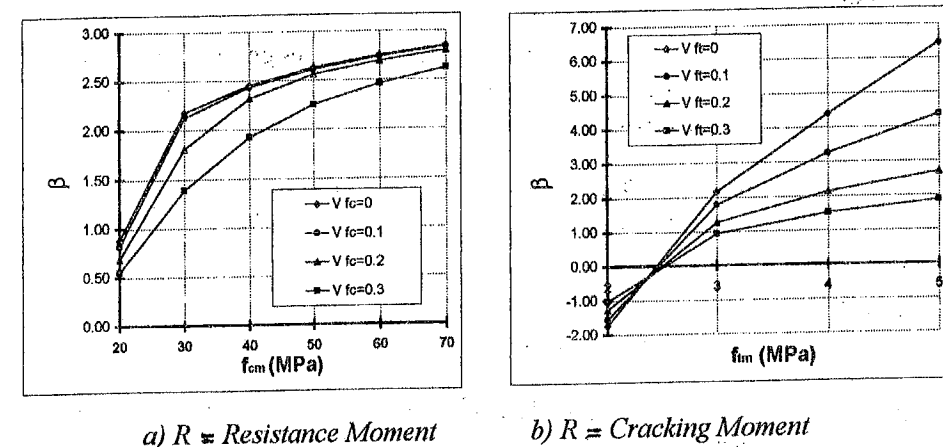
Fig. 3   The compressive and tensile strength of concrete versus β using different coefficients of variation

5. SUMMARY AND CONCLUSIONS

The study provides an example how unfavourably can the high relative standard deviation of tensile strength influence the structural safety of a reinforced concrete beam. In reinforced concrete structures the structural resistance often depends on the tensile strength of concrete significantly, and in many cases linearly. Contrary to that, compressive strength generally has not such a big effect on resistance except the cases of compressive strength generally has not such a big effect on resistance except the cases of elements under compression. In addition considering that the method to derive tensile strength from compressive strength encompasses major uncertainty (see Chapter 2) it is obvious that there is a contradiction in using exclusively compressive strength in the determination of tensile strength.

Three possible ways of solution:
1. Using the existing formulas, but considering their uncertainties.
2. To create more accurate formula for the relation between tensile-and compressive strength by involving other parameters which have effect on strength properties.
3. In cases when importance of tensile strength is particularly large it is necessary to determine it directly by test (splitting test, bending test, pure tensile test, etc.).

A designer should always be aware of the effect of all parameters involved and their relative uncertainty on the structural safety. In cases when the examined parameter has major impact on the safety level it requires special attention to determine its value with the least possible uncertainty.

REFERENCES

[1] Pulido,J.E., Jacobs,T.L., Prates de Lima,E.C., "Structural Reliability Using Monte-Carlo Simulation with Variance Reduction Techniques on Elastic-plastic Structures", *Computers & Structures*, Vol.43, No3,1992, pp.419-430.

[2] Tabsh, S.W.,"Stuctural Safety of Post-Tensioned Concrete Slab Bridges with Unbonded Tendons", *ACI Structural Journal*, Vol.92, No.4,July-August1995, pp.488-494.

[3] Ashraf,M., Rosowsky,D.V., Chen,W., "Partial Factor Design for Reinforced Concrete Building During Construction", *ACI Structural Journal*, Vol.91, No.4, July-August 1994,pp.475-485.

[4] Al-Harthy,S., Frangopol,D.M., "Reliability Assessment of Prestressed Concrete Beams", *Journal of Structural Engineering*,Vol.120, No.1,January 1994, pp.180-199.

[5] Szalai,K.,"Design Models for Reinforced Concrete Structures", *Newsletter Technical University of Budapest*, Vol.7, No.3,1989, pp.32-47.

[6] Rokugo,K., Uchid,Y., "Fracture Mechanics Approach to Evaluation of Flexural Strength of Concrete", *ACI Materials Journal*, Vol.92, No.5, Sept-Oct.1995,pp.561-566.

[7] CEB-FIP Model Code 1990, *Thomas Telford London*, 1993.

[8] CEB Bulletin d'Information No.202.,"Reliability of Concrete Structures", July 1991.

[9] CEB Bulletin d'Information No.222.,"Application of High Performance Concrete", Nov. 1994.

[10] Szalai K.,"Vasbetonszerkezetek (Reinforced Concrete Structures)", *Tankönyvkiadó Budapest*,1988.

[11] Mistéth E.,"Erőtani méretezés valószínűségelméleti alapon (Detailing with probabilistic method)", *ÉMI kidványsorozata*, 23. szám,1974.

[12] Balázs Gy.,"A beton húzószilárdsága (The tensile strength of concrete)", *BME Építőanyagok Tanszék 11/74. sz. kutatási jelentése*, 1974.

[13] Balázs Gy.,"A beton húzószilárdságának viszonyszámai (Tensile to compressive strength ratios)", *BME Építőanyagok Tanszék 23/76. sz. kutatási jelentése*, 1976.

[14] Deák I.,"Véletlenszám-generátorok és alkalmazásuk (Random number generators and their applications)", *Akadémiai Kiadó Budapest*, 1986.

LOCAL SHRINKAGE AND TEMPERATURE GRADIENTS IN REINFORCED SURFACE LAYERS OF CONCRETE STRUCTURES

Dipl.-Ing. S. Kranz
Universität (TH) Karlsruhe, Institut für Massivbau und Baustofftechnologie
D-76128 Karlsruhe

1. INTRODUCTION

Concrete structures which are reinforced near the surface are damaged by shrinkage of the concrete surface layers, especially under the influence of wind action and high local temperature gradients.

The latter are of importance, if long-term warming of concrete structures is followed by quick cooling together with the influence of moisture, as can happen e.g. after storms with wind and rain. In addition to these defects, stresses in concrete structures are created if they are strengthened by the addition of a top layer of new-cast concrete. These stresses must be transmitted between new and old concrete.

This project will explore, to what extent damage through shrinkage of the surface layers and locally high temperature gradients can be expected in these layers due to inclined principal tension stresses, as well as the degree at which such stresses can be mechanically influenced by reinforcement.

2. CALCULATION OF TEMPERATURE AND MOISTURE FIELD

As a first step a finite element programme was developed, which allows the numerical solution of the coupled temperature and moisture transport problems. The knowledge of the moisture distribution allows the calculation of shrinkage and swelling due to changes of the moisture content. By means of the coupled calculation it is (among others) also possible to consider the cooling of a surface, resulting from the evaporation of water from the surface. The programme further considered the possibility of the calculation of the process of hydration depending on actual temperature. The last-named point in particular is necessary for determining the chronological development of the material characteristics of concrete depending on the degree of hydration.

The temperature distribution is calculated according to the Fourier equation. The consideration of the temperature-dependent process of hydration was done according to the formulation of Laube [6].

For the calculation of the moisture field the formulation of the so-called moisture potential according to Kiessl [5] is used. To describe the mechanism of moisture flow in multilayer structure elements, Kiessl derived a relation between the water content u of a material and the corresponding "moisture potential" Φ. Fig. 1 shows this relationship schematically with an example for concrete.

The system of these differential equations which have to be solved, sounds:

$$c_\vartheta \cdot \dot{\vartheta} - \nabla^T \left(k_\vartheta \cdot \nabla \vartheta \right) = Q_\vartheta + \left[\nabla^T \left(k_\vartheta^\Phi \cdot \nabla \Phi \right) - c_\vartheta^\Phi \cdot \dot{\Phi} \right] \tag{1.1}$$

$$c_\Phi \cdot \dot{\Phi} - \nabla^T \left(k_\Phi \cdot \nabla \Phi \right) = Q_\Phi + \left[\nabla^T \left(k_\Phi^\vartheta \cdot \nabla \vartheta \right) - c_\Phi^\vartheta \cdot \dot{\vartheta} \right] \tag{1.2}$$
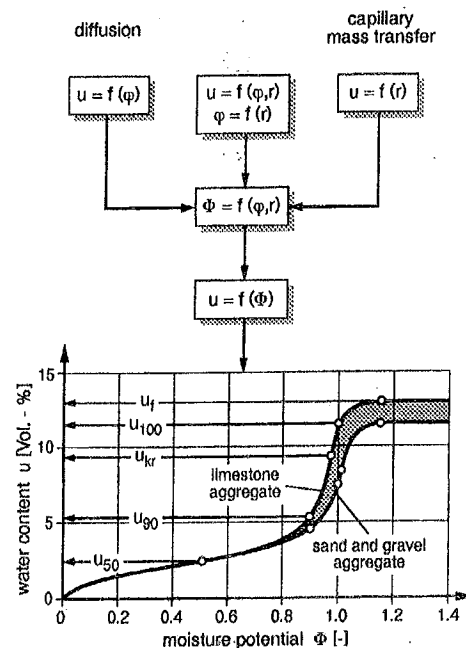
Fig. 1 *Definition of the moisture potential according to Kiessl [5] on the basis of the sorptionisotherm and the integral pore-size-distribution*

Equation (1.1) describes the heat conduction, equation (1.2) the moisture flow. The term Q_ϑ contains among others the heat produced by hydration. The bracketed term of equation (1.1) describes the influence of moisture on the heat conduction (e.g. evaporation). The coefficients c_Φ and k_Φ of equation (1.2) contain the contributions from diffusion process and capillary mass transport respectively. The influence of the temperature on the diffusion process is considered in the bracketed term of equation (1.2).

3. NUMERICAL MODEL FOR STRESS CALCULATIONS

After calculating the distribution of temperature, moisture content and the degree of hydration within the structure at different time points, their consequences on the structure can be calculated in the following stress analysis.

The rheological model to describe the material properties is composed of three elements in numerical order (Fig. 2): (1) an element, which describes cracking of concrete under tensile stress, (2) a visco-elastic element for the description of elasticity and creep, as well as (3) an element for the description of strains due to shrinkage and thermal dilatation.

The central element of the material model is the mathematical description of the visco-elastic behavior of concrete. Alongside the elastic behavior creep has also to be considered in the stress calculation. Creep as part of the model is described by means of a compliance-function. Here the double power law is used according to Bažant [1], with an extension for young concrete developed by Emborg [4].

To describe cracking a smeared crack-model according to de Borst/Nauta [3] is used.
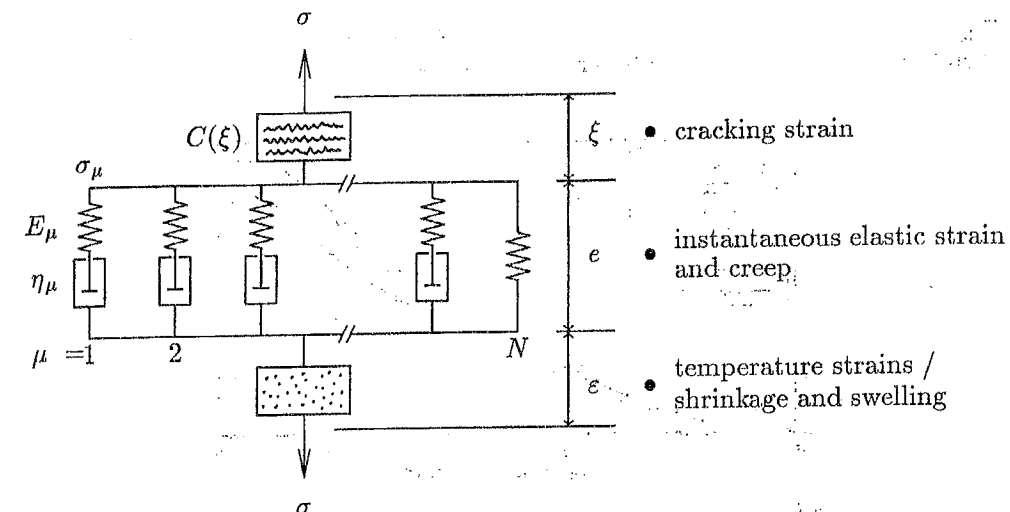
Fig. 2 *Rheological model to describe the deformation of concrete under tensile load (according to [1])*

The last element describes the strains due to temperature and/or shrinkage and swelling due to the changes of the moisture content. Shrinkage, which is understood as a strain resulting from the drying process, is considered to be a function of the moisture potential Φ. Within the calculation, it is described incrementally:

$$\Delta\varepsilon_s = \kappa \cdot \Delta u = \kappa \cdot \frac{du}{d\Phi} \cdot \Delta\Phi \qquad (2.1)$$

in which κ is an (incremental) shrinkage coefficient and $du/d\Phi$ is the first derivative of the moisture potential curve. The influence of the concrete composition is reflected both in the course of the moisture potential curve, as well as in the coefficient κ.

4. ACCOMPLISHED EXPERIMENTS

To be able to perform an investigation of the problems presented above, the material model had to be checked by means of experiments.

Non-linear moisture gradients in concrete structures lead to a deformation gradient in the plane of the cross-section. Its linear part causes elongation and deflection, which lead to stresses if the structure is restrained by other stuctures or supports. Due to the condition that the cross-section has to remain plain, the non-linear part of the deformation is prevented and leads to residual stresses.

In a first series of tests shrinkage deformations due to the drying process were determined. The start of drying was at a concrete age of 1 day. For all test series a concrete of quality B35 (according to German standard) with a water-cement-ratio of 0.60 was used. At the end of a certain drying time the thermal expansion coefficient and the tensile strength were determined.

In addition to the tests described above, further investigation for the estimation of the order of diffusivity was accomplished by means of separately manufactured specimens.

Fig. 3 and 4 show the results obtained from the tests on the history of drying and shrinkage. The numerical results are presented too.
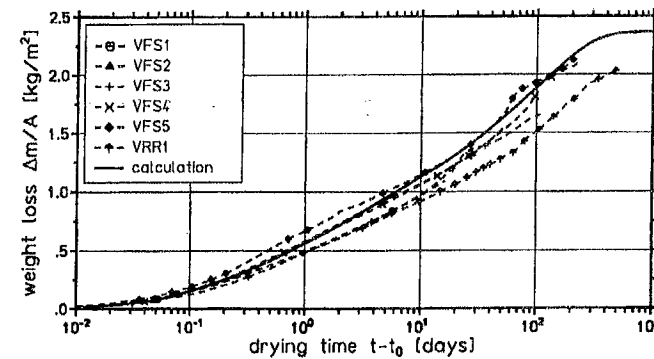
Fig. 3 *measured and calculated weigth loss of the specimens*
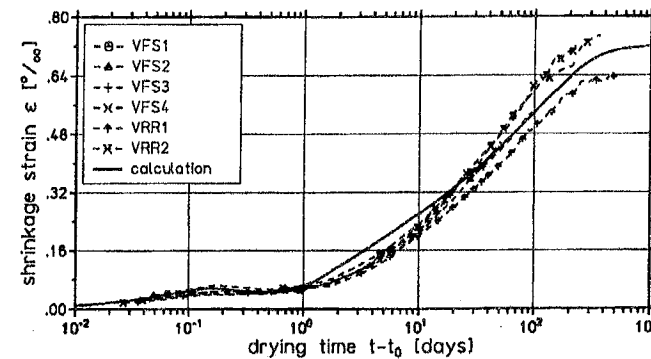
Fig. 4 *measured and calculated shrinkage strains*

In the second series of tests the development of stress was determined, by restraining the deformation due to shrinkage. For this the principle of a cracking frame was chosen allowing continuous measurement of stress development [2].

Three similar cracking frames were constructed with dimensions ensuring that 70-75% of the expected deformation could be prevented. The proportion of shrinkage deformation not prevented was also measured using 3 separate control specimens. The difference between the two deformation measurements corresponds to the deformation of the concrete, which causes stress.

The temperature measurement which was done in addition, showed a cooling of the specimens of about 3°C within the first 12 hours after the start of drying. This was due to evaporation of water from the surface.

The measured deformation-history of the specimens and the development of the stresses are presented in Fig. 5 and 6. The results calculated were recorded for purposes of comparison.

By combining the measured stress and the equal point in time of the measured concrete strain in one diagram and doing that for all time points measured, one obtains a "stress-strain-relation", which also shows the influence of creep. To elucidate this influence, the determined stress-strain-curves, which were obtained by direct tensile tests at the age of 28 and 56 days respectively, are presented in Fig. 7. As Fig. 7 shows, the calculated curve correlates well with the test results.
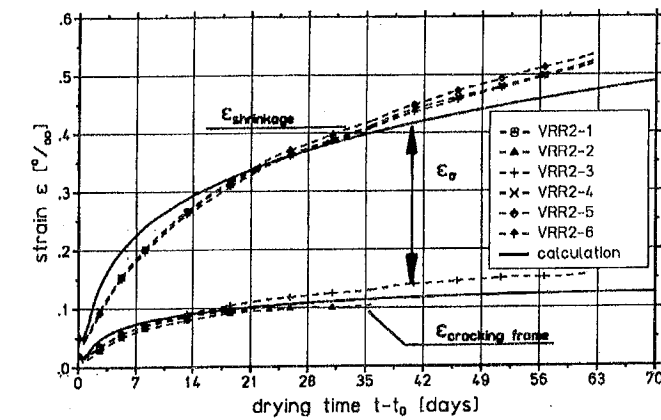
Fig. 5 *measured and calculated deformations of the unrestrained specimens (upper curve) and of the restrained specimens (lower curve)*
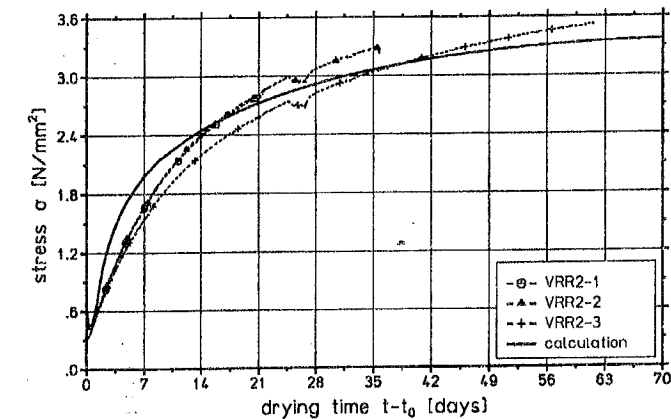
Fig. 6 *measured and calculated stresses of the restrained specimens*
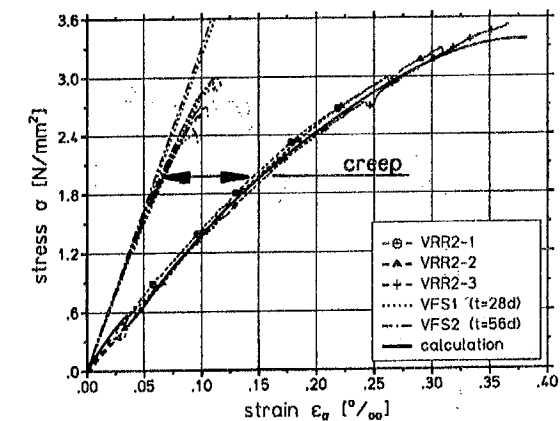
Fig. 7 *measured and calculated stress-strain-relation of the restrained specimens*

5. STRESS CALCULATIONS IN PROGRESS

On the basis of the influences outlined and the comprehensively presented material model initial precalculations for determining the demands of additionally strengthened cross-sections with reinforcement were carried out. A concrete slab with an additional concrete layer was simulated by means of FE-technology. The "old" concrete slab had a thickness of 20 cm and the additional concrete top layer was 5 cm thick.

In a first calculation the temperature distribution $\vartheta(\mathbf{x}, t)$ resulting from the process of hydration of the young concrete and the moisture distribution $\Phi(\mathbf{x}, t)$ from the drying process were determined. For simplification the non-stationary temperature and moisture movement was considered one-dimensional over the whole cross-section.

As a basis for calculation, the following procedure was undertaken: The concrete top layer was cured for 1 day and afterwards allowed to cool and dry unhindered. The environmental conditions had a temperature of 20°C and a relative humidity of 78%, similar to average European conditions. The existing slab, which was already several years old, therefore had the same pre-requisites. The slab was not wetted before the casting of the young concrete. The initial temperature of the top layer was measured at $\vartheta = 20°C$ and the initial moisture content at $\Phi = 1.0$. For the calculation of the moisture transport, the transport coefficients and the moisture potential curve were taken from the work of Kiessl.

Fig. 8 represents the temperature distribution resulting from the process of hydration within the top layer for different points in time. Fig. 9 shows the calculated distribution of the moisture content and the volumetric water content over the whole cross-section for different points in time.
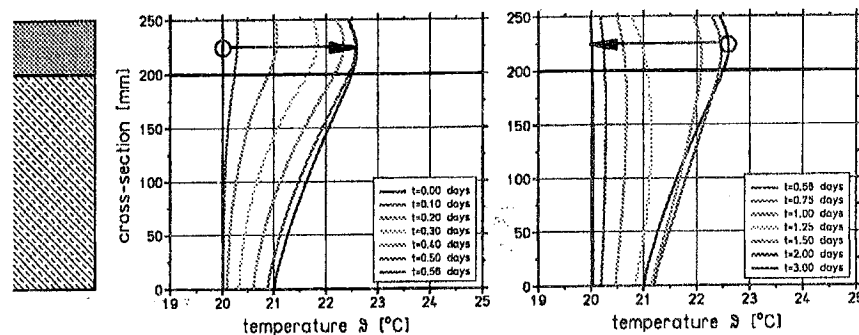
Fig. 8 *calculated temperature distribution over the whole cross-section at different time points (left: heating phase ; right: cooling phase)*
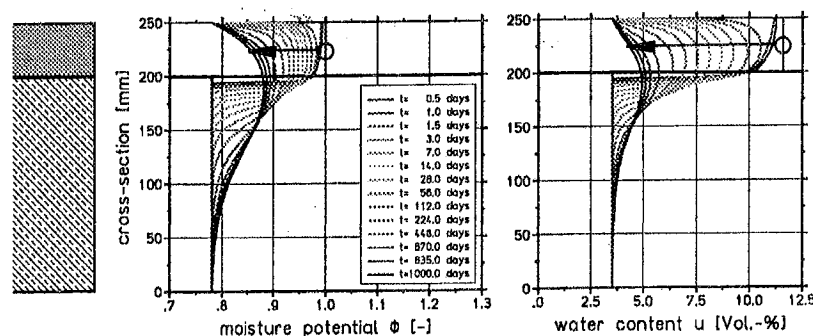
Fig. 9 *calculated distribution of moisture potential and volumetric water content over the whole cross-section at different time points*

In the following stress analysis the calculated state-variables "temperature" and "moisture potential" were procured in each element for the determination of the respective deformations. The material parameters of the young concrete could be set depending on the degree of hydration, which was determined in the prior calculation. For this the correlations published by Laube [6] were used.

Fig. 10 shows the calculated stress distribution over the entire cross-section at different points in time. Beside the non-linearity of the stress distribution of the top layer, the development of the crack depth is clear to see. Reinforcement was not considered in these first precalculations. This leads to the next stage of the project, and entails variation of several parameters.
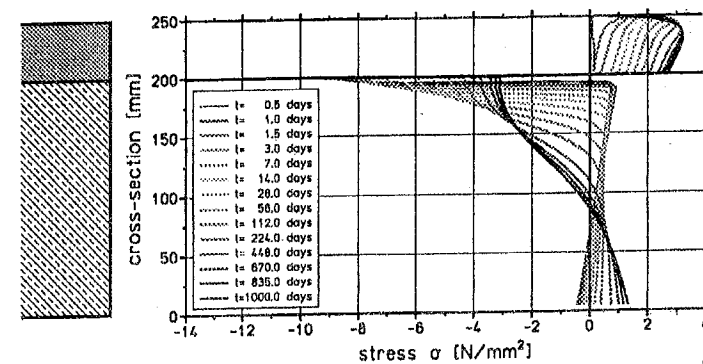
Fig. 10 *stress distribution over the whole cross-section at different time points*

7. CONCLUSIONS

First of all, a finite element programme was developed, allowing the calculation of the coupled heat and moisture movements. Further, a model for the non-linear calculation of the resulting stresses was presented. With the help of experiments, the necessary input parameters for the realistic description of shrinkage and creep were determined. By means of an initial precalcultion mathematical results could be obtained, which reflect the essential effects of the system explored.

In the next stage of the project a parameter study will be carried out, in which the essential influencing parameters will be varied systematically, to develope guidelines in the choice of a suitable reinforcement for additional top layers of concrete.

8. REFERENCES

[1]   *Bažant, Z.P.*(Editor) : Mathematical Modeling of Creep and Shrinkage of Concrete, Jon Wiley & Sons, 1988

[2]   *Breitenbücher, R.* : Zwangsspannungen und Rissbildung infolge Hydratationswärme, Dissertation Technische Universität (TU) München, 1988

[3]   *de Borst, R. / Nauta, P.* : Non-orthogonal cracks in a smeared finite element model, Eng. Comput., Vol. 2, March, 1985

[4]   *Emborg, M.* : Thermal Stresses in Concrete Structures at Early Ages, Doctoral Thesis, University of Technology Luleå, 1989

[5]   *Kiessl, K.* : Kapillarer und dampfförmiger Feuchtetransport in mehrschichtigen Bauteilen, Dissertation Universität (GH) Essen, 1983

[6]   *Laube, M.* : Werkstoffmodell zur Berechnung von Temperaturspannungen in massigen Betonbauteilen im jungen Alter, Dissertation Universität Braunschweig, 1990

BEHAVIOUR OF NON-METALLIC REINFORCEMENTS

Mazen Makt
Technical University of Budapest
Department of Reinforced Concrete Structures
H-1521 Budapest

1. INTRODUCTION

Mechanical behaviour of non-metallic (FRP) reinforcements (made of carbon, Aramid or glass fibers) is different from that of steel reinforcements. Modelling, design and application of non-metallic reinforcements requires special concern [1].

These materials are generally used for prestressing of structural elements owing to their high strength. Non-prestressed applications are also possible.

Non-metallic reinforcements are composites made of two components:

1. parallel 5 to 20 mm diameter high strength fibers
2. embedded into epoxy or polyester resin.

2. DISCUSSION

Strength and modulus of elasticity of the matrix are much less, however, strain at failure of the matrix is much higher than those of the fibers. Nevertheless, the bahaviour of the composites is governed by the behaviour of the fibers themselves.

Available test results generally reflect the behaviour of fibers and reinforcing elements. However, some tests have been already carried out on structural elements as well.

2.1 Advantages

Non-metallic reinforcements provide the following advantages [2]:

- non-susceptibility to electrolytic corrosion
- high strength
  (high strength to weight ratio)
- high fatigue strength
- lightness
  (easy to handle)
- non-magnetic conductivity
- low relaxation

2.2 Disadvantages

Following disadvantages of non-metallic reinforcements should be considered as well [2]:

- high price
- brittle type failure
- low strain at failure
- low transverse strength
- low modulus of elasticity (for some of them)
- need for special anchoring element

3. APPLICATIONS

Application of non-metallic prestressing reinforcement is still rather limited. Main reason is their high price. There have been already a bridge constructed in Canada over the Assiniboine River, in Minatoba [3] totally reinforced by FRP reinforcements. Both the prestressing cables and the stirrups were made of carbon fibers. The bridge consists of five spans, 32.5 meters each, covering a total length of 165.1 m. All the bridge girders are precast pretensioned and simply supported. The bridge girders have an I section transversely spaced at 1.8 m and supporting 187 mm thickness deck slab (Fig.1)
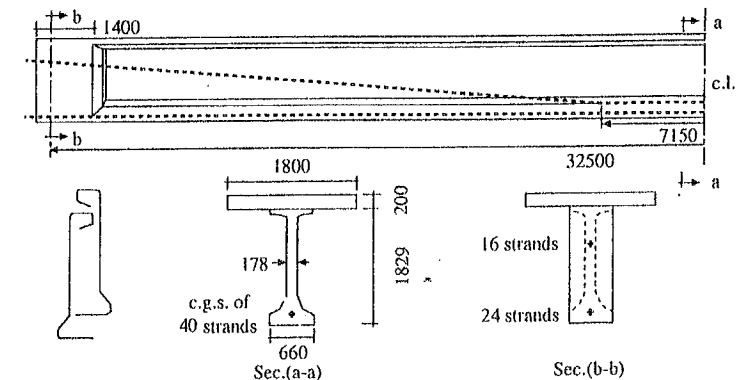
Fig.1 Pretensioned concrete bridge girders totally reinforced by FRP reinforcements (Assiniboine River, Minatoba, Canada) [3]

Another large field of application is the retrofitting of structures using carbon fiber strips.

4. CONCLUSIONS

From point of view of corrosion, static and fatigue strengths, weight, non-magnetic conductivity and low relaxation, non-metallic reinforcements are very promising.

Some disadvantages like high price, brittle type failure, low transverse strength and need for special anchoring elements are to be overcome.

5. ACKNOWLEDGEMENTS

6. REFERENCES

[1] RILEM, "Non-Metallic (FRP) Reinforcement for Concrete Structures", *Proceedings of the 2nd International RILEM Symposium (FRPRCS-2)*, ed. L. Taerwe, E & FN Spon Lodon, 1995

[2] Rostásy, L., "Non-Metallic Reinforcements" *State-of-the-Art Report* (in preparation as an FIP report), 1996

[3] Fam, A.Z., Abdelrahman, A.A., and Rizkalla, S.H., "FRP Flexural and Shear Reinforcements for Highway Bridges in Manitoba, Canada", *Proceedings of the 2nd International RILEM Symposium (FRPRCS-2)*, ed. L. Taerwe, E & FN Spon Lodon, 1995, pp. 395-402.

ON THE STATICAL PROBLEMS FOR DETERMINATION OF THE FORM OF PRESTRESSED TENTS

Dóra Pálfalvi
Technical University of Budapest, Department of Reinforced Concrete Structures
H-1521 Budapest

1. INTRODUCTION

The main attribute of tent structures is the negligibly small bending stiffness. That is why tents are perfect applications for the membrane shell theory. Critical load of shells is in connection with the bending stiffness, thus, critical compressive stress at tents is also negligibly small. If compressive stress should rise, the tent becomes wrinkled and performs as a rule, greater displacements than permitted at engineering structures. That means, compressive stress must not rise on any place of the tent under any load cases. That can only be achieved with prestressing the canvas. There are two possibilities for prestressing tents. The one is a stretch along the borders, the other operates with internal pressure of air or sometimes of liquid. My research deals with stretched tents.

The behaviour of tent structures is somehow analogous to soap-films [4]. Putting a wire frame into soap-solution and lifting it out, a membrane will stretch on the frame. Ignoring the negligibly small dead-load the membrane can assumed as unloaded, that is, its shape is determined by the action of uniform tensile surface stress. The membrane is in a hydrostatic self stress state. The shape of the surface is called minimum-surface, because the surface stress stretches the membrane onto the smallest surface area.

The analogy between tents and soap-films suggests a way for finding the optimum form of a tent where the task is to determine a shape that can be prestressed by uniform membrane tension: surfaces developing hydrostatic membrane self stress states are the same as surfaces having the smallest surface area, that is, minimum-surfaces.

There are two varieties of membranes that exhibit stress states called hydrostatic stress states. One is the "real membranes" when membrane stresses themselves are hydrostatic, another when principal projected stresses are equal. Membranes exhibiting the latter state of stress are called after the Hungarian professor, József Pelikán, "Pelikán membranes" [3]. Pelikán's idea was that membrane stresses and reduced membrane stresses slightly differ from each other, if the slopes of the membrane are not too high, hence, surfaces exhibiting hydrostatic reduced membrane self stresses may be good approximations for "real membranes". Actually, in case of flat surfaces the difference between "Pelikán membranes" and "real membranes" is small, but it becomes significant if the slope increases. The main advantage of "Pelikán membranes" is that their shape is defined (as shown in the sequels,) by a simple linear partial differential equation while that of real membranes emerges as the solution of a rather complicated non-linear differential equation.

The aim of the lecture is to show how Pelikán's idea can be used in determining optimum shapes of tents as minimum-surfaces or "real membranes".

2. PUCHER'S DIFFERENTIAL EQUATION FOR "PELIKÁN MEMBRANES", AND "REAL MEMBRANES"

The equilibrium equations of forces [2] acting on at a surface element cut from an unloaded membrane are two equations that are automatically met by membrane forces obtained by a stress function F and a third one, that is met if F meets Pucher's differential equation:

$$\frac{\partial^2 z}{\partial x^2} \cdot \frac{\partial^2 F}{\partial y^2} - 2 \cdot \frac{\partial^2 z}{\partial x \partial y} \cdot \frac{\partial^2 F}{\partial x \partial y} + \frac{\partial^2 z}{\partial y^2} \cdot \frac{\partial^2 F}{\partial x^2} = 0 , \qquad (2.1)$$

where z - equation of the shell-surface,
$\quad\quad\quad F$ - Pucher's stress function.

In the equation (2.1) the derivatives of F mean the projections of membrane forces (also called reduced forces):

$$\frac{\partial^2 F}{\partial y^2} = n_x, \quad \frac{\partial^2 F}{\partial x \partial y} = -n_{xy}, \quad \frac{\partial^2 F}{\partial x^2} = n_y,$$

where n_x, n_y - tensile reduced forces,
$\quad\quad\quad n_{xy}$ - shearing reduced force.

Pucher's differential equation expresses the equilibrium of vertical components of forces acting on at the surface element. Replacing the derivatives of F for the reduced forces it takes the form:

$$\frac{\partial^2 z}{\partial x^2} \cdot n_x + 2 \cdot \frac{\partial^2 z}{\partial x \partial y} \cdot n_{xy} + \frac{\partial^2 z}{\partial y^2} \cdot n_y = 0 , \qquad (2.2)$$

Substituting the conditions of "Pelikán membranes" into equation (2.2), it becomes a harmonic differential equation because no shearing reduced forces act:

$$n \cdot (z_{xx} + z_{yy}) = 0 , \qquad (2.3)$$

where $z_{xx} = \dfrac{\partial^2 z}{\partial x^2}$, $z_{yy} = \dfrac{\partial^2 z}{\partial y^2}$, n is the principal reduced force.

Introducing the "real membrane" conditions into equation (2.2) yields the following rather complicated differential equation for z:

$$\frac{N}{\sqrt{1+z_x^2+z_y^2}} \cdot \left(z_{xx} \cdot (1+z_y^2) - 2 \cdot z_{xy} \cdot z_x \cdot z_y + z_{yy} \cdot (1+z_x^2) \right) = 0 ,$$

where $z_x, z_{xx}, z_y, z_{yy}, z_{xy}$ are interpreted as before, N is the principal membrane force. Since the denominator of the first coefficient term cannot take zero value, this coefficient can simply be dropped. Then after some algebraic manipulations the remaining equation for the shape function of "real membranes" can take either the form:

$$z_{xx} + z_{yy} = 2 \cdot z_{xy} \cdot z_x \cdot z_y - z_{xx} \cdot z_y^2 - z_{yy} \cdot z_x^2 , \qquad (2.4)$$

or by adding $\left(z_{xx} \cdot z_x^2 + z_{yy} \cdot z_y^2 \right)$ to both sides of the equation, and then dividing them by $\left(1+z_x^2+z_y^2 \right)$ an alternative form with the same left-hand side:

$$z_{xx} + z_{yy} = \frac{2 \cdot z_{xy} \cdot z_x \cdot z_y + z_{xx} \cdot z_y^2 + z_{yy} \cdot z_x^2}{1+z_x^2+z_y^2} . \qquad (2.5)$$

3. THE CONNECTION BETWEEN "REAL MEMBRANES" AND MINIMUM-SURFACES

A minimum surface stretched on a closed curve Γ has to meet the conditional equation

$$A = \iint_T \sqrt{1+z_x^2+z_y^2}\ dxdy = \min ! ,$$

where A means the superficies, T is the domain of integration bounded by Γ and z is the function that describes the minimum surface in Cartesian co-ordinate system xyz and bottom indices refer to partial derivativations. Function z is called the extreme of the variational problem stated by the minimum condition.

If z is the extreme of the variational problem, then its small variations do not affect the extreme value of A, that is, producing the variation function by replacing $(z+\varepsilon \cdot \delta z)$ for z the following equation must hold:

$$\lim_{\varepsilon \to 0} \frac{\partial}{\partial \varepsilon} \iint_T \sqrt{1+(z_x+\varepsilon \cdot \delta z_x)^2 + (z_y+\varepsilon \cdot \delta z_y)^2}\ dxdy = \iint_T \frac{z_x \cdot \delta z_x + z_y \cdot \delta z_y}{\sqrt{1+z_x^2+z_y^2}}\ dxdy = 0 .$$

Derivatives of δz can be eliminated from the minimum condition using partial integration. After doing so, the integral takes the form

$$\iint_T \left\{ \frac{(z_{xx}+z_{yy}) \cdot (1+z_x^2+z_y^2) - z_x^2 \cdot z_{xx} - z_y^2 \cdot z_{yy} - 2 \cdot z_x \cdot z_y \cdot z_{xy}}{\sqrt{1+z_x^2+z_y^2}^3} \right\} \delta z\ dxdy = 0 .$$

Taking equal to zero the expression closed by figure brackets one obtains the so called Euler-Lagrange's differential equation of the extreme. Since the denominator of the fractional cannot be zero, it can be dropped out of the differential equation. The remaining expression can be rearranged into the same form as (2.5), thus, extremes of the minimum surface problem also have to meet Pucher's differential equation for self stressed "real membranes", that is, the two problems define the same surface.

4. DETERMINATION OF MINIMUM SURFACES AS "REAL MEMBRANES" USING "PELIKÁN MEMBRANE" SOLUTIONS

Formally, equation (2.2) is a linear differential equation for z, easy to solve numerically, provided we know the reduced membrane forces. We may suppose that reduced membrane forces approximately form a hydrostatic state of stress as in (2.3). By so doing, we obtain the shape function of a "Pelikán membrane". Then, assuming a hydrostatic membrane state of stress on that membrane we can calculate a reduced membrane stress distribution supposedly closer to that defined by a "real membrane" than the hydrostatic reduced stress distribution. Computing again the shape function with the modified reduced stress distribution we obtain a new shape, supposedly closer to the shape of a "real membrane" than the "Pelikán membrane". Repeating this two steps may give an iteration that produces the minimum surface. A disadvantage of this method is the long running time because in every step a new coefficient matrix and its inverse has to be computed.

The conditional differential equations (2.4) and (2.5) are non-linear equations. However, the structure of these differential equations affords the way to use another iterations that do not need a step by step reconstruction and inversion of the coefficient matrix. We make use that left-hand sides of equations (2.4) and (2.5) are the same as that of (2.3), and their non-zero right-hand sides can be interpreted as a fictitious load determined by a formerly computed approximation for z.

Surprisingly, iterations based on both formulas behaved basically different. Iteration based on (2.4) proved divergent but the iteration based on equation (2.5) was convergent and produced in some steps a form close to that obtained by the extremely lengthy surface minimization. The differences mainly were found along the borders. These could also be moderated by applying there a higher order approximation formulas for the numeric derivatives of z.

5. EXPERIENCES

The MATLAB was used for programming. First the minimum-surface stretched on the membrane boundary was computed using approximate triangulation. The iteration applied the optimisation toolbox of the MATLAB. It took several hours to compute rather small surfaces: using 4×9×9 triangulated elements and 81 degree of freedom the running time was about 10 hours or more, depending on the shape of the edges. Then we determined the shape of the "real membrane" with the same borders. As mentioned before, only the iteration based on (2.5) gave a good approximation to the form of the "real membrane", and the maximum running time was below two minutes.

1. Example:
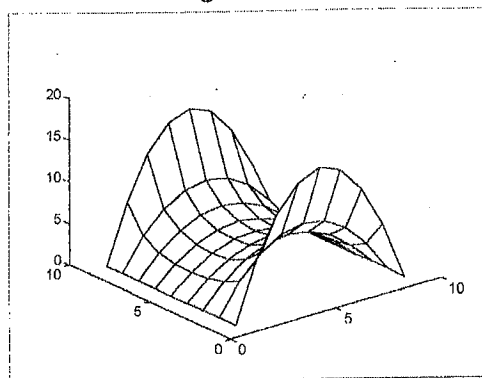
Inputs:
The measure of the matrix is 9×9, the distance between two points in one direction is 1, the edges are parabolic on two opposite sides and zero on the other two opposite sides.

Results:

area of the surface as a minimum-surface: 485.8129,
area of the surface as a "real membrane": 485.8279.

2. Example:
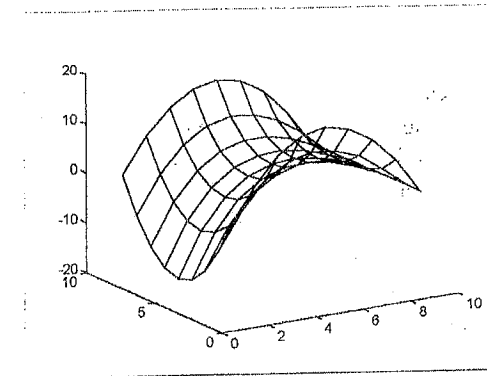
Inputs:
The measure of the matrix is 9×9, the distance between two points is 2, the edges are parabolic on two opposite sides and parabolic on the opposite direction on the third side, zero on the forth side.

Results:

area of the surface as a minimum-surface: $1.6204*10^3$,
area of the surface as a "real membrane": $1.6205*10^3$.

6. CONCLUSION

Numerous examples have shown that it is possible to construct a convergent iteration that uses a series of modified "Pelikán membrane" solutions and determines minimum-surfaces stretched on closed boundary curves as membranes with uniform hydrostatic membrane self stress. A comparison of the results of this iteration and those computed directly on the base of the geometric definition of minimum surfaces has shown very good coincidences both in the area of the surfaces and the co-ordinates of the surface points. Also a comparison was made between elapsed time that needed to determine the same surface using the one and the other principles. That has shown that computational time needed to solve the "real membrane" problem is less by magnitudes than that needed to solve directly the minimum surface problem.

7. REFERENCES

[1] Hegedűs I., "Mérnöki kontinuum feladatok differenciálegyenleteinek származtatása variációs elven", *Építési kutatás, fejlesztés*, 1986/2., pp.65-76.
[2] Hegedűs I., "Héjszerkezetek", *Manuscript*, 1992.
[3] Pelikán J., "Tartószerkezetek", *Tankönyvkiadó*, 1966.
[4] Pelikán J., "Szerkezettervezés", *Műszaki Könyvkiadó*, 1981.

WIND EFFECTS ON CABLE-STAYED STRUCTURES

Attila Péczely
Technical University of Budapest, Department of Reinforced Concrete Structures
H-1521 Budapest, Hungary

1. INTRODUCTION

Long-span cable-stayed bridges are very sensitive to dynamic effects because of their important flexibility, therefore they must be designed to withstand aerodynamic forces. Prediction of the response to wind load of line-like structures is very difficult due to the complexity of mathematical description of the atmospheric turbulence and the wind-structure interaction.

The turbulent wind brings the bridge into motion and its structural members - the deck, the pylons and the cable-stays - behave differently due to their different shapes and stiffnesses. A stochastic method has been used to determine the response of the structure and most particularly the contribution of the different structural elements.

2. WIND MODEL

2.1. Vertical wind speed variation

The airflow near the ground surface is retarded by friction forces. This effect is diffused by turbulent mixing throughout a region referred to as atmospheric boundary layer. The depth of the boundary layer normally ranges from a few hundred meters to several kilometres. The wind speed at the surface is zero and there is a continuous increase of velocity from the ground to the gradient height. A number of laws defining the variation of mean wind speed with height has been suggested, the most widely used are

- the logarithmic profile $\quad \overline{U}(z) = \dfrac{\ln(z/z_0)}{\ln(10/z_0)} \cdot \overline{U}_{10} \quad$ and $\qquad\qquad$ (2.1)

- the power law profile $\qquad \overline{U}(z) = \left(\dfrac{z}{10}\right)^{\alpha} \cdot \overline{U}_{10} \qquad\qquad\qquad$ (2.2)

where z is the height above the ground level, z_0 is the surface roughness length, α is a constant for a particular site and terrain and $\overline{U}_{10}$ is the mean wind speed measured at height 10 m.

2.2. Decomposition of the wind speed

A three-dimensional flow will have three components in three mutually perpendicular directions. In most flows of interest in wind engineering, the wind can be represented as the sum of a horizontal mean vector and three orthogonal fluctuating components:

$$U(t) = \begin{bmatrix} \overline{U} \\ 0 \\ 0 \end{bmatrix} + \begin{bmatrix} u(t) \\ v(t) \\ w(t) \end{bmatrix} \qquad\qquad (2.3)$$

the means of u, v and w being zero.

2.3. Quasi-stationary process

In the power spectrum of atmospheric wind speeds a region of low energy extends over a frequency range centred on about 1 cycle per hour. For periods corresponding to this frequency range the wind speed can be regarded as quasi-stationary. According to observations in the boundary layer, such wind speeds are suitable for estimating the wind loads on flexible structures. Consequently, for structural design the turbulent wind can be described by a quasi-stationary random process, that is, its statistical parameters, namely the mean wind speed $\overline{U}$, the mean square of velocity fluctuations σ_u, σ_v, σ_w and their covariance functions $R_u(\tau)$, $R_v(\tau)$, $R_w(\tau)$ are independent of time. The meteorological data used in the calculations consist of wind speed records measured in three directions at high sample rate during about one hour near the site of the future construction. From these records the mean wind speed, the mean square of fluctuations and other parameters are estimated by dividing the time series into subranges and averaging the results calculated on every subrange. A fast Fourier transform (FFT) is executed on the measurements to obtain the power spectra $S_u(n)$, $S_v(n)$, $S_w(n)$ of the fluctuations by adjusting an empirical function to the experimental data.

3. AERODYNAMIC FORCES

In most cases the wind loads on the structure are not directly known. The connection between the wind speed and the aerodynamic forces acting on the cross-section of the structure is taken into account by the steady aerodynamic coefficients C_x, C_y and C_m. The aerodynamic forces are then defined by the following equations:

$$f_x = \frac{1}{2} \cdot \rho \cdot B \cdot U_\perp^2 \cdot C_x(\theta)$$

$$f_z = \frac{1}{2} \cdot \rho \cdot B \cdot U_\perp^2 \cdot C_z(\theta) \qquad\qquad (3.1)$$

$$m_y = \frac{1}{2} \cdot \rho \cdot B^2 \cdot U_\perp^2 \cdot C_m(\theta)$$

where f_x is the drag force, f_z is the lift and m_y is the moment expressed in local coordinates (Fig. 1), ρ is the density of air, B is the width of the cross-section and $U_\perp$ is the velocity component perpendicular to the spanwise direction.

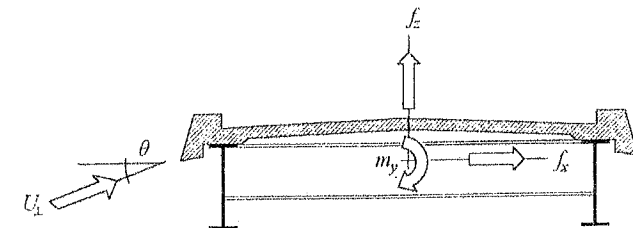*Fig. 1 Aerodynamic forces acting on the cross-section*

Since in high winds the fluctuations are sufficiently small compared to the mean velocity, higher degrees of u, v and w can be omitted. The steady coefficients are provided by reduced section model tests in wind tunnels and are used in conjunction with the theory of stationary flows. When the angle of attack is small, they can be approximated at the

first order. After a transformation into global coordinates the following equation can be derived for the aerodynamic forces:

$$f = f^{st} + f^d = \bar{f}(s) + f_u(s) \cdot u(s,t) + f_v(s) \cdot v(s,t) + f_w(s) \cdot w(s,t) \qquad (3.2)$$

where $\bar{f}$ represents the steady wind load and the remaining terms stand for the dynamic wind load.

4. DYNAMIC RESPONSE TO A STATIONARY RANDOM LOAD

As an experimental fact, it may be regarded that a continuously distributed elastic structure with low damping, submitted to an excitation, will vibrate in resonance at certain sharply-defined characteristic frequencies. Associated with each natural frequency there will also be a modal form which is independent of the loads and represents fundamental dynamic properties of the structure. By means of the set of modal forms any general deflection of the structure can be expressed.

$$x(s,t) = \sum_q \mu_q(s) \cdot x_q(t) \qquad (4.1)$$

where $\mu_q(s)$ is the modal deflection and $x_q(t)$ is called the general coordinates of the mode q. It can be shown (see [1], [2]) that if the damping ratio is small the general coordinates can be approximated by the differential equation:

$$\ddot{x}_q(t) + 2 \cdot \xi_q \cdot (2\pi n_q) \cdot \dot{x}_q(t) + (2\pi n_q)^2 \cdot x_q(t) = \frac{f_q(t) - K_q \cdot \dot{x}(t)}{m_q} \qquad (4.2)$$

with ξ_q the damping ratio, n_q the natural frequency, m_q the generalised mass and f_q the generalised force of the normal mode q. On the right-hand side of the equation the negative force represents the damping effect due to the modification of the resultant velocity by the structure's oscillation. This force, proportional to $\dot{x}(t)$, can be considered after a transformation as the aerodynamic damping.

$$\xi_q^{ae} = \frac{K_q}{4 \cdot \pi \cdot m_q} \qquad (4.3)$$

Since K_q is calculated by integration on the whole structure, the participation of the different structural elements in the response is reflected in the aerodynamic damping.

The method, known as the spectral analysis, is used to solve the differential equation Eq. 4.2. by substituting the variables $x_q(t)$ and $f_q(t)$ with their spectral density function obtained by Fourier transformation. This transformation implies a switching from the time domain to frequency domain which leads to simple linear relations between the exciting forces and the dynamic response. The differential equation takes the form

$$S_{x_q}(n) = |H_q(n)|^2 \cdot S_{f_q}(n) \qquad (4.4)$$

with $H_q(n)$ the mechanical admittance function (see [2], [4]), $S_{x_q}(n)$ and $S_{f_q}(n)$ respectively the spectral density of the general coordinates and generalised forces. This latter can be derived through the spectral density of fluctuations:

$$S_{f_q}(n) = |J_q(n)|^2 \cdot S_u(n) \qquad (4.5)$$

where $J_q(n)$ the aerodynamic admittance represents an adjustment of the correlation of various effects to preserve the validity of the above equation over the frequency range being considered. The area under the spectral density function of the general coordinates gives the mean square of the response (Fig. 2).

$$\sigma_{x_q}^2 = \int_{-\infty}^{\infty} S_{x_q}(n) \cdot dn = \int_{-\infty}^{n_0} S_{x_q}(n) \cdot dn + \int_{n_0}^{\infty} S_{x_q}(n) \cdot dn = \left(\sigma_{x_q}^{QS} \right)^2 + \left(\sigma_{x_q}^D \right)^2 \qquad (4.6)$$

In this equation $\sigma_{x_q}^{QS}$ is the quasi-static and $\sigma_{x_q}^D$ the dynamic part of the response.

5. CASE STUDY

5.1. Dynamic model

In a numerical example of a cable-stayed bridge, we will test the response of the structure to the turbulent wind. In practice, the structure's model is often simplified to its deck for dynamic analysis. We consider here the full dynamic model of the bridge examining separately the contribution of the deck, pylons and cable-stays. The structure considered here is the model of the Karkistensalmi Bridge in Finnland [3] during construction (Fig. 2). The most important vibrations due to turbulent wind are expected at the largest cantilever length just before central closure.
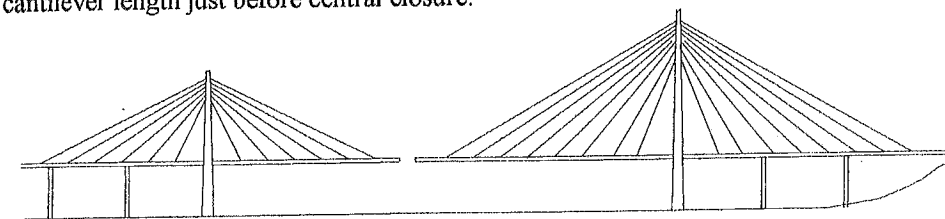
Fig. 2 The Karkistensalmi bridge - construction phase

5.2. Analysis of the response

The first ten natural frequencies and mode shapes have been calculated by the finite element program SYSTUS using beam elements and concentrated mass loads. The root mean square (r.m.s.) of the generalised coordinates is computed using the program VENTOSE [4] developed by the author, which also calculates the quasi-static and the dynamic part of the response. In our example, we study three typical vibration modes:
  - balancement of the deck,
  - the bending of the pylon perpendicular to the longitudinal axis and
  - the vertical bending of the deck.
The natural frequencies and the r.m.s. values are given in Tab 1.

Mode	Frequency Hz	Direction	Quasi-static $\sigma_{x_q}^{QS}$	Dynamic $\sigma_{x_q}^D$	Total σ_{x_q}
1	0,4037	u	0,0163	0,0218	0,0272
		v	0,0000	0,0000	0,0000
		w	0,0019	0,0088	0,0090
2	0,5524	u	0,0065	0,0065	0,0092
		v	0,0000	0,0000	0,0000
		w	0,0001	0,0006	0,0006
3	0,5625	u	0,0032	0,0084	0,0090
		v	0,0044	0,0046	0,0064
		w	0,0213	0,0781	0,0810

Tab. 1 R.m.s. values of the generalised coordinates

Values of $\sigma_{x_q}^D$ reveal the importance of the structure's dynamic amplification. $\sigma_{x_q}^{QS}$ here reflects the quasi-static variations of the wind speed corresponding to the low turbulence. It can be seen that the influence of the lateral fluctuation is small and it is mainly due to the pylon's movement in Mode 3. The major part of the response is concentrated in vertical bending modes of the deck, where the importance of the vertical fluctuation is preponderant. The contribution of the deck, the pylon and the cable-stays has been analysed separately (Fig. 3).
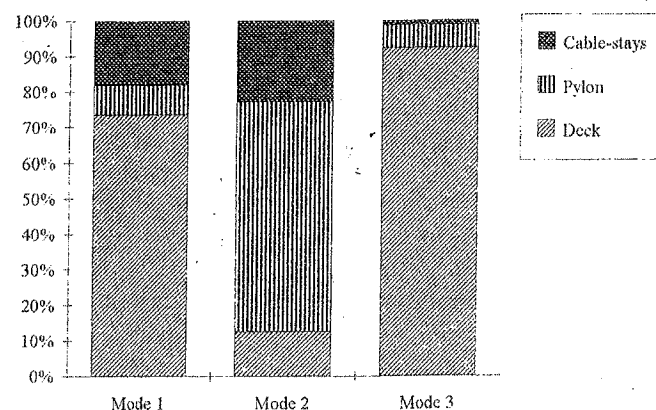
Fig. 3 Contribution of the structural members in the buffeting response

The increased participation of the cable-stays and the pylon in the horizontal balancement (Mode 1 and 2) is clearly shown. However, in vertical bending modes with growing natural frequencies the influence of the deck becomes dominant.

6. CONCLUSION

The dynamic response to turbulent wind of cable-stayed bridges has been examined, using spectral analysis with quasi-stationary approach. Numerical analysis is conducted to compare the participation of structural elements in the dynamic response with respect to the different vibration modes. According to computations, in the case of cable-stayed bridges the common way of modelling the structure by its deck alone can lead to underestimation of the buffeting response because of the significant role of pylons and cable-stays.

7. REFERENCES

[1] VÉRTES, GY. (1976): Építmények dinamikája (Dynamic of Buildings). Budapest, Tankönyvkiadó, pp.175-193 (in Hungarian)
[2] SIMIU, E. AND SCANLAN, R.H. (1986): Wind effects on structures. New York, John Wiley and Sons
[3] LE FAUCHEUR, D. et al. (1993): Le pont r haubans de Karkistensalmi. Paris, Ouvrages d'art, Vol. 16 (in French)
[4] CONTI, E and PÉCZELY, A. (1994): Programme Ventose, Notice Utilisateur, Paris, SETRA, internal report

APPLICATION OF FIBER REINFORCED PLASTICS (COMPOSITES) IN CIVIL ENGINEERING

Ákos Sapkás
Techical University of Budapest
Department of Reinforced Concrete Structures
H-1521 Budapest, Bertalan L. u. 2

1. INTRODUCTION

Fiber reinforced plastics (composites) are widely used in the aerospace engineering for decades. Popularity of composites is due to their good performance [1,2].

Composites consisted of fibers and matrix. The previous carries the load; the later protects the fibers and keep them together. There are several materials to form the fiber and the matrix, for example the fibers can be made of glass, graphite, aramid and metal; as a matrix we may use epoxy, polyesther, polyethelene or metal. The most frequently used composites are the graphite or glass fiber reinforced epoxy or polyester. We will discuss these in the following sections.

2. ADVANTAGES AND DRAWBACKS

The main advantage of composites is their small weight. Composites have high tensile strength. The stiffness of a graphite/epoxy composite is relatively high, while that of a glass/epoxy composite is small (Fig. 1.) [1].
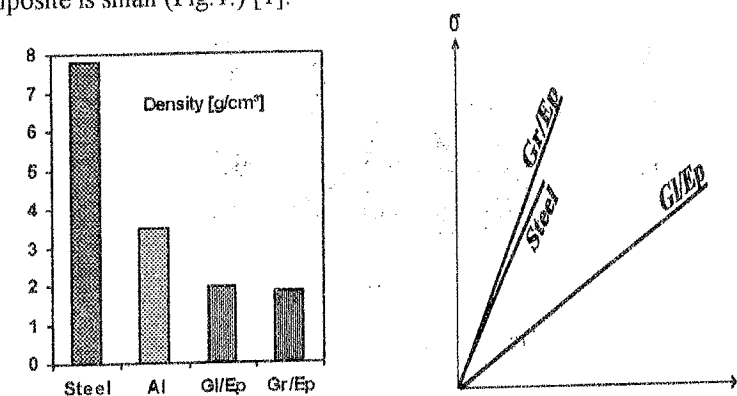
Fig. 1 Main properties of composites

Recently composites are also used in civil engineering. The main drawbacks in the application are the high price, low stiffness (in case of glass) and the lack of experience and standards.

3. APPLICATIONS

The most important applications are strengthening of existing structures, making non-metallic prestressing tendons, and last but not least the application of composites as primary load bearing structures [3,4,5,6]. In my presentation these load bearing structures will be discussed.

Composites are competitive with steel if the weight of the structure plays an important role. Urs Meier [3] showed that the maximum span of a cable-stayed bridge made out of steel is 4500 m, while that of a composite bridge is 14500 m. An other very important advantage of composite bridges is their corrosion resistance.

Analysis and design of civil engineering structures made of composites is very challenging, because of the new material characteristics new design aspects should be considered.

In my Ph.D. work composite pedestrian and bicycle bridges will be designed, analyzed and hopefully manufactured. Because of the previously mentioned reasons special attention should be paid on the design of connections, the possible vibration caused by the traffic and the buckling of the elements taking the effect of shear deformations into account [7].

Due our very rough preliminary calculation the price of the super-structure of a small span (l<10 m) composite bridge is competitive to the price of bridges made of conventional materials (Fig. 2) [8].
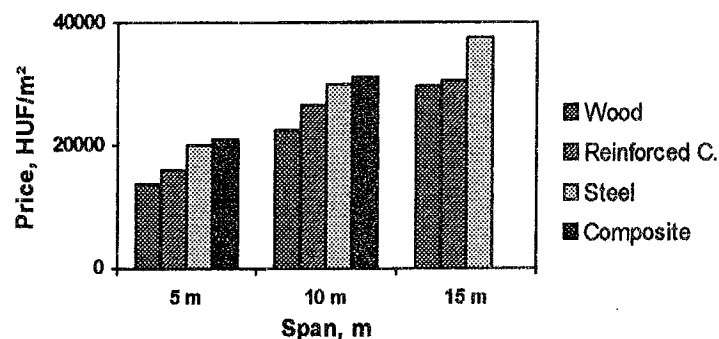
Fig. 2 Specific price of the bridge super-stucture

4. CONCLUSION

Composites are excellent candidates for load bearing elements of civil engineering structures. However attention must be paid because of the special characteristics of the material on the design of joints, on the effect of vibration and on the possible buckling of the elements.

REFERENCES

[1] Gibson, R.F. *Principles of Composite Material Mechanics* McGraw-Hill, Inc. New York etc. (1994)

[2] Czvikovszky, T. "New Qualities in Structural Plastics" (in Hungarian). *Magyar Tudomány,* Vol. 39, No. 4, August 1994, pp. 912-928

[3] Mufti, Erki, and Jaeger *Advanced Composite Materials with Application to Bridges.* The Canadian Society for Civil Engineering (1991)

[4] Mufti, Erki, and Jaeger *Advanced Composite Materials in Bridges and Structures in Japan.* The Canadian Society for Civil Engineering (1992)

[5] Barbero, and GangaRao "Structural Applications of Composites in Infrastructure" *SAMPE Journal,* Vol. 27, No. 6, November/December 1991, pp. 9-16

[6] Taewre, L. (editor) *Non-Metallic (FRP) Reinforcement for Concrete Structures* Proceedings of the Second International RILEM Symposium, London (1995)

[7] Ódor, P., Varga, L., Kollár, L. P., and Horváth, A. "Preliminary Feasibility Study on the Application of Composite Bridges in Hungary" (oral presentation), Canadian-Hungarian Conference on the Application, Manufacturing and Research on Advanced Composite Materials, 4-6th of October, 1995. Budapest

[8] "Comparative Study of Pedestrian Bridges", FŐMTERV Rt.

REAL LOAD MEASUREMENTS ON BRIDGES

Dipl. Ing. Johann BOGATH
University of Agricultury, Forestry and renewable natural resources
Institute for Structural Engineering
Peter Jordanstraße 82
A-1190 Vienna

1. INTRODUCTION

Structural reliability analysis has a rapid growth expiered in the last years and now this technology has reached a stage to implemet this basic research in design codes. In deterministic structural design the designer looks to the margin condition which are fixed in the code and in practice estimated values are compared with target values which are as well fixed in the code. The probabilistic design philosophy knows about the large uncertainties that exists in real situations and they were take into consideration in the codes.

2. THE BRIDGE LOAD MODEL FOR ROAD TRAFFIC IN EUROCODE 1-3

The Eurocode follows the probabilistic design philosophy in a wide range. The measurements of traffic made in France, on the A6 motorhighway near Auxerre, are considered that this traffic corresponds to an „European" traffic. This recorded datas are extrapolated by mathematical simulations and build the basis for modells in the Eurocode 1.

The load modell shown in Fig.1 has a range of validity for the Ultimate Limit State (ULS) ant the Serviceability Limit State (SLS). The Fatigue Live Assessment proof has its own load model called FLM3.
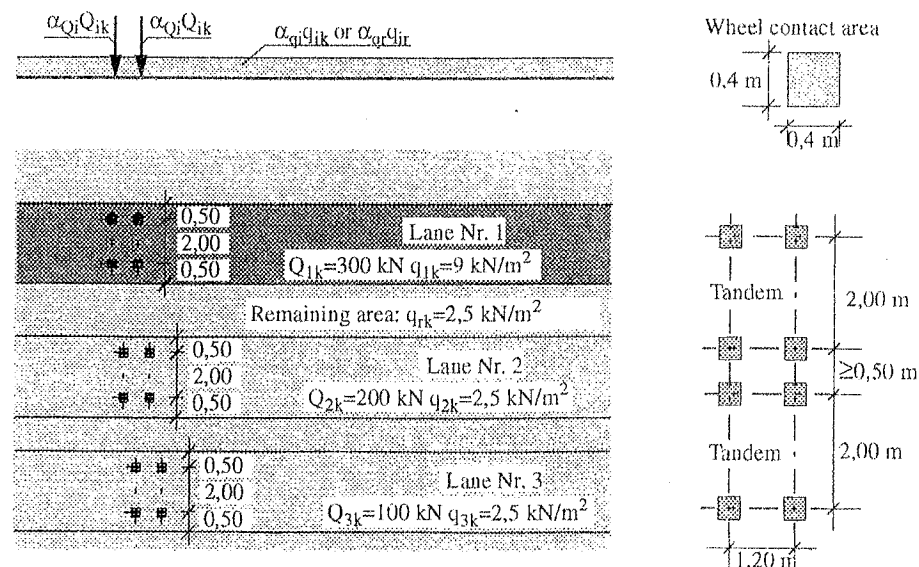
Fig.1 Description of Eurocode 1-3: load model 1

3. REAL LOAD MEASUREMENTS

Real load measurements are carried out on the highly loaded Brenner-Highway A13. The datas were continuosly meassured and recorded. The Institute for Structural Engineerinanalyses this datas and trays to develop a stochastic load model. In the following capter the EC1-load model will be compared with the existing Austrian Code B4002.

4. COMPARISON EUROCODE 1-3 WITH AUSTRIAN CODE B4002

For this comparision a simple beam has been choosen and the relation of the bending moments under the two load models are for different span length and carriagewidth determined. This comparison is shown in Fig.2.

$$comparisonvalue = \frac{maxM_{eurocode}}{maxM_{B4002}}$$
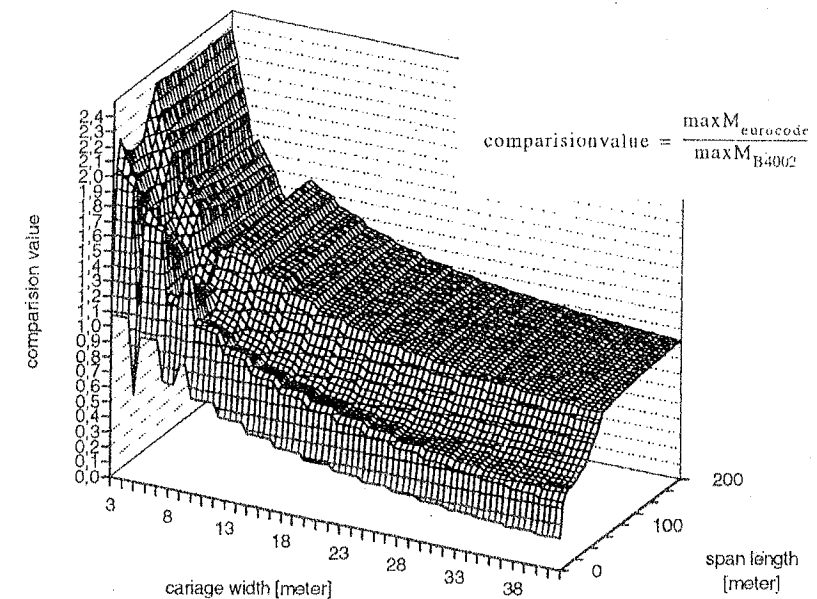
Fig.2 Comparision ot the Eurocode with the austrian national design code B4002

This comparison be shows, that the eurocode gives higer bending moments in the range of small carriage with. The reason is the higer traffic load in the first lane of the eurocode load model with a distributed load with $9kN/m^2$ and the axle load with 2x300kN. In the eurocode it is planed to modify the load values by α-values (see Fig. 1) witch may be fixed in national aplication documents like all boxed values.
In orter to establish this α-values in the national application document further investigations are needed. For this purpose, the load measurements wil be analysed to evaluate this reduction factors „α".

5. MEASURING DEVICE AND RECORDED DATA

In the first lane of the Brenner-highway a measuring device built into the pavement. This installatione register axles wich passes the meassuring strip. In a first utilization this registered axles are classified into vehicles and the vehicles themselves are classified into twelve vehicle groups.

For each registrated vehicle the folowing datas are recorded:
- record time
- distance betwen two vehicles
- velocity of the vehicle
- length of the vehicle
- numbers of axles per vehicle
- vehicle group
- each axle load
- total load of the vehicle

The vehicle classes are shown in Fig.3.
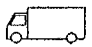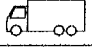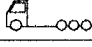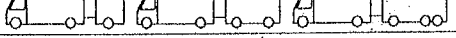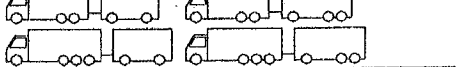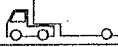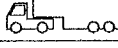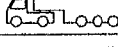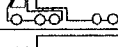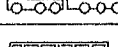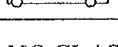
Fig. 3 vehicle groups at the Brenner highway measuring device

6. FIRST EVALUATION OF THE MEASURED AXLE LOADS

In a first step of evaluating the measurements, the defective values are checked. In a second step the measurements are devided into the vehicle groups (shown in Fig 3) and the vehicle groups are further devided into groups with the same axle numbers. Then the absolut density distribution will be analysed for the following values:
- total load of an vehicle for each vehicle group
- load from each axle of a vehicle for each vehicle group
- velocity of the vehicle for each vehicle group
- length of the vehicle for each vehicle group

- total loads and axle loads for all vehicles
- velocity and length for all vehicles
- total loads and axle loads for the heavy vehicles (vehicle group from 2 to 12)

An example is shown in Fig. 4
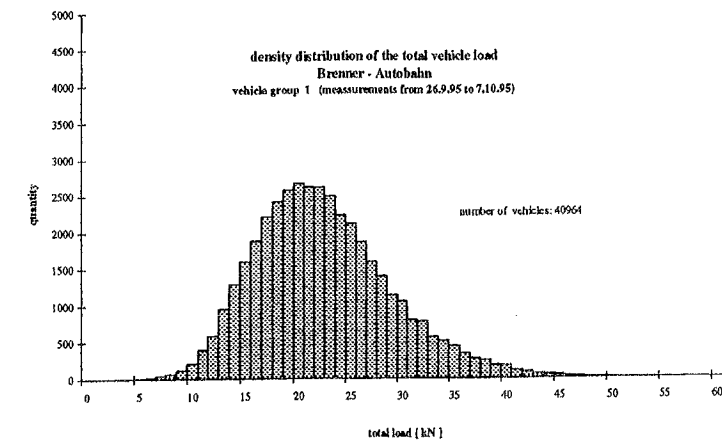
Fig. 4 density distribution of the total vehicle load - vehicle group 1

7. CONCLUSIONS

The Eurocode 1 is based on a traffic measured in Auxerre (France) in the year 1986. The first evaluation of the measurements at the Brenner highway (1996) shows that the total load of the vehicles are lower as the Auxerre meassurements and the total load is not normal distributed. In further investingations we will elaborate the different density distributions which are the basis for a stochastic load modell.

8. REFERENCE

[1] Eurocode 1: „Basis of Design and Actions on Structures, Volume 3 - Traffic loads on Bridges (Draft 8: October 1992)"
[2] Bogath J., „Brückenbelastung - Vergleich der Modelle für Verkehrsbelastungen auf Straßenbrücken nach Ö-Norm und Eurocode", Veröffentlichungen des Institutes für Konstruktiven Ingenieurbau, BOKU - Vienna
[3] Bruls A., Calgaro J.A., Mathieu H., Prat M., „The main models of traffic loads on road bridges - Background studies", IABSE Colloquium Delft 1996

SESSION 2

Road construction

SYSTEMATIC PROMOTION OF NON-MOTORIZED TRANSPORT IN THE TRAFFIC DEVELOPMENT

Tünde HAJNAL
Technical University of Budapest
Department of Highway and Traffic Engineering
H-1111 Budapest, Műegyetem rkp. 3.

1. INTRODUCTION

Near the turn of the millennium our individual transport is characterized by the extension of motorization and the increasing number of car use. The increasing tendency of traffic and its injurious effects also can be observed in Hungary. Therefore we have to throw light on the possibility of the use of environmental-friendly traffic modes. We would like to turn the attention to the most important questions by overviewing the different investigations and studies.

The present traffic situation is marked by the strong dominance of motorised private transport. The consequences of this dominance for man, for the environment and for the towns are so serious that at present many possibilities for reducing car traffic are under consideration. In this connection, however, it is also necessary to examine the promotion of each individual alternative traffic modes which could lead to the replacement of car trips. This is at present in the focus of the attention in urban transport.

2. MODAL CHOICE

The different modes of private transport can be observed as
- pedestrian movements and
- vehicle movements: by private vehicle and by public transport.

Those modes of transportation which are not harmful to the urban life, like pedestrian, bycicle and public transport traffic, are named environmental-friendly transportation.

The selection of transport modes by the population is permanently changing, and due to the increasing number of private cars and the development of motorization it is turning to the increased individual car use. For an average day of the years of the late seventies, the modal choice of Hungarian inhabitants of urban areas are illustrated on Fig. 1 compared to that of a German city. We note, that in the small domestic settlements and in the large cities the dominant transport mode was the use of bicycle and of public transport, respectively.

The environmental-friendly transportation is 82-88% of the urban transportation in that period in Hungary. We can follow the tendecy of the development on Fig. 2, where the actual modal splits are shown in different European settlements. The selection of transport modes by the population of Western European and Hungarian survey territory shows a sharp increase in the level of motorized individual traffic.
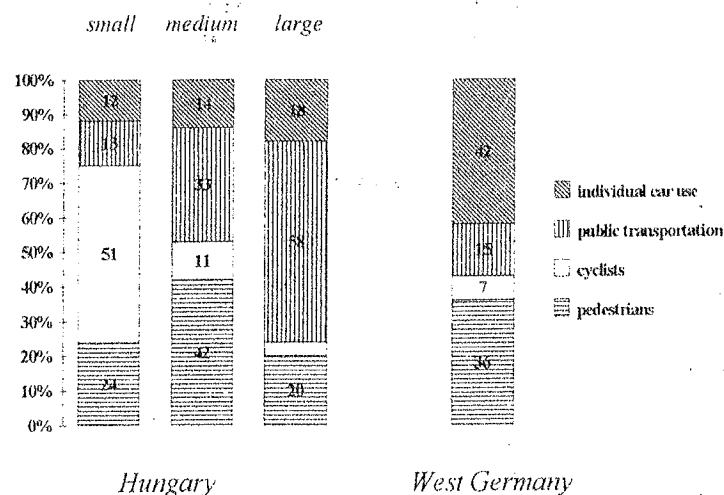
Fig. 1 The modal split in Hungarian settlements of different size, and in a German city in 1978
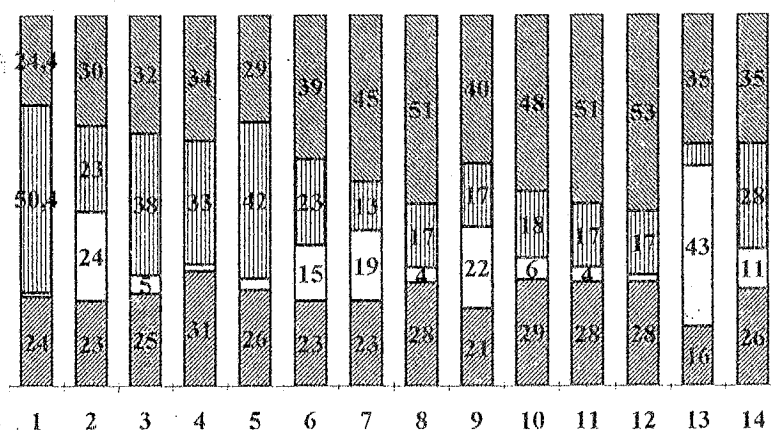
(the legend is the same as above)

Cities: 1- Budapest, 2- Amszterdam, 3- Stockholm, 4- Bolonga, 5-Zurich, 6- Hannover.
Middle-size towns: 7- Salzburg, 8- Linz, 9- Bremen, 10- Kassel, 11-Weisbaden, 12-Saarbrücken, 13-Groningen 14- Basel.

Fig. 2 Modal choice in European settlements of different size

3. MOBILITY

Mobility is described by the average daily number of journeys. Modal choice is one of the most important indicators to characterize the structure of the mobility: it descibes the distribution of mobility between different kind of traffic modes. In spite of the increasing number of car use the key values of mobility do not undergo radical changes. The measurements in the German surveyed territory gave an average of 2,9 journeys per person daily in 1990, which was the same in 1976. The distance covered in 1976 was 17 kilometers, the distance in 1990 was 20 kilometers. This reflects the increase of speed so the acceleration of urban life can be expressed by simple numbers as well. The number of journeys in Budapest shows the same tendency; according to a dweller survey in 1993-1994 the average specific journeys were 2,39 journeys per person daily.

3.1 Duration of travel

The discussion on mobility and traffic behaviour is concentrated primarily on the period during we are "on the road" and, therefore, "actively" participating in traffic events. An average person on an averange day spends only one hour actively in traffic. Six hours per day on average are spent off home, however, the greater part of the day is spent at home. But even there we participate passively in the traffic events: traffic noise and air pollution caused by those who are just completing their active hours effects the others as well.
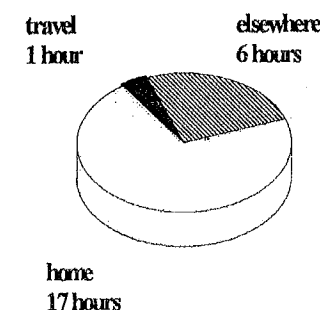
Fig. 3 Time spent by active transportation on an average day

The average travel time in Budapest fits in the European tendency, we spend usually 55-68 minutes with the daily transport.

3.2 Distances

The most important trip purposes (with almost equal shares of 25% each) are work, leisure and shopping (including the use of services such as post office, doctor etc.). In accordance with Hungarian measurements, the 32,4 % of the trips are shorter than one kilometer and further 29,7% of the journeys are below four kilometers, so the 62,1% of the trips in the capital are short distanced and ideal for walking or cycling. Looking at the results of a German survey about the distance and speed of car trips in city centers, Fig. 4, we can see the same tendency: the residents use their cars more than it would be indispensable.
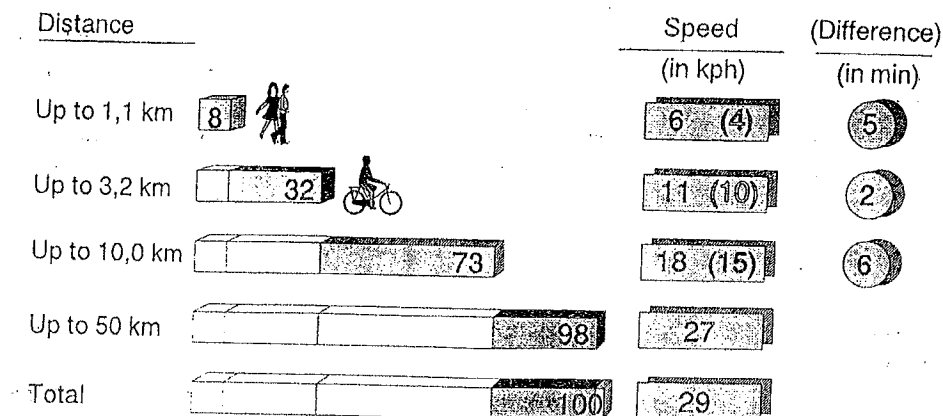
Fig. 4. Rates of car trips' distances (%) in German cities in 1990

4. REPLACEMENT OF CAR TRIPS

Generally speaking almost 60% of car use could be substituted by other, environment-friendly transport modes. In Budapest the development of public transport could give a good solution for individual transport problems, but the rate of use of public transport is significantly getting worse.

There was an interesting domestic survey in 1994-95 about cycling customs in Budapest. In contrast to the western European experiences the main goals of cycling in Budapest are leisure and sport. The investigations in Budapest demonstrate that the potentional cycle use could be increased up to 2,9-3,9 % instead of the actual 1.2%. Similar investigations were done in German cities as well, where it was provable that a very moderate behavioural change would already increase the bicycle use by 20%.

5. CONCLUSIONS

Working on our days' transport strategy we have to face the facts that the increasing individual car traffic can hardly find room on the urban road network, the congestion is growing, therefore the emission of pollutants intensifies. The actual rate of public transport and the environmental-friendly transportation is decreasing. To stop this process it is very important to hinder the increase of individual car use. The key word of the practical solution are the good *transport policy* and the *behavioural changes*.

REFERENCES

[1]. 1994.évi budapesti háztartásfelvétel feldolgozása és elemzése. *Transman Kft.*, Budapest, 1994.

[2]. A budapesti kerékpározási szokások elemzése az 1994. évi forgalomfelvétel adatai alapján. *Közlekedés Fővárosi Tervező Iroda Kft.*, Budapest, 1994.

[3]. Proceedings of the 8th Velo-City Conference, Basel, 1995.

[4]. Strategy for the Systematic Promotion of the use of Bicycles, *SOCIALDATA Institute für Verkehrs- und Infrastrukturforschung GmbH.*, 1995.

[5]. Tánczos L.né Dr.: A városi közlekedéspolitika néhány időszerű kérdése; *Városi Közlekedés*, 6/1995.

[6]. Koller S.: Forgalomtechnika , *Tankönyvkiadó*, Budapest, 1976.

[7]. Koller S.: Forgalomtechnika és közlekedéstervezés, *Műszaki Könyvkiadó*, Budapest, 1986.

[8]. Koller S.-né: Javaslat a kerékpáros közlekedés fejlesztési programjára, *Közlekedéstuddományi Intézet*, Budapest, 1984.

[9]. Knoflacher H.: Fussgeher und Fahrradverkehr.

[10]. Csorja Zs., Doborcsi T., Hajnal T., Rhorer Á.: Vizsgálat a fővárosi rövidtávú, személygépkocsival történő utazások kerékpárral történő kiváltására, *Fővárosi Polgármesteri Hivatal Közlekedési Ügyosztály*, Budapest 1995.

[11]. Csorja Zs., Golarits P., Hajnal T.: Kerékpáros forgalom fejlődésének és fejlesztésének tendenciája, a különböző intézkedések hatékonyságának vizsgálata, *Útgazdálkodási és Koordinációs Bizottság*, Budapest 1995.

SESSION 3

Steel structures

SEISMIC RESPONSE OF BUILDING STEEL FRAMES WITH SEMI-RIGID CONNECTIONS

Dinu Florea
Centre of Advanced Technical Sciences, Romanian Academy, The Timisoara Branch
Mihai Viteazul 24, Timisoara, RO-1900

1. INTRODUCTION

The cost of a building steel frame is considerably influenced by the nature of its beam-to-column connections and particularly by their degree of stiffening. Substantial economies may be easily achieved by using bolted connections without stiffeners, which are easy to fabricate in work-shop and to assembly on site and therefore ensure minimum cost.

Steel structures with semi-rigid joints have a greater possibility of deformations, in comparison with the rigid ones, which means that they are more sensitive at the second order effects, and, consequently, to the influence of imperfections. The semi-rigid joints are also influencing the dynamic response of the steel structures, modifying the structural coefficient q and the plastic hinges biography.

Promotion of steel structures with semi-rigid joints in Romania has to satisfy the seismic criteria of strength and deformability.

On the basis of an extensive numerical investigation, the present paper summaries the main conclusions in regard with the influence of different structural parameters on the seismic response of steel building frames with semi-rigid connections.

2. NUMERICAL SIMULATION PROGRAM

A numerical simulation program with DRAIN-2D computer code was designed to find out the influence of the structural and seismic characteristics on the behaviour of steel building frames with semi-rigid joints. The four steel frames presented in Fig.1 were selected for numerical simulations. HEA and HEB section for columns and IPE section for beams were used. Different ratios between the beam and column rigidity were chosen, i.e. strong column and weak beam (SCWB), weak column and strong beam (WCSB) and column and beam with almost the same rigidity (CBSR). The beam-column joints taken into account were either of rigid or semi-rigid type.

The Eurocode 3, Revised Annex J rules were used to evaluate the joint characteristics, i.e. the plastic resistant moment, M_{Rd}, and the initial stiffness, S_j. The characteristics of the joints selected for this parametrical study are:

- $M_{Rd} = 1.2; 1.0; 0.8 M_{pl.beam}$
- $S_j = K_{sup}, 0.8K_{sup}, 0.6K_{sup}, 0.4K_{sup}$ and K_{inf}

The S_j values are limited by K_{sup} and K_{inf} as shown in Fig.2.
The K_{inf} values are determined as follows:

- according to Eurocode 3 provisions

- on the basis of the ultimate plastic rotation capacity evaluated either with Mazzolani & Piluso method or with DUCTROT program [3].

The accelerogram of Vrancea (Bucharest 1977) earthquake was used for dynamic analysis.

The main purposes of this parametrical study were to analyse the time history of the plastic hinge appearance up to the collapse mechanism and the change of the q factor. Eurocode 8 provisions, the Ballio-Setti [7] and Gioncu [3] methods were used to evaluate the q factor values.

In order to model the cumulative damage of frame members, after the attainment of M_{pl}, a 5% degradation was considered in the bilinear M-ϕ curve during the dynamic simulation with DRAIN-2D.

The P-Δ effect was also introduced.
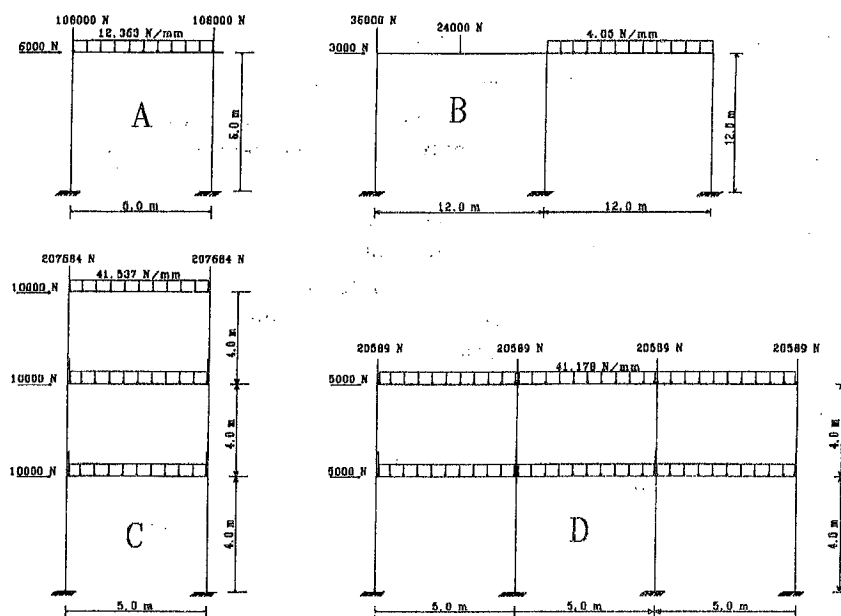
Fig.1
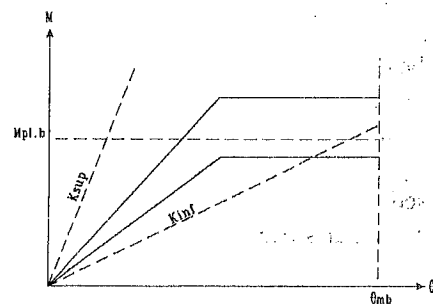
Fig.2

$K_{sup} = 25EI_b / L_b$ *

$K_{inf} = \max[(0.5EI_b)^*, (M_{pl.b} / \theta_{mb})^{**}]$

*   - Eurocode 3

** θ_{mb} - determined after the method of Mazzolani & Piluso and Gioncu

3. NUMERICAL RESULTS

Tables 1 to 4 show the values of q factor, determined by Ballio-Setti method using displacements, q_d, and plastic rotations, q_ϕ (see Fig.3a and 4a), and by Eurocode 8, q_m, respectively.

Tab.1 - q factor values for frame A

		Frame A								
		WBSC			CBSR			WCSB		
M_{Rd}	Stiffness	q_d	q_ϕ	q_m	q_d	q_ϕ	q_m	q_d	q_ϕ	q_m
1.2$M_{pl.b}$	k_{sup}	5.35	-	2.33	4.50	-	1.41	4.05	-	1.33
	0.8k_{sup}	5.25	-	2.20	4.50	1.25	1.41	4.10	-	1.33
	0.6k_{sup}	4.65	-	2.12	4.58	1.22	1.41	4.10	-	1.33
	0.4k_{sup}	4.0	-	2.0	4.72	1.42	1.47	4.10	-	1.33
	k_{inf}	2.2	2.53	2.55	1.95	1.22	3.32	1.85	1.70	2.60
1.0$M_{pl.b}$	k_{sup}	7.92	10.4	3.82	4.55	-	1.41	4.05	-	1.33
	0.8k_{sup}	7.10	9.20	3.50	4.50	-	1.41	4.10	-	1.33
	0.6k_{sup}	6.25	7.95	3.15	4.50	-	1.41	4.10	-	1.33
	0.4k_{sup}	4.95	3.85	2.60	4.75	-	1.47	4.10	-	1.33
	k_{inf}	2.18	2.54	2.55	1.95	2.20	3.32	1.85	1.70	2.60
0.8$M_{pl.b}$	k_{sup}	11.6	16.2	6.0	1.35	-	1.41	4.05	-	1.33
	0.8k_{sup}	11.7	16.3	5.87	1.15	-	1.41	4.10	-	1.33
	0.6k_{sup}	11.9	16.4	5.75	1.3	-	1.41	4.10	-	1.33
	0.4k_{sup}	10.15	14.5	5.22	1.5	-	1.47	4.10	-	1.33
	k_{inf}	2.15	2.54	2.55	1.95	2.15	3.32	1.85	1.70	2.60
Rigid		**3.40**	**-**	**2.0**	**4.40**	**-**	**1.35**	**4.05**	**-**	**1.27**

Tab.2 - q factor values for frame B

		Frame B								
		WBSC			CBSR			WCSB		
M_{Rd}	Stiffness	q_d	q_ϕ	q_m	q_d	q_ϕ	q_m	q_d	q_ϕ	q_m
1.2$M_{pl.b}$	k_{sup}	-	1.10	1.29	2.0	1.27	1.65	2.0	1.30	2.02
	0.8k_{sup}	1.32	1.08	1.39	2.05	1.28	1.65	2.05	1.30	2.03
	0.6k_{sup}	1.30	-	1.51	2.04	1.30	1.67	2.0	1.30	2.04
	0.4k_{sup}	2.60	1.31	2.09	1.98	1.26	1.73	2.0	1.30	2.08
	k_{inf}	1.60	2.62	2.64	2.20	2.90	2.90	2.10	2.20	3.54
1.0$M_{pl.b}$	k_{sup}	-	-	1.03	-	-	1.63	2.0	1.30	2.02
	0.8k_{sup}	1.5	1.58	1.98	1.95	1.08	1.63	2.05	1.30	2.03
	0.6k_{sup}	-	1.57	2.27	2.0	1.20	1.66	2.0	1.30	2.04
	0.4k_{sup}	-	1.33	1.80	1.95	1.27	1.73	2.0	1.30	2.08
	k_{inf}	1.60	2.63	2.63	2.25	2.90	2.90	2.10	2.20	3.54
0.8$M_{pl.b}$	k_{sup}	-	2.25	2.40	-	1.57	1.60	2.0	1.30	2.02
	0.8k_{sup}	-	2.95	4.40	6.20	1.50	3.04	2.05	1.30	2.03
	0.6k_{sup}	-	3.10	4.21	4.80	2.56	2.59	2.0	1.30	2.04
	0.4k_{sup}	3.7	2.55	3.75	3.75	1.95	2.15	2.0	1.30	2.08
	k_{inf}	2.2	2.90	2.63	2.15	2.90	2.90	2.10	2.20	3.54
Rigid		**-**	**-**	**1.36**	**1.85**	**-**	**1.42**	**1.95**	**-**	**1.46**

Tab.3 - q factor values for frame C

M_{Rd}	Stiffness	CBSR			WCSB		
		q_d	q_ϕ	q_m	q_d	q_ϕ	q_m
1.2M$_{pl.b}$	k_{sup}	2.35	1.43	5.40	-	-	1.47
	0.8 k_{sup}	3.32	1.36	7.70	-	-	1.47
	0.6 k_{sup}	3.56	1.17	7.70	-	-	1.47
	0.4 k_{sup}	3.57	-	6.75	-	-	1.44
	k_{inf}	2.04	3.0	1.35	1.38	1.53	3.0
1.0M$_{pl.b}$	k_{sup}	-	-	7.28	1.20	-	1.41
	0.8 k_{sup}	4.88	3.9	7.27	-	-	1.41
	0.6 k_{sup}	5.43	2.9	8.57	1.10	-	1.53
	0.4 k_{sup}	5.17	3.40	10.7	-	-	1.58
	k_{inf}	2.10	3.0	1.35	1.38	1.54	3.0
0.8M$_{pl.b}$	k_{sup}	4.73	1.83	7.0	2.40	-	2.54
	0.8 k_{sup}	6.04	1.90	8.5	2.10	4.25	3.10
	0.6 k_{sup}	10.84	2.10	9.0	2.10	4.27	3.0
	0.4 k_{sup}	11.10	-	7.0	1.82	2.55	2.83
	k_{inf}	2.05	3.05	1.35	1.38	1.53	3.02
Rigid		**2.40**	-	**5.50**	..	-	**1.40**

Tab.4 - q factor values for frame D

M_{Rd}	Stiffness	CBSR			WCSB		
		q_d	q_ϕ	q_m	q_d	q_ϕ	q_m
1.2M$_{pl.b}$	k_{sup}	2.40	-	2.39	3.73	-	3.33
	0.8 k_{sup}	2.45	-	3.50	3.67	-	3.33
	0.6 k_{sup}	2.10	-	3.40	3.72	-	3.33
	0.4 k_{sup}	1.84	-	3.25	3.84	-	3.50
	k_{inf}	1.30	1.30	3.08	1.28	-	2.64
1.0M$_{pl.b}$	k_{sup}	-	1.45	2.75	3.72	-	3.33
	0.8 k_{sup}	-	1.55	5.08	3.68	-	3.33
	0.6 k_{sup}	-	1.58	5.38	3.73	-	3.33
	0.4 k_{sup}	-	2.25	5.0	3.80	-	3.50
	k_{inf}	1.32	1.32	3.08	1.24	-	2.64
0.8M$_{pl.b}$	k_{sup}	-	-	4.60	3.81	1.22	4.0
	0.8 k_{sup}	-	7.5	6.20	3.82	-	4.0
	0.6 k_{sup}	-	-	11	4.16	1.26	4.0
	0.4 k_{sup}	-	-	11.28	3.85	-	3.67
	k_{inf}	1.30	1.30	3.12	1.24	-	2.64
Rigid		**1.15**	-	**2.42**	**3.50**	-	**3.33**
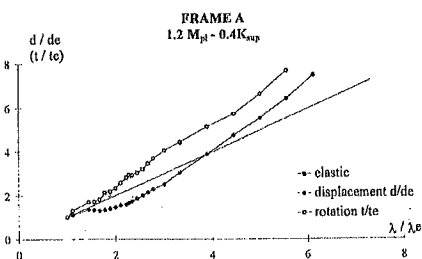
Fig.3.a SBWC
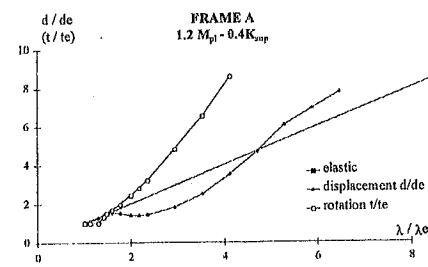
Fig.4.a CBSR
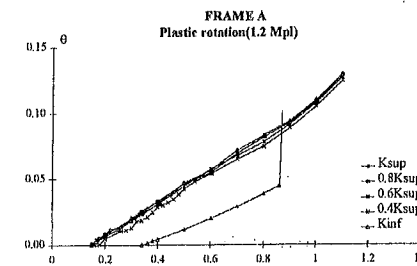
Fig3.b SBWC
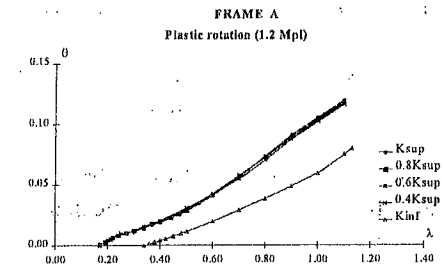
Fig.4.b CBSR
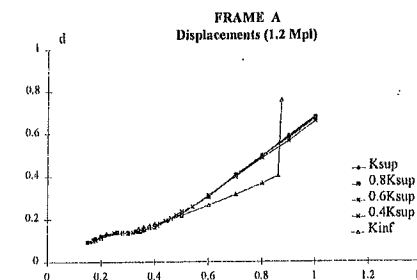
Fig.3.c SBWC
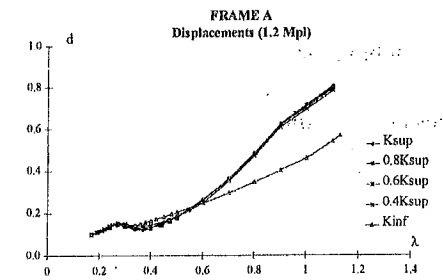
Fig.4.c CBSR

For C and D frames the WBSC results are similar to the CBSR one.

4. CONCLUSIONS

On the basis of the results previously presented, we have tried to obtain some answers to the following problems i.e..

4.1 Influence of the beam/column rigidity ratio

In case of SBWC frames, a floor mechanism located within the first storey occurs. The corresponding sway displacements are important. The q_m factor obtained according to Eurocode 8 is very close to the values obtained by Ballio-Setti method for q_d (Fig.3a).

For WBSC frames, the yield mechanism is a global one, in which the plastic hinge rotations are dominant. The q factor obtained according to Eurocode 8 is rather close to the values obtained by Ballio-Setti method for q_ϕ.

In case of CBSR frames, the yield mechanism is a combined one, in which the plastic hinges may appear both in columns and in beams. The q_m factor calculated according to Eurocode 8 has a value between q_ϕ and q_d (Fig.4a).

Regarding the q factor, it can be also observed that, in case of SBWC frames, the values of q for the rigid frames are closed to the semi-rigid ones. These values are increasing with the reduction of the joint rotational stiffness and ultimate resisting moment (semi-rigidity effect), excepting frame A, as seen also in Ref.[7].

So, the recently proposed formula by Mazzolani & Piluso [5],to reduce the q factor for semi-rigid frames, via a coefficient $\eta \leq 1$, seems to be not generally valid.

4.2 Change of ultimate resisting moment of the joints

In case of SBWC frames, if the ultimate resisting moment of the joint, M_{Rd} is changing, there are no differences in structural response (the yield mechanism is identically).

In case of WBSC frames, the specific M-ϕ curves influence both the q values and the collapse mechanism. The mechanism is global.

For CBSR frames the behaviour of the structures is rather similar if the joints are full resistant (i.e. $M_{Rd} = 1.2M_{pl.b}$; $1.0M_{pl.b}$), but it changes in case they are partial resistant joints (i.e. $M_{Rd} = 0.8M_{pl.b}$).

4.3 Influence of initial rotational stiffness

Behaviour of the structures (i.e. yield mechanism, q factor, displacements, rotations), is not significantly influenced by the change of initial joint rotational stiffness ($S_j = 1.0K_{sup}$; $0.8K_{sup}$; $0.6K_{sup}$; $0.4K_{sup}$), excepting $S_j = K_{inf}$, when appears great differences (Fig.3b,c and Fig.4b,c).

Some results already obtained with El Centro (1940) accelerogram, prove the fact that the type of seismic ground motion may strongly influence the structural dynamic answer. Thus, numerical simulations with El Centro, Northridge (1994) and Kobe (1995) accelerograms are in progress.

REFERENCES

[1] EUROCODE 3. "Design of Steel Structures", Commission of the European Communities, February 1992.

[2] EUROCODE 8. "Earthquake Resistant Design of Structures", Commission of the European Communities, October 1993.

[3] Gioncu V.,Mateescu G., Iuhas A., "Contributions to the study of plastic rotational capacity of I steel sections", *STESSA'94 - Behaviour of steel structures in seismic areas*, Timisoara, 1994.

[4] Guerra C.A., Mazzolani F.M., Piluso V., "Evaluation of the q Factor in Steel Framed Structures", *Ingegneria Sismica*, anno VII, No.2, 1990.

[5] Mazzolani F.M., Piluso V., "An Attempt of Codification of Semirigidity For Seismic Resistant Steel Structures", *Third International Workshop on Connections in Steel Structures*, Trento, 1995.

[6] Powell G.H., "DRAIN-2D User's Guide", *University of California*, 1973.

[7] Sedlacek G., Koo M.-S., Ballio G., "The Response of Steel Structures with Semi-Rigid Connections to Seismic Actions", *Connections in Steel Structures*, May 1987, pp. 362-374.

CYCLIC DETERIORATION MODELLING OF STEEL-TO-CONCRETE CONNECTIONS

Sándor Ádány
Technical University of Budapest
H-1521 Budapest, Hungary

1. INTRODUCTION

This paper deals with end-plate-type steel-to-concrete connections under cyclic loading conditions. After some basic definitions the behaviour of this type of connection is presented on the basis of test results, then a model is introduced which can be an effective tool for numerical analysis.

2. DEFINITIONS

The connection which is under investigation is defined in a general sense (i.e. connectors plus connected elements) and consists of four main components:
– a steel beam or column with arbitrary shape,
– a concrete or reinforced concrete element,
– an end-plate, welded to the connecting steel element,
– anchor bars, situated either in the middle part of the connection (nominally pinned connection) or in the edge zone of the end-plate (nominally fixed connection).
A typical structural arrangement is shown in Fig. 1.

Concerning the loads the following conditions are assumed:
– the connection is subject to bending moment and axial force,
– shear force is not taken into consideration,
– loading can be either monotonic or cyclic, this paper, however, is focusing on the cyclic behaviour.
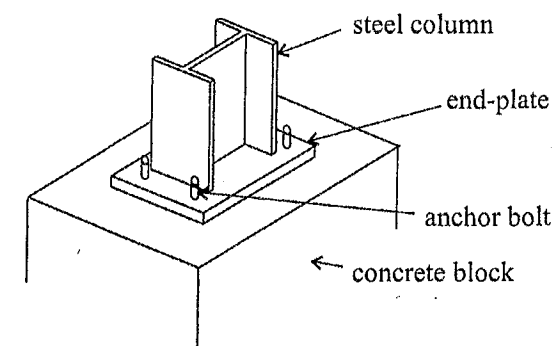
Fig. 1 A typical structural arrangement

3. CYCLIC BEHAVIOUR OF THE CONNECTION

3.1 General

In order to understand the behaviour of the connection, first the local behaviour of the connection components has to be understand. Each component has its own special behaviour which determine the connection behaviour. The characterizing phenomena are the following:
- plastic deformations in the end-plate,
- plastic deformations combined with local buckling in the steel beam or column,
- deterioration of the concrete,
- pulling out and/or elongation of the anchor bolts.

In this Chapter first the local behaviour of the connection components is summarized, then the global behaviour of the connection is discussed.

3.2 Local behaviour of the connection components

3.2.1 Plastic deformations in the end-plate

End-plate deformations are caused by the plastification of its material. The cyclic behaviour of steel material is presented in Fig. 2 , where typical σ-ε and τ-γ diagrams are plotted (based on [1]), σ being the normal stress, τ the shear stress, ε and γ the corresponding strains. As it can be observed, the steel material shows very good cyclic characteristics: high energy dissipation capacity, high ductility, without any rigidity degradation.
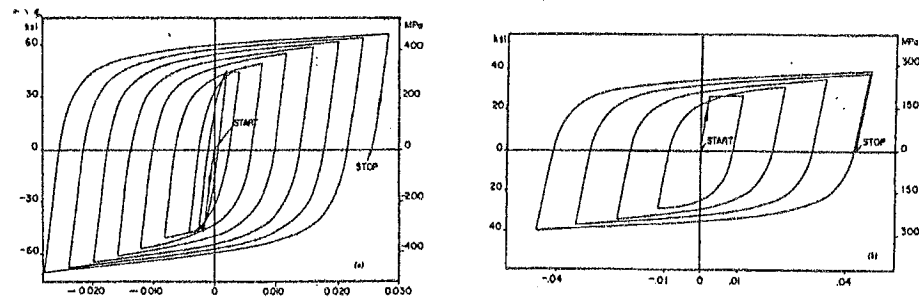
Fig. 2 Cyclic stress - strain curves of steel material

3.2.2 Plastic deformations plus local buckling in the steel bar

The behaviour is similar to that of steel material, the plastification, however, is limited due to local buckling (e.g. flange buckling in case of an I-section). This effect results in a degradation of cyclic characteristics. Two typical moment-curvature diagrams are presented in Fig. 3, according to [2].

3.2.3 Deterioration of concrete

Fig. 4 shows the cyclic σ-ε diagram of concrete material on the basis of [3]. In the envelope curve a softening branch takes place after reaching the maximum point, while, in case of cyclic loading, a significant rigidity degradation can be observed.
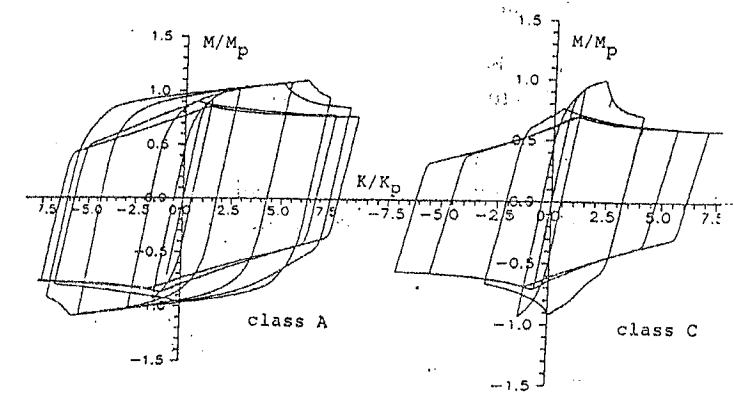
Fig. 3 Cyclic moment - curvature diagram of I-beams with variable slenderness
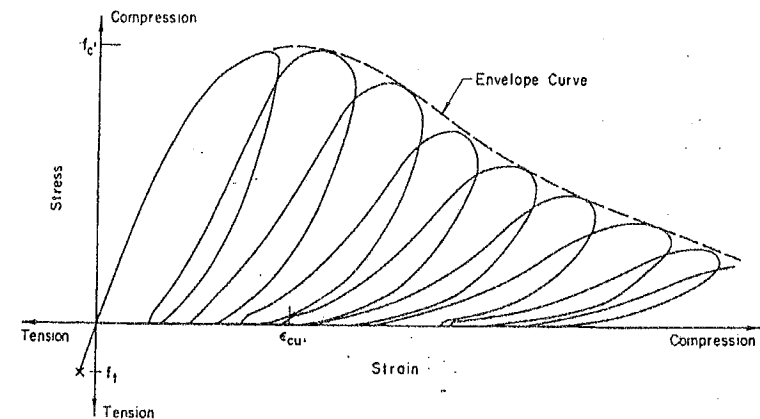
Fig. 4 Cyclic stress - strain diagram of concrete material
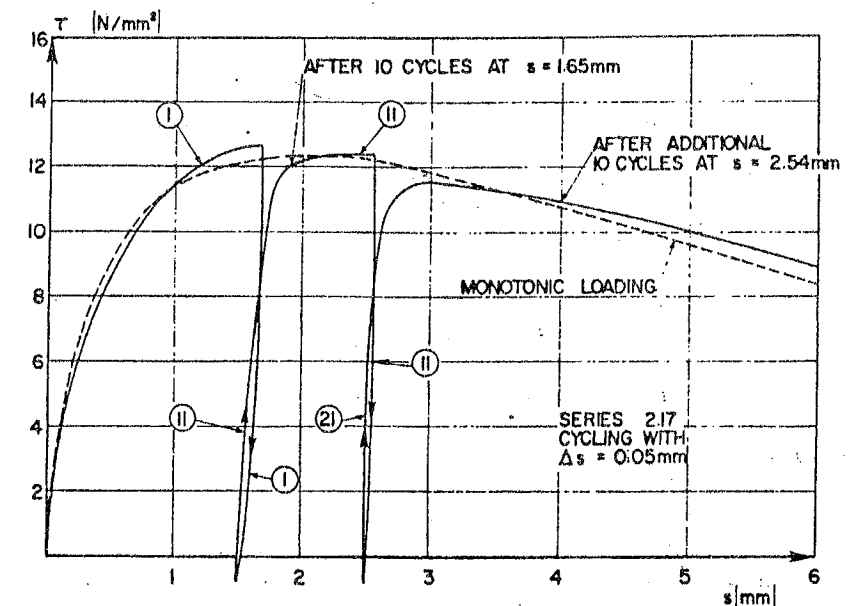
Fig. 5 Cyclic bond stress - slip curve of anchor bars

3.2.4 Pulling out and/or elongation of anchor bolts

The behaviour of the anchor bolts crucially depends on the structural details of the connection. Two types of structural solution are used.

In the first case the anchor bar is restrained at its end only, there is no bond between the steel and the concrete, the elongation of the anchor bolt can take place freely. Thus, the force-displacement characteristic is determined by the plastic deformation of the anchor bar.

In the second case the anchor bar is embedded in the concrete, the anchorage is ensured by the bond between the steel and concrete. The cyclic behaviour is determined by the combination of two phenomena: the elongation of the bar due to either elastic or plastic deformations, and the slip between the steel bar and concrete. This latter is illustrated in Fig. 5, where a bond stress versus slip diagram of an anchor bar subject to repeated tension force is plotted, according to [4].

3.2. Global behaviour of the connection

The global behaviour of the connection, which can be well demonstrated by its moment-rotation characteristic, is determined by the previously described local phenomena. It is obvious that none of these phenomena can take place independently of the others, but, in practical cases, there is a strong interaction between them. This interaction, however, is highly influenced by the parameters of the connection. In other words, the structural arrangement, the materials, as well as the dimensions of the connection have a very significant effect on the cyclic characteristics. For this reason, it is difficult to give a general description of the connection behaviour. As an example, the moment-rotation curve of a typical steel-to-concrete end-plate connection is shown in Fig. 6, as it can be found in [5]. The most important feature of the presented curve is the considerable rigidity degradation.
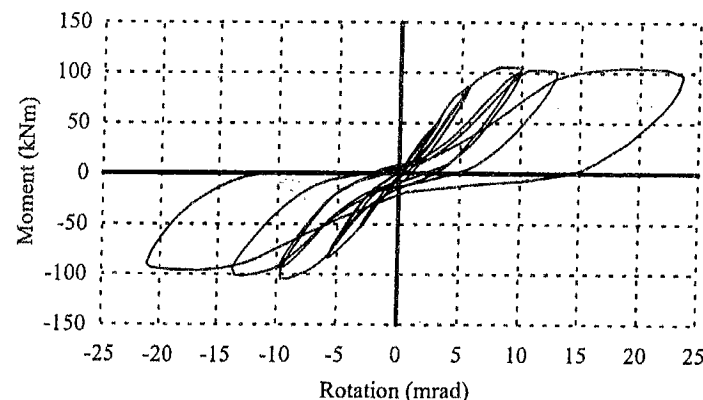
Fig. 6 Cyclic moment - rotation curve of a connection

4. NUMERICAL MODEL

After understanding the behaviour, a model can be introduced. To have an accurate model it is necessary to cover all the phenomena which crucially determine the behaviour. It is to be noted that, up to this time, such models are not developed.

The proposed model has the intention to be able to follow the local behaviour of all the connection components. In this way there is a hope to accurately predict the global moment-rotation behaviour as well. The most important characteristics of the proposed model are summarized as follows:

- the finite element method is proposed;
- layered shell elements are used to model the end-plate and the steel beam or column, (8-node serendipity element, 5 degrees of freedom per node);
- the concrete block is considered as a foundation layer;
- the anchor bolts are modelled as a special ("negative") foundation layer;
- Winkler-type foundation is used;
- a cyclic plasticity model is implemented as steel material model, (an extended Mroz model is proposed, as it is described in [6]);
- a cyclic deterioration model is applied for the concrete material, (envelope curve can be derived either from tests or by using an appropriate analytical model, while the rigidity degradation is considered in a simplified way according to [7]);
- cyclic force-displacement relationship is considered for the anchor bars, (the relationship is proposed to establish on the basis of experiments);
- geometric non-linearity is taken into consideration.

It is to be noted that, for the concrete and anchor bolts refined analytical models can also be used.

5. CONCLUSIONS

In this paper a model is proposed for the numerical analysis of end-plate-type steel-to-concrete connections. Based on experimental observations, the main characteristics of the model are defined so as to cover the most important phenomena which govern the cyclic behaviour of the connection. To verify the model, a numerical comparative study is necessary, which can be the next step of the investigations.

6. REFERENCES

[1] Popov, P. E. and Petersson, H.: "Cyclic Metal Plasticity: Experiments and Theory", *Journal of the Engineering Mechanics Division*, ASCE, Vol. 104, December 1978, pp. 1371-1388.

[2] Vayas, I. and Psycharis, I.: "Local Cyclic Behaviour of Steel Members", STESSA '94, International Workshop and Seminar on Behaviour of Steel Structures in Seismic Areas, 26 June - 1 July 1994, Timisoara, Proceedings

[3] Darwin, D. and Pecknold, D. A.: "Analysis of Cyclic Loading of Plane R/C Structures", *Computers & Structures*, Vol. 7, pp. 137-147.

[4] Eligehausen, R., Popov, E. P. and Bertero, V. V.: "Local Bond Stress-Slip Relationships of Deformed Bars Under Generalized Excitations", Report No. UCB/EERC-83/23, Earthquake Engineering Research Center, University of California, Berkeley, California, October 1983.

[5] Dunai, L., Fukumoto, Y. and Ohtani, Y.: "Behaviour of Steel-to-Concrete Connections under Combined Axial Force and Cyclic Bending", *Journal of Constructional Steel Research,* Vol. 36, No. 2, 1996, pp. 121-147.

[6] Mosaddad, B. and Powell, G. H.: "Computational Models for Cyclic Plasticity, Rate Dependence, and Creep in Finite Element Analysis", Report No. UCB/EERC-82/26, Earthquake Engineering Research Center, University of California, Berkeley, California, November 1982.

[7] Karsan, I. D. and Jirsa, J. O.: "Behavior of Concrete under Compressive Loadings", *Journal of the Structural Division,* ASCE, Vol. 95 (ST12), December 1969.

CALCULATION OF COMPOSITE BEAMS WITH ELASTIC CONNECTION

Zsuzsa Zsilák
Technical University of Budapest
H-1521 Budapest Pf. 91

ABSTRACT

This paper is to give a short summary on the theory and the different calculation methods of composite beams presuming elastic behaviour for the connectors.

1. INTRODUCTION

The majority of engineering structures consists of elastically connected girders. For instance both in case of railway and highway bridges elastic connection can be observed between the main and the floor beams and the stringers. In spite of this well known fact elastic composite behaviour is usually not considered in practice due to the difficult calculation method. Instead the regarding standards presume rigid connectors.

Composite structures give the most common example of elastic connection. In this case the assumption of elastic composite behaviour is justified by the problem of big spans that is that the thickness of the concrete slab cannot be increased beyond a certain limit which means that it will not follow proportionally the dimension changes of the structure. Thus, while the increase of the span results in a higher steel girder the thickness of the slab practically will not differ from the original one. Therefore the center of gravity of the composite cross section moves farther from the concrete part and the stresses at the edge of the slab on the compression side reach their limit value before those of the steel beam do on the tension side. It means that the steel structure is not used with its full capacity.

The elastic connection decreases the overloading of the concrete slab. The M_0 bending moment acting on the entire cross section is balanced with M_c (concrete), M_s (steel) and $N \cdot a$ bending moments: $M_0 = M_c + M_s + N \cdot a$

Generally the M_c bending moment is considered zero as the stiffness of the concrete slab can be ignored compared to that of the steel beam. It leads to the fact that the stresses in the concrete can be moderated by decreasing the N normal force.

2. CONVENTIONAL CALCULATION METHOD FOR ELASTIC CONNECTIONS - RESOLVING THE DIFFERENTIAL EQUATION [1]

This method is based on such a model of the composite girder where the connection of the concrete and the steel part is given by an elastic layer between the two elements. The change of the length of this layer is: $\delta_r(x) = c \cdot T(x)$,

the longitudinal strain is: $\dfrac{d\delta_r(x)}{dx} = c \cdot \dfrac{dT(x)}{dx}$. (1)
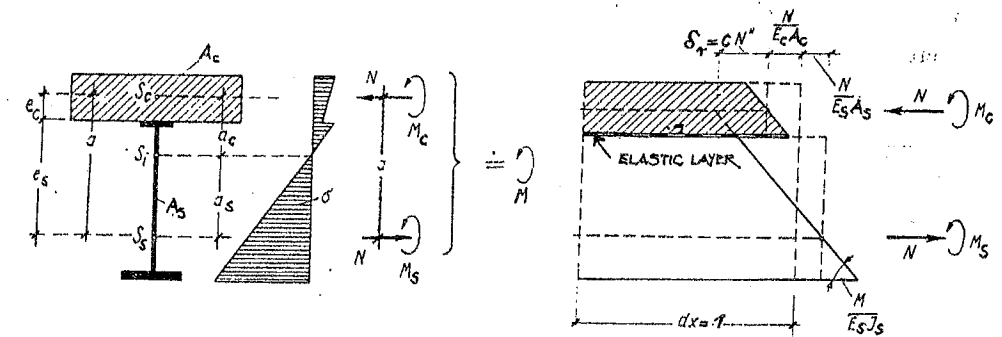
Fig. 1. The composite cross-section with the internal forces and the deflections

Determining this strain as the difference between the deflections of the connected elements: (Fig. 1.)

$$(dx + \Delta dx_s) - (dx + \Delta dx_c) = \delta_r(x)$$

Considering (1):

$$\frac{\Delta dx_s}{dx} - \frac{\Delta dx_c}{dx} = \frac{d\delta_r(x)}{dx} = c \cdot \frac{dT(x)}{dx} \qquad (2)$$

and

$$\frac{\Delta dx_s}{dx} = \frac{N}{E_s \cdot A_s} - \frac{M_s}{E_s \cdot I_s} \cdot e_s , \quad \frac{\Delta dx_c}{dx} = -\frac{N}{E_c \cdot A_c} + \frac{M_c}{E_c \cdot I_c} \cdot e_c , \quad e_s + e_c = a,$$

and also the equality of the curvatures:

$$\frac{M_c}{E_c \cdot I_c} = \frac{M_s}{E_s \cdot I_s} ,$$

equation (2) becomes :

$$N(x)\left[\frac{1}{E_s \cdot A_s} + \frac{1}{E_c \cdot A_c}\right] - M_s(x)\frac{a}{E_s \cdot I_s} = c \cdot \frac{dT(x)}{dx} \qquad (3)$$

From the equilibrium condition:

$$\sum N(x) = N(x) + T(x)dx - N(x) - dN(x) = 0$$

thus

$$\frac{dN(x)}{dx} = T(x) \text{ and } \frac{dT(x)}{dx} = \frac{d^2 N(x)}{dx^2}$$

From the equilibrium of the bending moments:

$M = M_s + M_c + a \cdot N$, ignoring M_c: $M_s = M - a \cdot N$

so equation (3) becomes:

$$N''(x) - \omega^2 \cdot N(x) + \lambda \cdot M(x) = 0 , \qquad (4)$$

where

$$\lambda = \frac{a}{c \cdot E_s \cdot I_s} \quad \text{and} \quad \omega^2 = \frac{\dfrac{1}{E_c \cdot A_c} + \dfrac{1}{E_s \cdot A_s} + \dfrac{a^2}{E_s \cdot I_s}}{c}$$

Solving the second order inhomogeneous differential equation for loadings frequently used in practice the following results can be obtained. (Tab. 1.)

Because of the relatively difficult formula the effect of creep and the statically indeterminate structures can only be calculated using approximating methods.

An example for applying the solution of the differential equation is presented in [2]. In the paper the results of calculating on the basis of elastic connection and also of the specifications of the Hungarian Standards are compared with experimental data. The calculated values show good coincidence with the experiments thus the assumption of elastic connection is verified. On the other hand it is noteworthy that the Hungarian Standards overestimate the values of the slip shear force.

3. CALCULATION WITH THE POTENTIAL ENERGY METHOD [3]

The main disadvantage of the conventional method is characterized by the fact that it is the normal force that is given as the result of the analysis. However considering statically indeterminate girders deflections are of greater importance and they can be determined only by approximating methods. Using the potential energy function the deflections can be derived directly.

The potential energy function is given as follows:

$$\Pi = \sum_{i=1}^{n} P_i \cdot w(x_i) + \int_0^l p(x) \cdot w(x) dx - L_b$$

The first two parts refer to the work of the external forces, these can be determined e.g. with the Ritz method. The L_b work of the internal forces is taken with the help of the differential equation (4) which expresses the equality of the strains.

The N normal force performs work on the

$$N(x) \left[\frac{1}{E_s \cdot A_s} + \frac{1}{E_c \cdot A_c} \right] + c \cdot \frac{d^2 N(x)}{dx^2}$$ relative displacement and the bending moments

on the $\dfrac{M_c(x)}{E_c \cdot I_c} = \dfrac{M_s(x)}{E_s \cdot I_s}$ curvatures.

Therefore the internal work is :

$$L_b = \frac{1}{2} \cdot \int_0^l \frac{M_s^2}{E_s \cdot I_s} dx + \frac{1}{2} \int_0^l \frac{M_c^2}{E_c \cdot I_c} + \frac{1}{2} \int_0^l K \cdot N^2 dx + \frac{1}{2} \int_0^l c \cdot N \cdot N'' dx ,$$

Tab. 1. Internal forces in case of elastic and rigid connection for different loadings

Loading	Normal force	Shear force	Stiff connection
	$N = N_0 \left[1 - \dfrac{2}{x(l-x)\omega^2} \left(1 - \dfrac{Cosh\,\omega\left(\frac{l}{2}-x\right)}{Cosh\,\omega\frac{l}{2}} \right) \right]$	$T = T_0 \left[1 - \dfrac{Sinh\,\omega\left(\frac{l}{2}-x\right)}{\left(\frac{l}{2}-x\right)\cdot\omega\cdot Cosh\,\omega\frac{l}{2}} \right]$	$N_0 = \dfrac{A_s \cdot a_s}{I_t} \cdot M$ $\quad T_0 = \dfrac{A_s \cdot a_s}{I_t} \cdot Q$
	$N = N_0 \left[1 - \dfrac{l \cdot Sinh\,\omega \cdot \xi}{x \cdot \xi \cdot \omega \cdot Sinh\,\omega \cdot l} Sinh\,\omega \cdot x \right]$ $\quad x \le \xi$	$T = T_0 \left[1 - \dfrac{l \cdot Sinh\,\omega \cdot \xi}{\xi \cdot Sinh\,\omega \cdot l} Cosh\,\omega \cdot x \right]$ $\quad x \le \xi$	$N_0 = \dfrac{A_s \cdot a_s}{I_t} \cdot M$ $\quad T_0 = \dfrac{A_s \cdot a_s}{I_t} \cdot Q$
	$N = N_0 \left[1 - \dfrac{Sinh\,\omega \cdot x}{x \cdot \omega \cdot Cosh\,\omega\frac{l}{2}} \right]$ $\quad x \le \frac{l}{2}$	$T = T_0 \left[1 - \dfrac{Cosh\,\omega \cdot x}{Cosh\,\omega\frac{l}{2}} \right]$ $\quad x \le \frac{l}{2}$	$N_0 = \dfrac{A_s \cdot a_s}{I_t} \cdot M$ $\quad T_0 = \dfrac{A_s \cdot a_s}{I_t} \cdot Q$
	$N = N_0 \left[1 - \dfrac{Cosh\,\omega\cdot\left(\frac{l}{2}-x\right)}{Cosh\,\omega\frac{l}{2}} \right]$	$T = N_0 \left[\dfrac{\omega \cdot Sinh\,\omega\cdot\left(\frac{l}{2}-x\right)}{Cosh\,\omega\frac{l}{2}} \right]$	$N_0 = \alpha_T \cdot \Delta T \cdot E_c \cdot A_c \cdot \dfrac{a_c}{a}$ $\quad \dfrac{\left(I_s + \frac{I_c}{n}\right)}{I_t}$
	$N_a = N_{a,0} \left[1 - \dfrac{Cosh\,\omega\cdot\left(\frac{l}{2}-x\right)}{Cosh\,\omega\frac{l}{2}} \right]$ $N_b = -(P - N_a)$	$T = N_{a,0} \left[\dfrac{\omega \cdot Sinh\,\omega\cdot\left(\frac{l}{2}-x\right)}{Cosh\,\omega\frac{l}{2}} \right]$	$N_{S,0} = \dfrac{\left(I_s + \frac{I_c}{n}\right)}{a} \cdot \dfrac{a_c}{a} \cdot P$ $\quad \dfrac{a_c}{a}$

where $K=\dfrac{1}{E_s \cdot A_s}+\dfrac{1}{E_c \cdot A_c}$.

Considering that

$$M_s(x)=-E_s \cdot I_s \cdot w''(x) \quad \text{and} \quad M_c(x)=-E_c \cdot I_c \cdot w''(x)$$

and introducing $\Theta=\dfrac{M_s(x)}{N(x)}$, the normal force follows as

$$N(x)=-\frac{E_s \cdot I_s \cdot w''(x)}{\Theta}.$$

Thus the internal work can be expressed as

$$L_b=\frac{E_c \cdot I_c + E_s \cdot I_s}{2}\int_0^l w''(x)^2\,dx + \frac{K(E_s \cdot I_s)^2}{2}\int_0^l \left[\frac{w''(x)}{\Theta}\right]^2 dx +$$

$$+\frac{c \cdot E_s \cdot I_s}{2}\int_0^l -\frac{w''(x)}{\Theta}\left[-\frac{E_s \cdot I_s \cdot w''(x)}{\Theta}\right]'' dx.$$

This way the potential energy function is determined, the deflection function can be replaced by an approximating $w(x)=\sum_i b_i \cdot f_i(x)$ that fulfils the boundary conditions and applying the Ritz method the b_i constants and the $w(x)$ function can be given so the internal forces can be calculated.

4. CALCULATING WITH FEM

Various softwares based upon FEM are available offering the possibility to examine the non-linear behaviour of the connectors of composite beams. Numerous researches have been done using FEM to obtain results regarding composite structures. In [4] the analysis of a composite girder was carried out where the concrete slab and the steel beam were modelled with surface elements positioned into the center plane of the regarding structural parts. The connectors were replaced by beam elements. As for the material properties in case of the steel the $\sigma-\varepsilon$ diagram formerly determined from experiments was applied, in case of the concrete an approximate model was used.

Drawing conclusion from the numerical analysis good coincidence was found between the FEM model and the experimental data as well as with the Hawranek-Steinhardt theory assuming elastic connection. On the other hand, however, the slip shear force distribution specified in the Hungarian Standards shows significant differences on the side of safety with the above mentioned results.
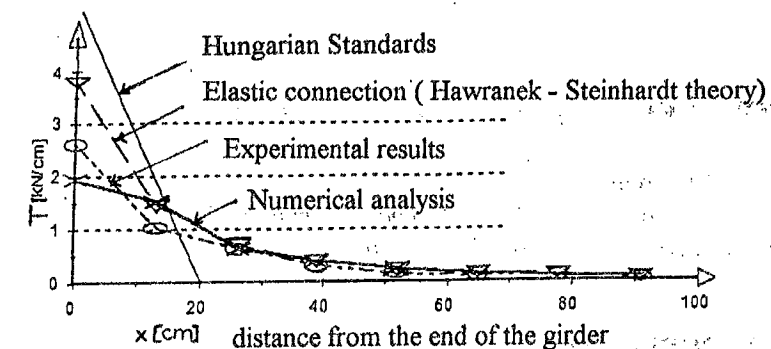
Fig. 2. Slip shear forces of the composite beam

CONCLUSIONS

Considering elastic composite behaviour in calculating composite structures leads to the decrease of the internal forces and results in a more economical design regarding the dimensions of the steel girder. The difficult formulas though hinder the method to become wide-spread and the lack of its use is partly due to the fact that it provides the internal forces as result while in case of statically indeterminate structures it is deflections that are needed to be available. This problem can be solved by applying the potential energy method which calculates the deflection function first and derives the internal forces from those data (e.g. using the Ritz method). Numerical FEM analysis can be carried out in order to examine the non-linear behaviour of the connectors and obtain more accurate results which tend to coincide with both experimental and theoretical ones. Comparing these above mentioned data with the specifications of the Hungarian Standards for composite structures a significant difference was pointed out (on the side of safety though) which strongly suggests the need for introducing new regulations in composite design.

REFERENCES

[1] Platthy, P.: "Vasbetonlemezzel együttdolgozó acéltartók elmélete"
(Theory of Composite Structures) Kézirat. Tankönyvkiadó Budapest 1965

[2] Platthy, P. - Szabó, B. - Fekete, L.: "Hőmérsékleti hatás laboratóriumi szimulálása öszvértartónál" (Laboratory Simulation of Temperature Effect on Composite Beams) Közlekedésépítés- és mélyépítéstudományi szemle XLIII. évf. 11. szám

[3] Platthy, P.: "Rugalmas kapcsolatú folytatólagos öszvértartók számítása"
(Calculation of Continuous Composite Beams with Elastic Connection) Építőipari és Közlekedési Műszaki Egyetem Tudományos Közleménye XI. kötet 3-4. szám Budapest 1956

[4] Horváth, L.: "Öszvértartók erőjátékának vizsgálata végeselem módszerrel"
(FEM Analysis of Behaviour of Composite Structures) Diploma work Dept. of Steel Structures TUB 1993

COUPLED INSTABILITIES IN THIN-WALLED STEEL BEAMS

Viorel Ungureanu
Centre of Advanced Technical Sciences, Romanian Academy, The Timisoara Branch
Mihai Viteazul 24, Timisoara, RO-1900

1 INTRODUCTION

The slender members loaded by transversal loads or ended moments acting in the plane of greatest stiffness, may collapse by lateral-torsional buckling before reaching the full plastic moment, M_{pl}. In the case of short members ($\overline{\lambda}_{LT} \leq 0.4$) with slender walls, the local buckling occurs and the failure is produced when the plastic moment $M_{pl,eff}$ of the effective cross-section, $M_{pl,eff} = W_{eff} \cdot f_y$, is reached. For usual thin-walled cold-formed steel beams, with the $\overline{\lambda}_{LT}$ slenderness size the local-overall buckling interaction always occurs. The practical way to introduce the local buckling effect into the overall lateral-torsional buckling of the beam is to reduce the flexural stiffness by means of the effective modulus, W_{eff}. Geometrical and material imperfections as well as the erosion of critical bifurcation load, due to the coupling phenomenon of two different instability modes, must be taken into account to evaluate the ultimate resistance of such beams.

Two relevant design codes i.e., ENV 1993-1-3, 1996E Eurocode 3 Part 1.3 and AISI LRFD (1990), and the ECBL approach [1], [2], were used to evaluate the ultimate lateral-torsional buckling moment. Tested specimens collected from literature [3], [4], [5] were selected for comparison with theoretical results.

The actual Eurocode 3-Part 1.3 buckling curves used to predict the ultimate load of cold-formed steel member have been obtained for hot rolled sections. Due to the different nature of the imperfections and to the interaction between overall and local buckling, these curves cannot always appropriately describe the buckling behaviour of cold-formed steel members. An alternative approach is proposed, based on the Erosion of Critical Bifurcation Load (ECBL) theory.

2 THE ECBL INTERACTIVE LOCAL, LATERAL-TORSIONAL BUCKLING APPROACH FOR BEAMS IN BENDING

Related to Figure 1 it may be written for $\overline{\lambda}_{LT} = 1/Q_{LT}^{0.5}$

$$\overline{M}_{LT} = \frac{M}{M_{pl}} = (1-\psi_{LT})Q_{LT} \tag{2.1}$$

where:

$$\overline{M}_{LT} = \frac{1+\alpha_{LT}(\overline{\lambda}_{LT}-0.4)+Q_{LT}\overline{\lambda}_{LT}^2}{2\overline{\lambda}_{LT}^2} - \frac{1}{2\overline{\lambda}_{LT}^2}\sqrt{[1+\alpha_{LT}(\overline{\lambda}_{LT}-0.4)+Q_{LT}\overline{\lambda}_{LT}^2]^2 - 4Q_{LT}\overline{\lambda}_{LT}^2} \tag{2.2}$$

$$\overline{\lambda}_{LT} = [W_{eff,y} f_y / M_{cr}]^{1/2} \tag{2.3}$$

$$Q_{LT} = \frac{W_{eff,y}}{W_{pl,y}} \tag{2.4}$$

$\overline{\lambda}_{LT}=$ the reduced slenderness;

$W_{eff,y}=$ section modulus of the effective cross-section when subject only to moment about relevant axis;

$M_{cr}=$ the elastic critical moment for lateral torsional buckling for the gross cross-section;

$Q_{LT}=$ the reducing factor of section modulus in interactive local-lateral torsional buckling;

$W_{pl,y} =$ the full plastic section modulus of the cross-section;

$\overline{M}_{LT}$ given by Eq. (2.2) represents a solution of the Ayrton-Perry formula adapted to interactive local-lateral torsional buckling including the generalised imperfection coefficient, η_{LT}, e.g.

$$\eta_{LT} = \alpha_{LT}(\overline{\lambda}_{LT} - 0.4) \tag{2.5}$$
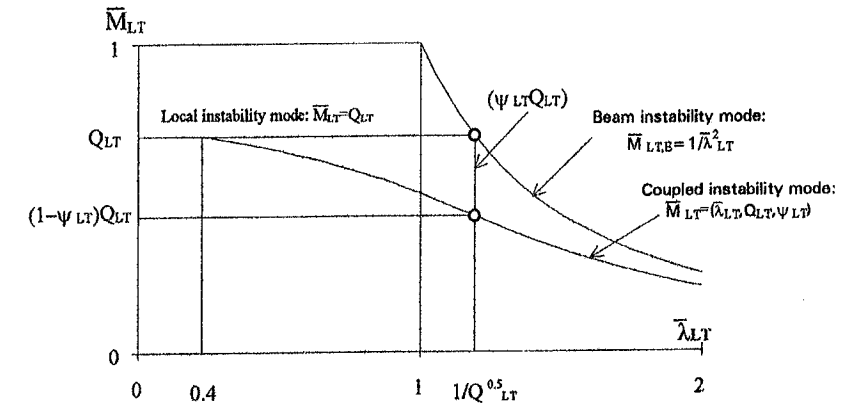
Fig. 1. The ECBL Interactive Model for Thin-Walled Beams

If $\overline{\lambda}_{LT} = 1/\sqrt{Q_{LT}}$ is introduced in Eq. (2.1), after some mathematical processing, it gives:

$$\alpha_{LT} = \frac{\psi_{LT}^2}{1-\psi_{LT}} \cdot \frac{\sqrt{Q_{LT}}}{1-0.4\sqrt{Q_{LT}}} \tag{2.6}$$

If $Q_{LT}=1$ (without local buckling) Eq. (2.6) becomes

$$\alpha_{LT} = \frac{\psi_{LT}^2}{0.6(1-\psi_{LT})} \tag{2.7}$$

respectively

$$\psi_{LT} = 0.3(\sqrt{\frac{20}{3}\alpha_{LT} + \alpha_{LT}^2} - \alpha_{LT}) \tag{2.8}$$

The new ECBL interactive approach for lateral torsional buckling of thin-walled beams is similar to that of EC 3-Part 1.3., but Eq. (2.5) is used to obtain the generalised imperfection in stead of the related formula given in the code.

That's means the ϕ_{LT} formula (see the EC3 code) becomes:

$$\phi_{LT} = 0.5[1 + \alpha_{LT}(\overline{\lambda}_{LT} - 0.4) + \overline{\lambda}_{LT}^2] \tag{2.9}$$

and α_{LT} should be calculated from Eq. (2.6) depending on ψ_{LT} erosion factor which has to be evaluated by statistical processing of relevant test specimens.

In the EC3 code, for lateral-torsional buckling of beams is used the same relation for the generalised imperfection as for compression members, e.g.

$$\eta_{LT} = \alpha_{LT}(\overline{\lambda}_{LT} - 0.2) \qquad\qquad (2.10)$$

Consequently, a significant jump of the χ_{LT} value is producing for $\lambda_{LT}=0.4$, respectively from 1.0 to 0.953 (5%). This jump is both physically and mathematically unjustified. Mateescu in [6] has also proposed the ϕ_{LT} formula given by Eq. (2.9), but with the imperfection coefficient $\alpha_{LT}=0.27$, for rolled I beams, and $\alpha_{LT}=0.60$, for welded I beams, respectively.

3 EXPERIMENTAL APPROACH FOR THE EVALUATION OF ψ_{LT} EROSION FACTOR

There are three distinct approaches [7] that can be used to evaluate the ψ_{LT} Erosion Factor i.e.: 1) the analytical approach; 2) the numerical approach and 3) the experimental approach.
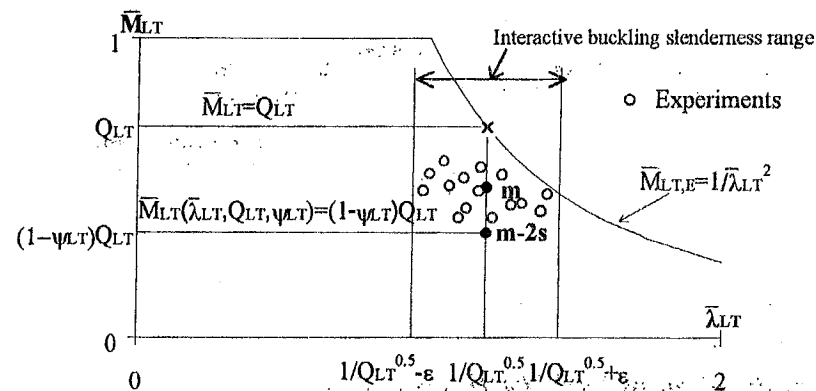
Fig. 2 Evaluation of ψ_{LT} Erosion Factor by means of experimental tests

The experimental approach for bending members includes the same steps like for columns [7]. There are used some representative series of beam test results corresponding to specified cross-section shapes. The beams are characterised by means of Q_{LT} factor and the experimental values of $\overline{M}_{LT}$, included in the *interactive buckling slenderness range*, only (see Fig. 2) are used for the statistical evaluation of ψ_{LT}.

The DATACOST [1] is used to calibrate the ψ factor and, on this basis, to obtain the new α imperfection coefficient and a new classification of cold-formed steel section for the stability analysis.

For instance, the experimental data carried out at the University of Salford [3] and University of Strathclyde, in Glasgow [4,5], included in DATACOST, are used on the following to evaluate ψ_{LT}.

In case of bent members the values of the Erosion Factor, for both Lipped Channel and Channel Section, calculated for different interaction range ε and scattering Δ are presented in Tables 1 and 2, respectively.

Table 1 Values of Erosion Factor for Lipped Channel Section Beams

Rhodes Lipped Channel Section (41 Tests)								
Scattering Δ	30%			50%			70%		
Inter. range	ψ_m	s	ψ_d	ψ_m	s	ψ_d	ψ_m	s	ψ_d
$1/Q^{0.5} \pm 0.15$	0.309	0.035	0.379	0.305	0.036	0.376	0.302	0.034	0.371
$1/Q^{0.5} \pm 0.20$	0.309	0.035	0.379	0.314	0.046	0.407	0.320	0.052	0.424
$1/Q^{0.5} \pm 0.25$	0.291	0.068	0.428	0.299	0.072	0.442	0.308	0.071	0.450

Table 1 (continued)

Lovell's Lipped Channel Section (27 Tests)								
$1/Q^{0.5} \pm 0.15$	0.233	0.039	0.311	0.233	0.039	0.311	0.224	0.037	0.297
$1/Q^{0.5} \pm 0.20$	0.238	0.078	0.394	0.211	0.055	0.321	0.231	0.072	0.374
$1/Q^{0.5} \pm 0.25$	0.238	0.078	0.394	0.213	0.092	0.398	0.234	0.103	0.440

Table 2 Values of Erosion Factor for Channel Tests

Lovell's Channel Section (20 Tests)		
Scattering Δ	30%; 50%; 70%	
Interaction range	ψ_m	s	ψ_d
$1/Q^{0.5} \pm 0.20$	0.226	0.015	0.256
$1/Q^{0.5} \pm 0.25$	0.199	0.048	0.294

4. COMPARISON BETWEEN NUMERICAL AND EXPERIMENTAL RESULTS

This chapter includes comparison of the results obtained by the EC3 Part 1.3, Mateescu and ECBL approaches with some relevant experimental results, and, on the other hand, includes a comparison between the interactive buckling curves obtained with Generalised Beam Theory (GBT) and ANSYS with those given by EUROCODE3-Part. 1.3, AISI LRFD (1990) and ECBL approaches and with test results.
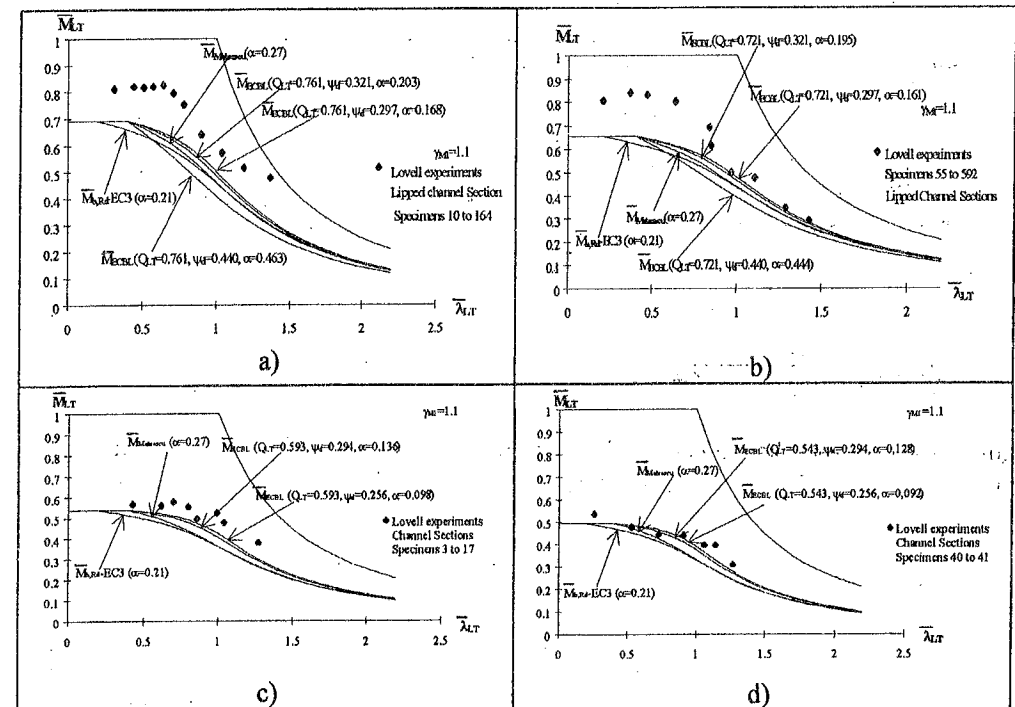
Fig. 3 Numerical-experimental comparative results

In case of Lovell's lipped channel tests, the best results for the ECBL approach, compared to EUROCODE 3-1.3 and Mateescu formulas, were obtained for $\psi_d=0.321$ ($\Delta=50\%$ and $\varepsilon=\pm20$), while for Rhodes tests the best ECBL results were resulted for $\psi_d=0.376$ ($\Delta=50\%$ and $\varepsilon=\pm15$). In the case of Lovell's channel tests the best results for ECBL approach are obtained for $\psi_d=0.256$; compared both to EUROCODE 3 and Mateescu formulas the correlation between test and numerical results is better in this case, but unfortunately, in all three approach, the safety level is too small.

The Generalised Beam Theory (GBT), seems to be a very convenient tool to analyse the individual and coupled buckling modes in the case of compression and bending thin-walled members. It was suitable to compare the results obtained with this method with those given by a standard Finite Element code, like ANSYS. On the other hand, the comparison of both the GBT and FEM results, via some selected series of tested specimens, with corresponding results given by relevant design code provisions, like EC3-Part. 1.3 and AISI LRDF (1990), or with the results of some recent interactive buckling approaches, like the ECBL method are, also, interesting and useful. GBT can be used both for bifurcation and general second-order problems [8], [9]. The independent modes are solved as bifurcation problems, while the coupled modes are of second-order ones.

The ANSYS FEM computer code, 5.1 version, with Elastic Shell 6.3 elements and the Subspace Eigen Buckling Method are used for the comparison with GBT Lovell's bending channel specimens [3] were selected for this comparison.

Figures 4 (a,b) show the comparison between GBT and FEM results. Local (L), distorsional (D) and overall (LT) independent instability modes and "all coupled modes" curves are plotted using GBT (no local modes are taken into account into "all modes" curve). The first eigen buckling modes overlap is plotted with ANSYS showing the ranges of different buckling modes [10].
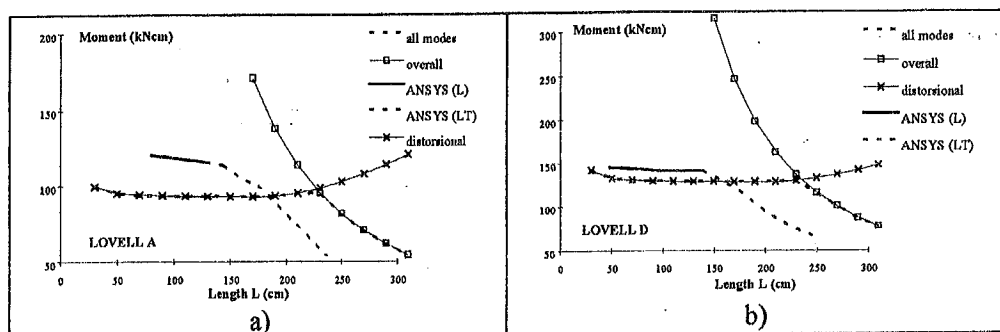
Fig. 4 GBT/FEM comparison for channel beams

Figures 5 (a,b) show the comparison between the interactive buckling curves obtained with GBT and ANSYS with those given by EUROCODE3-Part. 1.3, AISI LRFD (1990) and ECBL approaches and with test results [10].
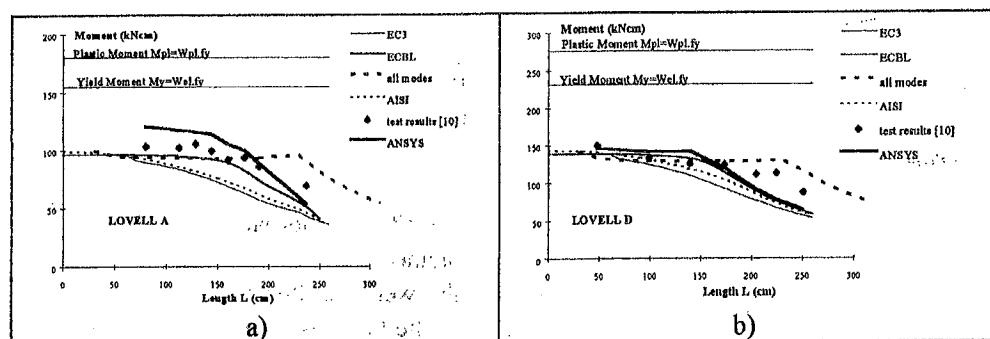
Fig. 5 Comparison with tests and design method for channel beams

5. CONCLUSIONS

The results obtained either with the code formulas or the ECBL approach are in a very good agreement with test results. In fact, this formulas are semi-empirical ones, and they were calibrated via a statistical processing of test results; consequently, it may be expected to have a such good agreement with the experiments.

If the comparison is limited only to GBT and ANSYS FEM results, the situation is rather different, especially because for short members the ANSYS model introduces the local buckling mode only, both for the compression flange and web, while in the case of GBT the distorsional mode is dominant. The FEM results are closed to the tests in case of Lovell's D specimen series, while GBT shows a good agreement with experiments, both for Lovell's A and D specimen series, but only for no long members.

The interactive buckling phenomenon of thin-walled cold-formed members is characterised by a strong erosion of critical load due both to the imperfections and coupling effect of instability modes. It could appear that both the GBT and FEM models used in this study are not suitable enough for these kind of problems, but this is not true because refined models can be obtained with both these methods. The effect of imperfections together with the plastic behaviour, which is important for short members especially, must be taken into account.

6. REFERENCES

[1] Dubina D. et al, "Calibration of Interactive Buckling Erosion Factor via a Cold-formed Steel Sections Experimental Database", *Proc. of Int. Coll. on Stability of Steel Structures, Budapest*, Hungary, September 21-23, 1995, Vol. II, pp. 133-144.

[2] Dubina D. et al, "Interactive buckling of cold-formed thin-walled members" *Structural Stability and Design*, ed. Kitipornchai S., Hancock G.J. & Bradford M.A. (Balkema, Rotterdam, 1995), pp. 49-54.

[3] Lovell M.H., "Lateral buckling of light gauge steel beams", Research Report, Department of Civil Engineering, University of Salford, 1985.

[4] Rhodes J. and Harvey J.M., *Proc. of the Fourth Conference on Experimental Stress Analysis*, 1970.

[5] Seah L.K., "Buckling Behaviour of Edge Stiffeners in Thin-Walled Sections", Doctoral Thesis, 1989.

[6] Mateescu D., "Considerations on the Value of Reduction Factor of Lateral-Torsional Buckling of Beams in Bending", *Proc. of First Int. Spec. Conf. on Coupled Instabilities in Metal Structures-CIMS'92*, Timisoara, October 12-14, 1992; Vol. 20, No. 1-4, 1994.

[7] Goina D., "Coupled instabilities in cold-formed thin-walled steel structures", in present volume.

[8] Davies J.M. and Leach P., "First-Order Generalised Beam Theory" *J. Construct. Steel Research.* **31** (1994), 187-220.

[9] Davies J.M. and Leach P., "Second-Order Generalised Beam Theory" *J. Construct. Steel Research.* **31** (1994), 221-241.

[10] Dubina D, Davies J.M. et al, "Recent interactive buckling approaches for cold-formed thin-walled members", *Coupled Instabilities in Metal Structures*, Liege, 5-7 September 1996, in print.

COUPLED INSTABILITIES IN COLD-FORMED THIN-WALLED STEEL COLUMNS

Dorina Goina
Centre of Advanced Technical Sciences, Romanian Academy, The Timisoara Branch
Mihai Viteazul 24, Timisoara, RO-1900

1. INTRODUCTION

In case of thin-walled cold-formed (TWCF) steel compression members, due to both wall slenderness and geometrical imperfections, an overall-local interactive buckling almost always occurs. The specific phenomenon of coupled instability, as a main design criteria for this type of steel profiles, is however extremely difficult to be implemented within simple formulas. The methods that are available to solve this problem may be classified in four categories:

1) *Analytic (theoretical) methods*, based on the theory of member post-critical behaviour, which unfortunately cannot give available formulas to current design;

2) *Semi-analytic methods*, where modelling of wall-buckling phenomenon is achieved using the "plate effective width" concept. The column overall non-linear behaviour is expressed using classic equations of structural mechanics, while the non-linear problem of the interaction between local and overall buckling is dealt by means of a step-by-step numerical algorithm;

3) *Semi-empirical methods*, which modify the buckling curves by means of reduced geometrical properties of member cross-section on the base of the "effective width" concept;

4) *Numerical methods*, which are the most powerful instrument to the analyse of thin-walled members behaviour. Finite Element method (FEM) using "shell" type elements and Finite Strip Methods (FSM) are both included in this category. However their use in practical design of structures is impossible since they allow only for the analyse of isolated members.

Generally, the design codes use semi-empirical methods. The actual Eurocode 3 - Part 1.3 buckling curves, used to analyse the behaviour of cold-formed steel member, have been obtained for hot rolled sections. Due to the different nature of the imperfections and to the interaction between overall and local buckling, these curves sometimes cannot appropriately describe the buckling behaviour of cold-formed steel members. An alternative approach based on the Erosion of Critical Bifurcation Load (ECBL) theory, is proposed.

2. THE ECBL APPROACH FOR INTERACTIVE BUCKLING OF COLD-FORMED THIN-WALLED COMPRESSION MEMBERS

On the basis of the ECBL theory applied to coupled instabilities [1], in Ref. 2 a new approach of overall-local interactive buckling load was proposed. This approach assumes the two theoretical simple instability modes that couple in case of thin-walled compression members, are the Euler instability mode, $\overline{N}_E = 1/\overline{\lambda}$ and the local instability mode, $\overline{N}_L$ described by means of the reducing factor of area, $\overline{N}_L = Q$. The resulting eroded curve describing coupled instability mode is $\overline{N}(\overline{\lambda}, \psi, Q)$ (see Fig. 1) Critical load maximum erosion (due to both imperfections and coupling effect) occurs in instability modes interaction point M ($\overline{\lambda} = 1/\sqrt{Q}$), where the erosion factor (ψ) is defined as:

$$\psi = \overline{N}_A - \overline{N} = \overline{N}_L - \overline{N} = Q - \overline{N} \tag{2.1}$$

where $\overline{N}(\overline{\lambda} = 1/\sqrt{Q}, Q, \psi)$ is the interactive buckling load.

It must be emphasised that $\overline{N}_L = Q$ is not precisely the theoretical local buckling curve, but it can be assumed (in a simplified manner, of course) as a *level* of the cross-section local buckling mode. However, Winter formula for computing effective width and Q is not a theoretical one because it was obtained in a semi-empirical way, modifying the theoretical formula given by Von Karman on the basis of experimental tests. On the other hand it is nevertheless evident that, even using Winter formula in Q computing, the fact of not considering at all the interaction between component walls of the cross-section, causes an under evaluation of the short member strength.
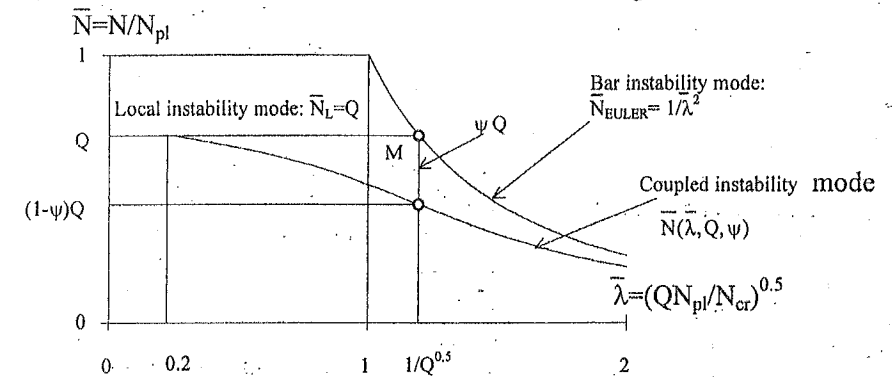
Fig 1. The Interactive Buckling Model based on the ECBL Theory

In order to obtain the interactive buckling curve $\overline{N}(\overline{\lambda}, Q, \psi)$ we have to start from the Ayrton-Perry formula adapted for the buckling of compression thin-walled steel members:

$$(Q - \overline{N})(1 - \overline{\lambda}^2 \overline{N}) = \eta \overline{N} \tag{2.2}$$

where: $\eta = \alpha(\overline{\lambda} - 0.2)$, is the generalised imperfection; $\overline{N} = N / N_{pl}$, is the relative compression load; $Q = A_{eff} / A$, the reducing factor of effective area; $\overline{\lambda} = \sqrt{QN_{pl} / N_{cr}}$, the member relative slenderness, $N_{pl} = Af_y$, the plastic strength of full cross-section and α is the imperfection coefficient.

Solving Eq. (2.2) in terms of $\overline{N}$ and imposing for $\overline{N}(\overline{\lambda} = 1/\sqrt{Q})$ to be equal to $(1-\psi)Q$ (see Fig. 1.) it gives:

$$\overline{N} = \frac{1 + \alpha(\overline{\lambda} - 0.2) + Q\overline{\lambda}^2}{2\overline{\lambda}^2} - \frac{1}{2\overline{\lambda}^2}\sqrt{[1 + \alpha(\overline{\lambda} - 0.2) + Q\overline{\lambda}^2]^2 - 4Q\overline{\lambda}^2} = (1-\psi)Q \tag{2.3}$$

the following relation between α, ψ and Q was obtained:

$$\alpha = \frac{\psi^2}{1-\psi} \cdot \frac{\sqrt{Q}}{1-0.2\sqrt{Q}} \qquad (2.4)$$

This represents the new formula of "α" imperfection coefficient which should be introduced in European buckling curves [3] in order to adapt these curves to overall-local buckling.

3. EXPERIMENTAL APPROACH FOR THE EVALUATION OF ψ EROSION FACTOR

There are three distinct approaches that can be used to evaluate the ψ Erosion Factor:

1. *the analytical approach*, that can be developed in the frame of the general theory of elastic stability, having as main goal to compute the low of axial rigidity of the related column in the vicinity of critical bifurcation point;

2. *the numerical approach* based on Finite Element (FEM) or Finite Strip (FSM) non-linear analysis of the behaviour of thin-walled columns in the vicinity of critical bifurcation point;

3. *the experimental approach* that is involving a statistical analysis of a representative series of column test results corresponding to specified cross-section shape which are characterised by means of Q factor in a *slenderness range of interactive buckling*; i.e. the vicinity of the point $\bar{\lambda} = 1/\sqrt{Q}$ (see Fig.2).

Due to the mathematical complexity of interactive buckling theory, the first approach is too difficult to be used in practice, only in some special cases should it be used.

There are no special problems to perform a numerical simulation of the behaviour of a thin-walled column in the vicinity of instability coupling point e.g. the critical bifurcation point, if a FEM or FSM non-linear computer code is available, but always an experimental calibration of the numerical model is necessary.

In these conditions, the experimental approach seems to be the most appropriate way to evaluate the erosion factor.
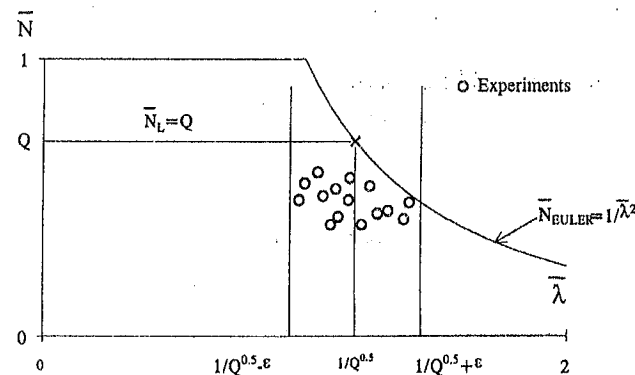
Fig. 2. Evaluation of ψ Erosion Factor by means of experimental tests

For a given specimen series of test results, if the interactive slenderness range is assumed to be $\bar{\lambda} = 1/Q^{0.5} \pm \varepsilon$, the experimental approach includes the following steps:

1. Compute the *individual* erosion for the i column specimen

$$\psi_i = Q_i - \overline{N}_{i,exp} \qquad (3.1)$$

where: $\overline{N}_{i,exp} = N_{i,exp}/N_{i,pl}$ $\qquad (3.2)$

with $N_{i,exp}$ - the experimental failure load and $N_{i,pl}$ - the full plastic resistance of the "**i**" column

2. Compute the mean value of ψ erosion factor for all **n** columns with the same cross-section shape, tested in the interactive buckling slenderness range:

$$\psi_m = \frac{1}{n} \sum_{i=1}^{n} (Q_i - \overline{N}_{i,exp}) \qquad (3.3)$$

3. Compute the *design* value of the erosion factor:

$$\psi_d = \psi_m + 2s \qquad (3.4)$$

in which s is the standard deviation related to ψ_i and ψ_m values.

It must be underlined that, after the specimen series was established for a predicted scattering, ψ_m and s, respectively ψ_d are calculated using experimental values within this specified series.

There are two parameters that characterise the specimen series i.e.

- the scattering of experimental results related to the mean value ψ_m:

$$\%\Delta = \frac{|\psi - \psi_m|}{\psi_m} \times 100 \qquad (3.5)$$

- the interactive buckling slenderness range, ε.

Both parameters can strongly influence the value of ψ, as will be shown in this paper.

In the aim to calibrate ψ erosion factor, an experimental cold-formed steel sections data bank (named DATACOST) is actually in progress in a combined research activity performed by the Department of Steel Structures at T.U. Timisoara and the Centre of Advanced Technical Sciences from Timisoara Branch of Romanian Academy (see [4]). This database is used to calibrate the ψ factor and, on this basis, to obtain the new α imperfection coefficient and a new classification of cold-formed steel section for the stability analysis.

The ψ factor evaluation for some series of compression members (channel and lipped-channel section) tested in Liège University [5], are presented in the following. Several interaction ranges ($1/\sqrt{Q} \pm \varepsilon$), as well as scattering values were proposed To study erosion coefficient ψ_d change. The related results are presented in tables 1 to 3. Regarding the interactive slenderness range, it depends on the experimental data at our disposal, but, as well known, the interaction erosion is theoretically maximum in coupling point $\bar{\lambda} = 1/\sqrt{Q}$. In fact, on the right hand of $1/\sqrt{Q}$, the theoretical value of critical load will be given by Euler buckling curve, and, consequently, $\psi_i = \overline{N}_{E,i} - \overline{N}_{i,exp}$; only in a very closed vicinity to $\bar{\lambda} = 1/\sqrt{Q}$ it can be assumed that $\psi_i = Q_i - \overline{N}_{i,exp}$. Consequently, if tests surrounding the coupling point are available enough, a smaller interactive slenderness range would be better. Unfortunately, this is not valid in our case, and larger ε should be used in order to obtain the design value of the erosion factor, ψ_d.

Tab. 1-Erosion coefficient.

Δ	100 lipped channel section tested in Liege								
	30%			50%			70%		
Inter. range	ψ_m	s	ψ_d	ψ_m	s	ψ_d	ψ_m	s	ψ_d
$1/Q^{0.5} \pm 0.15$	0.236	0.039	0.314	0.234	0.072	0.378	0.232	0.099	0.430
$1/Q^{0.5} \pm 0.20$	0.242	0.041	0.324	0.248	0.069	0.386	0.239	0.097	0.433

x

Tab. 1 (Cntd)

$1/Q^{0.5} \pm 0.25$	0.245	0.040	0.325	0.258	0.070	0.398	0.252	0.098	0.448

49 channel section tested in Liege

$1/Q^{0.5} \pm 0.15$	0.249	0.043	0.335	0.261	0.080	0.421	0.247	0.089	0.425
$1/Q^{0.5} \pm 0.20$	0.193	0.038	0.269	0.208	0.068	0.344	0.208	0.068	0.344
$1/Q^{0.5} \pm 0.25$	0.193	0.038	0.269	0.185	0.062	0.309	0.198	0.069	0.336

4. COMPARISON BETWEEN NUMERICAL AND EXPERIMENTAL RESULTS

This chapter includes comparison of the results obtained by both ECBL and EC3 Part 1.3 interactive approaches with experimental results. Fig. 3 (a and b) show the comparison between EC3 and ECBL buckling curves with some selected lipped channel and channel section compression specimens, respectively.
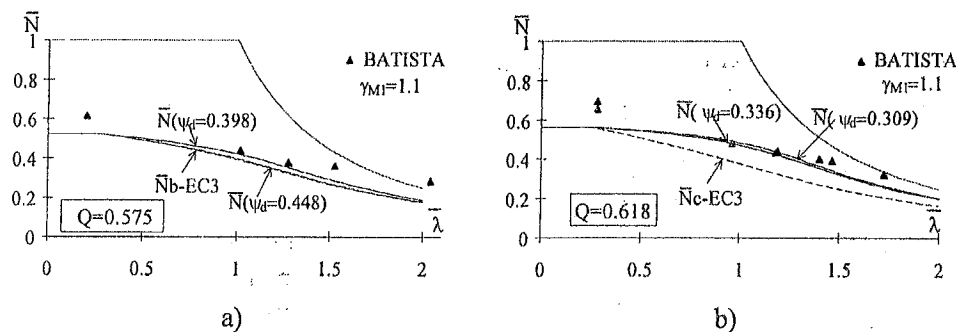
Fig. 3 Numerical experimental comparative results

Tab. 2 shows the statistical comparison (according to EC3-Annex Z procedure[6]) for all related specimens tested in Liège.

Tab.2 Statistical Values Lippped Channel and Channel Columns

Method		BATISTA's Lipped Channel Section (100 Tests)								
		ECBL								
		30%			50%			70%		
Stat. param.	EC3	$1/Q^{0.5}$ ±0.15	$1/Q^{0.5}$ ±0.20	$1/Q^{0.5}$ ±0.25	$1/Q^{0.5}$ ±0.15	$1/Q^{0.5}$ ±0.20	$1/Q^{0.5}$ ±0.25	$1/Q^{0.5}$ ±0.15	$1/Q^{0.5}$ ±0.20	$1/Q^{0.5}$ ±0.25
m	1.401	1.197	1.209	1.211	1.284	1.297	1.316	1.371	1.376	1.405
s	0.261	0.201	0.204	0.204	0.221	0.225	0.230	0.245	0.247	0.255
m-2s	0.879	0.795	0.801	0.803	0.842	0.847	0.856	0.881	0.882	0.895
v	0.187	0.167	0.168	0.168	0.172	0.173	0.175	0.179	0.179	0.181
ρ	0.913	0.917	0.917	0.917	0.913	0.912	0.910	0.905	0.905	0.902
BATISTA's Lipped Channel Section (49 Tests)										
m	1.547	1.253	1.173	1.173	1.388	1.265	1.219	1.396	1.265	1.254
s	0.197	0.131	0.119	0.119	0.163	0.134	0.126	0.165	0.134	0.132
m-2s	1.151	0.991	0.935	0.935	1.062	0.997	0.967	1.066	0.997	0.992
v	0.128	0.105	0.101	0.101	0.117	0.106	0.100	0.118	0.106	0.100
ρ	0.818	0.910	0.927	0.927	0.860	0.906	0.919	0.857	0.906	0.910

In case of lipped channel tests, the best results for the ECBL approach, compared to EUROCODE 3-Part 1.3, are obtained for $\psi_d=0.430$ ($\Delta=70\%$ and $\varepsilon = \pm0.15$), $\psi_d=0.433$ ($\Delta=70\%$ and $\varepsilon = \pm0.20$) and $\psi_d=0.448$ ($\Delta=70\%$ and $\varepsilon = \pm0.25$). The correlation between numerical and experimental results is very good ($\rho > 0.9$) both for EC3-Part 1.3 and ECBL approach but the safety level is slightly unsatisfactory (the best safety level was obtained for $\psi_d=0.448$). In the case of channel sections safety level is good in all the cases and the correlation between numerical and experimental results is very good for ECBL approach with $\psi_d=0.335$ ($\Delta=30\%$, $\varepsilon = \pm0.15$); $\psi_d=0.269$ ($\Delta=30\%$, $\varepsilon = \pm0.20$; $\Delta=30\%$, $\varepsilon = \pm0.25$); $\psi_d=0.344$ ($\Delta=50\%$, $\varepsilon = \pm0.20$; $\Delta=70\%$, $\varepsilon = \pm0.20$); $\psi_d=0.309$ ($\Delta=50\%$, $\varepsilon = \pm0.20$) and $\psi_d=0.336$ ($\Delta=70\%$, $\varepsilon = \pm0.25$). The best results were obtained for $\psi_d=0.344$

5. CONCLUSIONS

The ECBL theory is offering a suitable design model for thin-walled members in compression. In fact the Ayrton-Perry form of buckling curves, actually used in Eurocode 3, is maintained, but a new *imperfection* coefficient, depending on both imperfection effect and coupled instability, is introduced.

The correlation between ECBL interactive approach results and the experimental ones is very satisfactory and encourages researches in this area to be continued. The essential problem is that of ψ erosion factor evaluation.

Taking into account that experimental results on *interactive slenderness range* are interesting for ψ evaluation, only a relatively limited number of tests will be necessary. This is, in our opinion, the main advantage of the ECBL approach, because, on this way, the European buckling curves could be very easily adapted for cold-formed section.

REFERENCES

[1] Gioncu V., "General Theory of Coupled Instabilities", Elsevier Applied Science, *Thin-Walled Structures*, Volume 19, No. 2-4 1994, pp.81.

[2] Dubina D.; Goina D., "Interactive Buckling Approach on Thin-walled Cold-formed Members via an Ayrton-Perry Formula and Based on the Critical Load Erosion Theory", Research Report, Romanian Academy of Science, Timisoara Branch, January 1995

[3] *****EUROCODE3 Part 1.3 "Supplementary rules for Cold Formed Thin-Gauge Members and Sheeting", ENV 1993-1-3, 1996 E.

[4] Dubina D. et al, "Calibration of Interactive Buckling Erosion Factor Via a Cold-Formed Steel Sections Experimental Data Base", Int. Coll. on Stability of Steel Structures, Hungary, Budapest, September 21-23, Preliminary Report, Vol. II, 133-144.

[5] Batista, E.M., 1987, "Essais de profils C et U en acier plies a froid", Laboratoire MSM, Université de Liège, Rapport No. 157

[6] ***** EUROCODE 3- Part 1.1, "Design of Steel Structures, General Rules and rules for Buildings", Annex Z, February, 1992.

FATIGUE EXAMINATION IN STEEL RAILWAY BRIDGES BY USING THE HUNGARIAN TRAFFIC TYPE AND THE EUROCODE

Rafik Jaramani
Department of Steel Structures
Technical University of Budapest
H - 1521 Budapest, Hungary

ABSTRACT

In the past two years at the Department of Steel Structures, Technical University of Budapest a parametric study is done on the effects of fatigue on railway bridges.

The West European proposals (i.e. Eurocode 3) on railway bridge construction were used as a basis of this study. The results of the study indicated that a part of the Eurocode 3 proposals can be applied to Hungarian railway bridges.

1. INTRODUCTION

In previous years, West European fatigue examinations on railway bridges were conducted using the UIC proposals on traffic types. In these studies, the ideal (UIC) train loads were replaced with other load types. Different ideal loads were used for improving the accuracy, for example, differentiation between passenger trains and carriage trains. This differentiation of load types (4 - 12) depended upon the annual volume of traffic on the railway lines.

The use of the differentiated load types result an accepted tools but more complicated design procedures in the work. As a consequence, the UIC ideal load was used.
The following correction factor was included in the empirical analysis to compare the calculated stress with fatigue allowable stress [1] [2] :

$$\lambda = \lambda_1 \cdot \lambda_2 \cdot \lambda_3 \cdot \lambda_4 \tag{1}$$

where λ_1 : is a function of the span and traffic type

λ_2 : is a factor to take account of the annual volume of traffic

λ_3 : is a factor to take account of the design life of the structure

λ_4 : is a factor to be applied when the structural element is loaded by more than one track

The λ_2, λ_3 and λ_4 factors, however do not depend on load types or on the structure elements . Thus, λ_1 is the most important variable, and is a function of normal stress or shear stress (i.e. λ_1 can be differentiated into $\lambda_{1\sigma}$ and $\lambda_{1\tau}$). This study focussed on the two factors.

2. FATIGUE DESIGN ASPECTS IN HUNGARY

The previously mentioned Eurocode 3 proposals for fatigue examination to be used in Hungary required answers for the following two questions:

- Due to differences between West Eueopean and Hungarian load types, can the results of the calculation of $\lambda_{1\sigma}$ in the West European proposals be used in Hungary ?
- Can the West European proposals, which affirm :

$$\lambda_{1\sigma} \approx \lambda_{1\tau} \tag{2}$$

be used in Hungary ?

Referring to the first question, the proposal of Forgó Sándor for railway traffic types was accepted, considering his study in railway traffic of the Hungarian railway company (MÁV) [3] [4].
To answer the second question, Hungarian railway types were used in this study.

3. SIMPLY SUPPORTED BEAMS

3.1 Study on $\lambda_{1\sigma}$ factor

The calculation of $\lambda_{1\sigma}$ was conducted on the center points of 3, 5, 7, 10 and 50 meter span simply supported beams. The volume of traffic was 25 million tonne per annum. As a result, $\lambda_2 = 1$ and the design life of the structure is 100 years (i.e. $\lambda_3 = 1$). The structural element was loaded by one track (i.e. $\lambda_4 = 1$). Therefore, $\lambda = \lambda_1$.
In the study, the Standard S-N - curve (i.e. Wöhler - curve) and Palmgren - Miner cumulative damage calculation were used.

In the first step, influence diagrams were constructed for each load type , these influence diagrams were used to calculate stress range ($\Delta\sigma_i$) and the load cycles (N_i) using the Reservoir method. Following this, the reference value of fatigue stress at two million cycles ($\Delta\sigma_e$) was determined as :

$$\Delta\sigma_e = \frac{1}{\sqrt[3]{N_e}} \cdot \sqrt[3]{\sum_i \Delta\sigma_i^3 \cdot n_i \cdot \phi_i + \sum_j N_D^{0.4} \cdot \Delta\sigma_j^3 \cdot n_j^{0.6} \cdot \phi_i} \tag{3}$$

The Eurocode 3 proposal :

$$\lambda_1 = \frac{\Delta\sigma_e}{\phi_2 \cdot \Delta\sigma_{UIC}} \tag{4}$$

was then calculated, where

$\Delta\sigma_{UIC}$: is the stress range due to the UIC load diagram being placed in the most unfavourable position for the member under consideration.

ϕ_2: is the dynamic coefficient.

$$\phi_2 = \frac{1.44}{\sqrt{L} - 0.82} + 0.82 , \qquad (1.05 \le \phi_2 < 1.67) \tag{5}$$

ϕ_i: is the dynamic coefficient for each service train type.

$$\phi_i = 1 + 0.5(\varphi' + 0.5\varphi'') \tag{6}$$

$$\varphi' = \frac{K}{1 - K + K^{2.4}} \quad \text{with} \quad K = \frac{V}{160} \quad \text{for } L < 20 \text{ m}$$

$$\text{or} \quad K = \frac{V}{47.16 \cdot L^{0.408}} \quad \text{for } L > 20 \text{ m}$$

$$\varphi'' = 0.56 \cdot e^{-\left(\frac{L^2}{100}\right)}$$

$$V = \text{speed (m/s)}$$

As seen in Table 1, the results of $\lambda_{1\sigma}$ in this study are similar to the Eurocode 3 results, therefore, the Eurocode 3 proposals can be used in Hungary.

Table 1. The values of $\lambda_{1\sigma}$

L [m]	Type I.	Type II.	Type III.	TypeIV.	Mix	EUROCODE
3.0	1.63	1.61	1.39	2.19	1.68	1.36
5.0	0.88	0.92	0.76	1.20	1.00	1.02
7.0	1.07	1.01	0.79	1.31	0.96	0.94
10.0	0.79	0.62	0.68	0.93	0.75	0.82
50.0	0.59	0.48	0.55	0.62	0.56	0.62

3.2 Study on $\lambda_{1\tau}$ factor

$\Delta\tau_e$ was determined as :

$$\Delta\tau_e = \frac{1}{\sqrt[5]{N_e}} \cdot \sqrt[5]{\sum_i \Delta\tau_i^5 \cdot n_i \cdot \phi_i} \tag{7}$$

The same method of calculation of $\lambda_{1\sigma}$ was used to calculate $\lambda_{1\tau}$.

To compare $\lambda_{1\sigma}$ with $\lambda_{1\tau}$, the following ratio was used :

$$\alpha = \frac{\lambda_{1\sigma}}{\lambda_{1\tau}} \tag{8}$$

The results of this calculation are shown in Table 2. the values of α ratio are not similar to the Eurocode 3 results, therefore, the Eurocode 3 proposals can not be used in Hungary.

Table 2. The values of α ratio

L [m]	Type I.	Type II.	Type III.	TypeIV.	Mix	EUROCODE
3.0	0.60	0.76	0.60	0.60	0.68	1.00
5.0	0.98	1.28	1.03	0.86	1.06	1.00
7.0	1.20	1.41	1.48	1.18	1.42	1.00
10.0	1.16	1.87	1.31	1.25	1.48	1.00
50.0	1.61	1.90	1.67	1.52	1.66	1.00

4. ELASTICALLY SUPPORTED CONTINUOUS BEAMS

It is important to extend the previously mentioned study on continuous beams, because the maximum moment and maximum shear force in continuous beams are applied in the same cross - section.

The previously mentioned calculation method of $\lambda_{1\sigma}$ and $\lambda_{1\tau}$ was used here, too.

The results of the calculation of $\lambda_{1\sigma}$ was conducted on the cross - section of 3, 5 and 7, meter span elastically supported continuous beams, as shown in Table 3

Table 3. The values of $\lambda_{1\sigma}$

L [m]	Type I.	Type II.	Type III.	TypeIV.	Mix
3.0	4.1	2.12	2.50	4.23	3.41
5.0	1.66	1.00	1.13	1.79	1.45
7.0	1.28	1.14	0.96	1.31	1.05

During this study we calculated the ratio α for elastically supported continuous beams also. As seen in the Table 4

Table 4. The values of α ratio

L [m]	Type I.	Type II.	Type III.	TypeIV.	Mix
3.0	0.35	0.74	0.50	0.43	0.47
5.0	0.89	1.48	1.10	1.05	1.11
7.0	1.20	1.24	1.38	1.34	1.42

If we compare the Table 1 with the Table 3, and the Table 2 with the Table 4 we find a big different between the calculated results, which means we can not use the results of simply supported beams in the case of elastically supported continuous beams.

5. CONCLUSIONS

The results of this study show that the Eurocode 3 proposals for moment induced fatigue in simply supported beams can be used in Hungary, but the proposals for shear checking fatigue can not be used in Hungary.

The comparison between the calculated results of $\lambda_{1\sigma}$ and $\lambda_{1\tau}$ in simply supported beams and elastically supported continuous beams show that the ruselts of the calculation in simply supported beams can not be used in the case of elastically supported continuous beams. It means we have to do an independent calculation for the continuous beams, because the Eurocode 3 proposals for continuous beams have not yet been affirmed.

The study on continuous beams is especially important in welded connections, where normal stress has an interaction with shear stress.

6. REFERENCES

[1] Eurocode Einwirkungen auf Tragwerke "Vorschlag UIC" .Version : July 1991.

[2] Platthy, P. (1994): "New Hungarian Standards for railway bridges". XVII. Czech and Slovak Int. Conf. on Steel Structures. *Proceedings*. I. pp. 399 - 403.

[3] Forgó, S. (1995): "A vasúti acélhidak fáradása" (Fatigue of the Steel railway bridges). *Sinek világa*. XXXVIII. évf. pp. 179 - 188.

[4] Jaramani, R. (1995): "Vasúti hidak fáradásvizsgálata" (Examination of Fatigue in Steel railway bridges). *V. Törésmechanikai Szeminárium*. Miskolc. pp. 57 - 68.

[5] Platthy, P. (1975): "A rideg és a fáradt törés kapcsolata, valamint a fárasztó üzemi teher" (Relation of the brittle fracture to the fatigue crack and the value of the equivalent constant amplitude fatigue loading). *Mélyépítés - tudományi Szemle*, XXV. év. pp. 556 - 560.

MULTI-LEVEL APPROACH FOR THE STEEL FRAME CYCLIC BEHAVIOUR

Géza Varga
Technical University of Budapest, Department of Steel Structures
H-1521 Budapest

1. INTRODUCTION

Cyclic performance of structures is of importance when repeated loads in the inelastic range are applied. Cyclic behaviour here assumes no high cycle fatigue damage to occur. One of the main features of cyclic behaviour is its stability (Fig. 1). From experimental point of view, the behaviour can be defined as stable when the initial stiffness shown by each cycle is constant, and as unstable, when it is not. However, exact mathematical formulation of stability is difficult to construct.

Another feature of the behaviour is the deterioration of strength during load reversals. This deterioration means that, under strain controlled conditions, decreased values of forces are related to the same displacement level while applying reversed loading (e.g. see Fig. 1a). This process is due to several reasons, which are connected to different phenomena such as instability or low cycle fatigue based damage of the structural part concerned. The modelling of these phenomena is, as the most lucrative way, generally based on so-called physical theory models [1], and can be processed using different damage models [1] [2] [3].

In this paper, the idea of a multi-level approach for steel frame cyclic behaviour is presented, along with its realistic simplified form to be used in steel frame calculations. Testing aspects are reviewed from the point of view of this approach. Description difficulties of cyclic behaviour in relation with different loading programmes are emphasized.

2. MULTI-LEVEL APPROACH AND MODELLING ASPECTS

The multi-level approach assumes that the performance of the whole structure, or of a part of the whole structure, should somehow be based on the performance of the structural levels which are of lower order than the part in question. However, the derivation of the performance of one level from the other should include the consideration of some "external" phenomena. These "external" phenomena can be of two types: (a) those which could be incorporated into the derivation process with the application of higher mathematical accuracy (e.g. P-Δ and P-δ effects of frames), and (b) those which could not, referred to as "instability phenomena" [4]. Fig. 2 illustrates the levels of the multi-level approach in the case of steel frames, assuming that the type (a) "external" phenomena are incorporated into the derivation process.

No doubt, it is a long way to be able to track all the derivation processes represented in Fig. 2. For the present, a simplified approach should be used. The following simplifications are proposed:
- With the exclusion of Class 4 cross-sections [5], it can be assumed that instability phenomena in the inelastic range do not affect the behaviour of the cross-section.
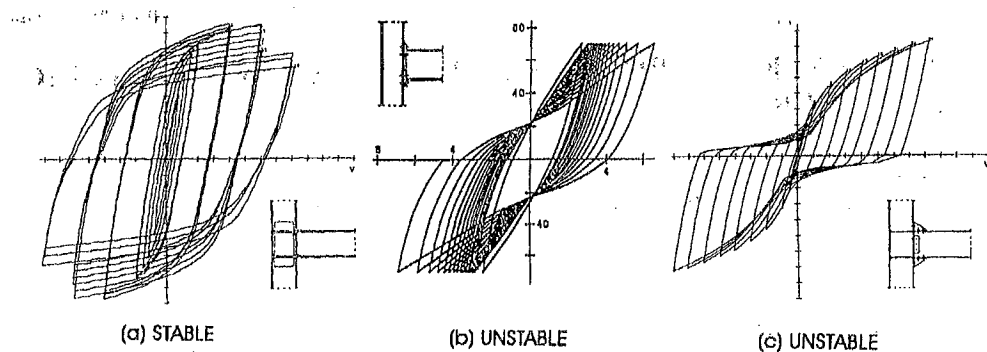
(a) STABLE   (b) UNSTABLE   (c) UNSTABLE

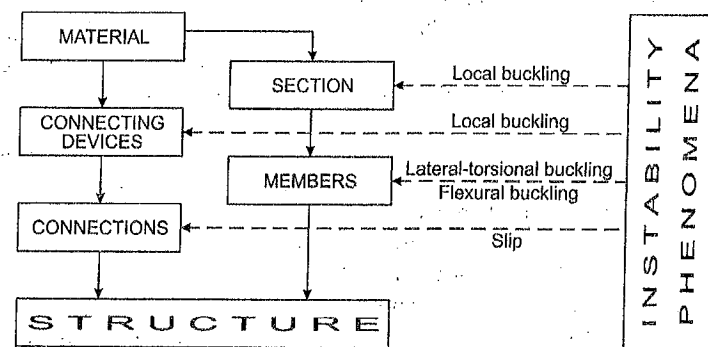*Fig. 1 Three types of cyclic behaviour*

Fig. 2 Multi-level approach. Idealized formulation

What concerns the instability phenomena in the plastic range, it can either be taken into account explicitly [6], or should be referred to in the connection model [7].

- The connecting devices–connections branch could be substituted with a simple idealized connection behaviour. Four possible modes of formulation can be established for the modelling of this behaviour:
  - (a) Rigid and pinned connections only;
  - (b) Idealized semi-rigid connections with stable, heuristic behaviour;
  - (c) More sophisticated idealized connection models (so called physical theory models [1], with stable behaviour, and explicit inclusion of instability phenomena, as in the case of the multi-spring type models such as those proposed in [7] or [8];
  - (d) Analytical connection models (so called phenomenological models [1]) based on parameters determined via tests, taking instability and slip into consideration [9].

This simplified model is illustrated in Fig. 3.

A very wide range of information, as well as many good predictive models, are already available concerning material behaviour [10]. However, it is anticipated that a relatively simple constitutive law [11] will ensure satisfactory results. From the material behaviour, which can be assumed to be stable in principle, the section behaviour can be derived according to the first simplification given above. The second simplification implies that there is no explicit connection between material and connection level, instead, connection behaviour is considered on the basis of available test results. An
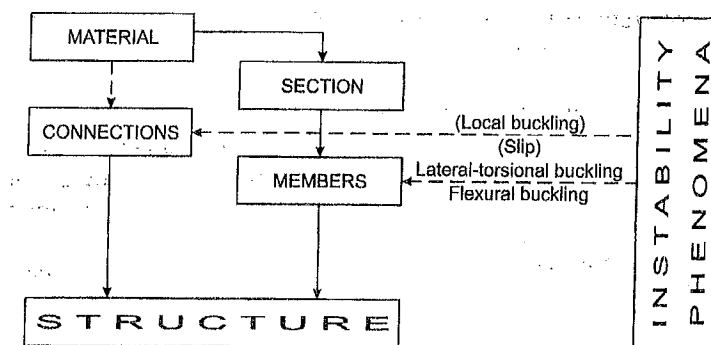
Fig. 3 Multi-level approach. Simplified formulation

interesting point of the approach can be the derivation of the member behaviour, for which a few models are already available [6]. It should be noted here that, according to the approach, the instability of the cyclic behaviour of the whole structure, when relevant, should arise primarily in this level.

3. TESTING ASPECTS

From the structural levels given in Fig. 2, only whole structures, members or connections separated, and certain connecting devices separated can be tested. In the context of the above described multi-level approach and its simplified version illustrated in Fig. 3, the role of the different tests of structural levels can be the following:

- Separated connection tests can serve as the basis for the derivation of the idealized connection behaviour;
- Separated member tests can provide predictive models for flexural and lateral-torsional buckling effects;
- Whole structure tests can serve as tool for the justification of the multi-level idea and the model simplifications applied in the simplified approach, and can show applicability limitations for those.

Separated connecting device tests, as connecting devices are not considered as an independent level in the simplified multi-level approach, are of no use in this context. It should be emphasized here that full scale tests are of relevant importance.

4. DESCRIPTION OF BEHAVIOUR

The behaviour of steel frames under cyclic loading should be described using the governing cyclic parameters as recommended in the ECCS Recommendations [12]. The following parameters are defined :

- partial ductility (μ_0), defined as the ratio of the total deformation in one direction and the yield deformation;
- full ductility (μ), defined as the ratio of the total deformation within a half cycle and the yield deformation;
- full ductility ratio (ψ), defined as the ratio of the total deformation within a half cycle and the overall deformation difference of the cycle with the yield deformation subtracted;
- resistance ratio (ε), defined as the ratio of the resistance and the yield resistance;
- rigidity ratio (ξ), defined as the ratio of the tangential rigidity observed at the beginning of the cycle and the initial rigidity;

- absorbed energy ratio (η), a ratio expressing the absorbed energy of a half cycle in terms of area of the characteristic curve.

These parameters are defined for each cycle, thus can be treated as functions of the number of cycles. Further, for a given structural part, the parameters are obviously functions of the loading programme (e.g. constant force, constant deformation, etc.).
This means that if the cyclic behaviour is to be described using these parameters, either their behaviour under different loading programmes should be known (and this implies transformation rules established), or every structural part should be described under the same agreed loading programme [12].

Figs. 4 to 6 show the variation of these parameters for the three types of behaviour given in Fig. 1. These are the three typical behaviour types of steel beam to column connections (a welded connection, a bolted end plate connection and a shear bolted connection, respectively), and are taken from the literature [9] [13].

5. CONCLUSIONS

Idea of multi-level approach presented can be useful for calculating steel frames under cyclic loads. The sophisticated rules incorporated, however, make it suitable only for use in research, e.g. in future Monte Carlo simulations. For the calibration of these rules (of which a few have already been established only), separated structural part tests are needed. Another difficulty is in relation with the description of the cyclic behaviour,
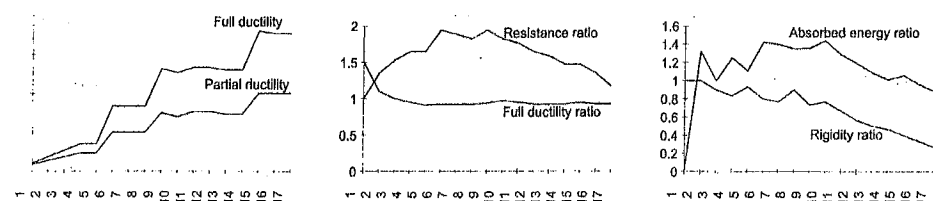

Fig. 4 First type behaviour
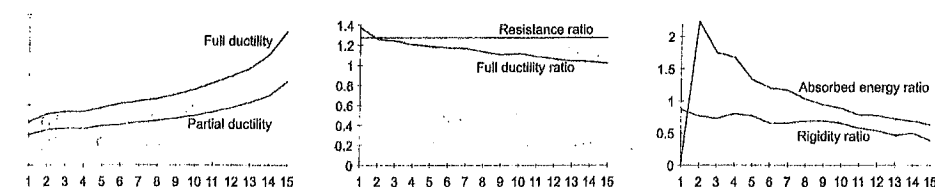
Fig. 5 Second type behaviour
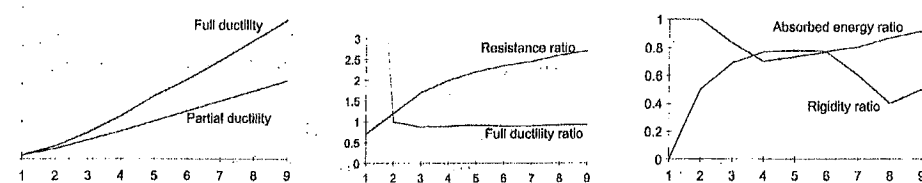
Fig. 6 Third type behaviour

which can be described via parameters which are functions of the number of cycles, and depend on the loading programme applied. Transformation rules between different loading programmes would be needed.

Consequently, the following open questions should be answered:
- What is the connection between/among the different levels of structural cyclic performance?
- What are the relations within one structural level and in case of one given configuration, between/among different test programmes?
- How does the sensitivity of the different governing cyclic parameters look like and how does it influence the frame behaviour?
- How is described, or, how can be read, stability or instability of cyclic behaviour by/from these parameters?

6. REFERENCES

[1]   Azevedo J. and Calado L.: Hysteretic behaviour of steel members: analytical models and experimental tests, *J. Constructional Steel Research*, Vol. 29, No. 1-3, 1994, pp. 71-94.
[2]   Calado L. and Azevedo J.: A model for predicting the failure of structural steel elements, *J. Constructional Steel Research*, Vol. 14, No. 1, 1989, pp. 41-64.
[3]   Ferry Borges J.: Safety Concepts for Non-Proportional and Repeated Loadings, *IABSE Reports of Working Commissions*, Vol. 12., 1973, pp. 101-124.
[4]   Takanashi K. and Nakashima M.: Stability Considerations on Seismic Performance of Steel Structures, *Proc. SSRC 50th Anniversary Conference*, Lehigh Univ., Bethlehem, Pennsylvania, U.S., 1994, pp. 119-133.
[5]   Eurocode 3 Part 1.1: Design of Steel Structures, General Rules and Rules for Buildings. European Prestandard ENV 1993-1-1:1992.
[6]   Ballio G. and Calado L.: Steel bent sections under cyclic loads: experimental and numerical approaches, *Construzioni Metalliche*, Vol. 38, No. 1, January-February 1986, pp. 1-23.
[7]   Ohi K. and Takanashi K.: Multi-Spring Joint Model for Inelastic Behaviour of Steel Members with Local Buckling, *Stability and Ductility of Steel Structures under Cyclic Loading*, ed. Fukumoto Y. and Lee G., CRC Press, 1992., pp. 215-224.
[8]   Elnashai A. S. and Elghazouli, A. Y.: Seismic behaviour of semi-rigid steel frames, *J. Constructional Steel Research*, Vol. 29, No. 1-3, 1994, pp. 149-174.
[9]   De Martino A., Faella C. and Mazzolani F. M.: Simulation of beam-to-column joint behaviour under cyclic loading, *Construzioni Metalliche* Vol. 36, No. 6, November-December 1984, pp. 346-356.
[10]   Shen C., Tanaka Y., Mizuno E. and Usami T.: A Two-Surface Model for Steels with Yield Plateau, *Structural Engineering/Earthquake Engineering* Vol. 8, No. 4, 1992, pp. 179s-188s.
[11]   Castiglioni A.: Numerical simulation of steel shapes under cyclic loading: effect of the constitutive law of the material, *Construzioni Metalliche*, Vol. 39, No. 3, May-June 1987, pp. 154-175.
[12]   Recommended Testing Procedure for Assessing the Behaviour of Structural Steel Elements under Cyclic Loads. ECCS Publication No. 45., 1986.
[13]   Ballio G., Calado A., De Martino A., Faella C. and Mazzolani F. M.: Cyclic behaviour of steel beam-to-column joints: experimental research, *Construzioni Metalliche* Vol. 39, No. 2, March-April 1987, pp. 69-90.

SESSION 4

Hydraulic engineering

WATER QUALITY CONTROL OF THE RÁCKEVE-SOROKSÁR DANUBE

Adrienne Clement
Technical University of Budapest,
Department of Water and Wastewater Engineering
H-1111 Budapest, Műegyetem rkp. 3.

1. INTRODUCTION

Among the problems that have threatened freshwater worldwide over the past two or three decades, man-made eutrophication has been the most prominent. Eutrophication literally means "rendering rich in nutrients". Although some lakes are naturally rich in nutrients, the term eutrophication is usually taken to mean the unintended enrichment by human activity, which leads the ecosystem of lakes, rivers and sea bays to change.

The Ráckeve-Soroksár Danube is only one case among others where the water, which has turned into a sickly green "pea soup" give rise to aesthetic and recreational interferences.

2. THE MODELING APPROACH

Obviously, the approach must cope with the characteristics of the problem, such as complexity, interdisciplinarity, and uncertainty. In addition, the approach must overcome the constant conflict between the need for scientific thoroughness and understanding, and the necessity to extract and provide information that can be employed at the policy making level. Thus, the scientific problem arises as how to integrate system processes that essentially differ on temporal and spatial scales such that the final result not only provides insights, but can also be used as a tool for decision making [3].

The water quality model building procedure has an outstanding role in the management practice constituting the basis of optimization and the eutrophication control models. Depending on the character of the problem, there can be any number of combinations, and this fact is well reflected by the large number of water quality models described in the literature. Our work does not focus on a development of a new version of eutrophication models but on the applicability conditions and limitations in the case of Ráckeve-Soroksár Danube study.

3. BACKGROUND OF THE RÁCKEVE-SOROKSÁR DANUBE WATER QUALITY PROBLEM

The 58 km long Ráckeve-Soroksár Danubian riverside is the second largest branch of the Hungarian Danube stretch. It is situated at the south part of the surrounding areas of the Capital, at the Isle of Csepel. The meandering channel is regulated by gates. Danube branch sector is one of the most dynamically developing recreational region of the country: the 3-400 m wide open expanse of water, the wildly romantic banks and quickly warming water entice hundreds of thousands of people seeking rest and relaxation at summer week-ends.

3.1 The "symptoms" in water quality

Water turning into mucous and becoming odorous because of the huge amount of algae can only deter bathers. Due to bacterial contamination virtually the most part of the Danube branch are unfit for bathing. Repeated occurrences of fish and shell-fish dying on a large scale, algae blooming changing the color of the water surface indicate that the Danube branch has reached the limit of its ability to absorb more [1].

The "diagnosis" is well-known: the eutophication. The situation is typical in rivers and lakes in the urban areas. What can we do to face future problems ?

3.2 The Reasons

At first sight it should be sufficient to concentrate on the watershed, its processes, and the ways in which they are influenced by human actions, in order to select the best management practices. Let us to see what is the situation in the Ráckeve-Soroksár Danube.

The Danube is a natural recipient of drain and excess surface waters from the related metropolitan sector and areas along the branch. It is the recipient of the second largest wastewater treatment plant of Budapest, which loads the Danube branch with 75 thousand cubic meters biologically treated waste water in every day. The majority of settlements surrounding the Danube branch are lack of sewerage and apart from point sources of the capital diffuse loads from surface and subsurface waters a fact which cannot be ignored when considering features determinant on water quality.

The situation is aggravated further that the quality of Danubian influent at the upper lock of the branch has been found to be unsatisfactory - and taking the prospects of infrastructures improvements in the metropolitan areas into consideration - more significant upgrading cannot be expected in the near future, either.

Other reason of water quality deterioration is derived from the special hydraulic conditions. Due to sluicing there is a slowdown in the flow rate of the danube water and it causes the sedimentation of the majority of suspended solids, the light intensity is increasing and a result of which is ongoing nutrient loads providing favorable conditions for biological production in the quickly warming water.

Neither the large numbers of external nutrient sources nor the role of the internal loads can be neglected. The considerable amount of sediment which is most likely to have settled on the river bed storing up large quantities of nutrients because of the high content of surplus of inorganic nutrients in the water.

3. APPLYING WATER QUALITY MODELS

3.1 The Vollenweider model

The core of this model is the OECD indicated study in the early 1970s to classify the lakes regarding their eutrophication level [3]. The result of this survey was a statistical model which gives a relationship between the phosphorus loads (as a normalized annual total P load) and the lake trophic status.

As the Ráckeve-Soroksár Danube is considered, it can be established that eutrophication processes are not limited by nutrients, the internal loads exceed the level which is enough to provide the biological processes. It means that the trophic status of the Danube branch depends only on the meteorological and hydrological conditions.

3.2 Simplified algae-phosphorus model

The largest group of water quality models means the dynamic models. These models based upon mass balance considerations, mostly in the form of differential equations, with time as an independent variable. There are various terms in the mass balance equation from a slightly different point of view: (a) hydrological and hydrodynamic transport terms; and (b) terms related to physical, biological and chemical transformations [3]. Since the time scales of these terms in most cases are different, most of dynamic models are ecology-oriented with simplified or completely ignored water transport.

The model applied for the Ráckeve-Soroksár Danube uses two variables: the algae phosphorus (AP) and the inorganic reactive phosphorus (IP). Considering the hydrodynamic terms a simplification is sought by analyzing steady state conditions only [2]. For the model calibration the results of a one-week measurement data was used (see Fig. 1).
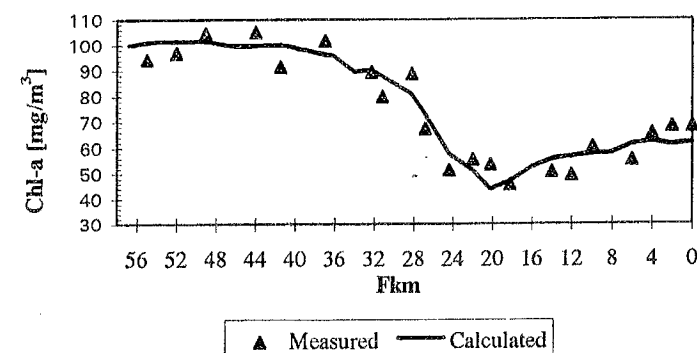
Fig.1 Result for AP-IP model: comparison of simulation with measurements

3.3 Model for eutrophication effects on dissolved oxygen

During photosynthetic cell synthesis, algae produce dissolved oxygen, whereas algal respiration consumes oxygen. The time variable rate of photosynthesis produces a diurnal variation of dissolved oxygen. The model is basically an expansion of the dissolved oxygen balance to include algal effects, taking into account not only spatial variations, but also temporal variations of dissolved oxygen concentration [4].

4. CONCLUSIONS

The paper gives a brief survey of the Ráckeve-Soroksár Danube, the major sources of nutrient loads and its impact on the water quality considering that special hydraulic conditions are in the channel because of the inflow-outflow regulation. The introduced three ecology-oriented water quality models serve as basic tools of the decision making processes.

5. REFERENCES

[1]   Clement, A., "Can it still be saved ? Survey of the Ráckeve (Soroksár) Danube", *Vízmű Panoráma*, Vol. 2, No. 3, 1994, pp. 30-32.

[2]   Thomann,R.V.-Mueller,J.A., "Principles of Surface Water Quality Modeling and Control" *Harper & Row, Publishers*, New York, 1987.

[3]   Somlyódy, L. - van Straten, G., "Modeling and Managing Shallow Lake Eutrophication", *IIASA*, 1986.

[4]   "Technical Guidance Manual for Performing Waste Load Allocations", Book II, Streams and Rivers, Chapter 2: Nutrient/Eutrophication Impacts, *U.S. EPA*, 1983.

DEPENDENCE OF DISCHARGE UPON WATER LEVEL

Tamás Dudás
Technical University of Budapest,   Department of Water Resources Engineering
H-1111 Budapest, Műegyetem rkp. 3.

1. THE PHENOMENA OF DEVIATION

1.1 The discharge rate curve

It has always been an important duty of the Hydrology to define a useable and adequate discharge rate curves for the rivers.
Certainly, it has been done by cross-sections and the velocity of the flow is supposed to be steady and uniform.
Accrediting the discharge rate curve of each significant cross-section of the river made the direct measurement of discharges superfluous. Using the discharge rate curve, the discharge time series can be generated from the stage series.

1.2 Historical records of deviation from the discharge rate curve

Although, the validity of using discharges derived from stage series by the discharge rate curve had been questionned in 1895, it has still been often applied.
By measurements of Sámuel Hajós, it has been proved, that regarding with the rivers with small slope, a significant deviation of discharges from the discharge rate curve might occur.
The falling branch of flood wave discharges might exceed the expected values, furthermore, in rising branches discharges are often less, than the ones derived from discharge rate curve [3].

2. REASONS OF DEVIATIONS

2.1 The slopes

Those measurements in 1895 have confirmed the importance of the loop-curve of discharge rates (hysteresis curve), which are to show the coherence of adequate stage seies and discharge time series.
The difference of rising and falling branch is shown clearly and it has been described as a consequence of changing slopes (see Fig. 1.) [3].
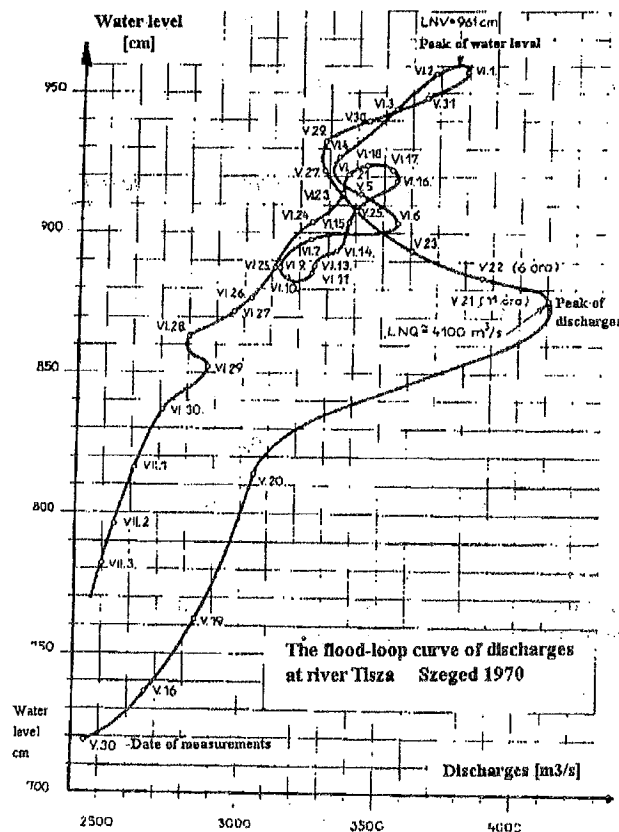
Fig. 1. The flood-loop (hysteresis) curve of river Tisza at town Szeged 1970

Though, in this theory some phenomena remained still unexplained and requires further investigations (for instance, the existence of similar characteristics in rising and falling branches of the flow has not been explained yet) [2].

2.2 Rising and falling of water level

Characteristics of behaving of the river are strongly influenced by conditions of smaller rivers and streams of the catchment area. Values of rising and falling of the water level can be calculated by theories of Benedek (1935) and Salamin (1948) [1].

In these methods the procedure of calculation is based on the slope of the water level. Difficulties and mistakes of the calculation at those points, where smaller streams or rivers join the main river, might indice discordances of these theories.

A theory by Vágás (1984) [2] gives a possibility to transform the water levels into various states of rising or falling condition for the given value of discharge.

The calculation proceeds upstreem along the flow. It occurs as a concordance of the method, that in case of water-inflow, the characteristics of the other branches can be ignored.

3. CALCULATION OF RISING AND FALLING WATER LEVELS

A water level regarded with its adequate discharge at the affected part of the river is concerned as "0" ordinate, as it is shown at (Fig. 2.) [2].

K_i — position of the cross-section
y_i — vertical coordinate of the water levels
i_a — slope of the "0" line (standard water level)
i_d — slope of rising water level
dx_i — distance of cross-sections
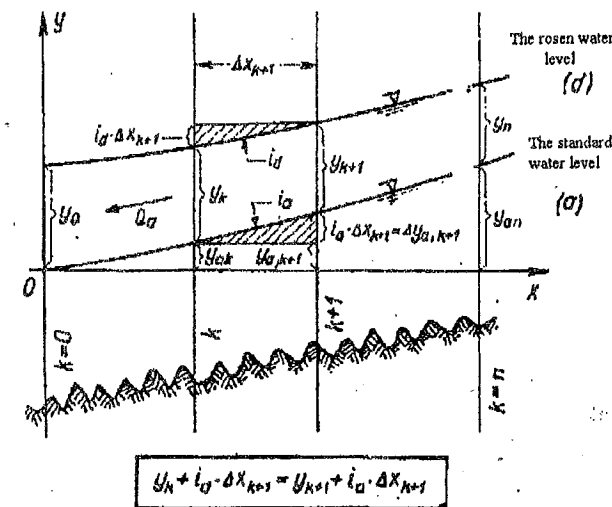
$$y_k + i_a \cdot \Delta x_{k+1} = y_{k+1} + i_a \cdot \Delta x_{k+1}$$

Fig. 2. The rising and falling water level

Between K and K+1 cross-sections, vertical coordinates are as follows

$$y_k + i_d * \Delta x_{k+1} = y_{k+1} + i_a * \Delta x_{k+1} \qquad (1)$$

Using the equation of rate of slopes and discharges

$$\frac{i_d}{i_a} = \frac{Q_a^2}{Q_d(y_k)^2} \qquad (2)$$

Q_a — discharge of standard level
$Q_d (y_k)$ — discharge of swelled water level at y_k

Replacing Eq. 1 into Eq. 2. :

$$y_{k+1} = y_k + [\frac{i_a}{i_d} - 1] * i_a * \Delta x_{k+1} \qquad (3)$$

With the notation of

$$i_a * \Delta x_{k+1} = \Delta y_{a,k+1} \tag{4}$$

Eq. 3 turns to be renaming :

$$\Delta y_{a,k+1} = \frac{y_{k+1} - y_k}{\dfrac{Q_a^2}{Q_d(y_k)^2} - 1} \tag{5}$$

Let us satisfy the next equation by definition of the adequate parts

$$y_{k+1} - y_k = \frac{y_n - y_0}{n} \tag{6}$$

Generating values for k=1;2;3...n we can summarize as follows:

$$y_{an} = \frac{y_n - y_0}{n} * \sum_{t=0}^{n-1} [\frac{Q^2}{Q_d(y_k)^2} - 1]^{-1} \tag{7}$$

Eq. (7) needs iteration (varying Q_a) , while y_{an} approximates its real value.
Using this method, we have to make restrictions. Only those coherences of Q_d (y_k) can be considered, where the slope was nearly equal to i_a, furthermore only those discharge measurements can be considered, where the difference of height at the examined cross-sections was close to y_{an} [2].

CONCLUSIONS

Actually the widely used measurements of discharges are often false, as a consequence of calculation without considering special conditions.
Using the method, mentioned above, data series can be corrected and further developing of the theory gives a chance to enlighten other, non-solved problems.

REFERENCES

[1]   Vágás, „A vízszín természetes duzzasztásának és süllyesztésének szerepe a Tisza és alföldi mellékfolyóinak vízjárásában",
        Hidrológiai Közlöny, 1981. 9.sz., pp.385-396.
[2]   Vágás, „Folyók vízhozamának és vízállásának kapcsolata",
        Hidrológiai Közlöny, 1984. 3.sz., pp.142-147.
[3]   „Az Alsó-Tisza vidéki nagy árvízvédekezés", 1970 pp. 139-142.,
        szerk: Vágás,
        Vízügyi Dokumentációs és Tájékoztató Iroda, Budapest 1972

FLOW THROUGH ORIFICES AT LOW REYNOLDS NUMBERS

Salaheddin N. Shmela
Technical University of Budapest
H-1521 Budapest

1. INTRODUCTION

In connection with a study concerning the hydraulic behaviour of perforated drain pipe systems, it seemed to be necessary to deal with the hydraulic resistance of small blunt or dull edged orifices (*Fig. 1/a*) simply drilled into a plate (e.g. a wall of a pipe).
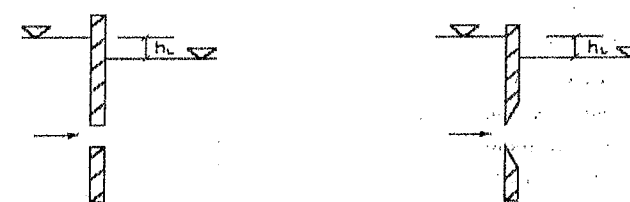
Fig.1   a)Blunt orifice   b)Sharp-edged orifice

In the literature available hardly could be found anything more than that the head loss factor $\zeta = \dfrac{2gh_L}{V^2}$ and the discharge factor $\mu = \dfrac{Q}{A\sqrt{2gh_L}} = \dfrac{V}{\sqrt{2gh_L}}$ are constant, or, exceptionally, that this statement is true for $Re = \dfrac{Vd}{v} > 4000$ [1], where Q is the discharge and V is the mean velocity through the orifice, A is the cross sectional area, and d is the diameter of the orifice, h_L is the head loss caused by the orifice, g is the intensity of the gravitational force field and v is the kinematic viscosity.

For sharp-edged orifices (Fig. 1/b) many data are available from very low up to very high Reynolds number, but in our case it was necessary to have reliable information for low Reynolds number values, because in practice the orders of magnitude of the orifice diameter and the wall thickness are the same, and so the orifice cannot be considered as sharp-edged. For practical reasons we decided to accomplish a hydraulic experiment series on blunt edged orifices with 3 mm of diameter each. The experiments were carried out at the hydraulic laboratory of the Department of Hydraulic Engineering of the Technical University of Budapest.

2. LABORATORY SET-UPS AND MEASUREMENTS

Three laboratory set-ups were used for determining the head loss and the discharge factors of the orifices. The Reynolds number ranged between 90 and 7250.
At our lowest Reynolds number regime, from 90 up to 1000, the laboratory set-up shown in *Fig. 2* was used.
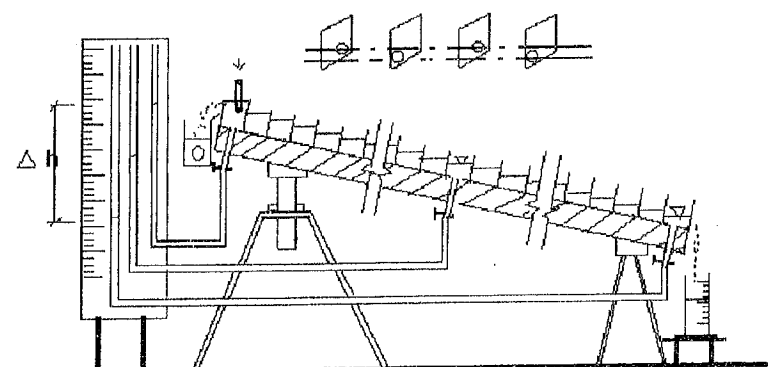
Fig.2   Set-up used for Reynolds number Re = 90 to 1000

It consisted of a flume with a series of cross wall plates in it. The thickness of plates was 1.7 mm. Each plate had a 3 mm diameter blunt edged orifice. The plates were fixed 4.5 cm apart in the flume. The orifices were arranged along two axes alternately. The flume slope could be changed. There was continuous constant level overflow at the upstream end bucket. The discharge was determined at the outflow end of the flume by means of volume and time measurements. The piezometric head and water temperature readings were taken at the first (upstream), the middle and the last (downstream) buckets. The total head loss of the series of orifices is equal to the head difference between the first and last bucket water levels. This, divided by 59 (the number of the orifices), gives the head loss caused by one orifice. The middle piezometric reading allows checking the uniformity of the head losses. The kinematic viscosity for each set of readings was determined, on the bases of averaging the water temperatures measured in the upstream, middle and downstream end buckets (stating at the same time that the temperature difference were insignificant).

For higher Reynolds numbers up to 7250 two laboratory set-ups shown in *Fig. 3* and *Fig. 4* were used. In that in Fig. 3, a 50 cm long PVC pipe with 4.65 cm internal diameter and 1.7 mm wall thickness was used.
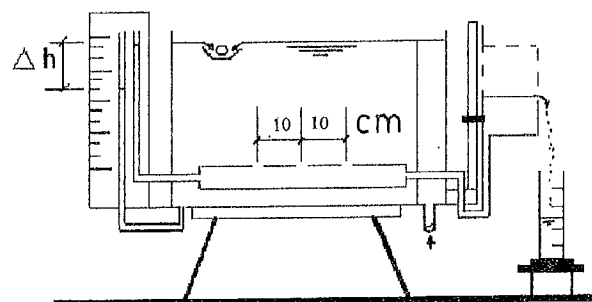
Fig.3   Set-up used for Reynolds nmber Re=1000 to 7250

Three circular blunt edged orifices of 3 mm diameter each and 10 cm apart, were drilled through the pipe wall. The pipe, which was closed at one end, was placed inside a tank filled with water. The water in the tank was kept at constant level. The flow rate, through the three orifices into the pipe, was controlled by a vertically adjustable overflow pot. Two piezometer tubes allowed the measurement of water head in the tank and inside

the pipe. Precautions were taken to prevent air trapping in the pipe and the connected tubes. The head loss through the pipe (between the orifices) could be neglected. Each set of readings consisted of volume, time, water temperature and piezometric level readings.

The laboratory set-up shown in Fig. 4 was also used for finding the discharge and head loss factors for the Reynolds numbers range from 1000 up to 7250.
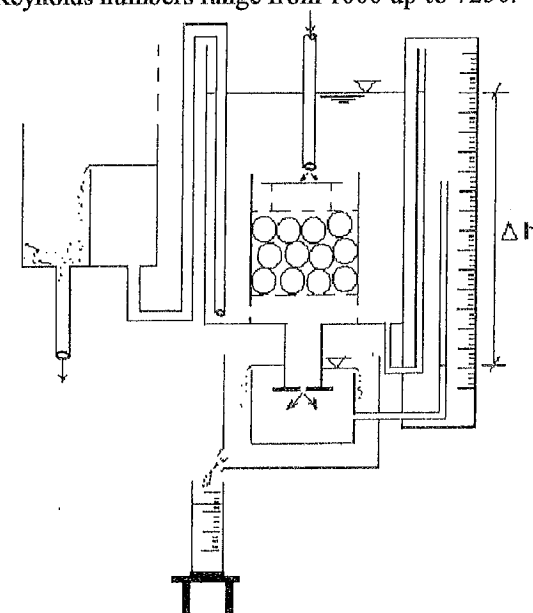
Fig.4   Set-up used for Reynolds number Re =1000 to 7250

The orifice was drilled through a PVC plate of 1.7 mm thickness. A constant head above the orifice was accomplished by an overflow pot. Each set of readings concerned volume, time, temperature and piezometric head measurements.

3. CONDITIONS OF SECONDARY IMPORTANCE

Three conditions of secondary importance were also checked :

a-In the set-up shown in Fig. 2 the flow through the channel is exposed to the atmosphere. The total surface area exposed was 1062 cm². The evaporation from this surface was calculated on the basis of measurements in an evaporation pan, and it was found negligible, with the exception of the lowest discharges, for which we corrected the directly measured discharge data. (Maximum evaporation = 0.00374 cm³/sec, i.e. less than 1.8% of the minimum discharge applied.)

b-In the same set-up, shown in Fig. 2, the change in the water temperature between the first and the last bucket was in the range of 0.2 to 2°C. In this narrow range the viscosity of the flowing water could be substituted by that belonging to the average temperature.

c-The thickness of all the plates and pipe walls, through which the orifices had been perpendicularly drilled in the laboratory set-ups, was uniformly 1.7 mm checked carefully. The orifice edge was left blunt, not made sharper, in conformity with the practice in such cases.
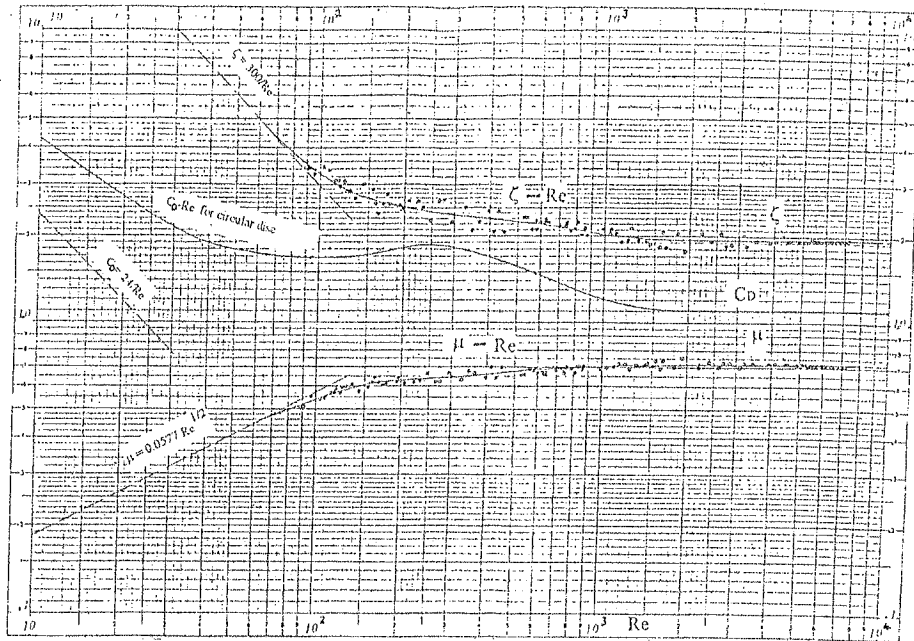
Fig. 5   *Discharge factor μ and head loss factor ζ of an orifice, and drag force factor*
C_D of a sharp edged disc as functions of Reynolds number Re
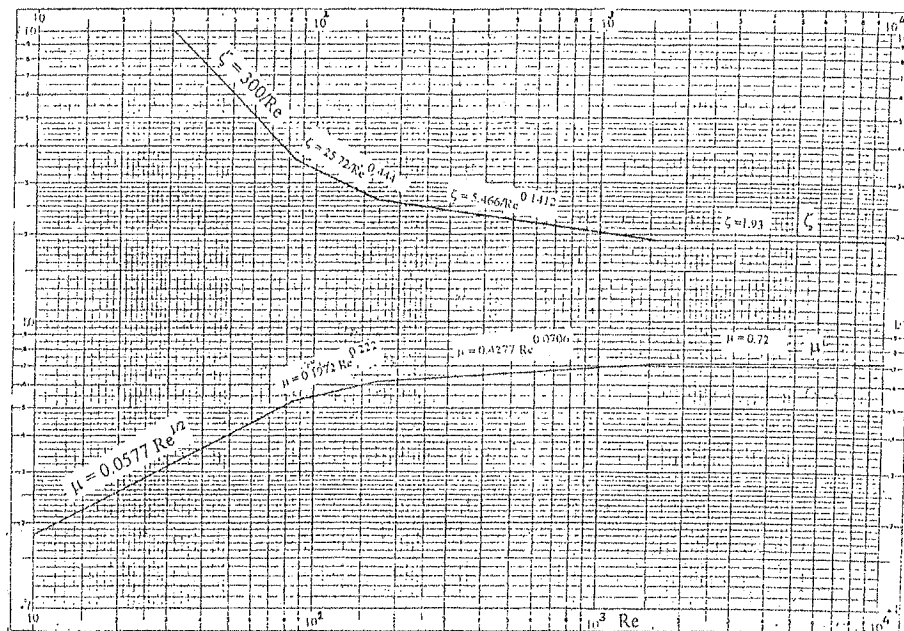
Fig. 6   *Discharge factor μ and head loss factor ζ as functions of Reynolds number Re*

4.DISCUSSION AND RESULTS

As expected, the laboratory results show that the discharge factor μ and the head loss factor ζ are functions of the Reynolds number Re, as it can be seen from the graphical presentation on log-log paper (*Fig. 5*). On the basis of a little extrapolation which must be yet checked for Reynolds numbers smaller than approximately 60, the head loss factor ζ is changing with the Reynolds number according to the equation ζ = 300/Re and consequently for the same range of Reynolds numbers the discharge factor μ is changing according to the equation μ =0.0577√Re (since μ =1/√ζ). For higher Reynolds numbers, up to 1700, the head loss factor ζ is decreasing with milder slopes, and finally it becomes constant (1.93) for Reynolds numbers higher than approximately 1700. It is worth mentioning, that the graphical shape of the relationship between ζ and Re is of more or less similar character to that between the drag force factor $C_D=2F_D/(\rho AV^2)$ and the Reynolds numbers Re for circular discs (Fig. 5) based on measurements of Schmiedel, Simmons, Dewey and Wieselsberger, [2]. This similarity is obviously due to the reciprocal character of the stream patterns around the disc and through the orifice respectively. As for the discharge factor μ, it is increasing with very mild slopes for the range of Reynolds numbers between 60 and 1700, and it obviously becomes also constant (0.72) for Re>1700 (Fig. 5). The relationships between the discharge factor μ and the head loss factor ζ on one hand and the Reynolds numbers Re on the other hand could be approximated with straight lines in the log-log network of *Fig. 6* and the μ and ζ values can be obtained from the following equations:

$$\mu = 0.0577\ Re^{1/2} \quad and \quad \zeta = 300/Re \qquad for \quad Re \leq 83 \qquad (still\ to\ be\ checked)$$
$$\mu = 0.1972\ Re^{0.222} \quad and \quad \zeta = 25.72/Re^{0.444} \quad for \quad 83 \leq Re \leq 170$$
$$\mu = 0.4277\ Re^{0.0706} \quad and \quad \zeta = 5.466/Re^{0.1412} \quad for \quad 170 \leq Re \leq 1600$$
$$\mu = 0.72 \quad and \quad \zeta = 1.93 \qquad for \quad Re \geq 1600$$

5. CONCLUSIONS

In the literature, many data are available concerning sharp-edged orifice from very low up to very high Reynolds number. In our case even though the orifices are of small diameters and thin edges but, the orders of magnitude of the orifice diameter and the wall thickness cannot allow the orifice to be considered as sharp-edged once. The change in head loss and discharge factors at low range of Reynolds number (less than 1700) is considerable and cannot be neglected in any practical application. For Reynolds number range less than about 80 more laboratory investigation has to be carried out.

6. REFERENCES

[1] Webber, N.B. (1979): Fluid Mechanics for Civil Engineers. *Spon Ltd*, London.
[2] Rouse, H. (1960): Elementary Mechanics of Fluid, *John Wiley and Sons*, New York.
[3] Naudascher, E. (1987): Hydraulic der Gerinne und Gerinnebauwerke. *Springer Verlag*, Wien, New York.
[4]Mérés méróperemmel(Measurements by orifice) MSZ 1709/3.

MANAGEMENT ASPECTS OF THE PHOSPHORUS REMOVAL FROM MUNICIPAL SEWAGE IN THE NETHERLANDS

Mrs E. Tomik
Technical University of Budapest
Department of Water Resources Engineering
1111 Budapest, Muegyetem rakpart 3, Hungary

1.   INTRODUCTION

Water is one of the most important lifelines for the Netherlands. In addition to the well-known program for flood protection Dutch water policy consists of two main subsectors: water supply and ground water protection and surface water quality management. The protection of the water quality is in the focus of interest since 1970, when the Pollution of Surface Water Act become operative. It has resulted in clearly demonstrable results for a number of substances.

In 1985 the memorandum "Living with Water" has added a new dimension to water management policy of the Netherlands. It has emphasized the integrated care for the condition and use of the water systems, comprising the media water, beds, and banks and shores with their physical, chemical and biological components.

2.   THE PHOSPHORUS IN MUNICIPAL SEWAGE

One of the substances receiving much attention in the water quality parameters is phosphorus. It is an essential component of organic substances. It is used as a fertilizer in agriculture, in washing powders, as an additive to cattle fodder and as phosphoric acid in many industrial applications. The environmental effect of phosphorus is well known, it contributes to the eutrophication of surface waters.

Phosphorus problem flows are:
1   Agriculture related flows;
2   Waste water from households, which reaches the surface waters as effluent from waste water treatment plants;
3   P ore industry.

The P load of surface waters in 1986 on the level of the European Community is shown in Table 1 [G. Huppes e.a. 1992].

Origin of surface water P load	kg 10⁶ P / year	as a % of the total load
agriculture	91	13
households	505	73
P ore industry	100	14

Table 1

The main source of phosphorus flows within the European Community is the import of phosphorus ore. For the most part this P ore is being transformed into fertilizer and used in agriculture. In arable soils, problems arise when soils become saturated with phosphorus. Any additional phosphate dosing will then almost entirely be lost, and will burden ground water and surface water in large quantities.

The P load of the surface water results mostly from household water. This emission can not be prevented on its final origin, but it can be tracked back to agriculture and so to the import of P ore.

The biological waste water treatment reduces the P concentrations by 35%. Techniques are available for dephosphatizing the sewage water with up to 90% of the original concentration. The results of those techniques in terms of substance flows however are different. Any reduction of phosphate in sewage water will result in an equal increase of phosphate in sewage sludge. This does not mean dephosphatizing is useless from environmental point of view: the phosphate flow in question is being concentrated and therefore easier to dispose of. Possibilities to recycle P from sewage sludge are being investigated; this could lead to diminished demand for P ore and so to a reduced economic inflow of P.

The P load from waste water treatment plants can be calculated from discharge and P concentration of the effluent. The majority of waste water treatment plants in the Netherlands measures the discharge continuously. The recommended frequency for measuring the P concentration for plants of 10 000 - 100 000 population equivalents is 56 times a year. In case if measured data are not available, the Dutch recommendation is to calculate with population equivalents and P production of 3.5 g / d / capita + the industrial production [Steenvoorden 1984]. The accuracy of the P load from sewage effluent is important by constructing P balance studies, because it reduces the errors of the diffuse P sources.

3.   THE DUTCH POLICY TO REDUCE THE PHOSPHORUS LOAD

The Pollution of Surface Waters Act(1970) distinguishes between national surface waters (the main rivers, the North Sea and the Waddensea) that are managed by the national government and other waters under the responsibility of sub-national level governments. This has created three levels of the surface water management: national, regional and local. Table 2 shows the levels, roles and actors involved into management of surface waters:

Level	Role	Actors
National level	Management	Ministry of Public Works Public Works Agency Ministry for Environmental Protection
	Consultation	Union of Waterboards Interprovincial Consultation Association of Dutch Municipalities Public Works Agency Ministry for Environmental Protection Association of Industries
Regional level	Management	Provinces Water Boards
	Consultation	Industries Farmers Municipalities
Local level	Management	Municipalities (responsible for sewage system)
	Production	Waste Water Treatment Works

Table 2

The legal basis for water quality parameters lies in National Environment Policy Plan (NEPP-1), published first in 1989, when the environmental awareness was at its highest level in the Netherlands. Based on NEPP-1 the 3. National Policy Document on Water Management(NPDWM) has been published [Ministry of Transport, 1989]. NPDWM formulates the goals for Water quality managers for the period 1990 - 2000 with interim goals 1995.

In its Package 2 (Nutrients) sets the following:

Final goal:
- decrease the emissions by households, industry and agriculture into surface water down to 75 % for phosphate and 70 % for nitrogen relative to 1985

Interim goal 1995:
- decrease of phosphate and nitrogen emissions from various sources to at least 50 % relative to 1985

Policy:
- complete replacement of phosphate detergents before 1990;
- dephosphating the municipal waste water to an average reduction efficiency of 75 %;
- halving phosphate discharges from the fertilizer industry;
- stimulation of new techniques of phosphate and nitrogen removal.

NEPP-1 was generally seen as well-researched document aimed at achieving sustainable development in the Netherlands within a generation. A reduction in emissions by 80-90 % was seen as the way to achieve that. It has suggested economic and market oriented instruments. The environmental groups advocated most for increasing the prices (by tax and levy) for the use of the resources and the emission of polluting substances. However the implementation deemed to be more complex, the polluting industries and the

industrial groups in general were against the economic instruments. Their arguments were based on fear that extra (eco) tax will make the Dutch products more expensive, and so less competitive on the international markets.

The report of RIVM [RIVM, 1993] has shown that aims in NEPP-1 cannot be achieved within the proposed time. At the end of 1993 National Environmental Policy Plan 2 (NEPP-2) was published. It focuses on the 'intensification of implementation, supplementary measures in cases where the aims can not be achieved'. Its preparation was marked by the same disagreement about the economic instruments as by NEPP-1.

The new financial policy instruments are studied on the level of the European Community, because on this way the legislation can be harmonized. Two instruments seems to have chances to be applied in practice incase of phosphorus:
- emission taxes;
- security deposits on hazardous substances.

Functionally the two instruments are quite similar: the substance deposit is another way of applying an emission tax. Administratively, however, there is a big difference. Emission taxes are based on direct measurement of emissions. The substance deposit is based on the measurement of economic inflow of a substance into a country (region) either by import or by primary production. There the deposit is paid. The outflow of the substance should be measured as well, either through export or acceptable disposal. There the deposit is refunded. Any amount lost in between (emitted somehow) implicitly is paid, as no refunding can take place. It functions as indirect emission tax. According to [G. Huppes e.a. 1992] after application of substance deposit the phosphorus emission can be reduced by 30 % between 1986 - 2000.

4.   CONCLUSIONS

The reduction of phosphorus emission needs not only technical methods but economical - financial instruments as well. This instruments could be applied only on the level of cooperating countries and for pollutants which have well described balance flows. On this way the "polluter pays" principle can be implemented. Phosphorus can be accounted in the municipal sewage only if we could measure its amount from entering into the municipality (from agriculture) up to the effluent of waste water treatment plant.

REFERENCES:

G. Huppes, E. van der Voet, W.G.H. van der Naald, G.H. Vonkeman, P. Maxson: New Market-Oriented Instruments for Environmental Policies, Graham & Trotman Ltd, London 1992

J.H.A.M. Steenvoorden, M.J. de Heus: Fosfaatbalansstudies en de bijdrage van diffuse bronnen, Instituut voor Cultuurtechniek en Waterhuishouding, Wageningen, 1984

Ministry of Transport and Public Works: 3. National Policy Document on Water Management, The Hague, 1989

J. van der Straten: Recent Developments in Dutch Environmental Policy, in Environmental Politics, Volume 3, Number 4, Frank Cass London, 1994

FLOW REGIME IN TABARROK ABAD RIVER AFTER CONSTRUCTING A RESERVOIR

Abolfazl Mosaedi
Technical University of Budapest
Department of Water Resources Engineering
H-1521 RKP-3 Budapest, Hungary

1. INTRODUCTION

The usual problem with the flow regime of a stream is that in a few times it is too much and makes flood, and for a long time it is too little and there is no enough water. Instead of the adaptation of demand to the random process of water supply, the transformation of the water regime by storage has proved to be a reasonable solution. This is the only way to achieve a proper development of limited water resources available on the continents and islands, or the individual regions and countries. However, due consideration must be given to an ever increasing demand, and the control of losses from harmful aspects of waters [2]. With constructing a reservoir we can control the regime of the stream, reserve water for drought period, decrease damage of flood, use the energy of water for producing electricity and many another purposes such as recreation.

As an example the present exercise is carried out to show how water is distributed over space and time in the Tabarrok Abad Basin, (one of the river basins in Iran) after the construction of a reservoir across the Atrak river.

2. DESCRIPTION OF THE STUDY AREA

2.1 Location

The study area (Tabarrok Abad catchment) is the upper part of the Atrak river, the catchment area is about 600 km^2. The average slope of this part of the river is 1.455%, average slope of catchment area is 1.7% and the average elevation of catchment is 1896.0 m above sea level. The main features of this part of the river are the considerable slope which goes up to 90% and the concentration time, that is 7.35 hours. Another important thing is that, there are favourable climatological and lithological conditions for forming high flow (huge amounts of precipitation, long period of snow cover, recharging from melting snow, rather small possibilities for infiltration, etc.).

2.2 Climate

The most important from the hydrological point of view is the amount of precipitation and its distribution in time and in space; the little rain is restricted to winter months, and in summer the amount of precipitation is close to zero. Because of the extreme variability of

rainfall in space and time, every year some days Tabarrok Abad experiences flood while in a long time suffers from drought. In the study area the average of precipitation is 334 mm/year, the average temperature is about 10 °C, the average specific runoff is 1.57 l/s per km^2, and mean discharge is 0.94 m^3/s.

The main characteristics of the area are high and violent rainfalls and big runoff coefficients that cause sudden and rapid water rises. For example while the maximum flood in 1971 was only 0.940 m^3/s in 1972 it was 125 m^3/s (133 times more, just after 1 year), the minimum discharge in 1975 was only 0.020 m^3/s while in 1973 it was 0.530 m^3/s (26 times more). Every year just in some days the area experiences floods while in a very long time especially in irrigation season there is not enough water for agricultural purpose, and farmers suffer from drought. Generally big floods in this area are because of snow melt, especially after some hours raining. The big floods usually occur in May and some floods with probability of 30 to 50 per cent may occur in April or June. When the flood occurs, after some days the regime of stream is decreasing. In September discharge is very low and it is the lowest amount of discharge in the year, from October till next May discharge is increasing (Tab. 1).

	Minimum	Maximum	Mean
January	0.20	1.28	0.55
February	0.16	26.50	0.65
March	0.24	18.50	1.04
April	0.18	30.10	1.61
May	0.10	125.00	3.09
June	0.02	23.75	1.32
July	0.02	25.00	0.53
August	0.03	23.06	0.38
September	0.03	7.47	0.33
October	0.06	29.73	0.46
November	0.10	38.37	0.60
December	0.14	1.62	0.57
Total character.	0.02	125.00	0.94

Tab. 1   Characteristics of daily discharge data (m^3/sec) for Atrak river in Tabarrok Abad station (first year 1963 last year 1989)

3. NEED FOR STOCHASTIC MODELS

River flow is considered as a random process, the appropriate word for this is stochastic. It is a function of precipitation and related factors which seem to evolve randomly in space and time. Even if the basic phenomena and their interaction were thoroughly understood, it would not be possible to describe mathematically the rate of discharge in a normal water course without involving unsystematic or unknown effects [1].

As is well known the water flow characteristics in a river at a particular time and place are principally caused by rainfall over an antecedent period and numerous hydrogeological,

climate and human induced factors. These elements can be analyzed as a system through stochastic models, which can try to explain the patterns and factors affecting the water flow. Mathematical model building is obviously of little importance when considered without empirical evidences.

4. HOMOGENEITY TEST FOR TWO SAMPLES OF SAME POPULATION

A special type of goodness of fit test derived by Smirnov can be used to determine whether two samples of data are from the same population or not and also to analyse whether they are identically distributed. From the analysis it appears that the homogeneity of the time series are uncertain, mainly because of the observed wet and dry period in the observed data, before 1977 there was a wet period and from 1977 there is a dry period. Because it is possible that in the next future the wet period or dry period or both occur, the whole available data (from 1963 till 1989) was used for Reservoir Computation.

5. DISTRIBUTION ANALYSIS

The goodness-of-fit test is required in order to ascertain whether a theoretical distribution can be fitted to the observed distribution through a set of measurements. The fit is generally determined by means of a criterion which depends on the differences between the observed and theoretical density functions or distributions [1].

Among the two most widely used tests of this kind one can mention the Chi - squared and Smirnov-Kolmogorov the second is more sophisticated in analysis than the first one. The distribution analysis is carried out for annual discharge data from 1963 till 1989, using the Smirnov-Kolmogorov fitting test. As the catchment area is about 600 km^2 the best distribution type for annual maximum can be Gumbel, Frechet and Log-Gauss. The Gumbel distribution type does not fit the base data series, the Frechet distribution type fits well to the base data but the discharge for return times more than 20 years seems to be very high. The Log-Gauss distribution type fits well to the data, D_{max} (maximum difference of the empirical and theoretical distribution function) is 0.057 and P_f (indicative, probability of the fitting test) is 1.000, considering 30 and 70 % as significance levels, as it can be seen in Fig. 1 the chosen distribution function fits well to the base data series. Because the range of available data (from 1963 to 1989) is short, it is not true to extrapolate return time period 3 times more hence, we can try to use the method of Todorovic and Zelenhazic for short time series, however the hypothesis of the exponentiality is not realised for any one of the base discharge levels. Therefore we choose the Log-Gauss distribution type for maximum distribution.

For determining the minimum value also Frechet, Gumbel and Log-Gauss distribution can be used, for Frechet distribution indicative probability for the fitting P_f is 0.759 but it seems to have high value for every return time more than 20 year. For Log-Gauss distribution P_f is 0.969 and also may be the value of discharge for every return time is a little bit high, but for Gumbel distribution P_f is 0.979 and the value of discharge for every return time is better for safety and consequently the Gumbel distribution is chosen for annual minimum distribution (Fig. 2).
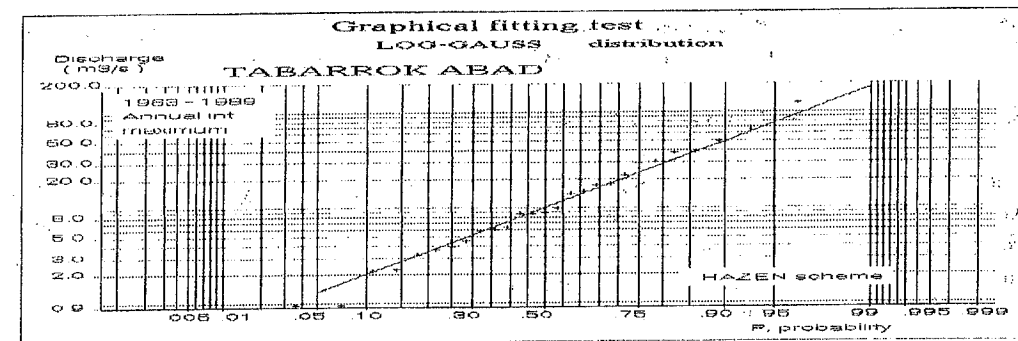
Fig. 1 Log-Gauss distribution for annual maximum discharge before the construction of the reservoir
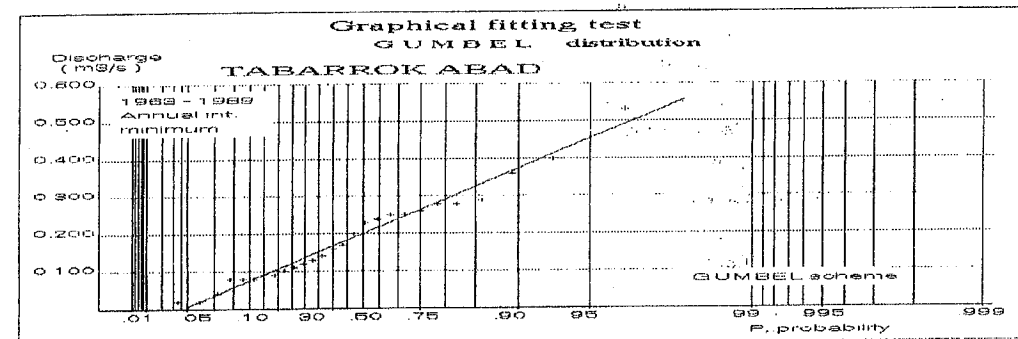
Fig. 2 Gumbel distribution for annual minimum discharge before the construction of the reservoir
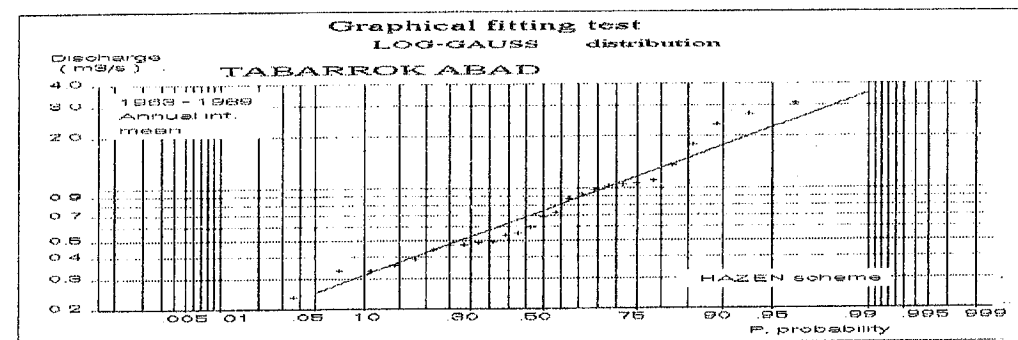
Fig. 3 Log-Gauss distribution for annual mean discharge before the construction of the reservoir

For determining mean annual Gauss and Log-Gauss distribution are examined, the first one does not fit the base data series, but for Log-Gauss distribution P_f is 0.855 and $D_{max} = 0.117$, this distribution function fits well to the base data series (Fig. 3). For irrigation season

(April - September), the Log-Gauss distribution function fits well the base data series, and for maximum, minimum and mean P_f is 0.932, 0.997, 0.810, respectively.

6. ESTIMATION OF FLOOD ATTENUATION

The daily discharge data from 1963 to 1989 is used but with little gap in between. The Reservoir Sizing by Transition Probability (RSTP) Moran model, developed by Zsuffa and Gálai [2], is applied for analysing the water flow regimes of the river and a number of alternative reservoir sizings are tried to match the demand and supply positions for Tabarrok Abad with different probability curves.

For flood attenuation effect of reservoirs, different variables such as weir size, weir level and starting water level for different input floods are examined. For all of the calculations the pre-draining time considered as 0.0 day and also the base flow during the flood as 0.00 m³/s, (the most dangerous It has seen that, the different base flow (from 0 to 9 m³/s) has not important role, regarding the reduction of peak of flood. If the chosen capacity for reservoir is 20.0 million m³ and the sedimented volume 15.0 million m³, the water level for 40 million m³ volume will be 34m, therefore for chosen weir size, the weir level and starting level considered as 34 m. With considering these 4 independent variables as constant (Weir level, Starting level, Base flow and Input flood as 34 m, 34 m, 0.00 m³/s and 2% probability respectively) to find the best weir size, different diameters are examined.

For diameters equal or smaller than 5m the problem is that, there will be too much water above weir and for big floods the capacity of weir will not be enough to pass a sufficient amount of water, also for diameters larger than 10m the reduction for floods with probability less than 2% will be too small. Reduction of flood with probability of occurrence larger than 2% and diameter of weir larger than 6m is too small. Therefore the best size of weir for attenuation of floods with return time smaller than 50 years is 6m (for its diameter). For big floods we need an emergency spillway, to pass the big floods and prevent the dam form broken.

By using a weir with 6 m diameter; starting water level and weir level as 34 m, base flow as 0.00 m³/s and pre-draining time as 0.00 day, the discharge of floods after passing spillway (Q_{output}) are analysed. The Log-Gauss distribution function fits well the base data series (Fig. 4), From this Figure it is observed that, the maximum of a flood with 100 year return time will be 110.3 m³/s, while the return time for a flood coming to reservoir for this amount of discharge is 37 year (Fig. 1). The Gumbel distribution and Frechet are examined, but Gumbel distribution function does not fit the best data series, and by using the Frechet distribution we will have a very high discharge for floods with return time longer than 10 years. Moreover, the method of Todorovic and Zelenhazic does not fit the base data.

Also the best distribution type for minimum and mean annual discharge after constructing the reservoir will be Gumbel and Log-Gauss distribution respectively, just like distribution types of discharge coming to the reservoir.
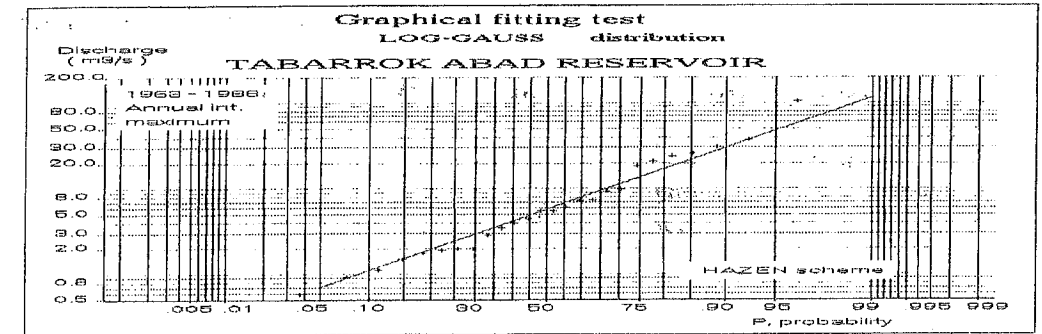
Fig. 4   Log-Gauss distribution for annual maximum discharge after constructing of the reservoir

CONCLUSIONS

From the analysis it appears that the homogeneity of the time series is uncertain, mainly because of the observed wet and dry period in the observed data, before 1977 there was a wet period and from 1977 there is a dry period. Because it is possible that in the next future the wet period or dry period or both occur, the whole available data (from 1963 till 1989) is used for Reservoir Computation. The distribution analysis is carried out for annual discharge data, using the Smirnov-Kolmogorov fitting test. the Log-Gauss distribution type fits well to the annual maximum data (Fig. 1), the Gumbel distribution chosen for annual minimum discharge (Fig. 2), and for mean annual Log-Gauss distribution fits well the base data series (Fig. 3). For irrigation season (April - September), the Log-Gauss distribution function fits well the base data series. By using a weir with 6 m diameter, starting water level and weir level as 34m base flow as 0.00 m3/s and pre-draining time as 0.00 day, the discharge of floods after passing spillway (Q_{output}) are analysis. The Log-Gauss distribution function fits well the base data series (Fig. 4), but Gumbel and Frechet distribution and the method of Todorovic and Zelenhazic do not fit the base data just like base data coming to the reservoir. Also the best distribution type for minimum and mean annual discharge after constructing the reservoir will be Gumbel and Log-Gauss distribution respectively.

REFERENCE

[1] Kottegoda N.T. "Stochastic Water Resources Technology". Macmillan press, 1980.

[2] Zsuffa I. and Gálai L. "Reservoir Sizing by Transition Probability - Theory, Methodology, Applications". Water Resources Publications, Littleton, Colorado, 1987.

SUBSURFACE DRAINAGE SIMULATION MODELS

Hossein Banejad
Water Resource Engineering Dept. ,
Technical University of Budapest, H-1521 Budapest

Abstract:

Artificial drainage system is needed where natural drainage is not may be due to many causes involving soil, climatic, hydrological, topographic and agricultural factors. The relations between all these factors and the drainage requirements and criteria are complex and sometimes are not easy to determine.

Simulation of a groundwater system refers to the construction and operation of a model whose behaviour assumes the appearance of the actual aquifer behaviour. The model can be physical, analogue, or mathematical.

Each model is described under the following sub-heading: type of theoretical approach, nature and management of the boundary condition, mathematical expression, surface runoff, discretization scheme, model input-outputs , model objectives.

Drain flow models can be used deterministic or conceptual approach based on fundamental soil-water flow theory or on a reservoir concept. The processes can be described at the field-scale or at the larger scale of the watershed. At each scale, models are developed using either a deterministic approach based on the fundamental laws of flow in porous media, or a conceptual one based on simple rules for managing one or several reservoirs. In all cases, a field- scale approach will be limited to unconfined aquifers. A regional scale approach will be used for both unconfined or confined aquifers.

1. INTRODUCTION

Subsurface drainage is very important in providing a root zone environment that is suitable for maximum growth of plants. A good drainage condition will increase production and sustain crop yield over long periods of time. One of the main reasons that poor drainage and high water table cause a decrease in crop production is the fact that the plant roots have only a limited amount of soil on which to grow.

Control of root-zone salinity and root-zone aeration are the main objectives of agriculture sub-surface drainage. Salinity control is imperative for the establishment of a permanent irrigated agriculture. Good aeration of the root zone prevents the nitrification and loss of valuable plant nutrient but, at the same time allows the plants root to carry on respiration in an unrestricted manner. Maximum production is obtained from the profile, well-drained soils (Ochs, W. J. et al., 1983). In arid areas, artificial drainage systems are install to control water-table level and salinity in the root zone.

2. GROUNDWATER MODELLING

Simulation of a groundwater system refers to the construction and operation of a model whose behaviour assumes the appearance of the actual aquifer behaviour. The model can be physical, analogue, or mathematical.

A mathematical model is simply a set of equations which , subject to certain assumptions, describes the physical processes active in the aquifer. While the model itself obviously lacks the detailed reality of the groundwater system, the behaviour of a valid model approximates that of the aquifer. Mathematical model maybe deterministic , stochastic, or some combination of the two. Deterministic models could be divided into : analytical, numerical and mixed. The analytical model concerned with the case when exact mathematical equations could be written to formulate the problem while from the hydraulic point of you could be approximate . This method widely used in the past .

The numerical method of modelling usually used when the problem is defined hraulicly but mathematically approximated .It is widely used now a days because of the advancement of the computer. The mixed method of modelling contains the use of the analytical approach up to the point where could not be solved mathematically so the solution is completed with numerical method.

2.1 Types of ground-water models

There are four general types of groundwater models. The problem of water supply is normally described by one equation, usually in term of hydraulic head This type is hydrodynamic that with this model problems could be solved like amount of water that we need .And from which region it is coming. The second type is Transport Models that they contain heat transport and solid transport. The fourth type is Deformation Models.

Ground-water flow models have been most extensively used for such problems as regional aquifer studies, ground-water basin analysis and near-well performance. This classification of ground-water model is no means complete. The type of model used will obviously depend on the application.

2.2 Numerical Methods:

Numerical method consist of certain procedures as a result of which the partial differential equation is replaced by an algebraic equation, or a system of algebraic equations. Usually these constitute a system of linear equations. The final solution then requires, the solution of this system of equations.

A numerical model is most appropriate for general problems involving aquifers having irregulars boundaries, heterogeneity, or highly valuable pumping and recharge test.

As mentioned there are some analytical solution, a great advantages of analytical solution, apart from its immediate availability, is that it can give a good insight into the dependence of the solution on various physical parameters, such as transmissivity, storativity, or geometrical dimensions. The main limitation of analytical methods of solution is that they are available only for relatively simple problem.

There are three kind of numerical method, Finite Different Method, Finite Element Method, and Boundary Elements. Finite difference method will used to solve the differential equation of steady and unsteady groundwater flow in aquifers. The general principle is that the unknown variable, the head φ, which is function of χ, y, and t, is represented, for every value of the time t, by a finite number of values $\varphi(i, j)$, where i and j indicate counter variables in χ and y direction, respectively. The form of the system of equations is that the values of the head in each point are related to the values in the surrounding points . In general, both the values in these points at the beginning and the end of time step. The various possibilities for the approximation by finite difference are usually denoted by forward, backward, and central finite differences.

A second very powerful numerical method is the finite element method. In groundwater flow problems one could imagine that a region is subdivided into small elements, such that for each element the flow is described in terms of the head in the nodal points, and then a system of equations is obtained from the condition that the flow must continuous at each node.

3. SUBSURFACE DRAINAGE SIMULATION MODEL

The design of an agricultural drainage system requires a good understanding of the occurrence, nature and movement of water in the soil as well as of the drainage related hydrological processes.

3.1 Criteria for model description:

Each model is described under the following sub-heading: type of theoretical approach, nature and management of the boundary condition, mathematical expression, surface runoff, discretization scheme, model input-outputs , model objectives.

Type of theoretical approach : Drain flow models can used deterministic or conceptual approach based on fundamental soil-water flow theory or on a reservoir concept. The processes can be described at the field-scale or at the larger scale of the watershed. At each scale, models are developed using either a deterministic approach based on the fundamental laws of flow in porous media, or a conceptual one based on simple rules for managing one or several reservoirs. In all cases, a field- scale approach will be limited to unconfined aquifers. A regional scale approach will be used for both unconfined or confined aquifers.

In application of the FEM, numerical stability and oscillation problems often occur. The numerical problems are mainly caused by (1) Improperly handling the time derivative term of the governing equation; (2) improperly choosing the time step sizes;

(3) improperly assigning a value to the weighting factor of the finite difference solution scheme (FDSS) ; and (4) improperly choosing element sizes and shape. There are two types of formulation in handling the time derivative, one being the consistent formulation and the other being the lumped formulation (Istok 1989). The consistent formulation treats the spatial derivatives and the time derivative of the governing equation consistently in terms of weight functions and basis functions. The lumped formulation , on the other hand , defines a set of special weight functions and basis functions to handle the time derivative. Consequently, the overal numerical formulation is consistent. However, the lumped formulation has been shown to be less susceptible to numerical oscillation and is more frequently used in practice (Xin Yu and Singh 1994)..

A drainage model that simulates surface and subsurface drainage systems can be effective management tool, with many application. Peak flood flows, water table levels, and flow volumes may be simulated for either drainage system. In addition, by changing the inputs to the models, the effect of different variables-for example, soil properties or rainfall patterns-may be evaluated. This feather can be valuable in determining the effect the effect of these changes in crop yield.

3.2 Calibration and Verification:

Loague and Freez (1985) distinguished between calibration and verification phases of model testing, defining the calibration of a model as being carried out using events from one pried of a data set, and verification of the model using events distinct from the calibration period.

The calibration process improves the simulation capability of the model by comparing the simulated results to the observed results. The model and its parameters can be adjusted and retested until the optimum results are obtained. Models often require calibration, depending on model performance, and this is accepted practice in model development.

The verification of a computer model shows the modeller how well the model responds to a set of data, with no calibration based on those data. This will determine whether the calibrations made by the modeller are realistic for that particular watershed, at least for the particular time period of the test.

The efficiency of the model is calculated by comparing the verification simulation to the observed verification events. It is a method of evaluating the calibration process. The verification efficiency selected by Loague and Freeze (1985) is calculated in the following manner.

$$E_f = (\Sigma(O_i - O)^2 - \Sigma(S_i - O_i)^2) / \Sigma(O_i - O)^2$$

where: E_f = verification efficiency; O_i = observed value for event I; O = mean value over the verification events; S_i = simulated value for event i.

James and Burges (1982) discuss several ways of measuring the efficiency of a model. These include statistical methods, time series analysis and scattergrams. They conclude that it is difficult for a model to perform well over all ranges of test data. It is

suggested that several coefficient of performance be used, for cases like peak flows, the parameters, wet periods and dry periods. However, to evaluate the model correctly, all coefficients should be considered, as high coefficient values may be obtained while poor modelling results are observed.

The most obvious impact of field drainage can be expected and have been experienced in the changes of runoff volumes and distribution. Especially surface drainage, by eliminating the natural surface storage capacity of the land, accelerate runoff and generally increase the peak flows. Shorter times of runoff concentration in the watershed cause rainstorms with shorter duration and, therefore, with higher intensity to become the critical rainstorms and the probability of higher peak flows, therefore increase even more(Penkeva, 1976).

4. CONCLUSIONS

Subsurface drainage is very important in providing suitable environment for maximum. In arid areas, artificial drainage to control water-table and salinity in the root zone.

With considering the usage of computer it has created solution for problems that there were no analytical solution for them. There are some method for modelling groundwater, subsurface drainage.

Each model has to calibrate and verify.. Models often require calibration and this is accepted practice in model development.

5. REFERENCES

Istok, J. (1989). " Groundwater modelling by the finite element meyhod." Water Resour. Monograph 13, American Geophysical Union, Washington, D. C.

James, L. D. And Burges, S.J. (1982). Selecting, calibration, and testing of hydrologic models. In: Haan, Johnson, and Brakensiek (Editors), hydrologic Modelling of Small Watersheds. A.S.A.E, Monograph No. 5, St. Joseph, MI.

Loague, K. M. And Freeze, R. A. (1985). A comparison of rainfall runoff modelling techniques on small upland catchments. Water Resour. Res., 21: 229-248.

Ochs, W. J., and Camp, R., and Donnan, W., and Winger, R. J. (1983). Drainage Requirement And Systems. Design And Operation Of Farm Irrigation Systems. Edited by M. E. Jensen. Published by American Society of Agricultural Engineering, Michigan, U.S.A, P 235-277.

Penkeva, F. (1976). Subsurface versus surface drainage water quality and environmental impacts. Environmental Aspects Of Irrigation And Drainage. Published by: American Society of Civil Engineerings, New York, USA, P 97-116.

Xin Yu, Fang and Singh, Vijay P. (1994). Modelling 3d Ground-Water Flow By Modified Finite-Element Method. Journal of Irrigation and Drainage Engineering. Vol. 120, No. 5, ASCE, p 892-909.

SESSION 5

Mechanics

INFLLUENCE OF THE HYDROSTATIC PRESSURE ON THE FRACTURE TOUGHNESS IN AN ANISOTROPIC GNEISS

Balázs Vásárhelyi

Department of Geology of Civil Engineering, Technical University of Budapest, 1111, Budapest, Sztoczek u. 2, Hungary

1. INTRODUCTION

Recently, the fracture mechanics has been applied in the solution of rock engineering problems, especially for competent brittle rocks under hydrostatic pressure or dynamic loading. Fracture toughness is one of basic parameters in fracture mechanics indicating the ability of rock to resist fracturing, i.e. the initiation and propagation of cracks. Although a number of authors have paid more and more attention to the investigation of fracture toughness of rocks, most of them have conducted their research with tensile loading. The standard testing procedure was proposed for determination of toughness in tensile mode fracture by three-point bending [9].

In the past 30 years, many investigations dealing with crack propagation in brittle rock have employed the well-founded discipline of linear elastic fracture mechanics, LEFM, with great success. Although this theory is based on linear elasticity and it is directly related to the Griffith [3] theory, plastic flow and other non-linear behaviour can occur on a small scale without affecting its predictive success. Purely brittle behaviour is not required and only when the size of the zone of non-linear behaviour at a crack tip cannot be considered small when compared to the crack length, does recourse to fracture theories such as the J-integral [4] become necessary.

Recent investigations have measured the fracture toughness, K_C, of the ortotrophic gneiss. Moreover, Schmidt and Huddle [5] and Abou-Sayed [1] indicated that the apparent fracture toughness of Indiana limestone increases with increased confining pressure. The anisotropic rocks were examined by Afassi [2]. The main objective of the present paper is to show the influence of the confining pressure and the anisotropy on the propagation of crack under mode I.

2. MATERIAL DESCRIPTION

The object of this research was a rock having anisotropic properties. Gneiss was chosen for this purpose. This metamorphic rock consist of small grains and during the metamorphosis the minerals deform in one direction which can be seen with unaided eye.

Table 1 shows the physical properties of the rock.

Physico-mechanical proprieties	Index	Unit	Result
Modulus of elasticity	E_1	GPa	41.69
Poisson ratios	$E_2=E_3$	GPa	70.05
	$\nu_{12}=\nu_{13}$	-	0.166
	$\nu_{21}=\nu_{31}$	-	0.262
	$\nu_{23}=\nu_{32}$	-	0.247
Maximal stress	σ_1	MPa	238
	$\sigma_2=\sigma_3$	MPa	267

Tab. 1. The physico-mechanical properties of the gneiss

3. SPECIMEN PREPARATION

Extensive specimen preparation is necessary for performing confined fracture toughness tests. This incudes initial specimen machining, fatigue pre-cracking, final machining, instrumenting and jacketing. For the best result the specimens were cut from one block.

Forty notched three-point bend specimens of gneiss were dry-machined to dimensions in accordance with ASTM standard [9] (Fig 1). All experiments were performed on 2 specimens.
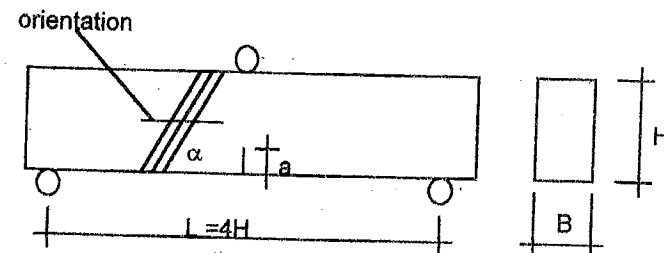

Fig. 1. Three-point bend specimen configuration used for fatigue pre-cracking

All specimens were 15 ($\pm$0.1) mm thick (B) and 25 ($\pm$0.1) mm wide (H) and were machined in the divider geometry in which the crack front is perpendicular to the bedding planes of the material. It was used in the initial phase of the tests in order to facilitate fatigue pre-cracking. It should be noted that all tests were performed on specimens of equal size with nearly equal crack lengths (a) (5 ($\pm$0.1) mm long). However, the size criterion often used for `valid` tests of K_{IC} requires the crack length to be larger than 2.5 $(K_{IC}/\sigma_y)^2$.

The measurements were elaborated in cases of anisotropy in the directions 0; 30; 45; 60 and 90 degrees to the horizontal line.

To perform tests under confining pressure, the specimens had to be jacketed with flexible material that would cover all machined surfaces including the notch, but not enter the crack.

4. TEST PROCEDURE

First, the jacketed and instrumented specimen was fastened inside the pressure vessel. Confining pressure was applied to the specimen while maintaining a slight tensile load on the external load cell. The specimen was then loaded to failure at a constant rate of increase in crack opening displacement.

The apparent fracture toughness, K_C, was determined from each test by using the following expression [6] :

$$K_Q = \frac{3PS}{2tW^2}\sqrt{\pi a}f_{(\alpha)};$$

$$\alpha = \frac{a}{W}$$

$$f_{(\alpha)} = \frac{1.99-(1-\alpha)(2.15-3.93\alpha+2.7\alpha^2)}{(1+2\alpha)(1-\alpha)^{3/2}}$$

(1)

where P was the maximum load measured.

6. RESULT AND DISCUSSION

The increase in fracture toughness of gneiss with increased confining pressure is shown in Table 2. The equations are shown below in function of the confining pressure with the variances:

0^0 :
$$K_{IC} = 8.551 + 1.084\,P \qquad (\sigma = 2.663)$$

30^0 :
$$K_{IC} = 9.819 + 1.078\,P \qquad (\sigma = 3.374)$$

45^0 :
$$K_{IC} = 10.288 + 1.070\,P \qquad (\sigma = 0.642)$$

60^0 :
$$K_{IC} = 6.964 + 1.124\,P \qquad (\sigma = 0.514)$$

90^0 :
$$K_{IC} = 8.048 + 1.048\,P \qquad (\sigma = 1.756)$$

I suppose that the connection between the toughness intensity factor and the hydrostatic pressure is linear. This assumption is supported by my investigations There are not large differences among the tangents (1.05 - 1.12) of the line. The

average value is 1.081, the variance is 0.024 [8]. The direction of anisotropy does not influence the slope of the line. Similar experiments were done by Schmidt and Huddle [5] on Indiana limestone and Terrien et al. [7] on sandstone. Examining their published results of experiments I have found that the line defined above can be fitted very close and the value of the slope characterise the rocks.

Direction	Pression [MPa]	K_{IC} [N/mm$^{3/2}$]	Average [N/mm$^{3/2}$]
0^0	0	6.63, 7.03	6.83 ±0.20
	10	18.95, 18.21	18.58 ±0.37
	30	45.98, 45.68	45.83±0.15
	60	73.77, 68.91	71.34±2.43
30^0	0	10.03, 9.34	9.69±0.35
	10	15.43, 19.44	17.44±2.00
	30	47.96, 47.37	47.67±0.30
	60	71.43, 73.04	72.23±0.80
45^0	0	11.18, 10.07	10.62±0.55
	10	21.33, 18.81	20.07±1.24
	30	42.92, 43.55	43.23±0.22
	60	71.10, 77.29	74.20±3.10
60^0	0	6.39, 5.85	6.12±0.27
	10	18.47, 19.97	19.22±0.75
	30	38.56, 42.79	40.68±2.11
	60	75.65, 72.80	74.22±1.43
90^0	0	7.39, 6.87	7.13±0.26
	10	19.78, 17.67	18.73±1.05
	30	44.36, 41.82	43.09±1.27
	60	65.55, 74.13	69.84±4.29

Tab. 2. Experimental data

8. CONCLUSION

The purpose of this study was determine the effect of the anisotropy and the confining pressure on fracture toughness of gneiss. Fracture toughness, K_{IC}, was measured on three-point-bend specimens as a function of hydrostatic pressure. I found that connection between the confining pressure and the facture toughness is linear and this is a constant which is in depend on the direction of the anisotropy.

9. ACKNOWLEDGEMENTS

10. REFERENCES

[1] Abou-Sayed, A. S. (1977): Fracture Toughness K_{IC} of Triaxially Loaded Indiana Limestone;
Proc. 17th U.S. Symp. Rock Mech. (Keystones), pp.: 2 A3-1 - 2 A3-8.

[2] Afassi, F. (1991) Caracterisation de la Resistance a la Propagation des Fissures dans une Roche Anisotrope: le Schiste.
These de Doctorat; Universite des Sciences et Techniques de Lille

[3] Griffith, A. (1924): Theory of Rupture;
Proc. 1st. Int. Cong. App. Mech., Delft, pp.: 55-63.

[4] Rice, J. R. (1968): A Path Independent Integral and the Approximate Analysis of Strain Concentration by Notches and Cracks
J. Appl. Mech. 35, 379

[5] Schmidt, R. A.; Huddle, C. W. (1977): Effect of Confining Pressure on Fracture Toughness of Indiana Limestone
International Journal of Rock Mechanics and Mining Science, 14, pp.: 289-293.

[6] Srawley; J. E. (1976): Wide Range Stress Intensity Factor Expression for ASTM E399 Standard Fracture Toughness Specimens.
Int. J. Frac. Mech., 12, pp.: 475-476.

[7] Terrien, M.; Sadra, J. P.; Chaye D'Albissin, M.; Bergues, J. (1984): Experimental Study of the Anisotropy of a Sandstone and a Marble
Coll. CNRS, Villard de Lans.

[8] Vásárhelyi, B. (1995): Etude de l'Influence de la Pression de Confinement et de l'Orientation de la Foliation sur la Propagation des Fissures dans un Gneiss;
Rapport de Stage, INPL, ENSG, Nancy.

[9] American Society for Testing and Materials: Tentative Method of Test for Plane Strain Fracture Toughness of Metallic Materials;
ASTM Designation E399 72T. Annual Book of Standards, Part 31;

STRESS ANALYSIS OF ARTIFICIAL JOINTS, IMPLANTS AND BONE – AN INTERFACE OF MECHANICS AND MEDICINE

Krisztina Polgár
Technical University of Budapest, Department of Civil Engineering Mechanics
H-1521 Budapest, Műegyetem rkp. 3.

1. INTRODUCTION

Bioengineering research plays an important role in the development of prosthetic joint replacement and implant design. Biomechanics provides theories and methods for mechanical analyses of complex structures, like combination of bone and biomaterials. The use of Finite Element Method was first introduced in orthopaedic literature about 24 years ago (around 1972) and has become a valuable tool in the field of analysing load transfer, stress and strain distributions in bones, artificial joint replacement, etc.

In the following chapters I cite examples – chosen my former and present research topics – to demonstrate a couple of possible application of Finite Element Analysis for the purposes of biomedical investigations.

2. THREE DIMENSIONAL FINITE ELEMENT ANALYSIS OF TOTAL HIP REPLACEMENT

In this section I present a few results of a previous research programme, when we worked in co-operation with the Dept. of Orthopaedics at Haynal Imre Postgraduate Medical University (ORFI–HIETE). The main object of this project was to determine the effects of a newly developed hip prosthesis on stress and strain distributions in human femur.

2.1 Materials and methods

Three dimensional linear and non-linear finite element analyses were performed using COSMOS/M (Explorer version 1.71) finite element programme. In order to obtain reference values, which are suitable for being compared the evaluated results with, I needed to build up three different finite element models: one for representing the whole bone without implant, and the others for studying the bone–implant system. Solid parts and volumes of the models were meshed automatically, generating 4-node tetrahedron elements. (Figs. 1-2)

The geometry of a realistic model of human femur was derived from a series of CT-scans along its height. Mechanical properties were obtained from literature [1], each material was assumed to be homogeneous and isotropic, material inhomogenity was taken into consideration by varying the value of Young's modulus throughout the bone. The applied loads reflecting single-leg stance with force vectors acting on the femur- or prosthetic head – respectively (representing joint reaction force), and on the trochanter major (caused by the abductor muscles).
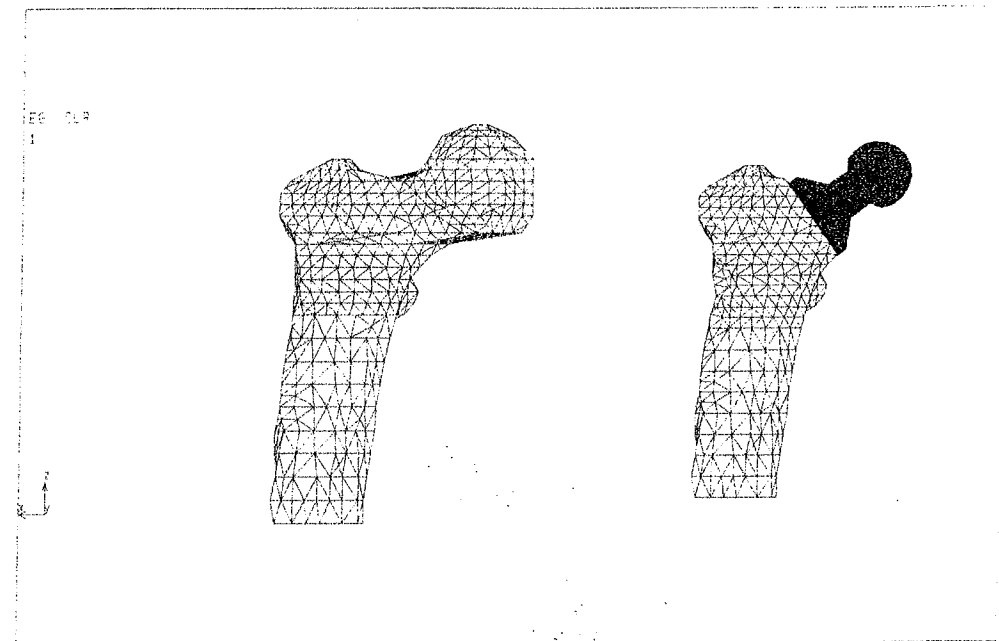

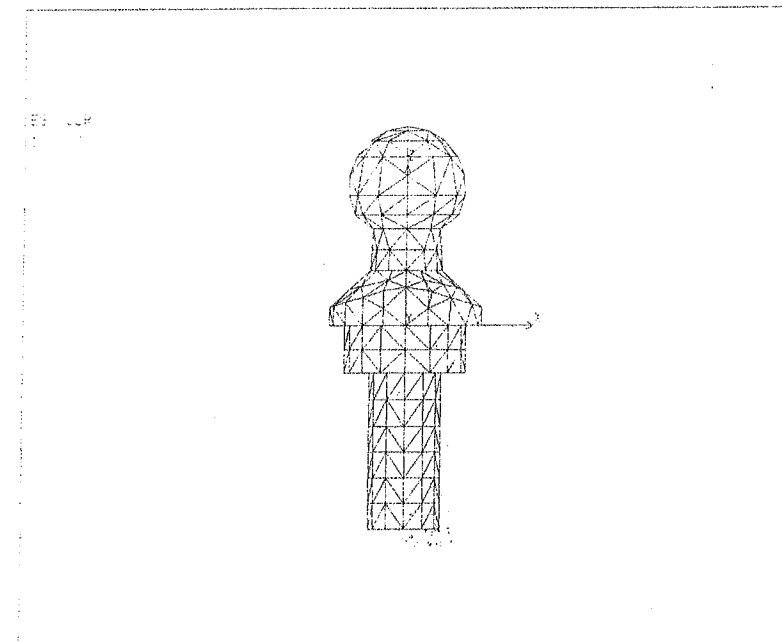Fig.1 Finite element mesh of bone without implant and bone-implant structure

Fig.2 Finite element mesh of prosthetic component for replacement of proximal femur

2.2 Conclusions

Comparison of calculated results, i.e. stress distribution in natural femur and in the same bone with implant, supposing perfectly bonded contact between surfaces of bone and porous-coated implant showed good agreement, however stress-level has slightly increased in the latter one. (Figs.3-4) Considering postoperative stage, i.e. unbonded and frictionless interface stress transfer was affected more dramatically, but significant stress concentration only occurred in diaphysis region at places of pin-fixation.
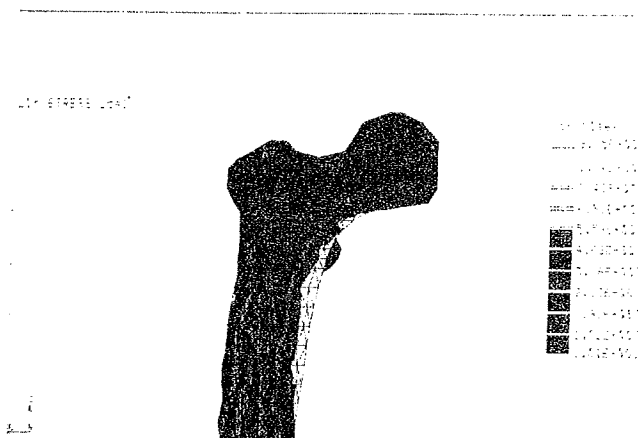

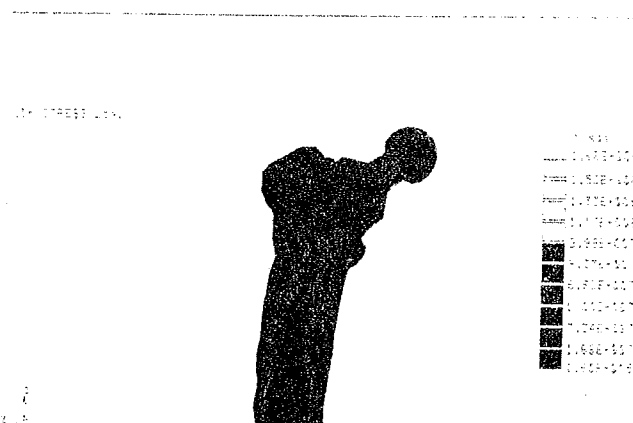*Fig.3   Stress distribution in bone without implant*

Fig.4   Stress distribution in bone with implanted prosthesis (considering fully bonded surfaces)

3. THREE DIMENSIONAL FINITE ELEMENT ANALYSIS OF DENTAL IMPLANTS

In recent years the use of osseointegrated dental implants has increased significantly. The function of these structures is supporting single-tooth or fixed prosthesis components. Presently a large number of implant designs exists with different geometrical features, so as to provide long-term stability. Although the success rate of dental implants is considerably high – reported to be above 90% – still there are questions have not been answered yet.

I currently work in a joint programme with physicians at the Department of Oral- and Maxillofacial Surgery of Semmelweis University of Medicine. Based on numerical results of our investigation we try to determine optimal shape, size and number of threads for "screw type" dental implants and demonstrate changes of stress distribution in cortical and cancellous bone by altering geometrical parameters such as length and diameter of implants.

3.1   Materials and methods

At the first stage of research, using COSMOS/M (Explorer version 1.71) finite element programme, three dimensional linear and non-linear finite element analyses were performed to evaluate load transfer of implants to surrounding bony matrix under vertical, horizontal and combined loading of the prosthetic component. In order to simulate connection between bone and implant surfaces – referring to different phases of healing process – I have calculated stress and strain distribution by applying interface contact elements (thus considering conditions that follow medical intervention) and also by supposing perfectly bonded surfaces.

Mechanical properties of cortical and cancellous bone of human mandible and maxilla were obtained from scientific literature. Each material was assumed to be homogeneous and isotropic.
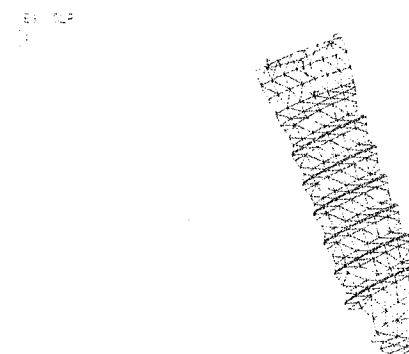

Fig.5   Finite element mesh of the quarter of a dental implant (length:10mm)

Fig.6 Stress distribution in bone surrounding a 12mm long implant

3.2 Future plans

The following step of this research has to provide more accurate results, which should be achieved by refinement of finite element mesh. Since limited version of the software used did not make possible any further increase in the number of nodes and elements, I intend to perform analyses using ABAQUS and PATRAN3 Finite Element Programme Systems running on workstation.

4. CLOSING REMARKS

The examples presented are, of course, only the first efforts to predict biomechanical behaviour of bone–implant structures quantitatively. Due to length limitations, basic and important questions of this field could not be mentioned, assumptions and symplifications were not discussed in detail in the scope of this article.

REFERENCES

[1]   Van Buskirk, W. C.; Ashmann R. B.:The elastic moduli of bone.; Mechanical Properties of Bone, AMD 45:131-143; ASME, New York, 1981.

[2]   Huiskes, R: Biomechanics of implants and bones.; The 6th Annual Meeting for the Orthopaedic Research of the Jap. Orth. Assoc., 1991.

CHAOTIC ADVECTION IN TWO-DIMENSIONAL FLOWS

György Károlyi

Research Group for Computational Mechanics of the Hungarian Academy of Sciences, Műegyetem rkp. 3, H-1521 Budapest, Hungary

ABSTRACT

We investigate the dynamics of tracer particles in time-dependent open flows. In cases when the time-dependence is restricted to a finite region, we show that the tracer dynamics is typically chaotic but necessarily of transient type. The complex behaviour is then due to an underlying nonattracting chaotic set that is also restricted to a finite domain. Examples are taken from the realm of two-dimensional incompressible flows. The case of the blinking vortex-sink system illustrates the phenomenon in inviscid fluids, while the von Kármán vortex street problem belongs to the class of viscous flows. Based on these examples, generic features of the scattering tracer dynamics are summarized.

1. INTRODUCTION

The advection of particles in hydrodynamical flows is a phenomenon having attracted great recent interest from the side of dynamical system community because these particles can exhibit chaotic motion [1-10]. By particle we mean a light granule of small extension. If it takes on the velocity of the flow very rapidly, i.e., inertial effects are negligible, we call the advection passive, and the particle a passive tracer. Its equation of motion is then

$$\dot{\mathbf{r}} = \mathbf{v}(\mathbf{r}, t),$$

where **v** represents the velocity field that is assumed to be known.

Here we consider passive advection in open flows in cases when complicated tracer movements caused by the time-dependent flow is assumed to be restricted to a finite region. This will be called the *mixing region* outside of which the time-dependence of the flow is negligible. It is worth emphasizing that a complicated flow field (turbulence) inside the mixing region is not at all required for a complex tracer dynamics and the corresponding fractal patterns. Even simple form of time dependence, e.g. a periodic velocity field is sufficient. For tracers injected into the flow outside of the mixing region, where the flow is still practically stationary, the motion is initially simple and becomes later gradually more complicated as the particle is being advected into the mixing region. The motion in the outflow region is then simple again. Thus, for such processes chaos is necessarily restricted to a finite region both in space and time. We claim that this *transient chaos* [11] is the only form of chaos which can appear in the situation studied.

The complicated form of trajectories implies a long time spent in the mixing region. In other words, tracers can be temporarily trapped there. Due to the incompressibility of the flow no attractors can exist, and *almost all* particles escape the mixing region. As a consequence, the underlying chaotic set is a *chaotic saddle* having a Cantor set type structure along *both* the unstable and the stable direction. In the next sections we study examples where the time dependence is the simplest possible one, periodic. Without giving mathematical details we introduce the problems and pictorially show some typical tracer trajectories, and the invariant sets obtained in numerical simulations.
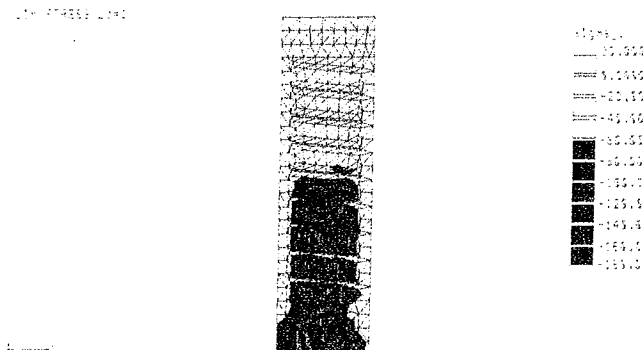
2. THE BLINKING VORTEX-SINK SYSTEM

Consider an ideal fluid filling in the infinite plane with a point vortex that is simultaneously sinking. This can be a model of a large bath tub with a sink since a rotational flow is formed around the sink in the course of the outflow. The blinking vortex-sink system introduced originally by Aref et al. [2] is obtained by having two such sinking vortex points some distant apart from each other and being active alternatingly for a duration of $T/2$. This models the outflow from a large bath tub with two sinks that are opened in an alternating manner. In the blinking vortex-sink system the velocity field is periodic with T but in a special way: it is stationary for a half period of $T/2$ and stationary again but of another type for the next half period of $T/2$.

The replacement of a tracer particle can easily be determined within any of the stationary regimes. The comparison of the particles' position right after the first flow field sets in, i.e. at $t = 0^+$ mod(T), leads to a stroboscopic map whose form can be given analytically [2].

The advection problem has two essential dimensionless parameters: the sink strength and the ratio of the vortex and sink strengths. We have carried out a detailed investigation of the tracer dynamics at different values of the parameters [13]. Two tracer trajectories are shown in Fig. 1 with long life time before reaching one of the sinks. The breakpoints are due to the sudden jumps between the two different streamline patterns at $t = 0$ mod($T/2$).
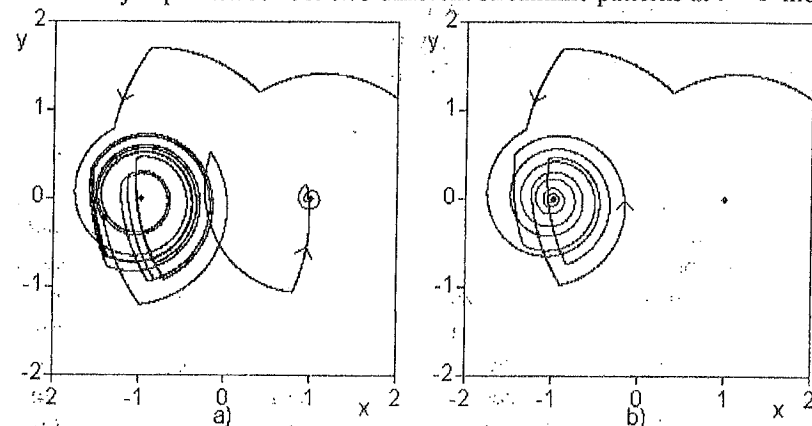

Fig. 1 Two complicated tracer trajectories of the blinking vortex-sink system. A change of 10^{-2} in the initial coordinates leads to completely different trajectories leaving the system through different sinks. The vortex-sink centers are denoted by black dots.

The invariant sets characterizing this problem are shown in Fig. 2 on a stroboscopic map taken at time $t = 0^+$ mod(T). The chaotic saddle (Fig. 2a) seems to be hyperbolic everywhere, i.e., to have a direct product structure. This set, just like a chaotic attractor, is the union of all bounded orbits, including periodic ones, never escaping the mixing region. In contrast to a chaotic attractor, however, these orbits are all unstable, and the chaotic saddle has practically no region of attraction. In other words, the chaotic saddle contains only those orbits which are trapped in the mixing region forever. They are rather exceptional ones and not even their closure covers a finite area of the plane, although they are infinite in number. Such orbits form a fractal subset of the mixing region.
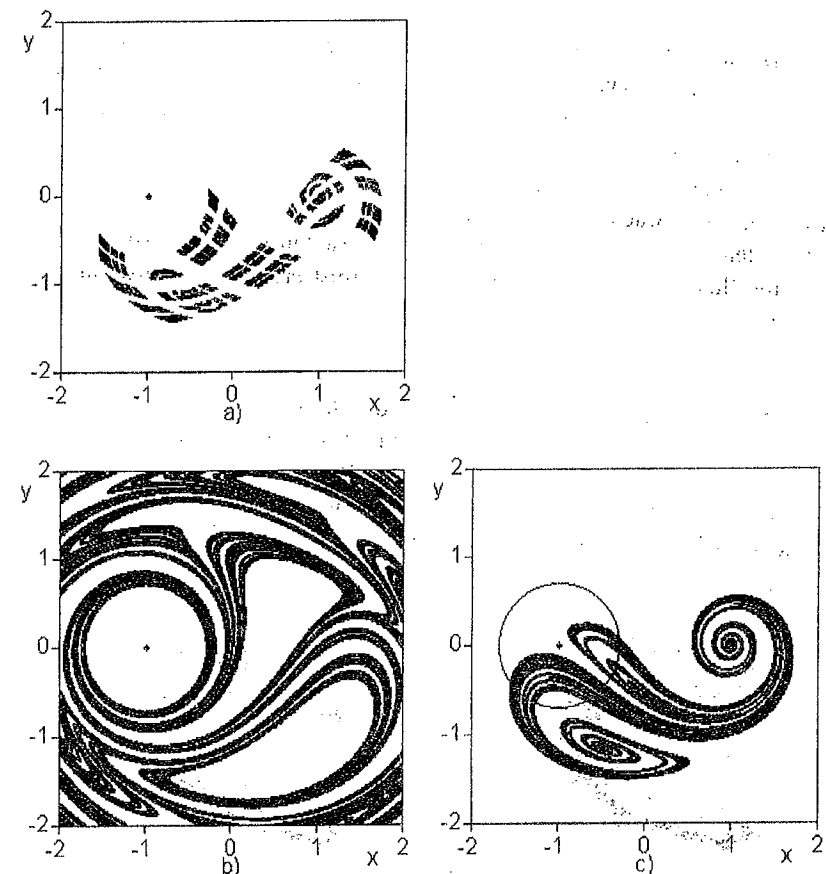

Fig. 2 Stroboscopic section of the invariant sets of the blinking vortex-sink system at $t = 0^+$ mod(T). a) Chaotic saddle, b) stable manifold, c) unstable manifold. The circle around the left vortex-sink center at $(-1,0)$ indicates the area from which the tracers leave the system via the left sink during the first half period.

The invariant manifolds are given in Figs. 2b and c. The chaotic saddle can be reached along the stable manifold (Fig. 2b), which is a complicatedly winding fractal curve reaching arbitrarily far away from the vortex-sink centers. Tracers with long lifetime can only be the ones approaching the chaotic saddle close along its stable manifold. It must have a vanishing area because in a Hamiltonian system no attractor can exist. In contrast, the unstable manifold (Fig. 2c) is a fractal curve bounded to a finite region. The unstable manifold of the saddle is the set of points along which particles, after entering a close neighbourhood of the set, leave this neighbourhood. In general this manifold appears on a stroboscopic map as a rather complicatedly winding curve and extends to the region where particles exit the flow. In our case it connects the chaotic saddle with the right sink closed at $t = 0^-$ mod(T), just before taking the stroboscopic map.

3. THE VON KÁRMÁN VORTEX STREET

We consider the flow of a viscous fluid around a cylinder with a background velocity pointing along the x-axis. At intermediate background velocities (whose dimensionless measure, the Reynolds number is on the order of 10^2) no stationary velocity field is stable, instead, a strictly periodic behaviour sets in with period T. Two vortices are created

behind the cylinder within each period, one above and the other one below the x-axis. These two vortices are delayed by a time $T/2$. Note that they are now extended vortices with finite velocities even in the vortex centers. The vortices first grow in size, then become detached from the cylinder and start to drift along the channel. This alternating separation of vortices from the upper and lower cylinder surface is called the von Kármán vortex street and is characterized by a strictly periodic velocity field of period T [8,12]. After a short length of travel, the vortices are destabilised and destructed due to the viscosity of the fluid. Far away from the cylinder upstream and downstream the flow is, however, practically stationary.

To obtain the velocity distribution one has to solve the two-dimensional inviscid Navier-Stokes equations with no-slip boundary condition along a circle [4,5]. For simplicity we use here an analytic model for the streamfunction introduced in [6]. It was motivated by a direct numerical simulation of the Navier-Stokes flow carried out by Jung and Ziemniak [5] at Reynolds number 250. Fig. 3 exhibits two complicated particle trajectories advected in this model flow, which are trapped for a while in the wake of the cylinder.
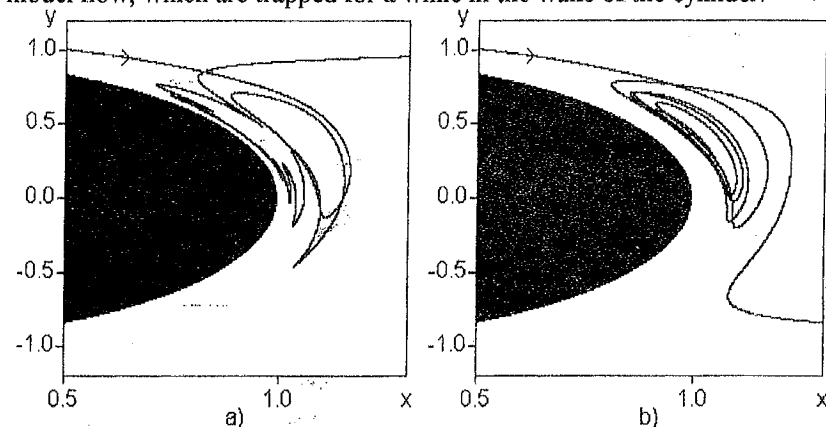

Fig. 3 Two complicated tracer trajectories in the von Kármán vortex street with initial y coordinates differing by 10^{-2}. The horizontal scale is multiplied by 3 for better visualization.

The invariant sets are shown again on a stroboscopic map taken at integer multiples of the period T in an area surrounding the cylinder. The chaotic saddle (Fig. 4a) contains now both a hyperbolic and a nonhyperbolic component. The former one is situated away from the cylinder, while the nonhyperbolic component seems to accumulate on the cylinder's surface. This is the manifestation of the no-slip boundary condition. Very close to the surface, i.e., in the boundary layer, the velocity must be small and therefore there can exist increasingly many trapped trajectories. In fact, the surface contains an infinity of parabolic orbits [6] and it plays a similar role as a KAM surface.

The invariant manifolds are exhibited in Figs. 4b and c. The stable manifold (Fig. 4b) surrounds the cylinder surface and extends to the infinitely far inflow region in a narrow band close to the negative x-axis. In contrast, the unstable manifold (Fig. 4c) touches the cylinder surface along a finite arch only, and extends to the outflow region at infinity in a strongly oscillating way.
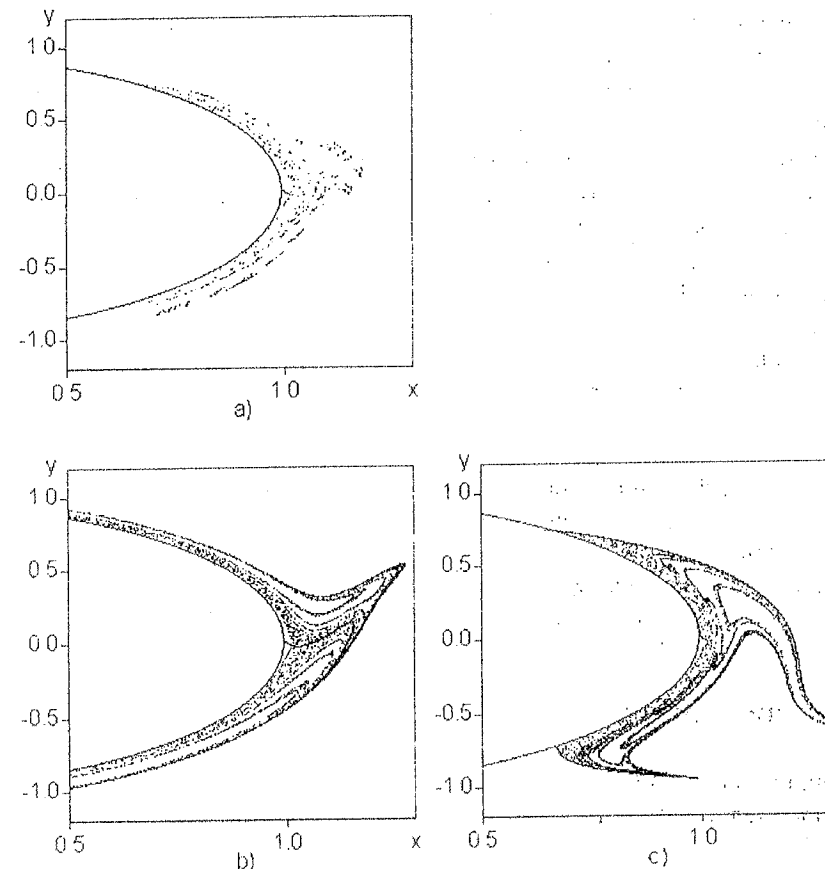

Fig. 4 Stroboscopic section of the invariant sets in the von Kármán vortex street at $t = 0 \bmod(T)$. a) Chaotic saddle, b) stable manifold, c) unstable manifold. The horizontal scale is multiplied by 3 for better visualization.

4. CONCLUSIONS

The existence of a chaotic saddle is the key observation in understanding the scattering tracer dynamics. The chaotic saddle contains those orbits which are trapped in the mixing region forever. These orbits are all unstable. Although they are infinite in number, not even their closure covers a finite area of the plane. Such orbits form a fractal subset of the mixing region.

The stable manifold of the saddle is a complicatedly winding curve along which the chaotic saddle can be reached. The stable manifold can also be considered as the "basin of attraction" of the saddle. The unstable manifold of the saddle is the set of points along which particles, after entering a close neighbourhood of the set, leave this neighbourhood. This manifold extends to the region where particles exit the flow. As a consequence, a droplet of particles injected into the flow in front of the mixing region will, after a long time, trace out the unstable manifold, provided the droplet overlaps initially with the stable manifold. This fact makes the unstable manifold a direct physical observable of the passive advection problem [1,8] and provides the easiest method to plot this manifold experimentally or numerically.

Trapped particles have some time delay τ relative to the background flow: the longer τ is the more complicated the trajectory becomes. Observe several trajectories with initial points taken from a closed domain of the flow. The quantity $P(\tau)d\tau$ is the probability to find a particle with time delay in the interval $(\tau, \tau+d\tau)$. Due to the hyperbolic structure of the saddle it typically decays exponentially as $P(\tau) \sim e^{-t/\bar{\tau}}$. $\bar{\tau}$ is the average time delay that can then also be considered as the average lifetime of chaos on the hyperbolic component. Particles starting not exactly on the stable manifold have finite lifetimes in the mixing region. Their motion can be considered as a random walk among the periodic orbits of the chaotic saddle. This time delay distribution is of great importance in practical applications The existence of the chaotic saddle determines the average time the pollution spends in the wake of the bridge-piers. An expanded chaotic set in a water-basin can result in long residence time of large mass of water, which may cause mustiness of the drinking water.

Finally we note that the features summarized here seem to be robust. Deviation from the flow's planar character does not change these properties. Similarly, if the particles have inertia, the dimension of the phase space doubles due to the appearance of physical momenta, but a chaotic saddle may exist in that case also. What we observe as tracer patterns is then related to the projection of the invariant manifolds to the space of the flow.

ACKNOWLEDGEMENTS

REFERENCES

[1] J. M. Ottino, *The kinematics of mixing: stretching, chaos and transport*, (Cambridge University Press, Cambridge, 1989); J. M. Ottino, Ann. Rev. Fluid Mech. **22** (1990) 207.
[2] H. Aref, S. W. Jones, S. Mofina, and I Zawadski, Physica **D37** (1989) 423.
[3] V. Rom-Kedar, A. Leonard and S. Wiggins, J. Fluid. Mech.**214** (1990) 347.
[4] K. Shariff, T. H. Pulliam and J. M. Ottino, Lect. Appl. Math. **28** (1991) 613.
[5] C. Jung and E. Ziemniak, J. Physica **A25** (1992) 3929.
[6] C. Jung, T. Tél and E. Ziemniak, Chaos **3** (1993) 555.
[7] E. Ziemniak, C. Jung and T. Tél, Physica **D76** (1994) 123.
[8] D. Beigie, A. Leonard, and S. Wiggins, Chaos Sol. Fract. **4** (1994) 749.
[9] Á. Péntek, T. Tél, and Z. Toroczkai, J. Phys. A **28** (1995) 2191 (1995); Fractals **3** (1995) 33.
[10] Á. Péntek, Z. Toroczkai, T. Tél, C. Grebogi, and J. A. Yorke, Phys. Rev. **E51** (1995) 4076.
[11] T. Tél, in: *Directions in Chaos*, vol. 3, Ed.: Hao Bai-Lin, (World Scientific, Singapore, 1990) pp. 149-221.
[12] M. Van Dyke, *An Album of Fluid Motion*, (The Parabolic Press, Stanford, 1982).
[13] G. Károlyi, Á. Péntek, T. Tél and Z. Toroczkai, to appear in the Proc. of the International Conference on Nonlinear Dynamics, Chaotic and Complex Systems, Zakopane, Poland, 7-12 November, 1995, (Cambridge University Press, 1995) pp. 119-132; G. Károlyi and T. Tél, to be published.

NUMERICAL SIMULATION OF BONDED GRANULAR MATERIALS WITH REINFORCEMENT

Klára Ledniczky
Technical University of Budapest, Faculty of Civil Engineering,
Department of Mechanics
1111 Budapest, Műegyetem rkp. 3.

1. INTRODUCTION

The aim of my work is the numerical simulation of bonded (concrete-like) granular materials with reinforcement. I deal with three main group of question: first, redistribution of stresses around the reinforcement, second the factors that influence the development and spreading of microcracks, such as grain distribution, rate of stiffness and strengths between the reinforcement and the concrete-like material, geometry of reinforcement, effect of different supports, and load-rate, and finally, the phenomenon of loosening of the material around the reinforcement are also examined. In this contribution I introduce the numerical model used for the simulations and show some examples to represent its work.

2. NUMERICAL MODEL

The computer program that I use to the investigations is called PFC ^{2D}. It was developed by Itasca Consulting Group, USA, and it bases on a dynamic model (DEM) made by Cundall. PFC ^{2D} works in 2D, it models circular particles. A particle generator allows the statistical generation of specified distribution of particles to be done automatically. Material properties are associated with individual particles and contacts. The contact physics consists of the following elements: linear springs, or modified Hertz-Mindlin law; Coulomb sliding; optional bonding (contacts may take tension and bending moment) and the bond may break due to excess tension or shear or bending moment. Assembly can be loaded in four ways: by gravity; by a set of forces applied to a given range of particles; by fixing velocities of a group of particles at a prescribed rate; by given arbitrary translation and/or rotation velocities of walls. Fig.1 shows the scheme of one calculation cycle.
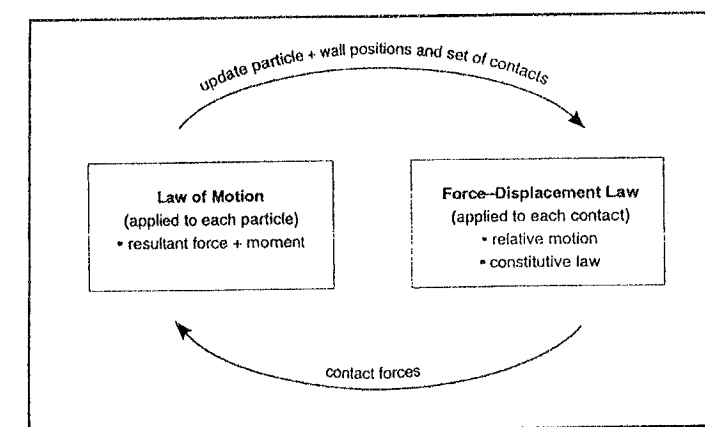

Fig.1 Calculation cycle in PFC ^{2D}

3. EXAMLPES

3.1 Pullout test

Pullout test of reinforcement of concrete-like material was simulated. The initial assembly is on Fig. 2. The load can be either a prescribed force acting on the first particle of the reinforcement, or prescribed velocity of this particle during given number of timecycle. (that means prescribed displacement)
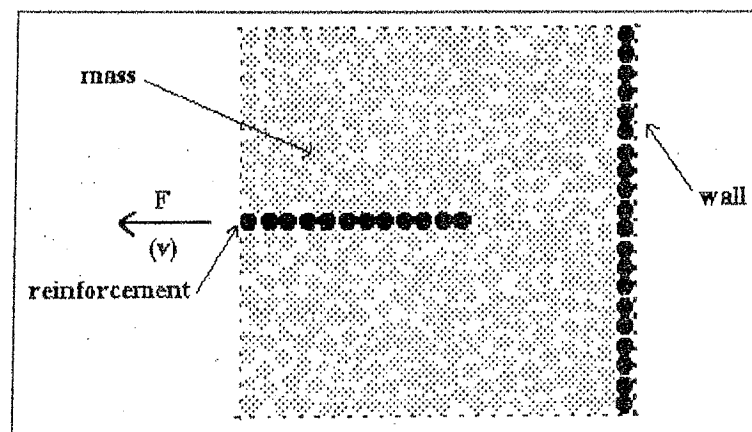

*Fig. 2 Initial assembly of the pullout test*

Distribution of forces around reinforcement and developing of cracks was investigated at different loadlevels, until the whole sample was destroyed.

The assembly at the different loadsteps is on Fig 3. Lines show contact forces, darker colour indicates particles around reinforcement which has broken contact. Diagrams under the pictures show normal force between the particles of the reinforcement.

At the first loadstep (F=3.0e+4) all the contacts are unbroken. Only the first few particles of reinforcement are loaded because forces are given on the mass. (Figure and diagram "a") At the second loadlevel (F=4.0e+4) some contacts are broken around the fore-part of reinforcement. That's why forces can be given to the mass at about half of reinforcement, so longer part of it is loaded. (Fig. and diag. "b") The next loadstep (F=4.72e+4) is the last steady-state of the assembly. Almost every contact of particles along the reinforcement is broken, so forces are acting on the mass behind reinforcement. (Fig. and diag."c") If the load is increased further (F=.4.75e+4), the whole sample is broken, as picture "d" shows.

This kind of simulation can be developed to be available for investigations mentioned in the introduction. The material parameters of reinforcement and mass, the geometry of reinforcement, the load, etc. are variable.
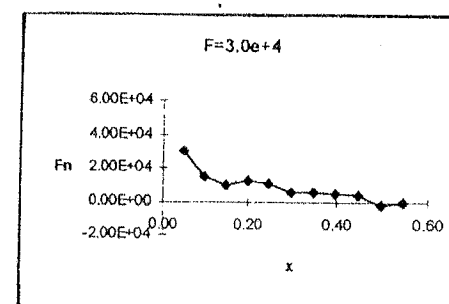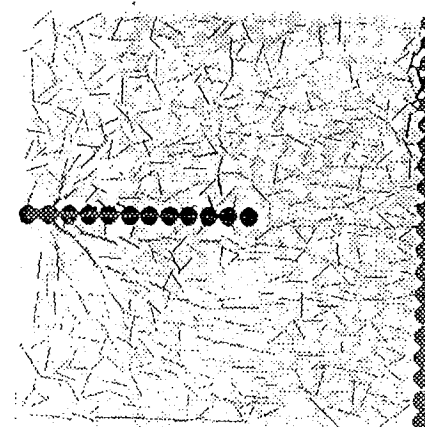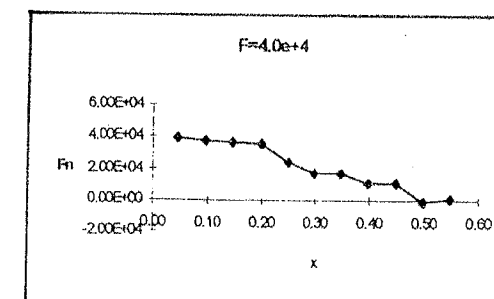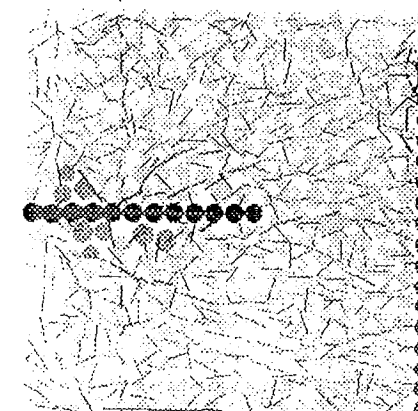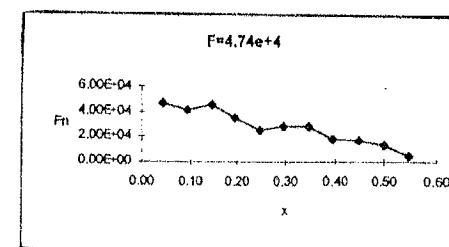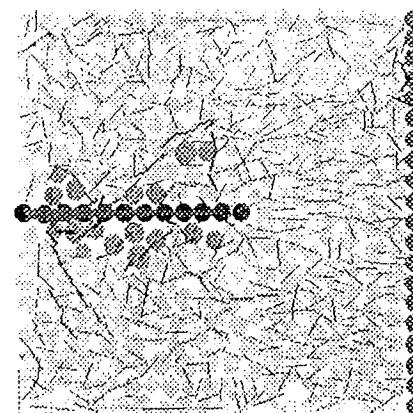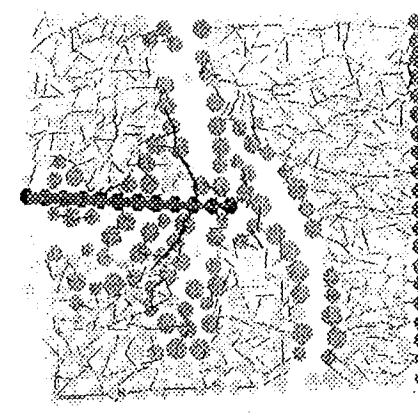
Fig.3 Loadsteps of pullout test

3.2 Push-out test

This example is shown to illustrate the flexibility of the model. Simulation of push-out test for investigation of ultimate strength of studs was done. The original test structure is on Fig.4. The numerical simulation models a part of the test, as it can be seen on Fig.5.
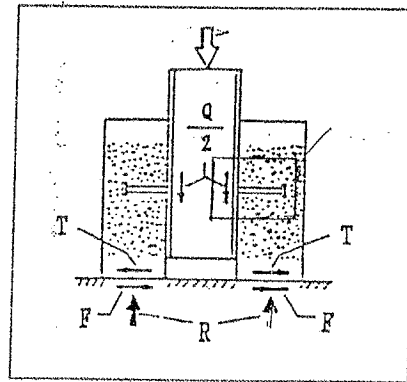
Fig.4 Push-out test
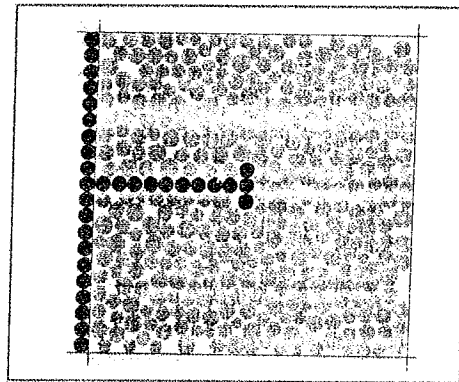
Fig.5 Numerical model of push-out test

Fig. 6 shows the sample at different loadlevel. At the first loadstep (F=1e+4) the sample is unbroken, large compression forces are acting on the right side of stub. (Picture "a") At the second loadlevel (F=2e+4) compression forces are increasing, some contacts next to the stub are broken. (Picture "b") The fracture of sample happens at the last loadstep (F=5e+4), all the contacts around the stub are broken, the stub is deformed considerably. (Picture "c")

"a"

"b"

"c"
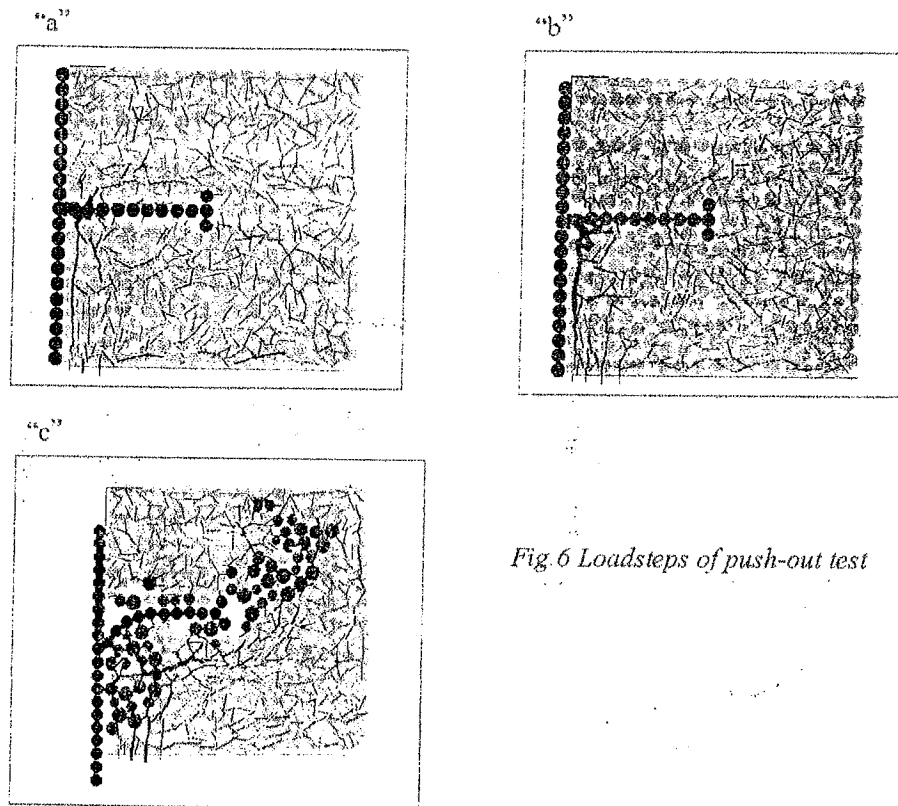
Fig.6 Loadsteps of push-out test

3.3 Identification of material parameters

The identification of material parameters is a very important question in the respect of the further investigations. The numerical model contains 11 material parameters, for example normal and tangential stiffness of a linear contact, the strength of a bonded contact, stiffness and strength of parallel bonded contacts which may take bending moment.

This example shows the determination of a microstructural parameter-set, which results the macroscopical properties of the sample to be in a good agreement with the real material. The material was concrete C25. Its standard parameters are as follows:

$$E = 3.05 * 10^7 \text{ kPa}$$
$$\sigma_{max} = 2.5 * 10^4 \text{ kPa}$$
$$\tau_{max} = 5 * 10^3 \text{ kPa} \qquad (\sigma_{max}/5)$$
$$G = 1.11 * 10^7 \text{ kPa} \qquad (\text{assuming } v = 0.35)$$

Different microstructural parameters are given for "balls" and contacts which model cement and aggregate. (Fig. 7)
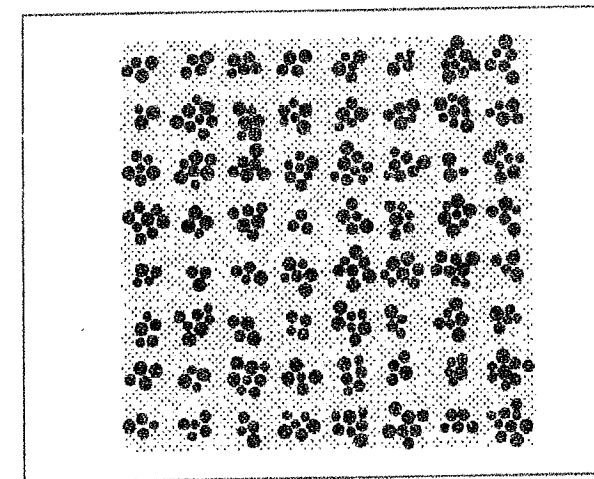
Fig. 7 Model of identification of material parameters

Fig. 8 and Fig. 9 show the model and load history of compression test. The load is the displacement of the upper horizontal wall by prescribed rate 10^7 unit/cycle.
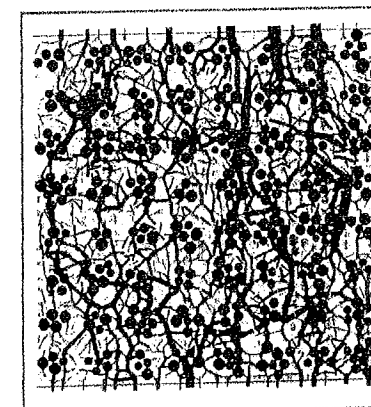
Fig. 8 Compression test
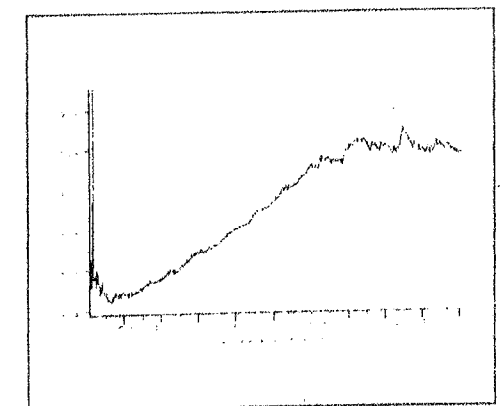
Fig. 9 Loadhistory of compression test

Fig. 10 and Fig. 11 show the model and load history of shear test. The load is also the displacement of the upper horizontal wall by prescribed rate 10^{-7} unit/cycle.
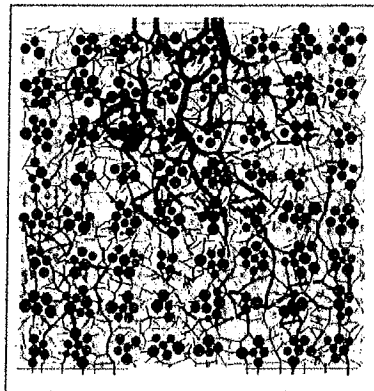
Fig. 9 Shear test
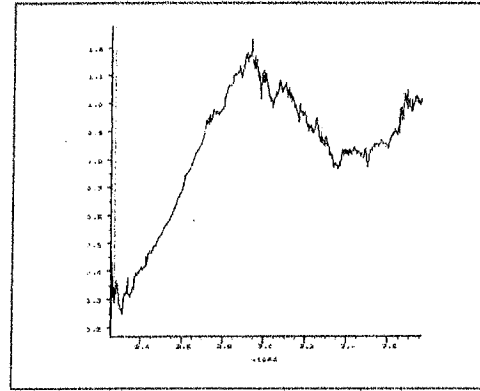
Fig. 10 Loadhistory of shear test

Macroscopical parameters calculated of the diagrams above are as follows:

$$E = 3.00*10^7 \text{ kPa}$$
$$\sigma_{max} = 2.5*10^4 \text{ kPa}$$
$$\tau_{max} = 6*10^3 \text{ kPa}$$
$$G = 1.0*10^7 \text{ kPa}$$

CONCLUSIONS

The presented numerical model is available for simulation of behaviour bonded granular materials with reinforcement. According to the first investigations the internal forces of mass considerably depend on the distance from the application point of load and the modification of the forcedistribution is significant during the loading process.

Flexibility of the model makes possible the investigation of very wide range of mechanical problems, for example material inhomogenity represented in Example 3.

REFERENCES

[1] PFC^{2D} User's Manual, Itasca Consulting Group, Inc

LIMIT STATE ANALYSIS OF DISKS

Tamás Fejér
Technical University of Budapest,
Laboratory of Informatics
H-1111 Budapest, Mûegyetem rkp. 3.
Tel: (36-1-)463 1933, E-mail: fejert@epito.bme.hu

## 1. THEOREMS OF LIMIT ANALYSIS

The engineering practice uses three basic types of analysis of structures. First of all maybe the most widespread and eximined method is the elastic analysis. The basic assumption of the method is the linear-elastic material behavior, based on Hooke's law.

In some cases this is not sufficient and we use an improved calculation based on the elastic-plastic material law. This yields in an iterative computation which may be slow and it does not converge always to the solution. If we apply a simplified material law which describes an ideally elastic – perfectly plastic material, we got a direct method to compute the collapse load of the structure. This is called limit analysis.

The limit Analysis consists of two theorems, namely the lower- and upper bound theorems, which are in primal-dual relationship with each other. In order to give a definition of them, first we have to define the statically admissible stress field and the kinematically admissible velocity field. A stress field, which satisfies the following conditions:
- fufills the equations of equilibrium,
- fulfills the stress boundary conditions, and
- nowhere violates the yield criteria,

is called a statically admissible stress field. For a given structure and external load, which is less than the limit load, we can always find a statically admissible stress field ([2]).

Similarly, a velocity field or deformation mode, which satisfies the following conditions:
- fullfills the geometric equtions
- fulfills the displacement boundary conditions, and
- the total rate of work done by the actual load on this field is positive,

is called a kinematically admissible velocity field. If we have a structure with external load greater than the limit load, we can always find a kinematically admissible velocity field.

If we use linear approximations, the greatest load which yields a statically admissible stress field and the smallest load which yields a kinematically admissible velocity field is equal and called the limit load.

In the present problem we used the lower bound theorem to get the limit load, because it fits better to the computer solution, however it is easier to visualize the results of the upper bound theorem, and it also gives directly the collapse mode and thus the weakest points of the structure.

2. MATHEMATICAL FORMULATION

The lower bound theorem states that an external load can be carried safely if a corresponding statically admissible stress field can be found. The first step to find the limit load is to establish a parameterized system of stress-fields which satisfies the equilibrium equations and the boundary conditions. Applying yield criteria to the system in form of inequalities, we have got the parameterized system of statically admissible stress field. Now maximizing the load factor subject to the previously established conditions, we get the highest load the structure can carry, i.e. the limit load.

This problem involves the use of mathematical programming, which has very effective algorithms to solve optimization problems if they are defined as linear functions of the variables. As a consequence, we have to set up both the yield conditions and the object function as linear functions of the stress parameters.

In the mathematical formulation we followed the common procedure used in the finite element method [1].

2.1 Geometric discretization

In the geometric discretization we used triangular elements defined by the three corners. Inside the element we used the triangular coordinate system which enables to treat all the elements similarly, they differ only in the global coordinates of the cornernodes.

2.2 Discretization of the function space

Following from the lower bound theorem, we have to deal only with the stress distribution and can completely ignore the strains and displacements. In general case, the stress distribution can be discribed by six stress parameters. For thin plates, loaded in its own plane we can assume the plane stress state, in which case three stress parameters are zero. The other three parameters can be derived from a common arbitrary function, called the Airy stress function ([4]) as follows:

$$\sigma_x = \frac{\partial^2 f}{\partial y^2}, \quad \sigma_y = \frac{\partial^2 f}{\partial x^2}, \quad \tau_{xy} = \frac{\partial^2 f}{\partial x \partial y} .$$

As a result, we have one unknown function, the $f(x,y)$ Airy function. Following from the geometric discretization, we defined the Airy function separately for every finite element as the function of the area coordinates. Inside the elements we assume linear variation of the stresses as an approximation. This involves the Airy function to be full third degree function of the coordinates and can be expressed as

$$f(\lambda_1, \lambda_2, \lambda_3) = \sum_{i=1}^{10} f_i s_i(\lambda_1, \lambda_2, \lambda_3) ,$$

where
$f(\lambda_1, \lambda_2, \lambda_3)$ is the Airy stress function as a function of the area coordinates, and
$s_i(\lambda_1, \lambda_2, \lambda_3)$ are specially selected weight functions.

A full third degree polinomial has ten degrees of freedom. The values of the weight functions are equal to 1 in one point out of the ten selected points and zero in all the other points. The values of the Airy function in the nodes (f_i) are the parameters of the problem.

2.3 Equilibrium equations

The internal equilibrium of the elements is automatically satisfied through the previous choice of the stress function, following from the definition of the Airy stress function. Later in this chapter we will only exemine the interelement equilibrium.

Along the sides of two neighbouring elements the normal stresses perpendicular to the side and shear stresses must be continuous. The normal stress paralel to the side may not be continuous. If we select the Airy stress function to be continuous over the whole structure, it can be proved that the continuity condition of the perpendicular normal stresses is automatically satisfied. To satisfy the equilibrium of shear stresses we have to build constraints. The variation of the shear stresses along the side is linear. This requires two constraints between every two neighbouring elements.

2.4 Boundary conditions

A serie of limitations follow from the lower-bound theorem and from the choice of the stress function. These are:

- within the scope of the lower bound theorem there is no way to prescribe support displacement,
- we assumed that the body forces are zero, therefore boundary conditions can be prescribed only at the outer boundary of the structure,
- following from the linear stress distribution, the external load function must be linear over the elements and it must be continuous,
- the load can be either paralel or perpendicular to the side,
- a support - in order to be effective - must be at least two element long,
- any support may be paralel and/or perpendicular to a boundary side.

3. COMPUTER IMPLEMENTATION

The program is divided into five phases. These are:

Phase 1 : Formulation of the constraints,
Phase 2 : Factorization of the equations,
Phase 3 : Formulation of the yield criteria,
Phase 4 : Optimization of the stress distribution,
Phase 5 : Postprocessing.

In the first phase we build up a linear equation system from the constraints, which in practical cases has free parameters, i.e. more variables than equations. We use a factorization process in the second phase to separate the free and non-free variables and thus eliminate the equations.

In general, the yield function is a non-linear function of the stress parameters and design variables. Since we use a linear programming solver, the applied yield criterion shuold be linearized in the following form:

$$k_1 \sigma_x + k_2 \sigma_y + k_3 \tau_{xy} \le 1 \ .$$

Here the k_i parameters are user defined and may depend on material properties. Using a set of yield criteria for every nodes, we can now build up the restrictions and the object function of the LP problem:

$$\text{maximize } \lambda$$

subject to

$$\mathbf{H} f_{free} \le \lambda r + r_0$$

where

$\mathbf{H}$ is the restriction matrix depending on the linearized yield criteria,
f_{free} is the vector of the free stress parameters,
r and r_0 is the parameterized load vector (variable and constant part),
λ is the scalar load parameter.

The optimization is done by an effective algorithm specially designed for structural applications [3] [5].

The result of the optimization is the maximum value of the object function, and the vector of the f variables which produces this value. The stress distribution described by the solution vector is a statically admissible stress field, which maximizes the external load, i.e. gives the exact collapse load of the discretized and linearized problem. Since we approximated the geometry and the stress distribution of the structure and also linearized a theoretical yield criterion, this collapse load can not be treated as an exact collapse load or even a lower bound solution of the real structure. However, if the mesh is dense enough and the yield criterion is linearized on the safer side, the result can be accepted as a good approximation of the lower bound solution.

CONCLUSION

A general numerical method for limit analysis of homogeneous plane structures has been established. The theoretical basis is the lower bound theorem and the finite element method which has been shown very effective in many numerical application. However the upper-bound theorem gives more visual results, this can be also calculated as the dual of the lower bound solution with simple postprocessing. On the other hand, the lower bound method gives results on the safe side and there is the possibility for further improvements.

The applied method makes the material optimization also possible, when some functions of selected material parameters (thickness, price, etc.) are to be optimized. An other improvement may include a special linear element type for the modelling of reinforced concrete structures and thus introduce inhomogenity into the system.

The method has been implemented in standard C language under Unix operating system. Due to the efficient algorithms and the used computer, the execution time of the problems were very modest. Since the program uses the ANSI C, it is easily portable to other platforms, including DOS.

REFERNCES

[1] Imre Bojtár and Zsolt Gáspár. *Tartók statikája IV. (in Hungarian)*. Mûegyetemi kiadó, H-1111 Budapest, Hungary, 1992. Textbook.

[2] W. F. Chen and D. J. Han. *Plasticity for Structural Engineers*. Springer, 1988.

[3] Lars Damkilde, Ole Høyer, and Steen Krenk. A direct linear programming solver in C for structural applications. *Computers & Structures*, 52(3):511-528, 1994.

[4] Y. C. Fung. *A first course in continuum mechanics*, pages 324-315. Prentice-Hall, second edition, 1977.

[5] Ole Høyer, Lars Damkilde, and Steen Krenk. General simplex algorithm implemented in C (in danish). Dokumentationsrapport 108, Dept. of Struct. Eng., Technical Univ. of Denmark, DK-2800 Lyngby, Denmark, 1992.

SESSION 6

Geodesy

DIGITAL IMAGE PROCESSING USING NEURAL NETWORKS

Árpád BARSI
Technical University of Budapest
Dept. of Photogrammetry
H-1521 Budapest

1. INTRODUCTION

Since the 60s we know the basic operation of artificial neural networks which are similar to the components of the human brain. The hardware and software necessary for the computation has become adequate just recently.

I'll discuss a special field of digital image processing in my paper, namely the thematic classification. I've made some experiments for doing this job with artificial neural networks.

2. NEURAL NETWORKS

The basic elements of a neural network are the neurons, connecting themselves networklike (Fig. 1).
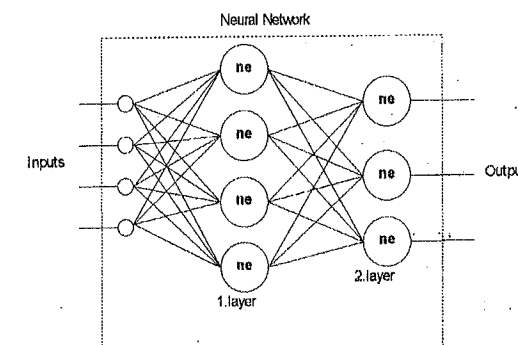

Fig. 1 Schema of a neural network

The neurons add the signals coming on their inputs by weighting and compute the output after an answer function. The answer function (called also transfer function) is mostly a logistic sigmoid

$$f(x) = \frac{1}{1+e^{-x}} \qquad (1)$$

The most popular network type is the so-called backpropagation network. The course of operation of a backpropagation neural network is the following:

1. Setup the network: determining the number of layers and the amount of their neurons.

2. Selection of the training set and training the network: In the first step of learning we choose the weights and biases randomly. (Biases characterize the transfer function.) Of course, there are special methods to accelerate the learning; these methods select the weights and bias values – network parameters – not so freely. After we calculate the net with these initial values (feed-forward), the given errors must be adjusted on the network parameters (backpropagation). The calculation must be repeated until the network error reaches a given rate.

3. Use of the trained network: A purely feed-forward phase.

Beside the mentioned method there are other organized neural networks e.g. Hopfield-networks [2].

3. THEMATIC MAPPING

The aim of the thematic mapping in digital image processing is to assign each pixel of a digital image (e.g. satellite image) to any thematic class meanwhile the classification error should remain as low as possible [3]. We can choose numerous mathematical solution to determine thematics from the input gray-level values. The generally used minimum distance method that belongs to the supervised classification methods, assigns the pixels to the nearest class in the intensity hyperspace. In contrast to that the maximum likelihood method will choose the most probable class for the image points. The mentioned methods need the determination of the parameters which can be computed from the training areas [1] [4].

4. NEUROCLASSIFICATION

In the experiment I made the classification for a LANDSAT TM image with six bands containing Budapest in it by traditional (minimum distance, maximum likelihood) and neural methods. The test area was about 125 km^2 (301 × 460 pixels). I used 2 and 3 layer neural networks with different number of neurons. Because of the six bands the number of the input neurons was given. I differentiated four classes, so the number of the output neurons was four. I've chosen two training areas pro thematic classes for which the means and covariance matrix were calculated. I trained the neural networks with eight input vectors containing only the band means.

The classification result shows that the operation is highly depending on the network structure. It's possible to find such a structure which is very similar to the result of the traditional methods. An advantage of the neural methods is the possibility to import other data into the classification, not only grayscale values [5].

5. CONCLUSION

It was proved in my experiment that the thematic classification using artificial neural networks is possible. The result depends on the network structure but a 3-layer neural network is able to produce acceptable thematic map. I'll refine the applied models and will try out further ones, too.

REFERENCES

[1] Barsi Á.,"Thematic Mapping of the Naivasha-region (Kenya) from LANDSAT Images", *Thesis work*, Budapest, 1994.

[2] Rojas R.,"Theorie der neuronalen Netze – Eine systematische Einführung", *Springer-Verlag*, Berlin, 1993.

[3] "Manual of Remote Sensing", ed-in-chief Colwell, R. M., *Sheridan Press*, Falls Church, 1983.

[4] "Remote Sensing: The Quantitative Approach", ed. Swain, Ph. H. – Davis, Sh. M., *McGraw-Hill*, 1978.

[5] Barsi Á.,"Thematic Classification of a Satellite Image using Neural Networks", *Essay*, Budapest, 1995.

GPS MÉRÉSEK FELDOLGOZÁSA ÉS TÉRINFORMATIKAI FELHASZNÁLÁSA

Szűcs László
Budapesti Műszaki Egyetem, Felsőgeodézia Tanszék
1521 Budapest, Műegyetem rkp. 3.

A geodéziában napjainkban olyan változásoknak lehetünk szemtanúi, melyekhez hasonlók a középkorban az osztott körökkel működő, modern formában napjainkban is megtalálható mérőműszerek megjelenésekor történtek. A változások érintik a műszereket, de alapvető fordulat történik a mérések feldolgozásának területén is.

A műszerek területén a nyolcvanas években megjelentek a könnyen kezelhető, műholdakat használó mérőműszerek. A gyakorlatban ma már a NAVSTAR-GPS rendszer a legelterjedtebb. Ezt a rendszert eredetileg az Amerikai Védelmi Minisztérium navigációs célokra hozta létre. Célja, hogy bárhol és bármikor, a Földön és közeli környezetében rövid idő alatt pontos helyzeti, idő- és sebesség-adatokat szolgáltasson a terepen mozgó katonák számára. A cél megfogalmazásából is látható, hogy a rendszer meglehetősen közel áll a földméréshez, melynek feladata a Föld alakjának és nehézségi erőterének, valamint a rajta található természetes és mesterséges objektumok helyzetének meghatározása.

A rendszer működésének elve, hogy hat műholdpályán 4-4 műhold kering 20000 km magasságban. Ez a kialakítás lehetővé teszi, hogy a műszer bárhol is van a szabad ég alatt, legalább négy mesterséges hold jelét képes észlelni. A műholdak által sugárzott pályaelemek alapján számíthatók a műholdak koordinátái. Megmérve az antenna távolságát a műholdaktól, meghatározható az antenna helyzete.

A távolságmérésre két módszer terjedt el. Az egyik lehetőség az, hogy a műhold által sugárzott jelek futási idejét mérjük a műhold és az antenna között. A futási időt a fény terjedési sebességével megszorozva megkapjuk a távolságot. Ezt a módszert hívjuk kódmérésnek. A másik lehetőség a távolság meghatározására a fázismérés. Ebben az esetben a sugárzott jel beérkezési fázisát mérjük. A hullámhossz ismeretében a beérkezési fázisból számítható a hullámhossznál kisebb távolság. A távolság meghatározásában ismeretlenként jelentkezik a hullámhossz egészszámú többszöröse, melyet a feldolgozás során határozunk meg. Mint a legtöbb esetben, a GPS méréseknél is az abszolút mérés sokkal pontatlanabb a relatív mérésnél. A pontok térbeli helyzetét abszolút módon csak több tíz méteres nagyságrendű hibával határozhatjuk meg. Relatív méréskor, azaz amikor a két pont közötti vektort keressük, a pont meghatározásának a pontossága kódméréssel legjobb esetben is kb. 80 cm, fázismérés esetében néhány milliméter, ezért geodéziai hálózatok mérésekor a fázismérést kell használnunk, de egyes feladatokhoz elegendő a kódmérés is.

Az 1995-ben rendezett szimpóziumon még csak a kódméréssel elért eredményeket tudtam ismertetni, azonban idén a Miskolci Egyetem Bányamérnöki Karának Geodéziai és Bányaméréstani Tanszéke jóvoltából kölcsönkaptunk egy fázismérésre alkalmas vevőt. Közösen használva a Felsőgeodézia Tanszék fázismérésre alkalmas vevőjével, geodéziai pontosságú méréseket tudtunk végrehajtani.

A Fotogrammetria Tanszékkel közösen kódméréssel dolgozó navigációs vevővel készítettük a Mosonmagyaróvár melletti autópálya térképezését, hogy feltüntessük a térségről készült GIS rendszerben. Mivel a GIS rendszert 1:10 000 vagy annál kisebb méretarányú térképek felhasználásával készítettük, a legnagyobb elvárható pontosság a pontok beméréssénél 2-3 méter volt. Erre a célra megfelelt a navigációs vevő.

A geodéziai vevő megérkezésekor az Egyetem előtt a Duna két partján egy hatpontos hálózatot hoztunk létre. A hálózat négy pontja a negyedéves hallgatók hálózatmérési gyakorlatában már több éve szerepelt, így koordinátáikat nagy megbízhatósággal ismertük. Ebbe a hálózatba illesztettünk be még két pontot. A létrehozott hálózatban igen sok, egymástól független mérés történt, melyek a GPS mérések pontossági vizsgálatát tették lehetővé. A vizsgálatok eredményei alapján arra a következtetésre jutottam, hogy a bázisvektoroknak a gyári feldolgozó szoftverrel számított a priori kovarianciamátrixa kb. 20-40-szer kedvezőbb képet mutat, mint a valóság. Ez megfelel a szakirodalomban hasonló vizsgálatokkal kapott eredményeknek.
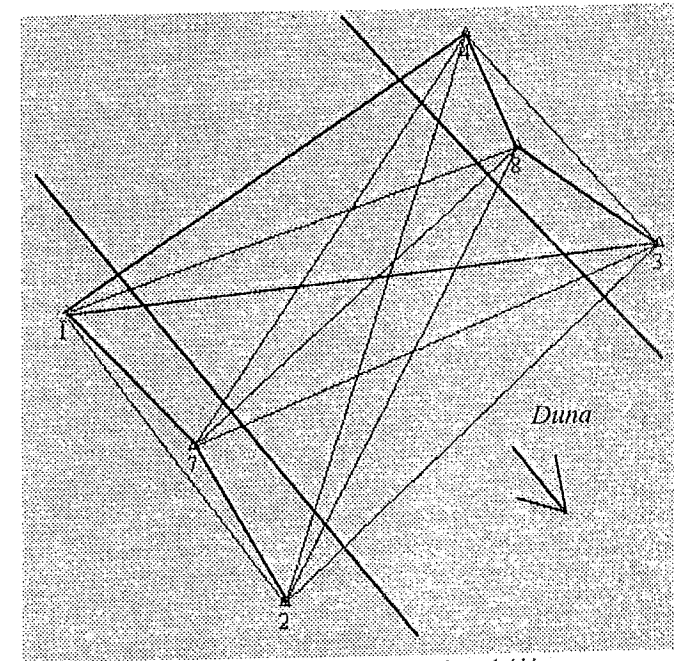
1. ábra Az Egyetem előtt létesített hálózat

Diplomatervezés keretében a hálózatba újabb pontokat illesztettünk kinematikus mérési eljárással. A kinematikus mérés lényege, hogy nem kell a vevőnek hosszú ideig egy-egy ponton állnia, hanem mozog a terepen. A bemérendő ponton csak rövid ideig tartózkodik. Hatékonysága a statikus mérésnek a többszöröse, ezért a GIS rendszerekben adatgyűjtésre használható.

Megvizsgáltuk a navigációs vevővel történő relatív kinematikus mérésekkel elérhető pontosságot. Tapasztalataink szerint a városi autónavigációhoz ez a pontosság megfelelne. Felszerelés hiányában az eredményeket csak utófeldolgozással tudtuk számítani, nem tudjuk a valósidejű feldolgozást megvalósítani.

A felhasznált két geodéziai pontosságú vevőt a Penci Kozmikus Geodéziai Obszervatórium területén létesített hálózatban kalibráltuk. Az ellenőrzés legérdekesebb eredményét a nulla hosszúságú bázisvonal mérése jelentette. Ekkor a két műszer közös antennát használ. Elvileg a bázisvonal hosszának nullának kell lennie. A feldolgozások tizedmilliméteres bázisvonalakat mutattak. Ez magukra a vevő műszerekre jellemző érték. A kapott eredmények alapján a műszereket hibátlannak tekinthetjük.

Diplomaterv keretében megmértük a Sóskúton létesített geodinamikai hálózatot, melyet a nyolcvanas évek elején létesítettek a geodinamikai mozgások kimutatására. 1990-ben történt az első GPS-szel végzett mérése. Az eltelt hat évben GPS-szel nem mérték a

hálózatot. Méréseink megfelelő összhangban voltak az alapmérésekkel, így nagyobb mozgásokra nem következtethetünk.
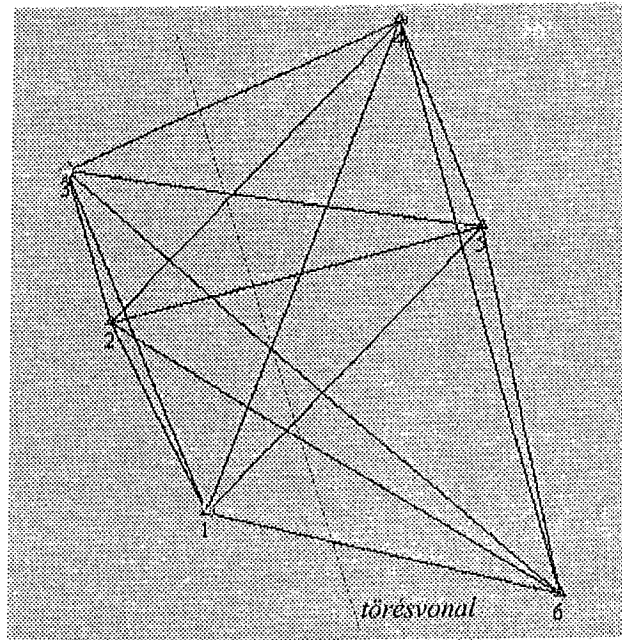
2. ábra. A BME Sóskúti geodinamikai hálózata

A fent leírtakból is látszik, hogy a GPS a geodézia egyre több területére tör be. Legfontosabb felhasználási területei a hálózatmérések és a térinformatikai adatgyűjtés. Az elmúlt időszakban a térképezéshez és a mérnöki hálózatok létrehozásához szükséges mérési és feldolgozási eljárásokkal foglalkoztam. A jövőbeni feladat a nagypontosságú hálózatok feldolgozási módszereinek vizsgálata lesz.

A MAGYARORSZÁGI GPS ÉS VÍZSZINTES HÁROMSZÖGELÉSI HÁLÓZAT ÖSSZEHASONLÍTÓ VIZSGÁLATA

Virág Gábor
BME Felsőgeodézia Tanszék
Bp. Műegyetem rkp. 3.

1. A MAGYAR-OSZTRÁK-SZLOVÁK-CSEH I. RENDŰ VÍZSZINTES HÁLÓZATOKAT ÖSSZEKAPCSOLÓ GPS MÉRÉSEK FELDOLGOZÁSA

A mérés célja, végrehajtása és feldolgozása

A mérés célja a hagyományos módszerekkel létrehozott magyar és csehszlovák országos geodéziai hálózatok hozzákapcsolása a nyugat-európai ED-87 rendszerhez. Ennek érdekében a határmenti sávban kiválasztottak I.rendű pontokat mind a négy országban, majd ezen pontokon méréseket végezve meghatározhatók a pontok GPS rendszerre vonatkozó koordinátái. Ezeket a koordinátákat már át lehet számítani az ED-87 vonatkozási rendszerbe. A méréseket 1993 októberében hajtották végre, melynek során 12 magyarországi ponton végeztek észleléseket. A mérési eredményeket az Osztrák Tudományos Akadémia Grazi Obszervatóriumában és a FÖMI Kozmikus Geodéziai Obszervatóriumában Pencen dolgozták fel [5,7].

A mérési eredmények vizsgálata

Az adatok korlátozott hozzáférhetősége következtében az elvégzett vizsgálatok csak Magyarországon található pontokra vonatkoztak.

Mivel a végleges feldolgozás eredményeit nem sikerült beszerezni, ezért a vizsgálat első lépéseként a pontok külpontossági elemeinek számítási eredményeit módosítottam a vetületi meridián konvergenciából adódó mértékben. Ezáltal rendelkezésünkre álltak a pontok térbeli derékszögű koordinátái az 1993.8 epochára számított ITRF91 rendszerben.

A vizsgálathoz szükséges másik adatcsoport a pontok HD72 dátumra vonatkozó térbeli derékszögű koordinátái. Ehhez először az y,x EOV síkkoordinátákból ellipszoidi földrajzi koordinátákat számítottam, majd az ellipszoid feletti magasság kiszámításához a H ortométeres magassághoz hozzáadtam az alábbi módon meghatározott geoidundulació értéket. Jelenleg Magyarország legpontosabb és legnagyobb felbontású geoidját Kenyeres Ambrus határozta meg a penci obszervatóriumban, mely geoid a GRS80 ellipszoidra vonatkozik. Az erre vonatkozó unduláció értékeket a Vening-Meinesz összefüggésekkel [4] átszámítottam az IUGG67 ellipszoidra. Erre azért is szükség volt mivel nem mindegyik ponton volt ismert az IUGG67 ellipszoidra vonatkozó geoidunduláció.

A lokális transzformáció vizsgálatához kihagytam a továbbiakban a területtől nagy távolságra lévő Penc nevű pontot. A Bursa-Wolf modell [1,6,8] felhasználásával a következő eredmények adódtak. A méretarány-tényező értéke ~4.5 ppm, amely jelentősen eltér az országos átlagtól [2,8], viszont nagyon jó egyezést mutat az országos hálózat nyugat-dunántúli részének 4-6 ppm-es értékével [8]. A transzformáció után visszamaradó javítások átlagos értéke mindössze 7 cm, amely messze alatta marad az országos hálózatra adódó 27 cm-es értéknek, de még a maximális érték is csak 10 cm körüli.

2. ÁTSZÁMÍTÁS A KÖZÖS PONTOK TÉRBELI DERÉKSZÖGŰ KOORDINÁTÁINAK KÜLÖNBSÉGE ALAPJÁN

A módszer alapelve

Ha rendelkezésünkre állnak a közös pontok térbeli derékszögű koordinátái a GPS vonatkozási rendszerében és az országos alapponthálózat vonatkozási rendszerében, akkor minden egyes közös pontra kiszámíthatók a koordináta – komponensek különbségei. A különbség értékek alapján minden egyes komponensre megszerkeszthető egy izovonalas ábra [3]. Ha van olyan pont, melynekkoordinátái adottak az egyik rendszerben, akkor a koordináták alapján megkereshetjük a pont helyét az ábrán, majd interpolációval erre a pontra megkaphatjuk a koordináta-különbség pontbeli értékét, amiből egyszerűen számíthatjuk a másik rendszerre vonatkozó koordinátákat.

A módszer gyakorlati alkalmazhatóságának vizsgálata

Az Országos GPS hálózat 43 közös pontja alapján megszerkesztettem a SURFER programrendszer segítségével az izovonalas ábrákat. Az 1. ábrán látható példaként az X koordináta különbség ábráját. Az ábrán a deciméteres izovonalak vannak ábrázolva, melyek felhasználásával remény van arra, hogy az átszámítás pontossága néhány cm legyen. Ez azonban még további vizsgálatokat igényel.
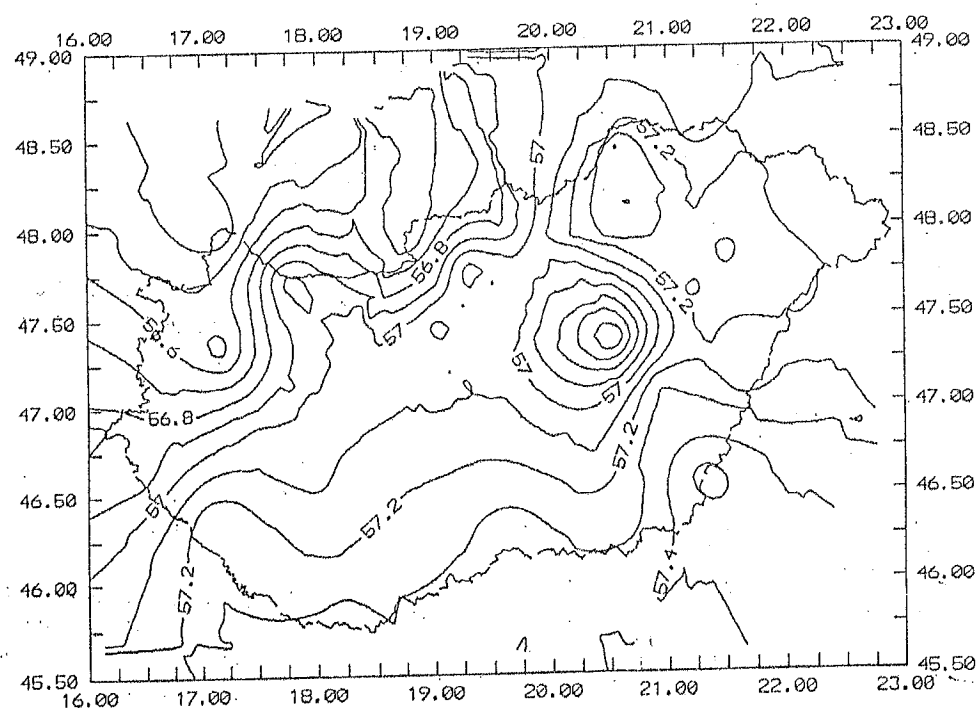
1. ábra Az X koordináták különbsége alapján szerkesztett izovonalas ábra

IRODALOM

[1] Ádám J.: Megfigyelő állomások koordinátáinak meghatározása kozmikus geodéziai módszerekkel, *Kandidátusi értekezés,* Budapest, 1980.
[2] Ádám J. - Borza T.: The GPS networks and their comparison with the traditional network of Hungary, *Reports on Geodesy,* No.(3)16,1995. pp. 211-219.
[3] Bácsatyai L.: Umwandlung der Budapester stereogtaphischen Koordinaten in österreichische Gauss-Krüger-Koordinaten, *Österreichische Zeitschrift für Vermessung & Geoinformation,* Vol.83, No.(4), 1995.
[4] Biró P.: Felsőgeodézia, *Kézirat, a BME egyetemi jegyzete,* Budapest, 1985.
[5] Kenyeres A.: A magyar-osztrák-szlovák-cseh I.rendű vízszintes hálózatokat összekapcsoló mérések feldolgozása, *FÖMI tanulmány,* 1993. december 15.
[6] Krakiwsky, E.J. - Thomson, D.B.: Mathematical Models for the Combination of Terrestrial and Satellite Networks, *The Canadian Surveyor,* Vol. 28, No,5, 1974.
[7] Stangl, G.: Interconnection 1993 Computational Strategies and Problems, *Reports on Geodesy,* No.(3)16,1995. pp. 157-165.
[8] Virág G.: A GPS és háromszögelési alaphálózatunk vonatkozási rendszere közötti transzformáció vizsgálata. *BME Diplomaterv,* 1993.

A DIGITÁLIS KÉPFELDOLGOZÁS LEHETŐSÉGEINEK VIZSGÁLATA AZ ARC/INFO ESZKÖZTÁRÁVAL

Nagyné Gerencsér Andrea
Budapesti Műszaki Egyetem
Fotogrammetria Tanszék
1111 Budapest, Műegyetem rkp.1-3.

1. BEVEZETÉS

Munkánk célja az volt, hogy a teljesség igénye nélkül bemutassuk azokat az eljárásokat, melyekkel különböző archiv alapanyagokból földhasználati térképeket állíthatunk elő. A munka során felépítünk egy környezeti, digitális adatbázist térinformatikai eszközökkel. Ez az adatbázis a későbbiekben a felhasználói igény szerint bővíthető egyéb információkkal. Az adatbázis alkalmas térbeli és időbeli változások vezetésére, tervezésekhez (pl. út-vasút), környezet- állapot vizsgálatra is.

A környezetvizsgálat és a környezetállapot megőrzése, illetve javítása napjainkban igen fontos kérdéssé vált. Reméljük, hogy a közeljövőben egyre több e témában jártas szakember (és nem szakember) veszi majd igénybe a térinformatikai rendszerek kínálta sokszínű felhasználási lehetőséget, mivel már sok területen igen elterjedt napjainkban ezeknek a rendszereknek a használata.

2. A RENDELKEZÉSÜNKRE ÁLLÓ ALAPANYAGOK

1:10000 topográfiai térkép (1985)
1:25000 topográfiai térkép (1972 és 1985)
1989-es légifénykép
1985-ös és 1986-os TM kompozitok nagyításai

3. A FELADAT MEGOLDÁSA SORÁN ALKALMAZOTT ELJÁRÁSOK

A rendelkezésünkre álló, az előzőekben felsorolt archiv alapanyagokból két különböző eljárással földhasználati térképek készítése térinformatikai rendszerben.

Az egyik eljárás, melyet a feladat megoldása során alkalmaztunk az osztályozás.

A másik eljárás során a topográfiai térképeket digitalizáltuk, illetve a légifényképet felüldigitalizáltuk, majd ezek kiértékelésével, interpretációjával elkészítettük a földhasználati térképeket.

Az osztályozást, valamint a digitalizált térképek szerkesztését az ARC/INFO szoftverrel hajtottuk végre, a térképeket pedig ArcView alatt hoztuk végleges formába.

3.1 Az osztályozás

A számítógéppel végrehajtott osztályozás feladata az, hogy az egyes képelemek (pixelek) spektrális jellemzőit összehasonlítva az adott képelemet a megfelelő osztályba sorolja.

Az osztályozó eljárások két csoportba sorolhatók:
-ellenőrzött,
-nem ellenőrzött osztályozás.

Az ellenőrzött (supervised) osztályozásnál a különböző osztályok spektrális jellemzője előre meghatározott az ún. tanító vagy tesztterületek alapján. Ezeket a tanítóterületeket a felhasználó teljesen szubjektív módon választja ki. Ez történhet például úgy, hogy kezébe vesz egy térképet és annak segítségével jelöli ki ezeket a tanítóterületeket. Pl.:ipari terület, település, gyümölcsös stb. Maga az osztályozás aztán a legismertebb és leggyakrabban használt módszerrel, a Maximum Likelihooddal történhet. A módszer a kiválasztott osztályok statisztikai jellemzői alapján valószínűségeket számol és a hozzárendelés a legnagyobb valószínűség szerint történik meg.

A nem ellenőrzött (unsupervised) osztályozásnál nincsenek előre kijelölt tanítóterületek az osztályozás megkezdése előtt. Más szóval ez a tanító nélküli osztályozás. Az eljárás során meg kell adnunk az osztályok számát (pl. 10 osztályt szeretnénk megkülönböztetni) és a csoportosítást a szoftver végzi el. Ez a klaszterezés[4].

3.2 A meglévő térképek digitalizálása

A meglévő térképek manuális digitalizálása a geometriai adatnyerés viszonylag olcsó és gyorsan elvégezhető módszere. A digitalizálás analóg-digitális átalakítás, amellyel a térkép egyes pontjaihoz számszerű koordinátákat és kódokat is rendelhetünk. Ennek következtében alkalmazása széles körben elterjedt.

A térképek manualizálásának munkafolyamata Detrekői-Szabó (1995) alapján a következő részekre bontható:

- előkészítés,
- a digitalizálás,
- az adatok szerkesztése.

Az előkészítés a rendelkezésre álló analóg térkép aktualitásának ellenőrzéséből és a digitalizálni kívánt tartalom kiemeléséből tevődik össze.
Az aktualitás ellenőrzése helyszíni bejárásból, a térképről hiányzó objektumok helyzetének meghatározásából (pl. GPS-vel), ill. a térképnél frissebb légifényképek interpretációjából áll. A digitalizálás során generalizálunk is.

A digitalizálás pontosságára a 0.05-0.10 mm érték a jellemző. Ez az érték azonban csak a digitalizálás műveletéből adódó hibákat jellemzi, s nem tartalmaz információt az eredeti térkép pontosságára vonatkozólag.

Az adatok szerkesztése a munkafolyamat harmadik lépése. A szerkesztés lépései a következők Detrekői-Szabó (1995) szerint:

- a hibák javítása,
- a hiányzó adatok pótlása,
- a topológia kialakítása.

A hibák javítása az eredeti térkép és a digitális állomány összevetése alapján lehetséges. A hiányzó adatok pótlása a hibák javításához hasonlóan vizuális összehasonlítás útján történhet. A topológia kialakítását a tárolási módnak megfelelően kell elvégezni.

Az eljárás előnyei:
- viszonylag nem drága eszközt,
- kevés szakismeretet igényel[3].

4. ÖSSZEGEZÉS

4.1 Az osztályozás eredménye

Első lépésként beszkenneltük a légifényképet és az űrfelvételeket.
Önmagában a légifénykép alkalmatlan volt az osztályozásra, ezért ezt az űrfelvételbe transzformáltuk. Így kaptunk egy 6 sávos multispektrális-kompozitot , mely már alkalmas a további feldolgozásra.

A képen 7 különböző osztályt sikerült elkülönítenünk. Egy-egy osztályhoz 3-4 tanítóterületet jelöltünk ki. Az osztályozást a szoftver Maximum Likelihood módszerrel hajtotta végre.

Összefoglalva: az osztályozás egészét tekintve, a kapott eredmény durva hibáktól mentes. Az osztályozás eredményét elfogadjuk.

Az osztályozás eredményét elfogadva szükség volt a képek szűrésére. Erre legalkalmasabb és mindig bevált szűrő a medián és a majority. A szűrés azért szükséges, hogy a néhány pixelből álló foltokat, illetve az egyedi pixeleket, melyeknek osztályba sorolása nem megfelelő (hibás) módosítsuk.
Szűrés után vektorizáltuk az osztályozott képet. Ez a vektorizált osztályozott kép már alkalmas arra, hogy az ArcView alatt mint térképet kezeljük és kiszinezzük.

4.2 Térképkészítés digitalizálással.

Ebben a pontban foglalkozunk a hagyományos úton készült, digitalizált térképeink létrehozásával és a megvalósítás esetleges problémáival.

Ezután a digitalizálást (ezt nevezzük felüldigitalizálásnak, megkülönböztetve a térképek manuális digitalizálásától) magán a légifényképen is elvégeztük, mivel úgy gondoljuk, hogy ez a módszer szolgáltatja a legaktuálisabb térképet. Ez a megoldás pontosabb, mint amikor a változásokat a meglévő térképen szerkesztéssel módosítjuk.

Digitalizálás után valamennyi térképünket a korábban már említett űrfelvételbe transzformált légifénykép geometriai rendszerébe transzformáltuk illesztőpontok segítségével.

Mint ismeretes a digitalizált térképek nem hibátlanok. Milyen gyakori hibák fordulnak elő? Pl.:
- 2 vonal nem egy csomópontban találkozik,
- poligon nem záródik,
- hiányzik vonal,
- egy vonal nem ér el egy másikat vagy éppen túllóg rajta stb.
A hibák kijavítása után felépítettük a topológiát. Erre minden esetben szükség van, mert enélkül nem tudunk tovább dolgozni, térképet készíteni.
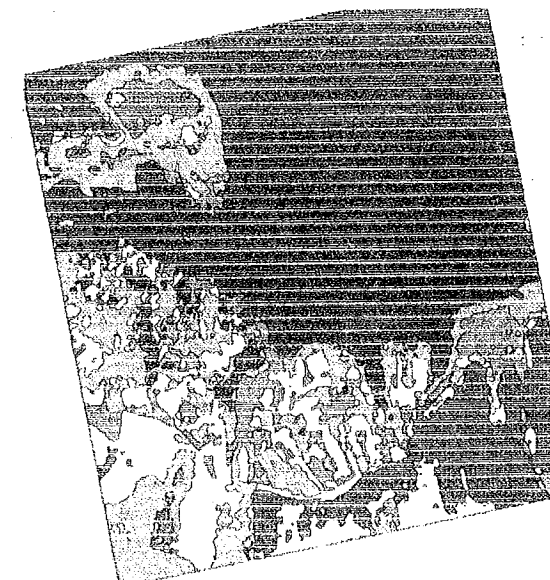
Vektor
- kopár terület
- erdő
- szántó
- füves
- szőlő,gyümölcsös
- bokros
- bánya

Vektoralaptérkép (osztályozás eredménye)
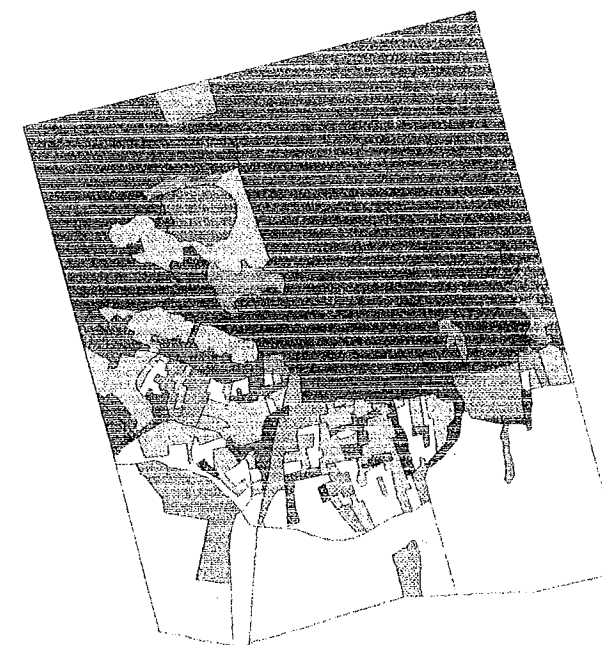
Terkep1
- bánya
- erdő
- kopár terület
- bokros,füves
- szántó
- kert, gyümölcsös
- szőlő
- füves
- mocsaras

Földhasználati kategóriák (digitalizálás eredménye)

5. REFERENCIÁK

[1] Álló G. - Főglein J. - Hegedűs Gy.Cs. - Szabó J.," Bevezetés a számítógépes
   képfeldolgozásba", Kézirat. *BME*. Budapest, 1985.
[2] Álló G. - Hegedűs Gy. Cs. - Kelemen D. - Szabó J.," A digitális képfeldolgozás
   alapproblémái", *Akadémiai Kiadó*. Budapest, 1989.
[3] Detrekői Á. - Szabó Gy.," Bevezetés a térinformatikába", *Nemzeti Tankönyvkiadó*.
   Budapest, 1995.
[4] Gerencsér A.,"Diplomamunka", Karlsruhe, 1992.
[5] "ArcView Version 1.0", Felhasználói Kézikönyv. *ESRI*. USA, 1992.
[6] "Understanding GIS. The ARC/INFO Method", *ESRI*. USA, 1994.

A MAGYAR ÉS A KÖZÉP-EURÓPAI GPS MÉRÉSEKEN ALAPULÓ MOZGÁS-VIZSGÁLATI PROGRAMOK ÉS AZ EDDIGI EREDMÉNYEK

Simon Ágnes
BME, Felsőgeodézia Tsz.
Budapest, Műegyetem rkp. 1-3
I. em. 61.

1. BEVEZETÉS

Napjainkban a műholdas helymeghatározási technika, a GPS (Global Positioning System) megjelenése forradalmi változást hozott a földtudományok területén. A kutatások legfontosabb eszköze lett a geodéziától a geofizikáig. Az elmúlt 5 évben Magyarországon és a közép-európai térségben egyaránt elkezdődtek a GPS méréseken alapuló geodinamikai kutatások.
A következőkben ezek a programok és eddigi eredményeik kerülnek ismertetésre.

2. A KÖZÉP-EURÓPAI REGIONÁLIS GEODINAMIKAI PROGRAM

2.1 A projekt célja

1993-ban lengyel és magyar szakemberek kezdeményezésére indult a Közép-Európai Regionális Geodinamikai Program (CERGOP). Célja, hogy a régióban folyó geodinamikai kutatásokhoz alapot nyújtson. Megpróbálja egyesíteni a különböző típusú korszerű mérési technikákat: abszolút gravimetriát, extenzometriát és végül, de nem utolsó sorban a különféle műholdas technikákat, mint például a GPS. Jelen pillanatban ez utóbbi vezető szerepet játszik a CERGOP műszerei között. A projekten belül az "alapeszköz" a Közép-Európai Geodinamikai Referencia Hálózat (CEGRN), mely 31 pontot tartalmaz (1. ábra).

Az ábrán fehér körrel jelölt pontok úgynevezett társult pontok, azaz a CEGRN mérésekkel egyidőben rajtuk is történik észlelés, de a feldolgozásba nem kerülnek be.
A pontok 11 ország területén találhatóak. A hálózat fő célja, hogy egy jól definiált referenciakeretet szolgáltasson a lokális és regionális geodinamikai kutatásokhoz. Másik nemkevésbé fontos feladata, hogy segítséget nyújtson a régió geokinematikai információkon alapuló tektonikai értelmezéséhez. A kitűzött célok elérésének útja a CEGRN hálózat évenkénti mérése GPS-szel.

A projekt céljainak megfelelően a pontok kiválasztásakor figyelembe vették többek között, hogy minden főbb geológiai szerkezeti egységen legyenek pontok, ugyanakkor megfeleljenek a GPS mérésekhez szükséges feltételeknek.
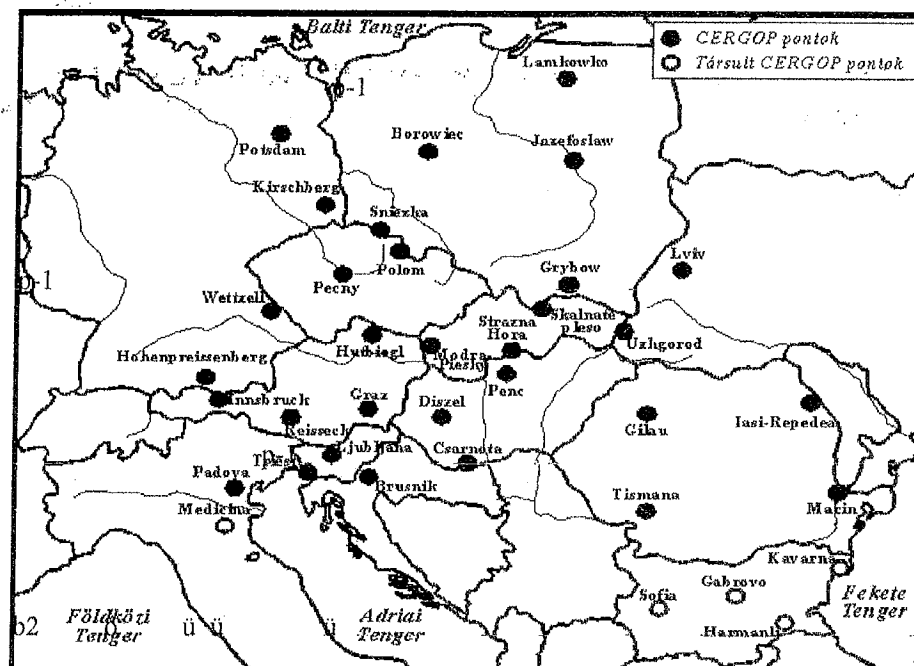
1. ábra A Közép-Európai Geodinamikai Referencia Hálózat pontjai

2.2 Feldolgozás

A feldolgozás öt feldolgozóközpont (Ausztria, Cseh Köztársaság, Németország, Magyarország, Szlovákia) által történik meghatározott stratégia szerint:

- Műholdpályák naponta, feldolgozás L3 frekvencián, L1-en és L2-n ambiguity meghatározás

- Troposzféraparaméterek meghatározása kétórás intervallumokra

- Két megoldás: szabad és rögzített

- A szabad megoldást geodinamikai célokra használják, ezért ennél a megoldásnál nem lesz rögzítve pont.

- A szabad megoldásból származó koordináta-kovarianciákat felhasználják a végső, kombinált megoldáshoz.

- A feldolgozó központok által produkált eredményeket összehasonlítják. Az 1 cm feletti horizontális, és 2 cm feletti magassági koordináta-különbséget szolgáltató megoldásokat kihagyják a végső feldolgozásból.

- A rögzített megoldást referencia-célokra (IGS) készítik, ahol IGS (Nemzetközi GPS Geodinamikai Szolgálat) pontokat vonnak be a feldolgozásba. Ennek a stratégiája jelenleg nincs kidolgozva. Még szükséges az IGS-szel egyeztetni az általuk támasztott követelményeket.

- A szabad megoldáshoz ún. CODE, a rögzített megoldáshoz IGS precíz pályákat használnak.

A fenti követelményeknek megfelelően megtörténtek a mérések két epochára: 1994-ben és 1995-ben. Elkészült a magyar feldolgozóközpont megoldása 1994-re a végleges, illetve 1995-re az előzetes.

A 2. ábrán a két megoldás összehasonlításának eredménye látható a magassági komponensre. Látható, hogy általában az eltérés 2 cm alatti. Kivételt képez BASO, LJUB és BRSK. Itt a különbség jóval több mint 2 cm. A probléma oka jelenleg még nincs tisztázva.

Néhány ponton (az ábrán szürkével jelöltük) 1994-ben nem történt mérés vagy nem volt megfelelő az adatok minősége.
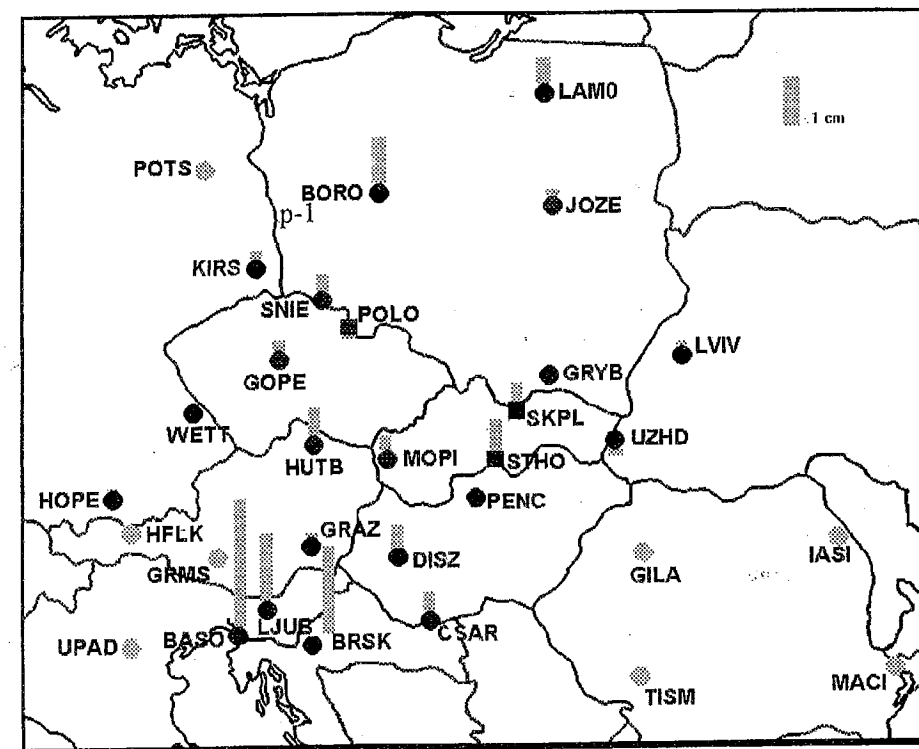
2. ábra Az 1994 és az 1995 évi CEGRN kampányok eredményeinek összehasonlítása

A CEGRN95 feldolgozása jelenleg is folyik. Geodinamikai eredmények csak a program befejezése után, az összes mérés eredményének értékelése után várható.

3. A MAGYAR GPS MOZGÁSVIZSGÁLATI PROGRAM

3.1 A program célja

A Magyar GPS Mozgásvizsgálati Program célja a Pannon-medencében zajló hosszú távú tektonikai mozgások detektálása valamint egy referencia hálózat létrehozása a lokális területek GPS technikán alapuló deformációvizsgálatához. A pontok (3. ábra) lehetőség szerint sziklán vannak elhelyezve és nemzetközi szabványoknak megfelelően állandósítva. Az állandósítási mód kidolgozását a penci Kozmikus Geodéziai

Obszervatóriumban végezték. A hálózat csatlakozik a globális IGS és a regionális CEGRN hálózathoz.

Az első három epocha mérésére 1991-ben, 1993-ban és 1995-ben került sor.
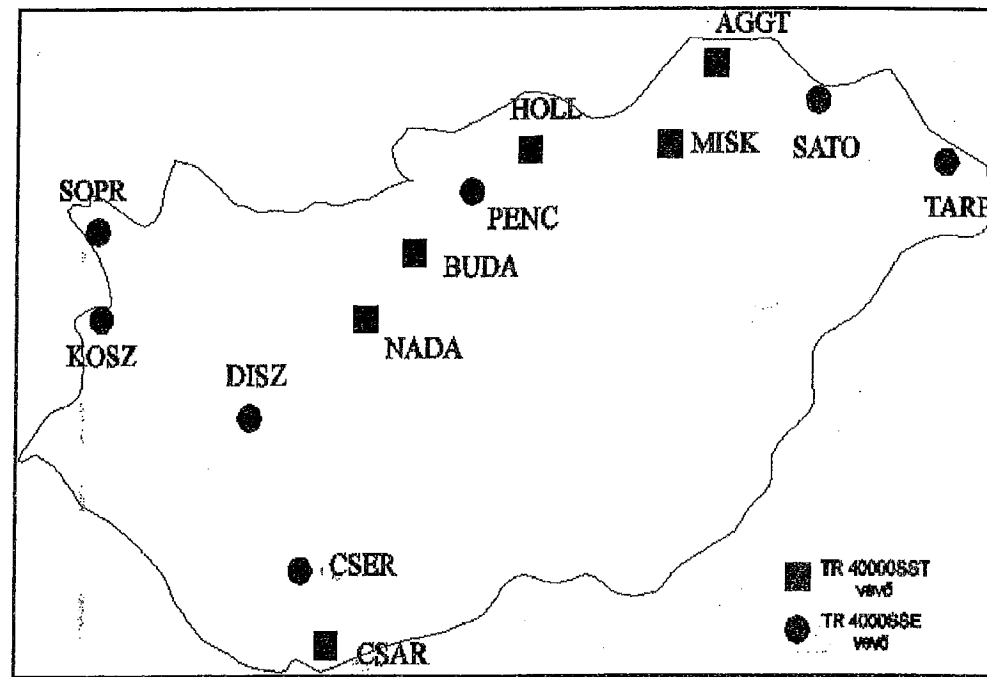
3. ábra A Magyar Geodinamikai Hálózat

3.2 Feldolgozás

A mérések feldolgozása a penci Kozmikus Geodéziai Obszervatóriumban történik Bernese V3.5 szoftverrel. A stratégia hasonló az előzőekhez. CODE precíz pálya felhasználásával egynapos pályaíveket számolunk. Ambiguity meghatározás "Sigma" stratégiával. A koordinátaszámítás L3 frekvencián történik, az összes mérési eredmény felhasználásával. Minden pontra troposzféra paramétereket határozunk meg kétórás intervallumokra.

Következő lépés lesz az eddigi három epocha eredményeinek együttes vizsgálata és természetesen a következő mérések feldolgozása.

ÖSSZEFOGLALÁS

A két mozgásvizsgálati program nagy jelentőségű a térség tektonikájának jobb megértése szempontjából. A geológiai mozgások évente kis mértékűek Közép-Európában illetve Magyarországon, ezért az esetleges mozgások kimutatása csak több éves mérési sorozat feldolgozásával lehetséges. Az eredmények értelmezéséhez pedig a földtudományok (geodézia, geológia, geofizika) szakembereinek együttműködése szükséges.

IRODALOM

[1] Gurtner W., Rothacher M., Friedhoff H., "BERNESE Version 3.5 Software Documentation" Astronomical Institute, University of Bern 1995.

[2] Simon Á, Kenyeres A. "Processing of the CEGRN'94 Campaign - the SGO solution", *Reports on Geodesy* No (3)16, 1995, pp. 323-329

[3] Gazsó M., Borza T., Fejes I., Busics I. "A GPS-Mozgásvizsgálati Program és földtani alapjai Magyarországon", *Geodézia és Kartográfia* 44. évf. 2. sz. 1992, pp. 73-85

[4] Fejes I. "The Central Europe Regional Geodinamic Project- CERGOP" *Reports on Geodesy* No (3)16, 1995, pp. 301-307

[5] Kenyeres A. "The Hungarian GPS Geodynamic Reference Network - HGRN: first results" *Proceedings of the 1st Turkish International Symposium on Deformation,* 1994. pp. 933-942

SESSION 7

Mechanics, materials

ÁTTÖRT FALAKKAL MEREVÍTETT ÉPÜLETEK MEREVSÉGI KÉRDÉSEI

Manninger Marcell
Budapesti Műszaki Egyetem, Magasépítési Tanszék
H-1521 Budapest

1. BEVEZETÉS

Az épületek merevítésének számítására többféle eljárás ismeretes. A megfelelő követelményeknek eleget tevő keret- illetve falszerkezetek diszkrét és kontinuum modelljének [3] tárgyalása is mindennapi rutinná vált a mérnökök körében. A végeselem programok adta lehetőségek mellet valójában nem ismerünk megoldhatatlan, vagy kiszámíthatatlan szerkezeteket.

Az előtervezés, a közelítő méretfelvétel során azonban még nem áll rendelkezésünkre a majdani, a fent említett eljárások valamelyikén végigfuttatandó szerkezet, hiszen épp ennek kitalálása a célunk. Kutatási programunkban felvállalt feladatként az előtervezéshez nélkülözhetetlen nyírásközéppont helyzetét vizsgáljuk. Az analitikus vizsgálat lehetőséget ad biztonságos általánosítások megtételére. Ennek szellemében alkalmazzuk a nyírásközéppont vizsgálatához az épületek áttört merevítő falainak szendvicsrúd modelljét [1]. Tesszük ezt más szempontból azért, mert e modell alkalmat nyújt a keretszerkezetek hajlítási és nyírási alakváltozásának együttes vizsgálatára. Ennek jelentőssége abban áll, hogy az áttört merevítő falak jelentenek alakváltozási szempontból átmenetet a - jellemzően hajlítási alakváltozást végző - tömör falak és a karcsú elemekből álló - jellemzően nyírási alakváltozást végző - keretek között.

Jelen tanulmányunkban a két különböző áttört falból álló rendszer nyírás- és csavarási középpontjának meghatározását mutatjuk be. Ehhez tehát egy-egy fal esetén a szendvicselmélet rúdmodelljét alkalmazzuk, amelynek alakváltozásai és terhei között a következő differenciálegyenlet-rendszer írható fel:

$$(B_0 B_1 / S) \, w_b^{VI}(x) - (B_0 + B_1) \, w_b^{IV}(x) = -q(x) \tag{1}$$
$$-(B_0 / S) \, w_b^{III}(x) = w_s^{I}(x) \tag{2}$$

ahol:
B_0 a merevítő fal oszlopainak globális hajlítási merevsége (Steiner-tag)
B_1 a merevítő fal oszlopainak lokális hajlítási merevsége
S a merevítő fal nyírási merevsége
$w_b(x)$ a merevítő fal hajlítási alakváltozásfüggvénye
$w_s(x)$ a merevítő fal nyírási alakváltozás függvénye
$q(x)$ a külső vízszintes teher
x változó a fal magassága mentén
(a teljes alakváltozás a nyírási és a hajlítási alakváltozás összegeként adódik: $w = w_b + w_s$)

2. A NYÍRÁSKÖZÉPPONT

A nyírásközéppont - definíciója szerint - az a pont, amelyben hattatva a külső terheket, a rendszer elcsavarodás nélkül eltolódik. Ez a merevítő falakra értelmezve azt jelentené, hogy az ebben a pontban ható külső terhek esetén a falak elhajlása azonos nagyságú lesz. A merevítő falaknál azonban (mivel nem csak hajlítási hanem nyírási alakváltozást is végeznek) nem egyetlen nyírásközéppont adódik, hanem a magasság mentén változó helyzetű nyírásközéppont, azaz nyírási középgörbe. Feltételezve, hogy a szélteherek megfelelő egyenletesen megoszló q nagyságú teher hat, a fenti differenciálegyenleteket alkalmazva a következő egyenletrendszer adódik:

az 1. számú falra:

$$(B_{01}B_{11} / S_1) w_{b1}{}^{VI}(x) - (B_{01} + B_{11}) w_{b1}{}^{IV}(x) = -q_1(x)$$
$$-(B_{01} / S_1) w_{b1}{}^{III}(x) = w_{s1}{}^{I}(x)$$

a 2. számú falra:

$$(B_{02}B_{12} / S_2) w_{b2}{}^{VI}(x) - (B_{01} + B_{11}) w_{b2}{}^{IV}(x) = -q_2(x)$$
$$-(B_{02} / S_2) w_{b2}{}^{III}(x) = w_{s2}{}^{I}(x)$$

és a fent írt két feltétel szerint:

$$q_1(x) + q_2(x) = q$$
$$w_{b1} + w_{s1} = w_{b2} + w_{s2}$$

Az egyenletrendszer átrendezésével a két fal hajlítási alakváltozásaira a következő differenciálegyenlet-rendszer kapható:

$$(B_{11} + B_{12} + B_{01}) w_{b1}{}^{IV} - (B_{01} / S_1)(B_{11} + B_{12})w_{b1}{}^{VI} + B_{02}w_{b2}{}^{IV} = q$$
$$(B_{11} + B_{12} + B_{02}) w_{b2}{}^{IV} - (B_{02} / S_2)(B_{11} + B_{12})w_{b2}{}^{VI} + B_{01}w_{b1}{}^{IV} = q$$

Mátrix alakban írva:

$$\underline{A}\, \underline{w}_b{}^{IV} - \underline{B}\, \underline{w}_b{}^{VI} = \underline{q} \tag{3}$$

amely alakilag megegyezik az (1) számú egyenlettel. Kettőnél több fal esetén sem esik szét az egyenletrendszer szerkezete, csak a mátrixok és a vektorok mérete növekszik.

A (3) számú mátrixegyenlet egy állandó együtthatójú, hatodrendű inhomogén differenciálegyenlet-rendszer, amelynek megoldása tulajdonképpen egy általánosított sajátértékprobléma megoldását jelenti. Ezt elvégezve a falak hajlítási alakváltozásaira a következők adódnak:

$$w_{b1} = C_{01} + C_{11} x + C_{21} x^2 + C_{31} x^3 + q x^4 / [24(B_{01} + B_{02} + B_{11} + B_{12})] +$$
$$+ C_{51} e^{\lambda 5x} + C_{61} e^{\lambda 6x} + C_{71} e^{\lambda 7x} + C_{81} e^{\lambda 8x}$$
$$w_{b2} = C_{02} + C_{12} x + C_{22} x^2 + C_{32} x^3 + q x^4 / [24(B_{01} + B_{02} + B_{11} + B_{12})] +$$
$$+ C_{51} w_{51} e^{\lambda 5x} + C_{61} w_{51} e^{\lambda 6x} + C_{71} w_{71} e^{\lambda 7x} + C_{81} w_{51} e^{\lambda 8x}$$

ahol:

C_{ij}	integrálási állandók (összesen 12)
$\lambda_5, \lambda_6, \lambda_7, \lambda_8$	a zérustól különböző sajátértékek
w_{51}, w_{71}	az egyes sajátvektorok komponenseinek aránya

A szendvicsrudakra végenként három-három peremfeltétel írható fel. Ez a két rúd négy végén összesen 12 peremfeltételt jelent. Minthogy a sajátértékek és a sajátvektorok komponensei arányának értékét a sajátérték-probléma megoldása szolgáltatja, az integrálási állandók a peremfeltételek segítségével egyértelműen meghatározhatók.

A hajlítási alakváltozásfüggvényekre kapott eredményeket az (1) számú egyenletbe helyettesítve megkaphatjuk a q egyenletesen megoszló teherből a két falra (azonos alakváltozásuk mellett) jutó terheket:

$$q_1(x) = (B_{01} + B_{11}) / (B_{01} + B_{02} + B_{11} + B_{12})q + K_{51}e^{\lambda 5x} + K_{61}e^{\lambda 6x} + K_{71}e^{\lambda 7x} + K_{81}e^{\lambda 8x}$$
$$q_2(x) = (B_{02} + B_{12}) / (B_{01} + B_{02} + B_{11} + B_{12})q + K_{52}e^{\lambda 5x} + K_{62}e^{\lambda 6x} + K_{72}e^{\lambda 7x} + K_{82}e^{\lambda 8x}$$

A két fal bármelyikére felírt nyomatéki egyensúlyból megkapható a **nyírásközépgörbe** egyenlete, pl.:

$$O_{ny}(x) = q_1(x)L / q$$

ahol:
L a két fal távolsága

3. A CSAVARÁSI KÖZÉPPONT

A csavarási középpont vizsgálatánál a két falra falanként egyenletesen megoszló, de ellentétes irányú terhet működtetünk (tiszta csavarás esete). Ekkor mindkét falra felírható egy-egy, az (1) és a (2) számú egyenletekből álló egyenletrendszer, amelyek megoldása után meghatározható a falak teljes alakváltozása (w_1, w_2) a nyírási és hajlítási alakváltozások összegeként. E két függvény lefutása tetszőleges két fal esetén nem arányos, sőt teljesen független egymástól. Ezért a csavarási középpont helye a falak magassága mentén változik. A **csavarási középgörbe** egyenlete geometriai megfontolások eredményeként megkapható; pl.:

$$O_{cs}(x) = L w_1 / (w_1 + w_2)$$

4. MUNKATÉTELEK

A külső idegen munkákra kimondott tételek vonatkozásában elmondható, hogy a változó helyzetű nyírás- és csavarási középpont ellenére továbbra is érvényben vannak. Eszerint, mivel a tiszta csavarás okozta alakváltozásokon a nyírási középgörbe mentén működő külső teherből a falakra eső terhek által végzett munka zérus, ugyancsak zérus lesz a nyírási középgörbe mentén működő külső teher okozta alakváltozásokon végzett munkája azon terheknek, amelyek a tiszta csavarásból adódnak a falakra. Továbbá, mivel a csavarási középgörbe mentén ható külső tehernek - s így az e teherből a falakra adódó terheknek - a tiszta csavarásból keletkező alakváltozások mentén végzett munkája zérus, zérus lesz a csavarási középgörbe mentén ható teher okozta alakváltozásokon a tiszta csavarásból a falakra adódó terhek munkája is.

5. KÖVETKEZTETÉSEK

Összegzésként megállapítható, hogy a nyírási alakváltozások figyelembevétele mellett nyírásközéppontról és csavarási középpontról nem beszélhetünk, mert helyzetük a falak magassága mentén változik. A két középgörbe csak speciális esetben esik egybe, mikor a falak megfelelő merevségeinek aránya megegyezik. A két görbe lefutását a teher megoszlása is befolyásolja, ahogyan közönséges tartókra ezt már Stüssi [2] is megmutatta.

IRODALOM:

[1]   Hegedűs I. és Kollár L. P., A szendvicselmélet eredményeinek néhány mérnöki alkalmazása. *A mérnöki stabilitáselmélet különleges problémái.* Szerk.: Kollár Lajos, Akadémiai Kiadó, Bp. 1991

[2]   Stüssi, F., Die Grenzlage des Schubmittelpunktes bei Kastenträgern. Abhandlung IVBH, Bd. XXV., 1965, 279-315

[3]   Szerémi L., Épületmerevítések számítása. Mérnöki Kézikönyv II. Szerk.: Palotás László, Műszaki Könyvkiadó, Bp. 1984

FIRE-RESISTANCE OF SANDSTONES

Mónika Hajpál
Technical University of Budapest, Department of Engineering Geology
H-1521 Budapest, Hungary

1. INTRODUCTION

Natural stones have been used as a construction material since prehistoric time. The knowledge of mechanical properties of natural stones is fundamental for conservation and exchange building stones of the monuments. In addition, it serves as a basis for the development of conserving materials and for structural calculations.

Sandstones are one of the most widespread building stones albeit our knowledge is rather limited in the sense of their mechanical behaviour in extreme conditions (e.g. in fire). The sandstones show great varieties in their particles (size and mineralogy), cement type and colour that all influence their weather- and heat resistance. The aim of this study is to examine the material properties and fire resistance of sandstones as building materials. The results can be directly implemented in the conservation work of monuments: stone exchange, static calculations of damaged structures, etc.

These studies form a part of a Ph. D. project. It was carried out both at the Mineralogical Institute of University Karlsruhe and at the Department of Engineering Geology, Technical University of Budapest.

2. APPLICABILITY OF FIRE-RESISTANCE SURVEYS

Many ancient buildings were demolished by fire. One of the best example is the Frauenkirche at Dresden, which was constructed from Elbaer sandstone. This 200-years-old building was collapsed due to the Second World War bombardments and following fire in 1945. The greatest damage is related to the heat effect of fire (1000-2000 °C). The sandstone blocks were flaking off, resulting the collapse of major load bearing structures. A current restoration and reconstruction project is in progress, aiming to rebuild the church that can be used as a religious site and concert hall. For this reconstruction project, the knowledge of the behaviour of sandstone structures in fire is essential. Furthermore, it is important to calculate with the effect of possible fires in future. Fire resistance standard does not exist for stone materials, thus examining the fire resistance of sandstones is very important. For our studies, sandstones were selected which have been used as building materials in monuments, ancient castles and churches.

3. ANALYTICAL METHODS OF SANDSTONES

3.1. Sandstone types

To understand the behaviour of sandstones in fire, sandstones with different cement types were selected. Up to the present, four German sandstones were studied:

- Cottaer Sandstone (pale grey, kaolinitic)
- Donzdorfer Sandstone (yellowish grey, ferrigenous clayey)
- Maulbronner Sandstone (reddish grey, clayey)
- Pliezhausener Sandstone (white, dolomitic)

In addition, three German and two Hungarian sandstones will be analysed in the future.

3.2. Test conditions

The selected sandstones were analysed in the following petrophysical states:

- air dry (22 °C)
- water saturated (22 °C)
- heated in an oven for 6 hours (300, 450, 600, 750, 900 °C)

Most of the fire damaged stone monuments are located in open-air. Therefore those are significantly effected by weathering. To model these conditions, it will be necessary to perform the following tests in the future:

- after 25 freezing cycle (22 °C)
- after heating water saturated state
- after heating 25 freezing cycle

3.3. Petrological analyses

The petrological analyses involve thin section description and X-ray diffractometry of different sandstones in different thermal states. Standard (30 µm) thin sections were analysed by polarising microscope and the most characteristic textures were documented on photographs. X-ray diffractometry gave a qualitative and quantitative mineralogical composition of sandstones. These tests inform us about the mineralogical and textural changes in relation to the heat. Tab. 1 shows the major mineralogical changes in examined sandstones. Dolomite, calcite and clay minerals disappeared above 600 °C, while quartz and feldspars were stable up to 900 °C. Results of petrological analyses in combination with petrophysical tests show the reason of changes in strength and durability of sandstones due heat-effect.

Temperature	Minerals [%]		
[°C]	Quartz	K - Feldspars	Kaolinite
Cottaer, 22	93	3	4
Cottaer, 300	93	3	4
Cottaer, 450	92	4	4
Cottaer, 600	97	3	-
Cottaer, 750	97	3	-
Cottaer, 900	96	4	-

Temperature	Minerals [%]					
[°C]	Quartz	K - Feldspars	Plagioclases	Hematite	Illite	Calcite
Maulbronner, 22	15	35	37	5	8	<1
Maulbronner, 300	13	35	40	4	8	<1
Maulbronner, 450	29	27	32	4	9	-
Maulbronner, 600	20	33	40	4	3	-
Maulbronner, 750	32	30	34	4	-	-
Maulbronner, 900	20	38	37	5	-	-

Temperature	Minerals [%]			
[°C]	Quartz	Plagioclases	Dolomite	Kaolinite
Pliezhausener, 22	80	4	2	14
Pliezhausener, 300	86	2	2	11
Pliezhausener, 450	88	2	2	9
Pliezhausener, 600	98	2	1	~0
Pliezhausener, 750	97	3	-	-
Pliezhausener, 900	98	2	-	-

Temperature	Minerals [%]		
[°C]	Quartz	K -Feldspars	Calcite
Donzdorfer, 22	97	3	<1
Donzdorfer, 300	98	~1	<1
Donzdorfer, 450	97	3	<1
Donzdorfer, 600	96	4	<1
Donzdorfer, 750	93	7	-
Donzdorfer, 900	97	3	-

Tab. 1 Mineralogical composition of different sandstone types (22-900 °C)

3.4. Petrophysical tests

3.4.1. Mass properties

The volume and mass of each sample were measured before and after the heating tests giving different densities. In addition, water adsorption tests were carried out. The specific densities were determined by pyknometer. Porosity (p) was calculated from specific (ρ_s) and bulk (ρ_o) density:

$$p = (1 - \rho_o/\rho_s) \cdot 100 \quad [\text{Vol.}\%]$$

With increasing heat, the volume of sandstone samples are increased while their weight are decreased. The specific density apparently remained the same while the bulk density decreased by elevation of temperature.

3.4.2. Indirect tensile strength test

Cylindrical 1:1 samples of 3,5 cm in diameter (d) were used for the tests (Fig. 1). The samples were drilled perpendicular to the bedding. During the loading, the load (F) and the maximal deformation were recorded. Surprisingly, tensile strength showed an increase at each sandstone type up to 450 °C which was followed by a gradual decrease (Fig. 2).
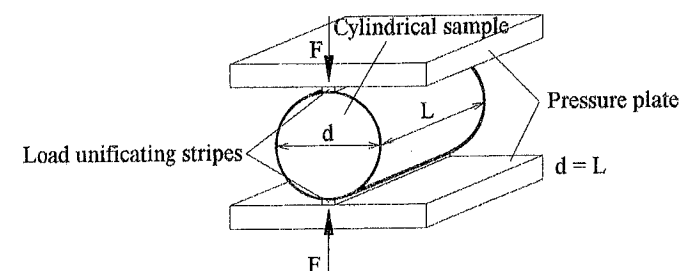

Fig. 1 Test configuration of indirect tensile strength measurements
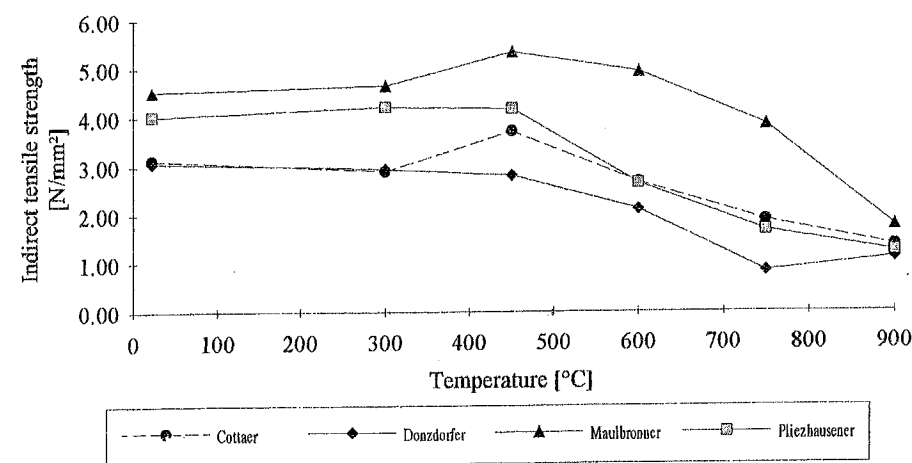

Fig. 2 Indirect tensile strength as a function of temperature, 4 different sandstone types

3.3.3. Uniaxial compressive strength test

Cylindrical 2:1 samples of 3,5 cm in diameter (d) were drilled perpendicular to bedding for compressive strength tests. Besides the load (F), the longitudinal (ε_y) and transverse deformation (ε_x) with 2-2 strain gauge were recorded (Fig. 3). Stress-strain diagrams ($\sigma - \varepsilon_x$ and $\sigma - \varepsilon_y$) were drawn as well as Young's modulus and Poisson modulus were calculated.
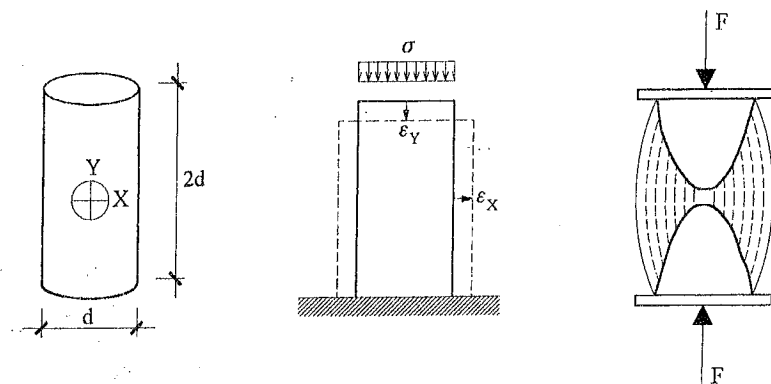

Fig. 3 Longitudinal and transverse deformations and the compressive strength test

Contrary to the tensile strength, no significant general changes were observed as a function of temperature (Fig. 4).
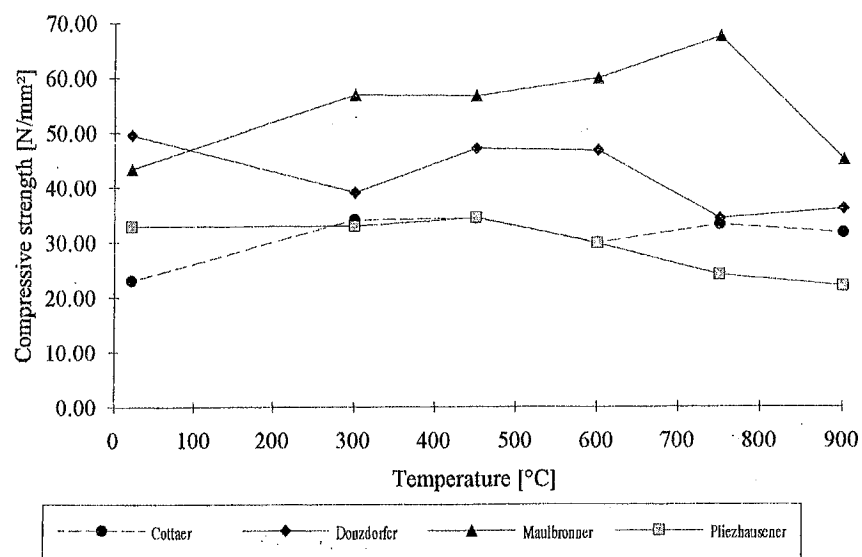

Fig. 4 Compressive strength as a function of temperature, 4 different sandstone types

3.4. Thermal analyses

According to the Hungarian and German Standards, the natural stones are ranged as "non combustible" materials. However it does not mean that their inner structure would not change by increase of temperature. Three major parameters can be used for the description of these changes:

- specific heat
- bulk density
- thermal conductivity and thermal expansion

The thermal conductivity and thermal expansion of natural stones are anisotropic, therefore measurements were carried out both parallel and perpendicular to bedding.

3.4.1. Specific heat

For the measurement of specific heat a calorimeter is used. A rock sample is placed into the calorimeter and the temperature of the calorimeter is measured as a function of time.

3.4.2. Thermal conductivity

The upper side of the isolated rock sample is heated which creates a thermal gradient between the upper and lower side of the sample (Fig. 5).

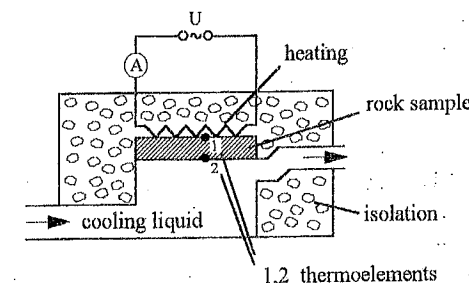*Fig. 5 Test apparatus for measuring the thermal conductivity of rocks*

3.4.3. Linear thermal expansion

The sample is placed into an isolated oven. The expansion is forwarded to the detector by quartz rods (Fig. 6).
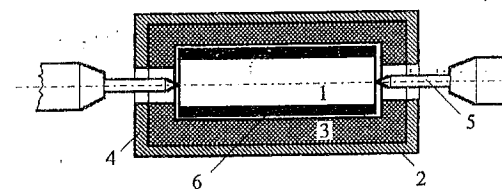

Fig. 6 Test apparatus for measuring linear thermal expansion (1-rock sample, 2-thermoelements, 3-isolating layer, 4-cover, 5-quartz rods, 6-heating)

3.5. Finite element modelling

Up to the present, the fire resistance was only on small samples analysed, but it is necessary to evaluate the load bearing capacity of larger stone structures such as walls, pillars, etc. Therefore the effect of fire on larger walls is planned to be studied. To obtain better results, a sandstone wall will be examined with the aid of a FEM software. The temperature-strain relation, thermal conductivity and thermal expansion factor of examined sandstones will be input data in addition to usual parameters. As output, the carrying capacity of the wall can be calculated to any given heat effect.

3.6. Model wall test

A small section of a sandstone wall is planned to be constructed and later tested in fire. The results of this small scale test will be compared with the computer modelling (FEM).

4. SUMMARY

Sandstones are considered as "non combustible" materials, although their internal structure and load bearing capacity can be endangered by fire (e.g. Frauenkirche at Dresden). As a consequence, the study of fire resistance of sandstones is necessary. Some minerals of the sandstones disintegrate in fire and their inner structure collapses at a given temperature, resulting the decrease of strength parameters of the building stone. Surprisingly, the strength of sandstone shows an initial increase with the increase of heat that is followed by a major decrease. The sandstones have different cement materials that reflects in their different behaviour by heat. Further studies in this field will help in the planning of reconstruction of sandstone monuments.

5. REFERENCES

[1] ALFES, Ch.; SCHIESSL, P., "Spannungsdehnungsverhalten, Schwinden und Kriechen von Sandsteinen", *Jahresberichte Steinzerfall-Steinkorservierung*, Verlag Ernst & Sohn, Berlin 1994.

[2] EGERER F.; KERTÉSZ P., "Bevezetés a kőzetfizikába", *Akadémiai Kiadó*, Budapest 1993.

[3] SCHUBERT, P.; FRIEDE, H., "Spaltzugfestigkeitswerte von Mauersteine", *Bautechnik* 4/1980.

[4] STIGLAT, K., "Zur Tragfähigkeit von Mauerwerk aus Sandstein", *Bautechnik* 2/1984.

[5] STROHMAYER, A.K., "Erhaltungszustand und Sicherung einer mittelalterlichen Ringmauer", *Diplomarbeit am Institut für Tragkonstruktionen Universität Karlsruhe*, 1994/95.

[6] GRIMM, W.D., "Bildatlas Wichtiger Denkmalgesteine Der Bundesrepublik Deutschland, Arbeitsheft 50", Bayerisches Landesamt für Denkmalpflege

---

SUGÁRVÉDŐ BETON MINŐSÉGELLENŐRZÉSE ÉS HŐMÉRSÉKLET ELLENŐRZÉSE

Salem Georges Nehme
Budapesti Műszaki Egyetem Építőanyagok Tanszéke
1111 Budapest Műegyetem rkp. 3.

1. BEVEZETÉS

A sugárvédő beton az ionizáló sugárzások ellen nyújt biológiai védelmet, mely megfelelően megválasztott összetételének következtében elnyeli a röntgen-, gamma és neutronsugarakat.

Vastag, speciális összetételű betonból, különleges körültekintéssel készítve, kiváló szerkezeteket építhetünk.

Alkalmazási területei a különféle kutató laboratóriumok, egészségügyi intézmények falai, stb. Megtalálhatók katonai létesítmények sugárzó anyagainak raktárainál, katakombák készülhetnek sugárzásvédő betonból. Az atomerőmű szerkezetei sugárzásvédő betonból készülnek , de nukleáris anyagok tárolására, sőt végleges elhelyezésre is ma szinte az egyetlen megoldás a nehézbeton, a hidrátbeton, és a közönséges beton szigorú feltételek mellett készített (nagy testsűrűségű) szarkofág.

Mivel a testsűrűség a sugárvédő beton legfontosabb tulajdonsága, az anyag minőségellenőrzésére fokozott figyelmet kell fordítani. Minőségellenőrzésen azokat az anyagvizsgálatokat értjük, melyek magukba foglalják a beton készítéséhez felhasznált valamennyi alkotóanyag, a frissbeton és a megszilárdult beton tulajdonságainak vizsgálatát.

A sugárvédő beton minőségének ellenőrzésekor vizsgáljuk a kötőanyag, az adalékanyag, valamint az adalékszerek kémiai és fizikai tulajdonságait, a frissbeton, valamint a szilárd beton fizikai és mechanikai tulajdonságait is. Bizonyos esetekben a vizsgálatok eredményei alapján módosítani kell a betonkeverék összetételét.

Az alkotó anyagok mellett nagyon fontos szerepe van a bedolgozás körülményeinek, és a beton szilárdulása közben kialakult hőmérsékleti viszonyoknak. Ez különösen fontos tömegbetonok esetén, mivel a nem statikai repedések döntő többsége még a beton szilárdulása közben képződik, és ennek leggyakoribb oka a hőmérséklet különbségek okozta felületi és átmenő repedések.

Előadásom célja e problémák leírása, tapasztalataim ismertetése. Részletesen szólok a minőségellenőrzés lépéseiről, a követelményrendszerről. Mindezeket konkrét példákon keresztül írom le, valódi kísérleteink eredményeiből.

2. MINŐSÉGELLENŐRZÉS

2.1 Laboratóriumi vizsgálatok

Adalékanyagra vonatkozó vizsgálatok

- szemmegoszlás vizsgálata
- tisztaság vizsgálata szemrevételezéssel
- testsűrűség vizsgálata
- alkáli érzékenység vizsgálata

Cementre vonatkozó vizsgálata

-kémiai összetételének és ásványi összetételének meghatározása
-kötési idő megállapítása
-kötési víz mennyiségének meghatározása
-csomósodás vizsgálata
-sűrűség vizsgálata
-fajlagos felület meghatározása
-térfogatállandóság meghatározása

Adalékszerre vonatkozó vizsgálatok

-sűrűségének meghatározása
-szín megállapítása

2.2 Helyszíni vizsgálatok

-szemrevételezés
-hőmérséklet mérése
-terülés mérése
-a folyósítószer mennyiségének meghatározása
-testsűrűség meghatározás
-frissbeton víztartalmának meghatározása
-beton összetételének ellenőrzése
-légtartalom meghatározása

2.3 A megszilárdult beton ellenőrzése

-próbakockák készítése a helyszínen
-a megszilárdult beton tulajdonságainak értékelése

3. A HŐMÉRSÉKLETVÁLTOZÁS ELLENŐRZÉSE

Tapasztalatból tudjuk, hogy a nagytömegű betonban a betonozást követő napokban fennáll az átmenő és a kéregrepedések veszélye. A terhelés okozta feszültségek és a sajátfeszültségek kialakulása egyrészt akkor következik be, ha a beton szilárdulása során egyenlőtlen hőmérséklet-eloszlás jön létre, másrészt egyenlőtlen zsugorodás alakulhat ki a, emiatt az ezekből adódó alakváltozások nem játszódhatnak le szabadon. Ez a gátolt alakváltozás esete, melyből feszültségek keletkeznek.

A repedések két csoportba oszthatók, beszélhetünk **kéreg** és **átmenő** repedésekről. A repedéseket a betonban kialakuló húzófeszültségek okozzák, ha azok túllépik a beton húzószilárdságát.
A kéregrepedések keletkezését befolyásoló tényezők az alábbiak

Környezeti

- a zsaluzat minősége
- a kizsaluzás időpontja
- a szél intenzitása
- a léghőmérséklet és a levegő nedvesség tartalma

- a napsugárzás intenzitása
- a párolgás mértéke

Betonösszetételi

-a beton hőmérséklete a betonozás időpontjában
-a beton hővezetési tényezője
-a betonfelület hőátadási tényezője
-a cementfajta (kötéshője) és a cementtartalom
-a vízcement tényező
-a késleltető adalékszerek adagolása
-a betonozás szakaszossága
-a beton kúszási tényezője
-a beton ill. vasbeton tömb (fal, lemez) méretei
-az utókezelés (a védelem, takarás jellege és időtartama)

Az átmenő repedések képződésének oka

-az alaptest hőmérséklete és a felmenőfal hőmérséklete közötti különbség, mely fenti tényezők szintén befolyásolnak.

A hőmérők elhelyezése a falban
1. ábra

A fal vastagsága, 1m

A hőmérséklet alakulása a falban

2. ábra

A betonozás kezdetétől eltelt idő, óra

A hőmérséklet időbeni alakulása a 3.helyen (falban)

(jelöléseket lásd az 1.ábra)

3. ábra

4.ÖSSZEFOGLALÁS

Az előadásban bemutatom a tömegbeton készítésének problémás kérdéseit, összefoglalom a legsúlyosabb hibákat okozó jelenségeket. A téma különösen fontos, amikor egyre nagyobb mértékben terjed a különféle sugárzó anyagok alkalmazása a tudomány és az ipar számos területén.

5. HIVATKOZÁSOK

1. CEB comité Euro-International du Béton. *Bulletin d'Information No 183.* Durable Concrete Structure. Lausanne. 1992. May.
2. Balázs Gy.: Építőanyagok és kémia *Tankönyvkiadó Budapest, 1983*
3. A paksi atomerőmű betonfalai hőtechnikai vizsgálata a betonozást követő időszakban (*Tudományos közlemények*, BME Építőanyagok Tanszék)
4. EUROCODE-2 beton és vasbetonszerkezetek tervezése, Kézirat Budapest (BME Vasbetonszerkezetek Tanszéke)
5. Balázs Gy.: Építőanyag praktikum, *Műszaki Könyvkiadó Budapest, 1983*
6. Balázs Gy.: Beton és vasbeton I. alapismeretek története, *Akadémiai kiadó, Budapest*
7. A beton húzószilárdsága (laboratóriumi kisérletek) tudományos közlemények Építőanyagok Tanszék II..
8. A Paksi Atomerőmű Átmeneti Hulladéktárolója Építése, Bp, 1995. november
9. A Magyar Építőanyagipari Szövetség, Műszaki Feltételei

RENDSZERELVŰ ÉPÍTÉS NEMNUMERIKUS PROBLÉMÁINAK GÉPESÍTÉSE

Salah BIRI
BME Épitőmérnöki Kar Informatikai Laboratórium
Budapest, Műegyetem rkp. 3.

1. BEVEZETÉS

A hagyományos szerkezet-tervezés abból indul ki, hogy szubjektiv döntéssel elhatározza, hogy milyen statikai vázlatot fog alkalmazni. A statikai vázlat és rá ható erőrendszerek ismeretében a belső erők, a mozgások, a feszültségek meghatározhatók. Ezeket a módszereket, amelyek lényegében numerikus algoritmusok, a tartószerekezetekkel foglalkozó különböző tantárgyak keretében lehet elsajátitani.

Vajon tudunk-e valamit gépesíteni az előbb említett numerikus modellek felállítása előtt, az eddig csak szubjektiv döntéssel meghatározott konfiguráció-felvétele során?
A rendszerelvű építést üzemben előregyártott szerkezeti elemekből valósítják meg. Egy építési rendszernek az építőelemeit a rendszerkatalogusok tartalmazzák. Azt, hogy ezekből a rendszer komponensekből hogyan lesz egy épület, a kérdéses építési rendszer összeépítési stratégiáját tartalmazó leírásokban szokták közétenni.

Vajon tudunk-e egy egyértelmű szabályt alkotni egy ilyen szövegesen leírt összeépítési stratégiához?

A válaszunk erre a kérdésre az, hogy igen, hisz az algoritmus fogalma nem kötődik kizárólag numerikus problémákhoz. Jelen dolgozatban szeretném megmutatni, hogy a matematikai nyelvészet és az ehhez kapcsolódó applikativ programozási nyelvek lehetőséget adnak a konfigurácó-generálás nemnumerikus algoritmusainak leírására és gépi kezelésére.

Az említett lehtőségeket kihasználva a tervkészítés gépesíthető szakaszát kiterjeszthetjük az eddig is alkalmazott numerikus problémamegoldások előtti szakaszra.

2. ELŐZMÉNYEK

2.1. A CLASP építési rendszer

A CLASP építési rendszer
- teherhordó váz alrendszerből,
- közbenső födém alrendszerből,
- tetőfödém alrendszerből,
- külső fal alrendszerből,
- válaszfal alrendszerből,
- lépcső alrendszerből,
- alapozás alrendszerből,
- álmennyezet alrendszerből,
- és még sok más többek között épületgépészeti alrendszerből áll, amelyek rendszer komponensei a CLASP építési rendszer katalógusaiban egyértelműen rögzítve vannak.[1]

Épületkonfiguráló mintapéldánkat természetesen első lépésben nem terjesztettük ki az összes alrendszerre. Mintapéldánk a teherhordó váz és a közbenső födém alrenszerekre terjed ki.
A CLASP építési rendszer egy nyilt rendszerű teherhordó vázon alapszik. A mintapéldában a teherhordó váz alrendszerének cellás, acél szerkezetű oszlopaival, kölönféle tartó gerendaival és kiegészítő szerkezeti elemeivel foglalkoztunk. Ezeknek az elemeknek a száma megközelíti a 200-at, nem beszélve a pillérek öltöztetéséről, amin azt értjük, hogy különböző csomólemezekkel ellátva szélrácsok fogadásara is alkalmassá tehetők, méghozza adott esetben négy irányból.
Minthogy ez önmagában nem mutatná be a nemnumerikus algoritmuskészítés lehetőségeit, ezért a közbenső födém alrendszer elemeit is bevontuk a mintapéldánkba.

A közbenső födém elemei alulbordás vasbeton elemek, amelyek attól függően, hogy szélső mezőben, sarkon, vagy közbenső mezőben foglalnak helyet mások és mások. Az elemek száma mint egy 20 db.

A teherhordó váz kialakítása a tér mind három irányában 90 cm-es szerkezeti modulhálóra építhető fel. Ahhoz, hogy fogalmat alkothassunk, a teher hordó váz elemeiről példaként bemutatunk egy tetőgerenda-elemet (1. ábra).

RB108 | RB99 | RB90 | RB81| RB72 |
RB63 | RB54 | RB45 | RB36 | RB27 |RB18
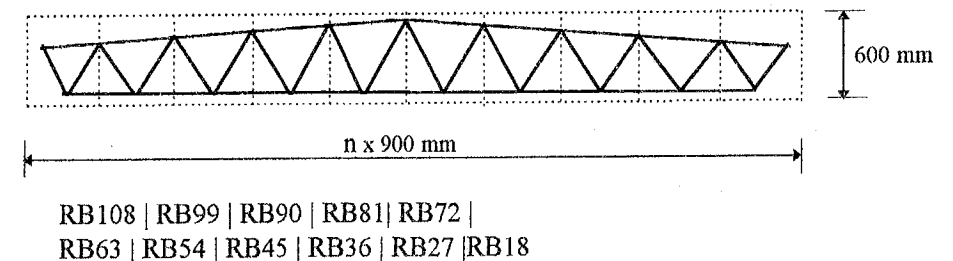
1. ábra Tetőgerenda elem

Látható, hogy a tetőgerenda-elemek minden esetben egy 600 mm-es szerkezeti sávban helyezkednek el és hosszúságuk 900 mm többszörösének megfelelő hálózatra illeszkednek.
Az ábrán fel vannak tüntetve azok a jelek is, amelyeket a CLASP építési rendszer az egyes tetőgerenda-elemek megjelőlésére használ. Látható, hogy egy sémához milyen változat tartóznak. Ugyan részletkérdés, de megemlítjük, hogy az ábrán látható RB az ilyen tipusú tetőgerendának a jele, a mögötte levő szám pedig deciméterben a gerenda fesztávát jelenti. A CLASP építési rendszer elem katalógusa ilyenformán tartalmazza a teherhordó vázszerkezet összes elemét.

Mint már eddig is említettük, hogy egy építési rendszer nem lehet teljes ha annak csak az elemeit alkottuk meg. Szükségünk van egy olyan leírásra, amely ezen építőelemek használatát összeépítési stratégiáját tartalmazza. Azt is említettük, hogy éppen ennek a leírásnak az egzakt formalizálása képezi vizsgálatunk tárgyát.

2.2. Mit értünk a nyelvtanon

Egy G generatív grammatikán, vagyis egy nyelvtanon, egy rendezett halmaz négyest értünk.

$$G = <T, N, S P >$$

Ebben a G grammatikában a T az úgynevezett terminális szimbólumok halmazát jelenti, amely egy nem üres halmaz, az alkalmazott jelek halmaza, más néven ábécé.[2]

Hogy is kell ezt elképzelnünk a rendszerelvű építés keretén belül? Míg a valódi ábécéből szavakat tudunk kialakítani, addig a teherhordó váz alrendszer jeleiből vázszerkezetet tudunk komponálni. Ez olyan mint egy mondat. Valóban az itt szereplő S, a mondatszimbólum, ami itt az egész épületet jelenti. Hogy az egész épület jelentő jel milyen helyettesítési sorozat után fog konkrét jelekből álló sorozattá alakulni, ezt a grammatika produkcióhalmaza írja le. P a produkcióhalmaz olyan szabályokat tartalmaz, amelyek segítségével az eddig még nem tárgyalt N halmaz elemeit, végső soron terminális szimbólumok sorozatával tudjuk helyesíteni. Az N halmaz elemei az úgy nevezett nem terminális szimbólumok. Az élő nyelv használatával élve ezek a gyűjtő fogalmak. Az élő nyelv példáján a terminális szimbólum-jel egy meghatározott "almának" a jele, amit meg tudunk enni. Ehhez a bizonyos "almához" tartozik eggyel magasabb szinten az "almák" gyűjtő fogalma, ami egy nemterminális fogalom. Efölött találjuk a "gyümölcs" fogalmat, mint nem terminális fogalmat, és így folytathatnánk tovább.

Építési rendszerekben a nemterminális fogalmak példájaként megemlítjük az oszlopokból és szélrácsokból kialakított "rácssíkot", vagy a födém alrendszer gerendáiból kialakított "födémet". Az itt említett " rácssík"-okból és " födém"-ekből, mint gyűjtő fogalmakból, egy magasabb hierarchia szinten kialakíthatjuk az " épület "-fogalmat, mint nem terminális fogalmat. A produkcióhalmaz egzat módon jelöli, hogy az " épület "-fogalom helyettesíthető " rácssíkok " és "födémek " fogalmával. A produkcióhalmaznak egy másik eleme lehetne, hogy a " rácssík" helyettesíthető " oszlopok " és " szélrács-rudak " fogalmával. Ugyanígy a produkcióhalmaznak eleme kell, hogy legyen az, hogy a "pillér " fogalma helyettesíthető pl. P1103-mal, ami egy konkrét pillér, amelyet az épületbe be lehet építeni. Olyan mint az a konkrét alma amelyet meg lehet enni. Látható, hogy egy épületkonfiguráció az építési rendszer terminális szimbólumaival, azaz a katalógusban szereplő jelek halmazával, a mérnöki gyakorlatban használatos gyűjtő fogalmakkal, vagy más néven nemterminális fogalmakkal tovább az összeépítési stratégiát tükröző összeépítési szabályhalmazzal leírható. Az összeépítési szabályhalmaz fogja képezni a konfiguráció-generálás implikáció jellegű kijelentéseit. Ugyanezek az implikatív kijelentések azok, amelyek a PROLOG-nak mint applikatív nyelvnek a klózait fogják alkotni.

3. A SZERKEZET KONFIGURÁCIÓT GENERALÓ NYELVTAN

A CLASP építési rendszer teherhordó váz alrendszer bemutatását célszerű a produkcióhalmaz bemutatásával kezdeni.

S = { clasp_h1_építési_rendszer_teherhordó_váz_alrendszer }
P = { clasp_h1_építési_rendszer_teherhordó_váz_alrendszer →
       cellás_szerkezetű_acélváz_alrendszerváltozat |
       csarnok_szerkezetű_acélváz_alrendszerváltozat;
cellás_szerkezetű_acélváz_alrendszerváltozat →
       tetőfödém_tartóelem | közbenső_födém_tartóelem |
       pillér | merevítőrács | faltartó | kapcsolóelem |
       tetőfödém_kiváltó | kötőelem | korláttartó;
tető_födém_tartóelem →
       tetőszegélytartó | tetőgerenda |
       tetőlezárógerenda | tetőkiváltó | tetőmerevítő |
       tetőszegélytartó_dilatációnál;
tetőszegélytartó →
       RP36 | RA36 | RA27 | RA18 }

2. ábra CLASP építési rendszer produkcióhalmaza

A clasp h1 teherhordó váz alrendszere lehet cellás szerkezetű acél váz alrendszerváltozat vagy csarnok szerkezetű acél váz alrendszerváltozat. Az útóbbival most nem foglalkozunk. A cellás szerkezetű acél váz alrendszer lehet tetőfödém tartóelem, közbenső födém tartóelem, pillér, vagy merevítőrács stb. A tetőfödém tartóelem mint gyűjtő fogalom, lehet tetőszegélytartó, tetőgerenda, vagy mindazok, amelyek a 2. ábrán fel vannak sorolva. A fogalomdefiníció értelmében az utolsó sorban látjuk, hogy tetőszegélytartó vagy RP36, vagy RA36, vagy RA27, vagy RA18 jelű raktárról szállítható konkrét gerenda lehet. A RP36, RA36, stb. jelek a terminális szimbólumok. Az ilyen jelek itt definált hierarchiájából építhető fel tehát az a legmagasabb nemterminális fogalom, amit mondatszimbólumnak is nevezünk, s ami nem más, mint " clasp h1 építési rendszer teher hordó váz alrendszere".

4. ÖSSZEFOGLALÁS

Az eddigiekben láttuk, hogy milyen a CLASP építési rendszer mérnöki szempontból. Láttuk azt, hogy milyen lehetőségeket nyújt nekünk a matematikai nyelvészet a nemnumerikus problémák formálizalásához, és bemutattuk, hogy a kérdéses építési rendszert hogy lehet a matematikai nyelvészet eszközeivel definiálni. Befejezésül szeretnénk megemlíteni, hogy az elsőrendű logikán alapuló PROLOG nyelvnek van olyan implementációja, amely a produkcióhalmaz jelölésrendszerét inputként eltudja fogadni.

A PROLOG applikatív programozási nyelv, amely most nem részletezhető módon tétel bizonyításra is alkalmas a produkcióhalmaz kódolása révén eldöntheti:
- hogy egy szerkezetleírás korrekt mondata-e az építési rendszernek, magyarán szólva ezekből az elemekből a szerkezet megépíthető, vagy pedig

- generálni lehet segítségével az összes lehetséges épületkonfigurációt.

Mivel a szakértői rendszerek, ha úgy tetszik keretrendszerek, PROLOG vagy ehhez hasonló applikativ nyelvet használnak a felhasználó elől elrejtve, mind az, amit a PROLOGgal kapcsolatban elmondhatunk, megismételhetnénk a szakértői rendszerek nómenklatúrája, elnevezés rendszere segítségével is. Ezzel tulajdonképpen befejezésül szerettük volna bemutatni, hogy építési rendszerek keretein belül a konfiguráció-generálás nemnumerikus problémái megoldhatók.

Reméljük, hogy a közel jövő számító autómatai a sebesség, a tárolókapacítás tekintetében olyanok lesznek, hogy az itt vázolt teljes leszámlalással dolgozó logikai nyelvek konkrét használatba is kerülhetnek, és a teljes leszámlálás miatti kombinatorikus robbanás ellenére reális feladatok megoldására is alkalmas lesz. Ennek reményében foglalkozunk a matematikai nyelvészet építési rendszerekre történő alkalmazásával.

5. IRODALOM

[1] CLASP-H építési rendszer, váz és közbenső födém alrendszer katalógusa.
[2] Holnapy D. : A matematikai nyelvészet és alkalmazása a tervezési folyamatban. *BME Építőmérnöki Kar Informatikai Laboratórium kiadványa*, Budapest 1994.

SESSION 8

Hydraulic engineering

MŰSZAKI SZABÁLYOZÁS A MEZŐGAZDASÁGI TERÜLETRENDEZÉSBEN

Gunyhó Edit
Budapesti Műszaki Egyetem, Vízgazdálkodási tanszék
H-1111 Budapest, Műegyetem rkp. 3.

1. BEVEZETÉS

Magyarország azon törekvése, hogy az Európai Unió tagja legyen reális, bár meglehetősen sok követelménynek kell megfelelnie a csatlakozás elött. A EU egyik legvitatottabb leginkább dotált ágazata a mezőgazdaság, így érthető, hogy a belépő országokat e témakörben alapos vizsgálat alá vetik. Egyik fő kritérium a szabványok harmonizálása a mezőgazdaságban. Ez nemcsak a termelési, feldolgozási, raktározási, áruminőségi szabványokra értendő, hanem a mezőgazdaság legfőbb termelő eszközének a termőterületre és a termőtalajra is vonatkozik.

A mezőgazdasági területek rendezését többféle módon is lehet szabályozni. Ennek három legismertebb módja a következő:

-jogi
-közgazdasági
-műszaki

Munkám során igyekeztem összehasonlítani a külföldi, elsősorban a német és az osztrák műszaki szabályozási módokat a meglévő magyar szabályozási módszerekkel.

2. CÉLKITŰZÉSEK

A téma célkitűzései három fő cspoprtba oszthatók:

-a területrendezés szabályozásának felülvizsgálata
-összehasonlítás az egyéb európai szabványokkal
-javaslat a változtatásokra

3. A TERÜLETRENDEZÉS FOGALMA

Mezőgazdasági területrendezésen a mezőgazdasági művelés alatt álló földterület, rét, szántó, legelő tereprendezési, talajvédelmi, tájvédelmi tevékenységeit értjük. A birtokrendezés a területrendezésnek egy jogi keretek között végrehajtott szabályozása, mely a tulajdonosi viszonyokra, és az ezekkel járó jogokra és kötelességekre vonatkozik. Ezt a két fogalmat egyébként a külföldi szakirodalom is szétválasztja.

4. MEZŐGAZDASÁGI TERÜLETEK RENDEZÉSE

4.1 Birtokrendezés

Jelenleg hazánkban a birtokrendezés szabályozása sem műszakilag, sem jogilag nem megoldott. Műszaki vonatkoztatások például a kialakítandó táblaméretekre léteznek,

mint irányadó tervezési alapadatok, de sajnos ezek a mezőgazdaságban végbement rendszerváltozás miatt nem megfelelőek. Azonban általánosítani sem lehet, hogy minden, a nagyüzemi mezőgazdasági termelésre vonatkozó feltevés elavult. Ilyen pl. a fásítás kérdése, mely nagytáblás gazdálkodás esetén korszerűnek mondható, s nem feltétlenül szükséges a teljes átalakítása csupán némi kiegészítést igényel a kisüzemi gazdálkodásra vonatkozóan.

4.2 Talajvédelem

Itt általában az agrotechnikai, erdészeti, és a műszaki talajvédelmi feladatok együttes alkalmazását értjük. Kapcsolata a témának a vízgazdálkodáshoz talán itt a legközelebbi. E támakör legérdekesebb részei a már fent említett fásítás és az erózióvédelem. Ez utóbbi esetén meglehetősen sok a rendelkezésre álló külföldi dokumentum, így viszonylag könnyű az összehasonlítás. Megállapítható, hogy a javasolt műszaki megoldások meglehetősen hasonlítanak, néhány országban az alkalmazott meghatározási módszerek (mennyiséget meghatározó képletek) eltérnek egymástól.

Ugyancsak ehhez a témakörhöz kapcsolódnak a talajtani minőségi és a vizsgálatokat leíró szabványok, előírások is. Itt az összehasonlítás szintén egyszerű, mivel általában konkrét jellemzők leírásáról van szó. A vizsgálatok egy része teljesen egyező, de pl a talajok savasságát különböző módon határozzák meg nálunk és Németországban. Ez félreértésekre adhat okot a későbbiekben. Az átállás, új műszerek beszerzése elég drága, de elképzelhető egy átszámítási mód kidolgozása a két rendszer közt.

4.3 Tájvédelem

Sajnos a hazai tájvédelmi szabályozási módszerek eléggé elavultak, így összehasonlításuk nem igazán ajánlott. Javasolt viszont a teljes, ide vonatkozó szabvány alapos felülvizsgálata. Pozitív lépések azonban már törvényi szinten is tapasztalhatók: pl. a természetvédelmi és a területfejlesztési törvényeket illetően, melyek deklarálják a táj és annak természetes és mesterséges tájalkotó elemeinek a védelmét, védelmi, fejlesztési tervek készítését.

5. MEGÁLLAPÍTÁSOK

A magyar műszaki szabályozási rendszer, a szabványok, műszaki irányelvek, műszaki előírások a mezőgazdasági területek rendezésére vonatkozóan tartalmilag korszerűnek mondhatók. Gondot csak az jelent, hogy ez a korszerű tartalom a nagyüzemi mezőgazdaságra vonatkozik, aminek a szerepe egyre inkább csökken, s kezdenek teret hódítani a kisebb táblákon gazdálkodó egyéni vállalkozók, társulások. Ez, és az EU-hoz való csatlakozási szándékunk együttesen indokolják a minél előbbi változtatásokat.

KISVÍZFOLYÁSOK VÍZKÉSZLETE ÉS AZ APADÁSI GÖRBE

Engi Detki Zsuzsanna
Budapesti Műszaki Egyetem, Építőmérnöki Kar
Vízgazdálkodási Tanszék
H 1521, Budapest, Műegyetem rkp. 3.

1.BEVEZETÉS

Az alapvízhozam recessziós görbéje magában hordozhat a gyakorlat számára szükséges információkat. A havi vízhozamok statisztikai elemzése gyakran utal szeriális korrelációra. E korreláció fő kiváltó oka lehet a hónap elei alapvízhozam. Az összvízhozam ezen összetevője értékelhető és előrejelezhető, így a hónapos vízhozam determinisztikus komponensének tekinthető.

Az alapvízhozam a felszín alatt tározódott vízből szivárog a mederbe. A felszínalatti lefolyást sok tényező befolyásolja, a talaj geológiai szerkezete, a szivárgási út mentén ható függőleges hatások, stb.

2.EMPIRIKUS MEGOLDÁSOK

A kutatások azt mutatják, hogy a recessziós görbe leírható a következő empirikus kifejezéssel:

$$Q_t = Q_0 e^{(-at)}$$

Az $e^{-\alpha}$ helyett k-val írva Barnes kifejezését kapjuk, mely magába foglalja a felszíni lefolyást is.

$$Q = Q_0 k^t$$

ahol k a recessziós állandó, amely kísérletek alapján az alapvízhozamra 0.93-0.995 értékeket veheti fel.

Yevjevich vizsgálatai a recessziós görbét a száraz időszakban a következőképpen írják le:

$$Q = Q_0 e^{-ct} \qquad \text{vagy} \quad Q = Q_0 e^{-ctn} \qquad \text{, ahol c és n koeficiensek.}$$

A kisvízfolyások főleg talajvízből, rétegvízből, tehát a felszínalatt tározódott vízkészletből táplálkoznak, így a recessziós görbe azon alsó szakasza érdekes csak számunkra, amely az alapvízhozamra utal. Szemilogaritmikus koordináta rendszerben ábrázolva a felszínalatti

vízből táplálkozó vízhozamokat, az exponenciális apadási görbe α hajlású egyenest követ, így leolvasható az apadási görbe Q_0, t_0 kezdőpontja.

3.MATEMATIKAI MODELLEK

Mivel a recessziós görbe kialakulását sok bizonytalan tényező befolyásolja, nagyon egyszerű matematikai modelleket alkalmaznak a vízhozam időben bekövetkező csökkenésének matematikai megközelítésére. Alapjuk egy függőleges tartályban levő vízoszlop szintjének fokozatos apadását leíró nem permanens mozgásegyenlet, vagy egy vízszintesen vízzáró réteg fokozatos megcsapolását jellemző nem permanens folyamatot leíró differenciál egyenlet.

Az első esetben a kis kiterjedésű karsztos víztartókból álló felszínalatti tározóteret prizmatikus üreggel és ezt az üreget megcsapoló, porózus anyaggal kitöltött járatú forrással, egyetlen lineáris tározóval helyettesíthetjük. A karsztforrás az alapvízhozam alakulásának tanulmányozására jól felhasználható, mert közvetlen kifolyója a mögötte elhelyezkedő tározótérnek, így vízhozamadatsora zavartalanul, más hatásoktól mentesen mutatja a tározó kiürülését. Felírva a mozgásegyenletet, majd összevonva a kontinuitási egyenlettel, a matematikai modell meghatározható, megoldásra exponenciális jellegű apadási görbét kapunk.

$$Q = Q_0 e^{-\alpha(t-t_0)}$$

ahol Q a t időpontbeli kezdőérték, t az idő, a vízgyűjtőterület hidromorfológiai tényezőitől függő fizikai paraméter.

Megtörténhet, hogy karsztos források esetében a recessziós görbe két vagy több, külön , exponenciális jellegű kiürülési görbe összegével állítható elő. Az első görbe jellemzi a nagyméretű karsztos csatornák, a második a szűk repedéshálózat vízmennyiségének kiürülését.

$$Q = b_1 e^{-\alpha_1(t-t_0)} + b_2 e^{-\alpha_2(t-t_0)}$$

Ha a kisvízfolyás jelentős kavicsrétegből táplálkozik, az apadási görbe negatív kitevőjű hatványfüggvénnyel közelíthető.

$$Q = Q_0(1 - t^{n/(n-1)})$$

4.KÖVETKEZTETÉS

Az alkalmazott matematikai modelleket csak nagy körültekintéssel ajánljuk hszanálni, a helytől függően.

5.IRODALOM:

[1]Kovács, Gy. :A felszíni víz és a talajvíz egymásra hatása. *Vituki*, Budapest, 1974.
[2]Zelenhasic, E.: Analiza malih rečnih voda. *Poljoprivredni Fakultet*, Novi Sad, 1985.
[3]Zsuffa, I.:A hidrológiai folyamatok elmélete és a műszaki hidrológia.. Budapest, 1993.
[4]Nathan, R.J.; McMahon,T.A.:Evaluation of Automated Techniques for Base Flow Recession Analysis.1990,*Water Resources Reseach*, 26(7), 1465-1473.
[5]Nutbrown,D.A.,Downing,R.A.:Normal-mode Analysis of the Structure of Base Flow Recession Curves. 1976, *Journal of Hydrology*, 30,327-340.
[6]Anderson,M.G.,Burt,T.P.: Interpretation of Recession Flow. 1980, *Journal of Hydrol.*, 46, 89-101.
[7]Jones,P.N.,McGilchrist,C.A.: Analysis of Hydrological Recession Curves. 1978., *Journal of Hydrology*, 36. 365-374.

VÍZELLÁTÓ HÁLÓZATOK REKONSTRUKCIÓJA

Kereszturi Péter
Budapesti Műszaki Egyetem
Vízellátás-Csatornázás Tanszék
1111 Budapest, Műegyetem rkp. 1 - 3.

1. BEVEZETÉS

Az előadás áttekintést ad a vízellátó hálózatok illetve vezetékeinek rekonstrukcióját
- kiváltó okokról és
- a hálózat állapotának minősítési-, értékelési és döntés-előkészítő módszereiről,
- valamint az elkészítendő szakértői rendszerről.
Továbbá definiálja a hálózat illetve vezeték rekonstrukció fogalmát, valamint a külföldi és
hazai értékelő és döntési eljárások mellett bemutat egy a szerző által készített értékelő
módszert.

2. HÁLÓZAT ILLETVE VEZETÉK REKONSTRUKCIÓ

A minden településre kiterjedő közműves ivóvízellátás megvalósítása hazánkban befejezés
előtt áll. Az elmúlt időszakban e szakterületre vonatkozóan a műszaki tudományos
tevékenység elsődlegesen és alapvetően a művek létrehozásához kapcsolódott. Ma
meghatározó igényként a vízellátó rendszerek tudományos alapokon nyugvó üzemeltetése,
az amortizálódott művek rekonstrukciója jelentkezik.

A vízellátás csővezetékei - mint a legrégebbi közművek - nagyobb városokban
megközelítik a 100 éves életkort. A hálózatok hossza ebben az évszázadban az egész
világon többszörösére nőtt, melyeknél napjainkban a csővezeték rohamos előregedése
tapasztalható. Nem elhanyagolható az a tény, hogy az urbanizálódási folyamat és a vele
együtt járó motorizáció a hálózatok használatát, az üzemeltetés műszaki és tárgyi
feltételeit megváltoztatta.

A **rekonstrukció fogalmát** azokra a tevékenységekre használjuk, amelyek a már meglévő
közmű vezetékek állapotát (szerkezetét, helyzetét, anyagát, méretét, állagát) vagy a
hálózatban betöltött feladatát megváltoztatják. A rekonstrukció fogalomkörében
tárgyalandók a rendszerelméletű beavatkozási módszerek is, amelyek segítségével a
meglévő vagy megnövekedett szolgáltatási igények kielégíthetők. De a
hálózatrekonstrukció és a vezetékrekonstrukció között lényegi különbséget kell tenni [1].

Hálózatrekonstrukciót elsősorban a területi fogyasztási (külső) igények, feltételek
változása teszi szükségessé. A hálózat rekonstrukció a teljes hálózatra vagy hálózatrészre
terjed ki, és esetleg kihathat a szivattyú, medence üzemelési rendszerére is, azaz nem egy
egyértelműen adott vezetékszakasz rekonstrukciójáról van szó.

Vezeték rekonstrukcióra a helyi, konkrét üzemeltetési (belső) feltételek változása miatt
kerül sor, amelyet egy adott vezeték gyakori sérülései, csökkent teherbírása, korróziója,
inkrusztációja stb. miatt végeznek.

A hálózat és vezeték rekonstrukció ennek ellenére a valóságban gyakran
összekapcsolódik. A hálózatrekonstrukció és a vezetékrekonstrukció viszonyát az 1. ábra
szemlélteti.
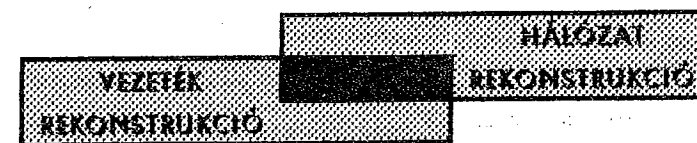
1. ábra Vezeték- és hálózatrekonstrukció kapcsolata

3. REKONSTRUKCIÓT KIVÁLTÓ OKOK

⇨ **_MŰSZAKI_** [4]

    a.) FENNTARTÁSI PROBLÉMÁK:

      ① *meghibásodások:* ⇨ *tervezési hibák,*

            ⇨ *kivitelezési hibák,*

            ⇨ *gyártási hibák,*

            ⇨ *üzemelési hibák,*

            ⇨ *üzemi feltételek változása:*
                ✦ **környezeti hatások változása:**
                    • fiziko-kémiai hatások,
                    • biológiai hatások,
                    • külső környezeti hatások:
                        - statikus hatások,
                        - dinamikai hatások,
                        - hőmérsékleti hatások.
                ✦ **ellátási igények változása,**

            ⇨ *elhasználódás.*

      ② *lerakódások, keresztmetszet csökkenés,*

      ③ *vízminőség változások.*

    b.) ELAVULÁS (kapacitáshiány, nyomáscsökkenés).

⇨ **_GAZDASÁGI_**
    KÖLTSÉGEK CSÖKKENTÉSÉT CÉLZÓ REKONSTRUKCIÓ [5]:

    ① **fenntartási, javítási költségek,**

    ② **energia költségek.**

# 4. A VÍZELLÁTÓ HÁLÓZAT ÁLLAPOTÁNAK ÉRTÉKELÉSI MÓDSZEREI

Az összemérési, minősítési, értékelési, elemzési módszerek jó összehasonlítási alapot teremtenek a hálózatok állapotfelmérésén keresztül azok értékeléséhez, beruházási,- (fejlesztési), rekonstrukciós döntések előkészítéséhez [1,5].

A hálózat állapotának értékelemzése a rekonstrukció szempontjából a döntés-előkészítés része, és a vízhálózat használati érték műszaki-gazdasági elemzését jelenti.

4.1 Németországban kifejlesztett módszer

A *Németországban* kidolgozott minősítő-, értékelő eljárás két meghatározó eleme:
-a műszaki állapot és
-a kapacitás (2.ábra) [2,3].
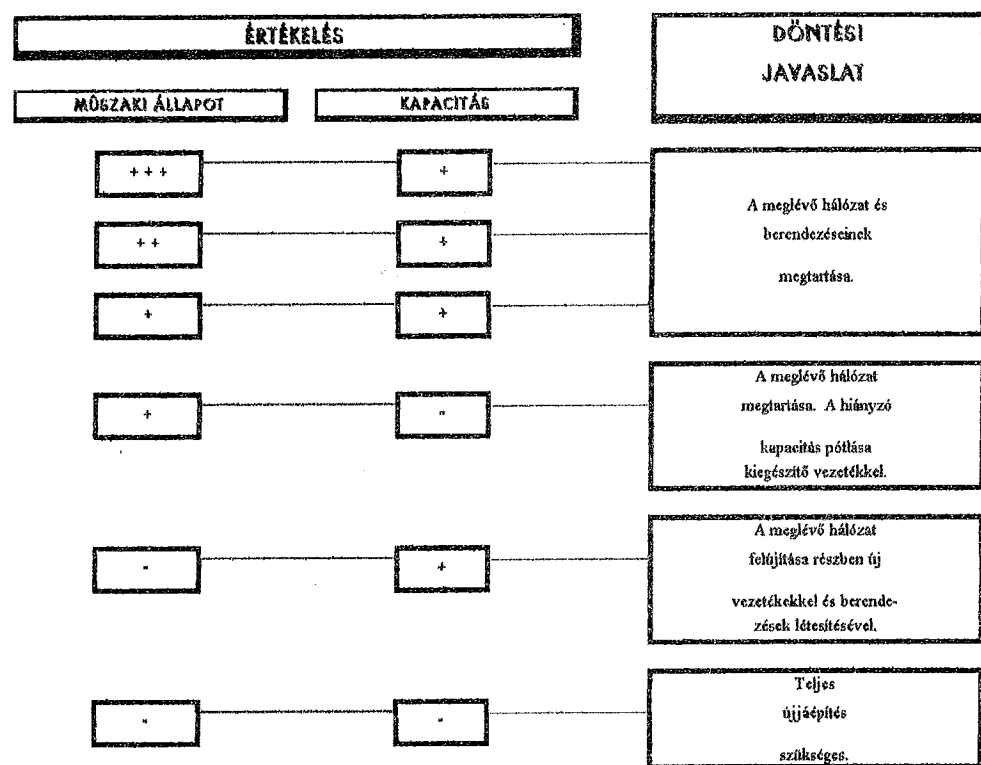
2. ábra Értékelő táblázat döntési javaslatokkal [2]

A műszaki állapotot három tényező alapján értékelik:
- a hálózat kora (A),
- a használati érték (B) és
- a meghibásodások aránya (C)   (1., 2. táblázat).

A MŰSZAKI ÁLLAPOT ÖSSZETEVŐI		ÉRTÉKELŐ SZÁM	FONTOSSÁGI SZÁM	MÉRŐSZÁM
A HÁLÓZAT KORA (A)	1900 előtt épült	0	0,1	0
	1900...1920	1	0,1	0,1
	1921...1945	2	0,1	0,2
	1945 után épült	3	0,1	0,3
HASZNÁLA- TI ÉRTÉK, [%], (B)	<25	0	0,3	0
	25...50	1	0,3	0,3
	51...75	2	0,3	0,6
	>75	3	0,3	0,9
MEGHIBÁSO- DÁSI ARÁNY [db/km/év], (C)	>1	0	0,6	0
	0,51...1	1	0,6	0,6
	0,25...0,50	1	0,6	1,2
	<0,25	3	0,6	1,8

1. táblázat A vízellátó hálózatok műszaki állapotának értékmérői [2]

A használati érték részletes számításának lehetősége.

HASZNÁLATI ÉRTÉK [30 % -on BELÜL 100 % -ot KÉPVISEL]	Szabványon kívüli átmérő		0	0,5	0
	Szabványnak megfelelő átmérő		1	0,5	0,5
	Végág		0 (1)	0,15	0
	Nem végág		1 (0)	0,15	0,15
	Rossz helyen van a cső		0	-	-
	Megfelelő helyen van a cső		1	-	-
	Csőanyag	ac	0	0,25	0
		pvc	0	0,25	0
		öv	1	0,25	0,25
	Beépítettség	belváros	0	0,1	0
		külterület	1	0,1	0,1

2. táblázat A használati érték mérőszámai

A műszaki állapot mérőszámát az

$$M_m = A + B + C \qquad (3)$$

képlet fejezi ki. Az M_m lehetséges értékei alapján végzett minősítést a 3. táblázat tartalmazza.

A MŰSZAKI ÁLLAPOT MÉRŐSZÁMÁNAK (M_m) HATÁRÉRTÉKEI		MINŐSÍTÉS
ALSÓ	FELSŐ	
0	0.75	NEM FELEL MEG (-)
0.76	1.75	MEGFELEL (+)
1.52	2.25	KIELÉGÍTŐ (+ +)
2.26	3.00	JÓ (+ + +)

3. táblázat Minősítés a műszaki állapot értékelése alapján [2]

4.2 Az USA-ban kifejlesztett módszer

A csővezetékek felújítása, a munkálatok időpontjának optimalizálása hosszabb ideje foglalkoztatja a szakembereket az *USA*-ban is. A csővezetékcsere ütemezésére ad megoldást egy analitikus eljárás, amelyet Calgasy város Alta nevű területére dolgoztak ki. Egy cső vagy hálózat *törési adatai alapján* meghatározható egy regressziós egyenlet, amely jól tükrözi a folyamat alakulását [10, 11]. Ez felírható

⇨ exponenciális alakban

$$N_t = N_{t_0} \cdot e^{A \cdot (t - t_0)} \qquad (1)$$

⇨ lineáris alakban

$$N_t = N_{t_0} + A \cdot (t - t_0) \qquad (2)$$

ahol
- t - a vizsgálat időpontja [év],
- t_0 - az építés éve [év],
- N_t - törések száma - 1000 m csőszakaszra a t-edik évben [db],
- A - növekedési együttható,
- N_{t_0} - regressziós együttható [10].

4.3 Hazánkban alkalmazott módszerek

A hazai módszerek közül az egyik legjobbat a *Főmtervben* dolgozták ki [6,7,8]. Konkrét statikus-vizsgálati módszert javasol, elemzi a meghibásodásokat, a hibák rendszerezésére, csoportosítására és a hálózati minősítésre ad konkrét javaslatokat. A megbízható, jó értékelő eljárások közös ismérve, hogy azok minden olyan *értékelési tényezőt* tartalmaznak, amelyek egy esetleges átépítést vagy egyéb elhatározást indikálhatnak. Természetesen kívánalom egy jó értékelő eljárással szemben, hogy az áttekinthető, könnyen kezelhető és megbízható legyen. A fenti célok elérését teszi lehetővé az *értékelő eljárás sémája* és az *értékelő táblázat*, amely 1983-ban több évi fejlesztőmunka után a *Mélyéptervben* került kidolgozásra [9].

4.4 A készített minősítő-, értékelő módszer bemutatása

Az eljárás a német módszert veszi alapul, azonban ezt jelentősen átdolgozza és újdonságként bevezetésre került az úgynevezett *"S"* sürgősségi tényező, amely a munkálatok elvégzésének időrendi fontosságát adja meg közel azonos állapotú csövek esetében.

5. A KÉSZÍTENDŐ SZAKÉRTŐI RENDSZER ELŐKÉSZÍTÉSE

Az elkészítendő szakértői rendszer feladata, egy adott település esetén kiválasztani a rekonstrukcióra megérett vezetékszakaszokat, az előbb említett minősítés után a megfelelő szempontok szerint az értékelést elkészíteni, a kiválasztott vezetékszakaszok esetében módszer(eke)t javasolni a rekonstrukció megvalósítására, és elemezni, értékelni az elvégzett beavatkozás várható hidraulikai-, vízminőségi-, üzembiztonsági hatásait.

6. MEGÁLLAPÍTÁSOK

Az előadás áttekinti az ivóvízellátó hálózat rekonstrukcióval foglalkozó szakterületet időszerű kérdéseit, feladatait, és az összegyűlt tudást végső célként az elkészítendő szakértői rendszerben szándékozik együttesen megmutatni. A szakértői rendszer feladata lesz egy adott hálózat minősítése, értékelése, döntés-előkészítése, döntéstámogatása. Ennek segítségével lehetőség nyílik az elöregedett illetve a rekonstrukcióra megérett hálózatok, vezetékek tudományos alapokon végzett vizsgálatára és a tervszerű rekonstrukciós programok elkészítésére.

A téma keretén belül azonban nyomatékosan hangsúlyt kell fektetni a kiváltó okok vizsgálatára, elemzésére (pl: csőtörések okai, nyomáslengések hatásai, légtelenítés problémái stb.), mely ismeretek által a rekonstrukció kérdése kezelhetőbbé válik, és ennek eredményeként a rekonstrukció megvalósítása időben kitolható, de el nem kerülhető.

7. HIVATKOZÁSOK

[1] *Bartos-Mészáros-Solti:* Víz- és csatornahálózatok rekonstrukciója. Műszaki Könyvkiadó, Budapest, 1989.

[2] Bauakademie der DDR. Institut für Ingenieur und Tiefbau: Problemstudie zur komplexen Erschliessung bei der Rekonstrukcion innerstadtischer Wohngebiete. Leipzig, 1980.

[3] *Beck, D.-Heins, D.- Jürgenlohmann, P.:* Sanierung von Rohrnetzen für Wasser, Gas und Abwasser. Strassen und Tiefbau. Nr. 2. 1985.

[4] *Becker Károly:* Elosztóhálózat rekonstrukciója. Víz- és csatornahálózatok rekonstrukciója, VI. Szeminárium, Miskolc, 1980.

[5] Budapesti Műszaki Egyetem Építés-kivitelezési Tanszék: Közmű-rekonstrukciónál alkalmazható komplex diagnosztikai vizsgálatok és értékelési módszerek a döntés-előkészítéséhez. Értékelő eljárás. (Kutató zárójelentés) Budapest, 1982.

[6] Főmterv: Közműhálózat-javítási munkák számítógépes feldolgozása és nyilvántartása I. rész. Alaptanulmány. Budapest, 1982.

[7] *Issekutz György:* Közműhálózatok életkorának és élettartamának vizsgálati módszerei és lehetőségei. Magyar Építőipar. Nr. 4. 1983.

[8] *Mészáros Pál:* Közműhálózatok és -rendszerek minősítése, a diagnosztika jelentősége a rekonstrukciós módszerek meghatározásában. Vízgazdálkodási és Közműépítési Konferencia, Budapest, 1985. IV. köt.

[9] *Mészáros Pál-Oelberg Gusztáv-Székely Csabáné-Balogh József-Fauszt László:* Közműhálózatok adatainak nyilvántartása és a rekonstrukció számítógéppel segített tervezése. Mélyépterv, Budapest, 1983.

[10] *Uri Shamir and Charles D. D. Howard:* An Analytik Approach to Schedulig Pipe Replacement. J. AWWA. Nr. 5. 1979

[11] *Walski, T. M.-Pelliccia, A.:* Aconomic analysis of Water main breaks. J AWWA. Nr. 3. 1983.

INFORMÁCIÓS RENDSZEREK A VÍZKÉSZLETGAZDÁLKODÁSBAN

Zilahy András
Budapesti Műszaki Egyetem
Építőmérnöki Kar, Vízgazdálkodási Tanszék
Műegyetem rakpart 3.
H-1111, Budapest, Hungary

1. SUMMARY

Today, with more and more demand for water and with the increasing number of environmental problems it is very important to develop and manage a safe water resources development with the help of a management information system (MIS). An MIS can support and supervise political and economical decision making, and therefore it is very useful also in the regional and countrywide water management. An information system (IS) is a subsystem of MIS, which makes it possible to manage big databases, to get and to process the information, and to make forecasts for the future. It also has great importance in the communication between subsystems and with other databases or information systems. The IS has to fulfill the needs of the users efficiently. In Hungary, there is a good and wide long-established IS in water resources development, but with the growing demand for water and with the increasing number of environmental problems, the information system in the field of water resources management needs further development.

2. BEVEZETÉS

Magyarországon igen nagy múltra tekinthet vissza a vízgazdálkodás, ezen belül is a vízkészletgazdálkodás. Az ezen a területen végzett magas színvonalú munkák méltán nagyhírűek és nemzetközileg elfogadottak. A vízkészletgazdálkodásra jellemző, hogy a víz körforgásának folyamatos követéséhez és a beavatkozások hatásainak figyelemmel kíséréséhez nagy mennyiségű adatot (információt) kell összegyűjteni, feldolgozni és értékelni. Sőt lényeges az is, hogy nemcsak a vízügyi szervek, hanem a vizet használók is hatással vannak vízkészleteink állapotára, ezért ezek tevékenységét is figyelemmel kell kísérni. Látható tehát, milyen összetett feladatokat kell ellátni a vízkészletgazdálkodás területén.

3. MENEDZSMENT INFORMÁCIÓS RENDSZER A VÍZKÉSZLETGAZDÁLKODÁSBAN

Korunk egyre nagyobb – ipari és társadalmi (lakossági) – igényei és az egyre jobban elszennyeződő és fogyatkozó vízkészleteink miatt úgy kell gazdálkodnunk a rendelkezésre álló vízkészlettel, hogy ez a készlet a jövő generációk számára is – legalább a mai szinten – megmaradjon *("fenntartható fejlődés")*. A vízkészletgazdálkodás, mint egy átfogó, egész országra, sőt ennél nagyobb területekre is (vízgyűjtő rendszerekre) kiterjedő rendszer megfelelő irányításához korszerű, integrált és hatékony menedzsment információs rendszer (MIS) alkalmazása nélkülözhetetlen. Ilyen integrált rendszer segítségével lehetőség nyílik a különböző vízügyi szervek munkájának és a vizet használók igényeinek összehangolására, a nagy

mennyiségű adatállomány megfelelő menedzselésére és gazdasági-politikai döntéselőkészítésre és döntésfelügyeletre is.

4. INFORMÁCIÓS RENDSZEREK ÉS FELADATAIK

Az információs rendszerek – melyek egy-egy MIS alrendszerei – az adatgyűjtés, adatfeldolgozás, valamint az értékelések és becslések (előrejelzések) készítésén túl – többek között – adatvédelemmel és a felhasználókkal, illetve más rendszerekkel, adatbázisokkal való kapcsolattartással (beleértve a felhasználók igényeihez való folyamatos alkalmazkodást, azaz a rendszeres fejlesztést is) kell foglalkozzanak. Ilyen komplex információs rendszerek tervezése körültekintő munkát igényel, melynek során ma már komoly szakirodalmi háttérre lehet támaszkodni (pl. [1],[2]).

4.1. Térinformatika és távérzékelés

A térinformatika és távérzékelés az információbeszerzés és -feldolgozás egyik legdinamikusabban fejlődő területe, melynek segítségével gyorsan és hatékonyan lehet olyan adatokra szert tenni, melyek más úton nem, vagy csak körülményesen szerezhetők be [3]. A mai technológiai színvonal és technnikai háttér ezen módszerek gyakorlati alkalmazását már Magyarországon is elérhetővé teszi (lásd a távérzékelés gyakorlati alkalmazásáról pl. [4]).

4.2. Magyarországi előzmények és a fejlődés lehetőségei

Magyarországon az adatfeldolgozás gépesítése és a számítástechnika alkalmazása a vízkészletgazdálkodásban komoly hagyományokkal rendelkezik. Az elmúlt időszakban több alkalommal történtek kísérletek a vízgazdálkodás informatikai rendszerének kialakítására, de többnyire csak részeredmények születtek (pl. VIFIR: vízföldtani információs rendszer, SHATIR: hidrológiai adatfeldolgozó és tároló rendszer) [5],[6]. A vízügyi informatika fejlesztésére egységes irányelveket dolgoztak ki [6], és a környezeti hatások előtérbe kerülésével elkészítették az egész Magyarországot felölelő környezetgazdálkodási információs rendszer tervét is, mely a vízkészletgazdálkodás mellett más területek környezeti problémáit is tárgyalja [7].

4.3. Környezeti hatásvizsgálatok

Bár a káros környezeti hatások vizsgálata, értékelése és megelőzése még az iparilag fejlett országokban is sok kérdést hagy maga után és az alkalmazott vizsgálati és értékelési módszerek még vitatottak, kialakulóban van egy olyan irányzat, mely a hangsúlyt a megelőző politikák kidolgozására helyezi. Ennek érdekében egyre több országban válik kötelezővé környezeti hatásvizsgálat, és újabban stratégiai környezeti vizsgálat [8] készítése is. A vizsgálatok egyrészt a kiindulási állapot felvételekor, a határadatok és egyéb tényezők megállapításakor építenek az információs rendszerek adatállományaira, másrészt a vizsgálatok elvégeztével maguk is hasznos információval járulhatnak hozzá a már meglevő adatállományokhoz. A környezeti hatásvizsgálatok elvégzésének jelentősége napjainkban egyre növekszik.

5. ÖSSZEFOGLALÁS

A magyarországi vízkészletgazdálkodás területe magas színvonalú hagyományos információs rendszerrel rendelkezik, de a növekvő igények kielégítéséhez, a készletek mennyiségi és

minőségi megóvásához, valamint az integrált formában jelentkező káros környezeti hatások kivédéséhez ennek további fejlesztése elengedhetetlen.

IRODALOM

[1] Blokdijk A., Blokdijk P., "Planning and Design of Information Systems", *Academic Press*, London, 1987

[2] Meyer-Uhlenried K.-H., "Metodische Grundlagen für die Planung von Informationssytemen", *Verlag Dokumentation*, München, 1977

[3] Detrekői Á., Szabó Gy., "Bevezetés a térinformatikába", *Nemzeti Tankönyvkiadó*, Budapest 1995

[4] Tauer W., Humborg G., "Runoff Irrigation in the Sahel Zone", *CTE (Verlag Josef Margraf)*, The Netherlands, 1992

[5] Szini I., "A vízgazdálkodási információrendszer fejlesztése", *BME*, Budapest, 1985

[6] —, "A vízügyi informatika fejlesztésének irányelvei", *Országos Vízügyi Főigazgatóság, Vízgazdálkodási Főosztály*, Budapest, 1992

[7] Csalagovits I., "Regional Integrated Monitoring", *Geographical Information Systems in Water and Environmental Management, Workshop, organised by Equipe Cousteau and TUB*, Budapest, 1992

[8] Dr. Juhász F., "Stratégiai környezeti vizsgálat (SKV)", kézirat, Budapest, 1995

HIDROGEOLÓGIAI VIZSGÁLATOK A BUDAI VÁRHEGYEN

Hajnal Géza
Budapesti Műszaki Egyetem, Mérnökgeológiai Tanszék
H-1521 Budapest, Hungary

1. BEVEZETÉS

A múlt század közepe óta számos kutató foglalkozott a Várhegy kialakulásával, földtani felépítésével és a hegy gyomrában képződött üregrendszerrel. A terület átfogó hidrogeológiai vizsgálatának megkezdésére azonban csak Kessler Hubert vállalkozott 1971-ben, felismerve a természetes- és mesterséges eredetű vizek jelenlétének sokrétű problémakörét. Az Alagút vágatainak vizesedése, a Várlejtők csúszásveszélye, az üregrendszerben megfigyelt vízbetörések mind azt indokolják, hogy szükséges folytatni Kessler kutatásait.

2. FÖLDTANI ÁTTEKINTÉS

A hegy fő tömegét a budai márga képezi, melynek a téma szempontjából három fontos tulajdonságát kell megemlíteni:

a.) az alsó összletrész nagy mésztartalmú, ezért karsztosodásra, üregképződésre hajlamos, jó vízvezető, míg a felső szakasz nagy agyagtartalmú és viszonylag rossz vízvezető

b.) a márga nyomószilárdsága víz hatására lényegesen csökken, egyharmad-egynegyedére

c.) a márgaösszlet padjai uralkodóan D-i, ill. DNY-i dőlésűek, aminek kiemelt szerepe van a felszín alatti szivárgóvizek mozgásában, az 5-30° között változó dőlési síkok mentén ugyanis a polgárváros felől a víz az Alagút felé áramlik (Dél felé).

A hegy tetejét sapkaként borítja az átlagosan 10 m vastag édesvízi mészkő, melyet a területen feltörő meleg hévforrások alakítottak ki. Ebben a kőzetben és ennek alsó határán jött létre a világon igen ritka mésztufa barlang- és üregrendszer.

3. BARLANGPINCÉK

A barlangpincéknél három szint különíthető el. A legfelső szint 2-3 m mélyen található a felszín alatt, ezek az épületek mesterségesen kialakított pincéi. A középső szintet 5-8 m mélyen vájták bele az édesvízi mészkőbe, kibővítve a természetes eredetű üregeket. A harmadik szinten az úgynevezett mélypincék húzódnak, amelyekből ismerünk egyedieket (kb. 60 db) és egy nagy összefüggő rendszert, melynek Nagy Labirintus a neve. Ezek a hévizes barlangképződés hatására jöttek létre, mai formájukat több évszázados emberi beavatkozásoknak köszönhetik. A Nagy Labirintus alapterülete 18.000 m², míg az egyedi mélypincéké 4.000 m² (1. ábra).

A kutatók és a gyakorlati szakemberek munkáját három tényező nehezíti:
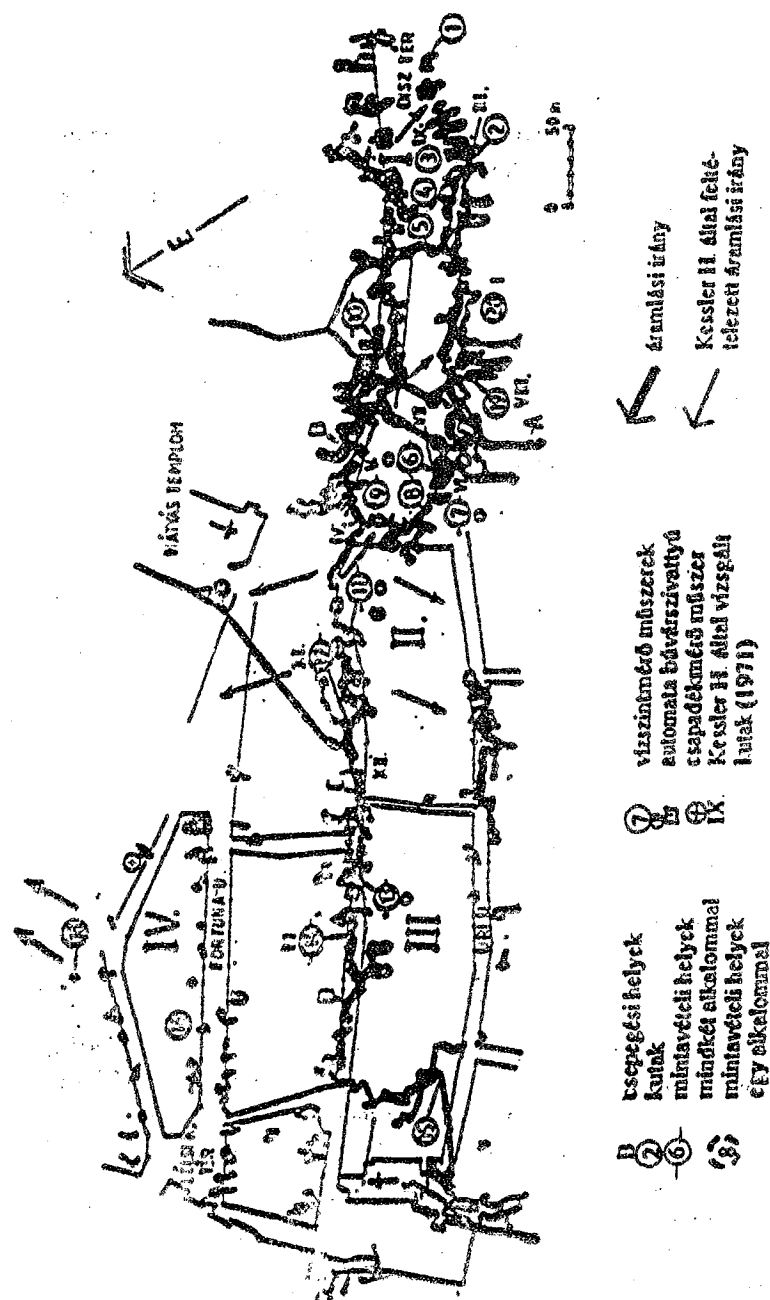
1. Ábra A Budavári Nagy Labirintus és a mélypincék alaprajza a mérési és mintavételi helyekkel

1., a területről nincsenek hiteles térképek, mind horizontális mind vertikális értelemben számtalan eltérés mutatkozik a száz év alatt készített alaprajzokon és metszeteken.

2., a barlangokat hadi- és polgári védelmi célokra is felhasználták, ami nehézzé teszi az adatszerzést.

3., sosem volt tisztázva a sziklapincék tulajdonviszonya, ami rengeteg jogi bonyodalmat okoz.

4. VÍZMÉRLEG

A Várhegy természetes vízkészletét a csapadékból kapott vizek tartják egyensúlyban. A csapadékmennyiség ismeretében különféle hidrológiai modellek segítségével előállítható a vízmérleg, melynek felhasználásával a vizes műtárgyak (csatornák, aknák, szivárgók) tervezéséhez nélkülönözhetetlen adatok nyerhetők. Az eddig végzett számítások eredményei- melyek a beszivárgás mértékét becsülik külön a platóra ill. a lejtőre jelentősen eltérnek egymástól. Ennek okai: a különböző területméretek alapulvétele, ill. a különféle számítási módok (párolgás figyelembevétele, lefolyási tényezők stb.)

Kessler Hubert kétféle, nagyságrendileg is óriási eltérést mutató eredménye (24.400 ill. 146.000 m³/év) úgy született, hogy Kessler az üregekben talált vízmennyiségből visszafelé is kiszámolta a beszivárgás lehetséges mértékét. Eredményei azt bizonyítják, hogy a barlangpincékben lényegesen több víz van, mint amennyi a csapadékból lejuthatna. Ezt a víztöbbletet egyértelműen a hibás közműhálózat okozza, ám ennek bizonyítása nem túl egyszerű feladat.

5. KÖZMŰVEK

A Fővárosi Vízművek 1985 óta végez rendszeresen időszakos vízveszteség méréseket a területen. Erre azért van szükség, mert egy kis hibahelyen lényegesen több víz szivároghat el, mint egy nagyobb csőtörés alkalmával (pl. 5 mm-es lyukon 24 l/perc). Ezek a hibahelyek főleg az illesztéseknél és a bekötéseknél jelentkeznek. 1990-es adatok szerint a Várnegyedben 7,7 m³/h volt a veszteség, ami 110 mm/év csapadéknak felel meg. Ez évi 70 000 m³ vizet jelent, ami jórészt lefedi a Kessler által feltárt különbséget. Fontos megemlíteni, hogy a Fővárosi Vízművek, csakúgy mint a Csatornázási Művek csak a közterületeken felelős a vezetékeiért, azok üzemeltetéséért és karbantartásáért. A házi bekötő vezetékek állapota még rosszab, mint a közterületeken lévőké, bár ezek rekonstrukcióját folyamatosan végzik. Rövidesen beépítik a folyamatos vízveszteségmérő műszereket a Vár platóján, ami nagyban hozzájárul a hibahelyek gyors kiszűréséhez. A Fővárosi Távfűtő Művek az idén végzi vezetékeinek cseréjét.

A Csatornázási Művek 1993-ban készített részletes állapotfelvételt a vári csatornahálózatról, mely 5000 fm hosszú, és egyesített rendszerű. Túlnyomó részüket az 1800-as évek végén fektették, ennek köszönhetően hidraulikai szempontból megfelelőek, sőt túlméretezettek. Viszont a statikai és vízzárósági követelményeknek nem felelnek meg, korrodálódtak, kiüregelődtek. A különféle műtárgyak, aknák állapota katasztrofális. A csatornákból elszivárgó vízmennyiséget csak nagyságrendileg lehet megbecsülni, amiben a kémiai és a biológiai vizsgálatok is nagy szerepet játszanak.

6. KUTAK

Távlati célunk egy sok paramétert figyelembe vevő, az eddigieknél pontosabb vízmérleg készítése, melynek első lépcsőfoka a hidrológiai észlelőhálózat kiépítése. Ennek keretében két évig működtettünk egy csapadékmérő műszert a Táncsics Mihály utcában (1. ábra), felkutatjuk a Várlejtőn található forrásokat (későbbi vízhozammérés), ill. begyűjtjük a közműhálózattal kapcsolatos adatokat. A legtöbb hasznos információ a kutak vizsgálatából nyerhető, az eddigi eredményeket a következőkben foglalom össze.

Az eredetileg létrejött mésztufa üregrendszer a csapadékból beszivárgó vizeknek természetes ciszternája volt, melyekből a XVII. században a korabeli leírások szerint 170 db működött. Ezen ciszternák megcsapolására mélyítettek kutakat a mészkőbe, illetve a kisvízű üregek aljából a márgába. Míg az 1700-as években 75 kutat ismertek, addig az elfalazások, tömedékelések következtében napjainkra csak 20 vízadó kút maradt. A kutaknak 3 típusát lehet megkülönböztetni:

1.) Sekély vízmerítő helyek, melyek csak a márgaréteget borító kavicsteraszig vannak lemélyítve (pl. Táncsics Mihály u. 5. alatti kút)
2.) Közepesen mély kutak, melyek a márga feszínéig, vagy abba 1 m-ig vannak lemélyítve (pl. Dísz tér 15.)
3.) Mélykutak, melyek a márgába mélyen be vannak ásva (pl. Dísz tér 10.)

A kútvizsgálatoknál a következő paramétereket kell megfigyelni:
   a.) vízállásváltozás, lehetőleg a csapadék függvényében;
   b.) visszatöltődési idő (vízadóképesség);
   c.) vízhőmérséklet, léghőmérséklet;
   d.) kémiai vizsgálatok;
   e.) kutak közti kommunikáció (áramlások).

Ezeken kívül fontos megfigyelni a csepegési helyeket, az itt betörő vizek kemizmusát, kiterjedését, valamint csepegési intenzitását.

A felsorolt megfigyeléseket és méréseket Kessler H. 1970. IX. 6-tól 1971. V. 30-ig végezte, míg a Debreceni Búvár Klub és a szerző hosszú szünet után 1993. V. 29-én kezdte meg újra az észleléseket. A Kessler és az általunk vizsgált kutak csak részben fedik egymást, mivel a hosszú idő alatt több kút hozzáférhetetlenné vált.

6.1. Vízállásváltozás

A hetvenes évekbeli méréseket heti egy alkalommal végezték, mm-es pontossággal. A hidrológiában nagyon rövid idejűnek tekintendő észlelésekből annyi megállapítható, hogy a vízállásváltozások nagyjából követték a csapadék eloszlását, a hóolvadások pedig egyértelműen nyomon követhetők a vízszintadatok tükrében. Arra viszont nem lehet teljes bizonyossággal választ adni, hogy a csapadék és a vízszint kapcsolata közvetlen-e, vagy a csatornákból lejutott vízmennyiség jelent meg a kutakban. Érdekes, hogy a legnagyobb heti változás 170 mm volt (IX. kút). Ez a nagyságrend tette elfogadhatóvá az általunk felszerelt mechanikus vízszintmérő órák alkalmazását, mivel ezek maximális holtjátéka 5 cm. Ezek a műszerek közel két éve üzemelnek folyamatos regisztrációt biztosítva (havonta kell őket leolvasni és újraindítani) és eddig mindegyik konstans vízállást mutat. Eszerint a vízállásváltozások 5 cm-en belül mozognak, ezért mm pontosságú nyomásérzékelő műszerek beszerelését tervezzük kb. 7 db kútba. Ezek a műszerek vízhőmérsékletet is tudnak regisztrálni.

6.2. Visszatöltődés-vízadó képesség

Kessler H. négy kutat vizsgált (III., VIII., IX., XII.), melyeknek a leszivattyúzás utáni visszatöltődési idejükből rendre a következő értékeket kapta: 3,9 l/nap; 43 l/nap; 16 l/nap; 9,3 l/nap. Az újabb eredmények alapján a terület hidrológiai szempontból négy részre osztható, melyet a térképen nagy római számok jelölnek.

6.3. Vízhőmérséklet

Megállapítható, hogy a kútvizek hőmérséklete követi a barlangi léghőmérsékletet, kivéve a próbaszivattyúzások után, mert akkor a visszatöltődéseknél felmelegedés tapasztalható. Ez azt látszik igazolni, hogy az utánpótlódás a réteghatáron tárolt statikus vízkészletből történik. Az állandó vízhőmérséklet mérést a fent említett nyomásérzékelő műszerekkel lehetne megoldani, így eddig csak kevés adat áll rendelkezésünkre.

6.4. Kemizmus

A huszonöt évvel ezelőtti vegyi vizsgálatok a víz SO_4^{2-} és az NO_3^- tartalmát mérték. Ezen anyagok jelenléte ott volt kiugróan magas (600 mg/l SO_4^{2-} és 940 mg/l NO_3^-), ahol nem lehetett kapcsolatot találni a csapadékvizekkel. Néhol az NH_4^+ is megjelent. A mai vizsgálatok eredményeit az 1.,2. táblázat tartalmazza, az eddigi két mintavételezés alapján

Kiugróan magas értékeket kaptunk a vezetőképességre a 7-es és a 12-es kútnál, valamint a 10-es kútnál, amit csak egy alkalommal volt módunk vizsgálni. Ennek a három kútnak a vízében a legmagasabb a klorid-ion- és a nátrium tartalom is, ami a szennyvíz jelenlétét igazolja. A 9-es kút vize jelentősen tisztult az első alkalomhoz képest, de most sem zárható ki a szennyeződések jelenléte.

1. táblázat Vízminták vizsgálati eredményei, (1994.VII.5.) * csepegési hely, vízbetörés

Mintaszám	pH	Vezetőképesség μS	Oxigénfogy.ps. mg/l	Na mg/l
6	8,50	1280	2,80	81,49
7	8,55	2080	2,00	315,70
9	8,77	1420	3,44	107,3
11	8,52	1330	2,72	68,3
12	8,31	3800	2,48	386,6
13	8,40	900	1,92	73,83
14	8,57	690	1,84	25,33
A*	8,68	650	2,40	11,42
B*	8,70	520	2,72	11,85
C*	8,50	530	1,52	11,72

2. táblázat Vízminták vizsgálati eredményei, (1994.IX.21.) ⁺fluoreszceines volt a minta

Mintaszám	pH	Vezető-képesség	Oxigénfogy. ps. mg/l	Klorid-ion mg/l	Na-ion mg/l
6	7,84	1080	3,04	148	78,14
7	8,03	2050	2,08	580	364,6
8	7,45	1700	2,80	208	109,5
9	7,69	670	2,96	50	35,12
10	7,78	1800	2,48	438	197,2
11	7,65	1190	2,80	134	66,38
12	7,64	3380	1,68	1076	415,00
13	7,79	800	1,60	72	79,29
14	7,69	530	1,04	36	19,02
18⁺	7,60	1260	12,8	270	99,03
A*	8,21	465	1,12	28	11,92
B*	7,91	520	2,32	32	25,74
D*	8,22	960	3,92	186	128,10

6.5. Áramlás

Kessler nem is próbálkozott a kútvizek megfestésével, mivel az áramlás sebessége rendkívül kicsi, hanem a vízszintekből próbált következtetni az áramlási irányokra. Néhány helyen próbálkoztunk a vízfestéssel, de ez a Nagy Labirintus területén nem járt eredménnyel, viszont a mi vízállásadataink alapján semmiféle áramlás nem regisztrálható. Külön érdekesség, hogy az egymáshoz nagyon közel lévő 6-os és 7-es kút között sem tapasztaltunk semmi kapcsolatot, amit a jelentősen eltérő vegyi paraméterek is bizonyítanak (1., 2. táblázat). Ezzel szemben a IV-es jelű területről a kútvizek egyértelműen a Várlejtő felé szivárognak, amit a vízfestések is igazoltak. (Pl. a Táncsics M. u. 15. alatti kút vize a Kagyló lépcső mellett szivárog ki, ami ÉNY-DK-i irányú áramlásnak felel meg, 1. ábra) Ez a támfalak megrongálódását, sőt megcsúszását is okozhatja, amire az elmúlt időszakban többször is akadt példa (pl. Halászbástya).

6.6. Csepegési helyek

Ahol magas a minta elektromos ellenállása és kicsi az ionkoncentráció, ott a csepegés valószínű vezetéki vízből származik, ahol ez a reláció fordított, ott szennyvíz jelenlétére kell gyanakodnunk. Ezeken a helyeken erre az elviselhetetlen szagokból is következtethetünk. A főtén a vizesedések 1-től 40 m²-ig terjedtek el, a csepegések intenzitását a közeljövőben kezdjük mérni. Kessler helyenként 6000 l/nap értéket is észlelt m²-ként. Mi a csepegési és vízbetörési helyeknél ugyanazokat a kémiai paramétereket vizsgáltuk, mint a kútvizeknél (1. ábra,1.,2. táblázat).

Az "A"-val jelölt részen mindkétszer tiszta vizet találtunk, ami azért érdekes, mert májusban állították helyre a pont felett húzódó vízvezetéket, ami addig el volt törve. Ennyi ideig nem tározódhatott a kőzetben az addigi hibából származó víz és így nincs magyarázat a folyamatos utánpótlódásra. A "B" pont közvetlen kapcsolatban van a

csapadékkal. Az első mintavétel előtti két napon összesen 57 mm csapadék esett, ami elöntötte a környező üregeket. A második alkalomra az intenzitás jelentősen lecsökkent, a víz minősége alig változott. A "C" pontbeli csepegésnél a vegyi paraméterek ivóvíz minőséget mutatnak, pedig az egész Labirintusban itt van a legkellemetlenebb szaghatás. Lehet, hogy a mészkő kiszűrte a szennyezőanyagok egy részét, vagy a helyi körülmények teszik lehetővé a baktériumok elszaporodását. A "D" vizsgálati pontnál több helyen a falakból dől a víz. Valószínűleg az Országház utcai közműépítések következtében sérült meg valamelyik vezeték, lehet, hogy fűtővezeték, de a kemizmusa alapján szennyvíz is lehet.

7. MEGÁLLAPÍTÁSOK

A Várhegyről, mint önálló hidrológiai egységről kevés ismeret áll rendelkezésünkre. A legtöbb hasznos információ a barlangi kutak vizsgálatából nyerhető, melyek alapján a következő megállapításokat tehetjük:

- A kutak vízszintje nem változott az 1 éves megfigyelés alatt az időnkénti kiugróan magas csapadék hatására sem.
- Néhány kút vize erősen szennyezett.
- A Nagy Labirintus kútjai között nincs kommunikáció, amit a vízfestések és a vegyi vizsgálatok is igazoltak.
- A különálló üregek néhány kútjából ÉNY-DK-i irányú áramlás figyelhető meg, ami komoly műszaki problémákat okozhat.

8. IRODALOMJEGYZÉK

Debreceni Búvárklub, "Összefoglaló jelentés a budai Várbarlang 1993. május 29. - 1994. január 28. között vizsgált és tisztított kútjainak hidrogeológiai megfigyeléseiről", Kézirat, 1994, p 34

Kessler H., "A budai Várbarlangban végzett hidrológiai mérések értékelése" Kézirat, 1971.

Krolopp E. et al., "Budai Várhegy negyedkori képződményei" Földtani Közlöny, 1976. pp 199-228

Author index

Supervisor index